PHOSPHOLIPIDS AND A PROTEIN-CONDUCTING CHANNEL REGULATE COTRANSLATIONAL PROTEIN TARGETING

Thesis by

David Akopian

In Partial Fulfillment of the Requirements for the Degree of Doctor of Philosophy

California Institute of Technology
Pasadena, California
2014
(Defended May 19th, 2014)

ACKNOWLEDGEMENT

During my stay at Caltech I was fortunate to be surrounded by talented, driven and supportive friends, colleagues, and mentors who have left an indelible mark on my development as a scientist. The time spent with them was very productive and intellectually enjoyable. There is indeed no place like Caltech, and I am glad to have decided to join its graduate program of Biochemistry and Molecular Biophysics. I am also fortunate to have been trained in the laboratory of Shu-ou Shan.

I would like to thank Dr. Shan for fostering scientific rigor and discipline in her trainees, for encouraging us to think deeply and carefully about the research topics and experimental results, and for incessant guidance on our journey of professional growth towards success and self-fulfillment. I benefited tremendously from an in-depth analysis of experimental data and multiple stimulating conversations with Shu-ou. She is always accessible and willing to discuss science.

I am very fortunate to have had a supportive and involved thesis committee. I would like to thank Doug Rees, Bil Clemons, and David Chan. I enjoyed and learned from all of my meetings with them. I would like to thank Andre Hoelz for advice and many insightful and stimulating conversations.

My work at Caltech is tied closely with the work of Ishu Saraogi, with whom I became close friends. Ishu was very supportive throughout my graduate program, especially during the times when the progress was very slow. We spent countless hours over the course of the years discussing topics as divergent as experimental set-ups and data on the one hand and the philosophy of a Ph.D. program on the other. The experimental tools that Ishu developed have become essential to the tool kit in the Shan laboratory and made interesting and incisive studies

possible, one of which we pursued together. Her departure to India left a void in the laboratory that I felt acutely and that could not be filled. I learned a great deal from Ishu, and am very fortunate that our paths crossed.

When I joined Shu-ou's lab, I had received no training in biochemistry and biophysics. As with any graduate student who ventures into an unfamiliar territory, I relied greatly on the expertise of senior students. I would like to thank Kuang Shen, with whom I worked in the same bay for almost five years. Kuang shared with me both his knowledge of the experimental aspects of research and deep understanding of chemical kinetics. I would like also to thank Xin Zhang, from whom I learned the key experimental procedures in the laboratory. The Shan laboratory, in general, is an amazing place to do science in a collaborative and collegial environment, and I would like to thank everyone who came before and after I joined the group. I extend special thanks to Aileen Ariosa, Sowmya Chandrasekar, Sandhya Chandrasekaran, Un Seng Chio, Doug Henningsen, Yu-Hsien Hwang Fu, Peera Jaru-Ampornpan, Vinh Lam, Jae Ho Lee, Fu-Cheng George Liang, Camille McAvoy, Thang Nguyen, Nathan Pierce, Samantha Piszkiewicz, Meera Rao, Michael Rome, and Dawei Zhang. I would like also to thank our volunteers, Irene, Kathy, Mark, and Chris for pouring countless gels and quench tubes. Their diligence and hard work in the laboratory has made our work easier.

Success in any research laboratory is linked to people in other research groups with whom we interact both in the work setting and outside the laboratory. Caltech is a small and closely-knit community that fosters interaction between different laboratories. I would like to thank the members of the Aravin, Chan, Clemons, Hoelz, Miller, Rees, and Varshavsky laboratories. I enjoyed very much the productive joint meetings with Tom Miller and Connie Wang, and am grateful to them for the rigorous treatment of our experimental data and fruitful

insights that it generated. I would like to thank our collaborators at the University of British Columbia, Franck Duong and his former graduate student Kush Dalal. Thanks to Kush, I became more comfortable dealing with SecYEG. I would also like to thank Jost Veilmetter in the Protein Expression Center from whom I learned to operate the BiaCore SPR apparatus. Santiago and Blanca deserve much gratitude for having stock solutions and glassware readily and continuously available. Special thanks go to Margo Hoyt for being always available and so helpful in scheduling meetings and reserving meeting locations. Biochemistry and Molecular Biophysics graduate students are fortunate to have Alison Ross as the option secretary. Alison was very helpful throughout the program, from the very beginning to the very end, and I would like to thank Alison for her support and guidance.

It would have been difficult to go through stressful times, let alone successfully complete the program, without the support of my family and friends, especially my parents. I am incredibly grateful to them for their unwavering support, understanding, and patience. My warm thanks go to Svetlana Ustyugova for her support and encouragement.

ABSTRACT

Signal recognition particle (SRP) and signal recognition particle receptor (SR) are evolutionarily conserved GTPases that deliver secretory and membrane proteins to the protein-conducting channel Sec61 complex in the lipid bilayer of the endoplasmic reticulum in eukaryotes or the SecYEG complex in the inner membrane of bacteria. Unlike the canonical Ras-type GTPases, SRP and SR are activated via nucleotide-dependent heterodimerization. Upon formation of the SR•SRP targeting complex, SRP and SR undergo a series of discrete conformational changes that culminate in their reciprocal activation and hydrolysis of GTP. How the SR•SRP GTPase cycle is regulated and coupled to the delivery of the cargo protein to the protein-conducting channel at the target membrane is not well-understood. Here we examine the role of the lipid bilayer and SecYEG in regulation of the SRP-mediated protein targeting pathway and show that they serve as important biological cues that spatially control the targeting reaction.

In the first chapter, we show that anionic phospholipids of the inner membrane activate the bacterial SR, FtsY, and favor the late conformational states of the targeting complex conducive to efficient unloading of the cargo. The results of our studies suggest that the lipid bilayer acts as a spatial cue that weakens the interaction of the cargo protein with SRP and primes the complex for unloading its cargo onto SecYEG.

In the second chapter, we focus on the effect of SecYEG on the conformational states and activity of the targeting complex. While phospholipids prime the complex for unloading its cargo, they are insufficient to trigger hydrolysis of GTP and the release of the cargo from the complex. SecYEG modulates the conformation of the targeting complex and triggers the GTP hydrolysis from the complex, thus driving the targeting reaction to completion. The results of

this study suggest that SecYEG is not a passive recipient of the cargo protein; rather, it actively releases the cargo from the targeting complex. Together, anionic phospholipids and SecYEG serve distinct yet complementary roles. They spatially control the targeting reaction in a sequential manner, ensuring efficient delivery and unloading of the cargo protein.

In the third chapter, we reconstitute the transfer reaction *in vitro* and visualize it in real time. We show that the ribosome-nascent chain complex is transferred to SecYEG via a stepwise mechanism with gradual dissolution and formation of the contacts with SRP and SecYEG, respectively, explaining how the cargo is kept tethered to the membrane during the transfer and how its loss to the cytosol is avoided.

In the fourth chapter, we examine interaction of SecYEG with secretory and membrane proteins and attempt to address the role of a novel insertase YidC in this interaction. We show that detergent-solubilized SecYEG is capable of discriminating between the nascent chains of various lengths and engages a signal sequence in a well-defined conformation in the absence of accessory factors. Further, YidC alters the conformation of the signal peptide bound to SecYEG. The results described in this chapter show that YidC affects the SecYEG-nascent chain interaction at early stages of translocation/insertion and suggest a YidC-facilitated mechanism for lateral exit of transmembrane domains from SecYEG into the lipid bilayer.

TABLE OF CONTENTS

INTRODUCTION AND SUMMARY

Proper and timely delivery of newly synthesized proteins from the cytosol to a correct subcellular compartment is essential for maintaining structural and functional integrity of the living cell. Nearly 30 percent of the proteome whose synthesis is initiated in the cytosol is delivered to the endoplasmic reticulum (ER) in eukaryotes or the inner membrane in bacteria (Shao, 2011; Pool, 2005). A large fraction of this subset of proteins in eukaryotes is further processed via a well-characterized secretory pathway and is either exported or integrated into the plasma membrane (Miller, 2013; Zanetti, 2012) (Figure 1A). A diverse set of disorders in humans is linked to functional anomalies in the secretory pathway, making various aspects of protein secretion an area of intense investigation (Wang, 2012).

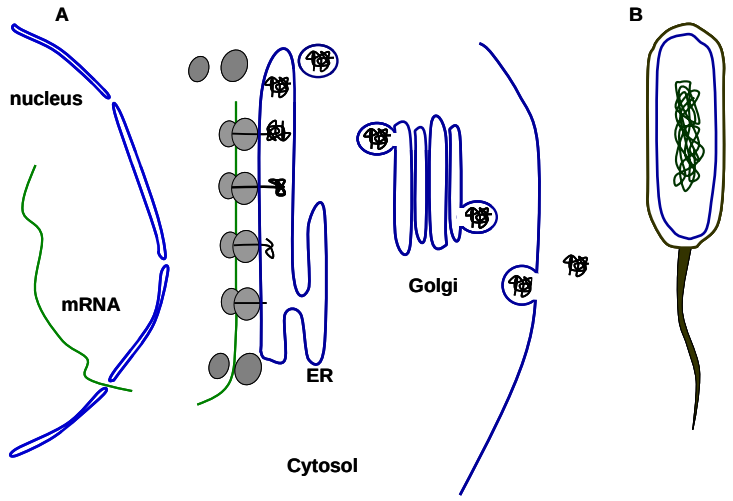

Figure 1. Main features of the secretory pathway. A. In eukaryotes, the secretory pathway begins with targeting of the translating ribosomes to the sites of translocation at ER. The protein is posttranslationally modified and trafficked via Golgi apparatus to the plasma membrane. **B**. In prokaryotes, ribosomes translating membrane proteins are cotranslationally targeted to the inner membrane (blue) of the cell.

Cotranslational targeting of nascent proteins to the sites of translocation at ER constitutes the first essential step of the pathway; its proper execution thus largely affects subsequent steps in the pathway and determines successful secretion or integration of a nascent protein. One of the

lines of research in the Shan laboratory focuses on understanding how ribosome-nascent chain complexes (RNCs) are delivered to the target membrane in a timely and faithful fashion.

Although bacteria lack the secretory pathway characteristic of the eukaryotic cell, the targeting machinery that engages RNCs and the translocation machinery at the target membrane are highly conserved across the living world, allowing us to use *E. coli* as a model organism to study the molecular details of cotranslational protein targeting and its regulation (Figure 1B and 2) (Akopian, 2013; Cross, 2009).

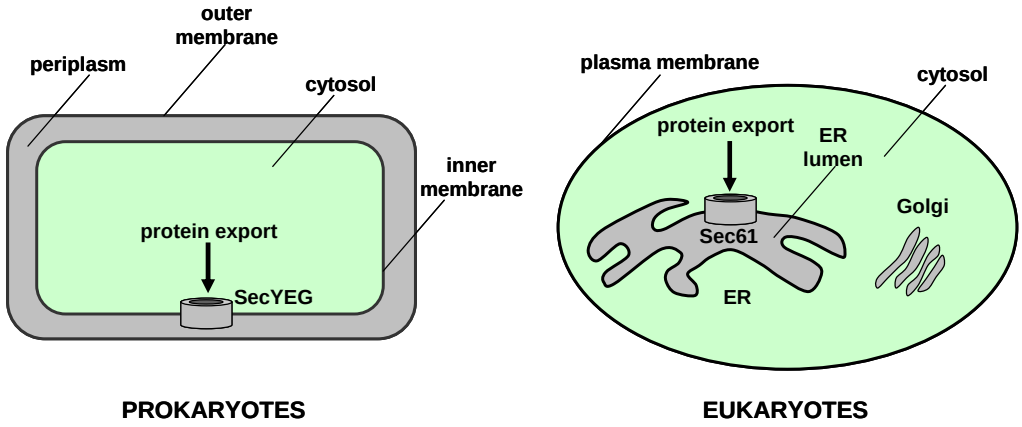

Figure 2. Protein export in prokaryotes and eukaryotes. In prokaryotes and eukaryotes a significant subset of proteins is delivered from the cytosol cotranslationally to conserved sites of translocation in the lipid bilayer. In bacteria, the translocation machinery is represented by a heterotrimeric SecYEG complex that mediates translocation of secretory proteins across the lipid bilayer into the periplasmic space and integration of membrane proteins into the lipid bilayer. In eukaryotes, the protein-conducting channel is the heterotrimeric Sec61 complex embedded in the lipid bilayer of ER and composed of Sec61α, Sec61γ, and Sec61β subunits homologous to the bacterial SecY, SecE, and SecG, respectively.

Cotranslational protein targeting is mediated by conserved GTPases, Signal Recognition Particle (SRP) and its receptor, SR (Kudva, 2013; Akopian, 2013; Saraogi, 2013; Shan, 2009). A universally conserved heterotrimeric protein conducting channel at the target membrane, Sec61 complex in eukaryotes and SecYEG in bacteria, is the site of destination of the cargo (Figure 2) (Cross, 2009; Driessen, 2008; van den Berg, 2004; Hanada, 1994; Gorlich, 1992; Brundage,

1990). While in eukaryotes the SRP-mediated protein targeting pathway handles both membrane and secretory proteins, in bacteria only the membrane proteome (~1000 proteins) and a small subset of secretory proteins are delivered to the SecYEG complex cotranslationally, with the majority of secretory, periplasmic, and outer membrane proteins (~ 400-500) being targeted to SecYEG posttranslationally via the SecB/SecA system (Chatzi, 2014; Kudva, 2013; Hartl, 1990; Lee, 1986).

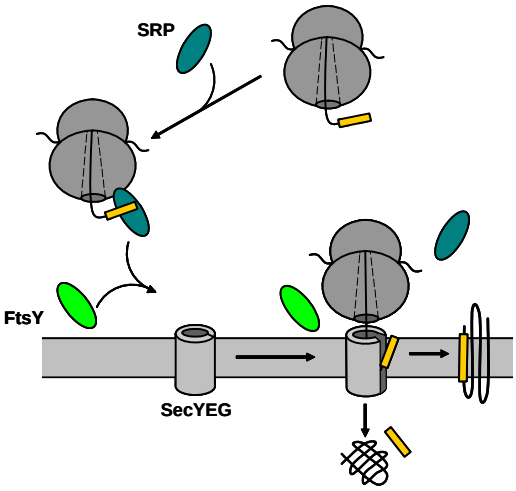

Figure 3. Main steps of the cotranslational protein targeting pathway. In the cytosol, SRP engages a ribosome translating a secretory or membrane protein by binding the signal peptide and the large ribosomal subunit at the ribosomal tunnel exit site. The cargo-loaded SRP is delivered to the target membrane via interaction of SRP with its receptor, FtsY in bacteria. The targeting SRP•FtsY complex unloads RNC onto the SecYEG translocon, and the ribosome continues to synthesize the nascent chain. In the case of a secretory protein, the polypeptide chain is translocated across the channel into the periplasmic space. If the nascent polypeptide is that of a membrane protein, transmembrane domains (TMDs) exit SecYEG via the lateral gate. The orange rectangle represents either a signal sequence or the first TMD of a secretory or membrane protein, respectively.

Cotranslational protein targeting begins with recognition of the N-terminal signal sequence of a secretory protein or a signal anchor (transmembrane domain, or TM) of a membrane protein by SRP, which binds RNC by contacting both the nascent polypeptide chain and the large ribosomal subunit at the ribosomal tunnel exit site (Hainzl, 2011; Janda, 2010; Schaffitzel, 2006; Pool, 2005, 2002; Ullers, 2003; Walter, 1981; Walter, 1980). The cargo-loaded SRP is then delivered to the target membrane by forming a complex with its receptor SR (Shan, 2004; Focia, 2004; Eitan, 2004; Luirink, 1994; Gilmore, 1982). The RNC is transferred from the targeting SR•SRP complex to the protein-conducting channel, and GTP hydrolysis

triggers dissociation of the complex, allowing SRP and SR to be recycled for another round of targeting (Connoly, 1994). As the polypeptide chain is elongated, it is either translocated across the membrane in the case of a secretory protein or integrated into the lipid bilayer in the case of a membrane protein. In the former case, the polypeptide chain passes through the aqueous pore of the translocon, while in the latter case TMs exit the translocon via its lateral gate (du Plessis, 2009; Rapoport, 2007; van den Berg, 2004) (Figure 3).

In bacteria, SRP is a ribonucleoprotein composed of a 48-kDa protein, Ffh (fifty four homologue), homologous to a 54-kDa subunit of SRP in eukaryotes, and 4.5S RNA (Poritz, 1990). The latter has been shown to play an essential regulatory role in the SRP pathway by increasing the rate of association of SRP and SR and accelerating the rate of GTP hydrolysis from the complex (Voigts-Hoffman, 2013; Shen, 2012; Ataide, 2011; Bradshaw, 2009; Neher, 2008; Peluso, 2001; Peluso, 2000). Ffh and FtsY are twin GTPases characterized by the presence of the conserved NG-domain, the main functional and structural component of the two proteins (Figure 4) (Egea, 2004; Focia, 2004; Eitan, 2004; Montoya 1997a, 1997b; Freyman, 1997). The NG-domain is subdivided into the GTPase G-domain and the regulatory N-domain. The G-domain shares homology with classical GTPases, such as Ras and EF-Tu. However, unlike Ras GTPases, both Ffh and FtsY contain a unique insertion box domain (IBD) with β-α-β-α composition, whose loops bear catalytic residues required for GTP hydrolysis. The N-domain is represented by a bundle of four α-helices that pack against the G-domain. In addition to the NG-domain, FtsY contains a highly acidic N-terminal A-domain important in its association with the membrane (Braig, 2009; Weiche, 2008; Parlitz, 2007; Angelini, 2006, 2005), while Ffh contains the C-terminal methionine-rich M-domain that binds 4.5S RNA and interacts with the signal sequence of the nascent polypeptide chain (Zopf, 1990).

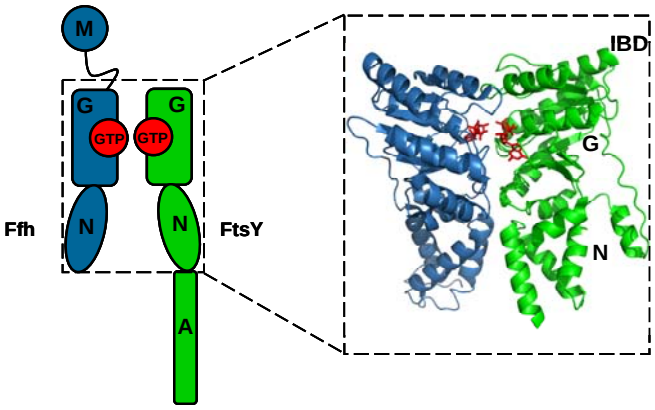

Figure 4. Domain organization and structure of the conserved core of the SRP•FtsY complex. Both Ffh and FtsY contain a structurally and functionally conserved core called the NG-domain, composed of the GTPase G-domain and the regulatory N-domain. Ffh contains an additional C-terminal methionine-rich M-domain that binds a signal sequence and 4.5S RNA, while FtsY has an acidic A-domain implicated in its association with the target membrane. The GTP analogue GMPPCP is shown in stick notation in the composite active site of the complex (red). The crystal structure of the Ffh•FtsY complex from *T. aquaticus* is reproduced with Pymol from Egea, 2004.

FtsY and SRP represent a unique class of GTPases that differ from a classical Ras GTPase in several ways. They do not undergo a major conformational change upon binding GTP, and they associate with both GTP and GDP with equally low affinity (Shan, 2009, 2004; Peluso, 2001). No guanine-nucleotide exchange factors (GEFs) or GTPase activating proteins (GAPs) are required for binding and hydrolysis of GTP. Instead, the GTPases in FtsY and SRP are reciprocally activated as the two proteins form a heterodimer in a nucleotide-dependent manner (Figure 4). Other members of this novel class of GTPases include dynamins, FlhF, MinD, MnmE, septins, and Toc proteins (Saraogi, 2013).

A significant amount of time and effort in the Shan laboratory was devoted to understanding how the activity of the SRP•FtsY complex is regulated. The research revealed that the heterodimer undergoes a series of discrete conformational changes that effectively couple activation of the GTPases to efficient delivery and unloading of the cargo at the target membrane in a timely and faithful manner (Saraogi, 2013; Akopian, 2013; Zhang, 2010, 2009; Shan, 2009;) (Figure 5).

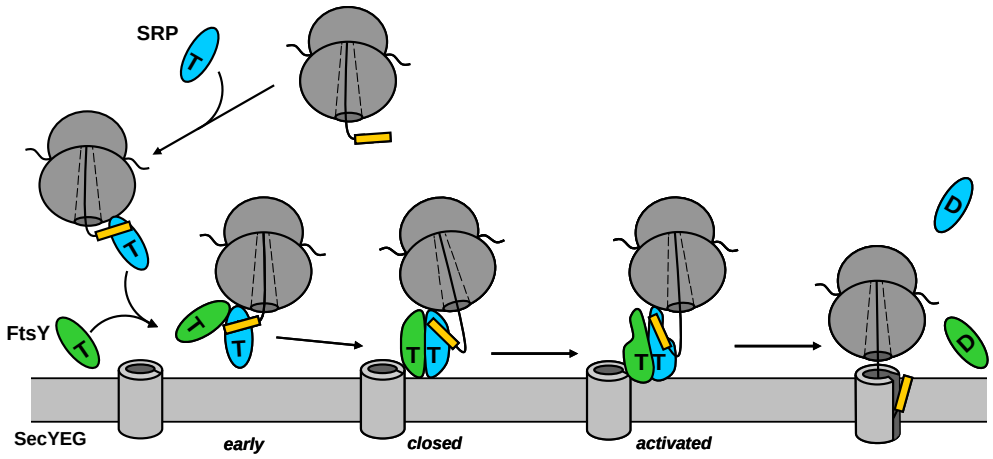

Figure 5. Conformational states of the targeting complex. From the initial heterodimerization to the disassembly upon the hydrolysis of GTP, the SRP•FtsY complex undergoes a series of discrete conformational changes. The two GTPases first form a transient early intermediate held by electrostatic contacts between the N-domains. The early complex then rearranges to the closed conformational state in a GTP-dependent manner. Finally, repositioning of the catalytic loops of IBDs bring the catalytic residues of SRP and FtsY in close proximity to GTP, converting the complex to the activated state and priming it for GTP hydrolysis. The hydrolysis of GTP triggers disassembly of the complex. While GTP hydrolysis is required for recycling of the GTPases, it is not required for unloading of the cargo onto SecYEG, which may occur concurrently with the GTP hydrolysis or precede it. The figure was modified based on Zhang, 2009. T and D denote GTP and GDP, respectively.

FtsY and SRP by themselves exist in an open conformation possessing a poorly organized active site and characterized by low basal GTPase activity (Shan, 2009, 2003; Peluso, 2001). Initial association of the two proteins results in formation of a highly labile (K_d ~ 4-8 μM) *early* intermediate held by electrostatic interactions between the charged surfaces of the N-domains (Zhang, 2011, 2008; Estrozi, 2011). The formation of the early complex is nucleotide-independent; however, subsequent conformational changes of the heterodimer occur only in the presence of GTP or a non-hydrolyzable GTP analogue. In the presence of GTP, the early complex is converted to the *closed* conformational state. This conformational change involves movement of the N-domains toward the center of the heterodimer and removal of the steric block imposed by the first helix of the N-domain of both Ffh and FtsY, αN1, resulting in a complex with a much larger number of stabilizing contacts between the NG-domains (Neher, 2008; Shan,

2004; Egea, 2004). The two GTP molecules in the composite active site are oriented head-to-tail and form contacts between the ribose hydroxyl group and the γ-phosphate. A final conformational change, the repositioning of the catalytic loops of IBDs with respect to GTP, converts the closed complex to the *activated* state, in which the GTPases are primed for GTP hydrolysis. Upon GTP hydrolysis, critical contacts between the two GTP molecules in the composite active site are lost, contributing to the weakening of the affinity between the two proteins. The negative charge of free phosphates further destabilizes the heterodimer, leading to dissociation of the complex and freeing of the SRP and FtsY for another round of the GTPase cycle (Shan, 2007, 2004; Connoly, 1991).

The role of the conformational states of the targeting complex in regulation of the protein targeting reaction can only be understood if considered in the context of the biological cues in the pathway capable of modulating the conformation of the heterodimer. One such factor is the cargo protein. It has been demonstrated in the Shan laboratory that correct SRP substrates, RNCs bearing nascent chains with engineered highly hydrophobic signal sequences (1A9L, 2A8L, 3A7L), dramatically alter the energy landscape of the conformational rearrangement of the complex (Zhang, 2009) (Figure 6). RNC stabilizes the early intermediate ~ 1000-fold by reorganizing the interacting GTPases and maximizing the number of contacts between them. The K_d of the early complex in the presence of a correct SRP substrate falls to approximately 40 nM. One consequence of such stabilizing effect of RNC on the SRP-FtsY interaction in the early complex is the proportionate stabilization of the RNC-SRP interaction. Calculations based on the known K_d values in the thermodynamic cycle of the early complex formation show that in this FtsY•SRP•RNC intermediate SRP binds RNC with affinity in the picomolar range, compared to

the nanomolar affinity in the SRP•RNC complex. The SRP is thus said to be in the cargo-binding mode in the early complex.

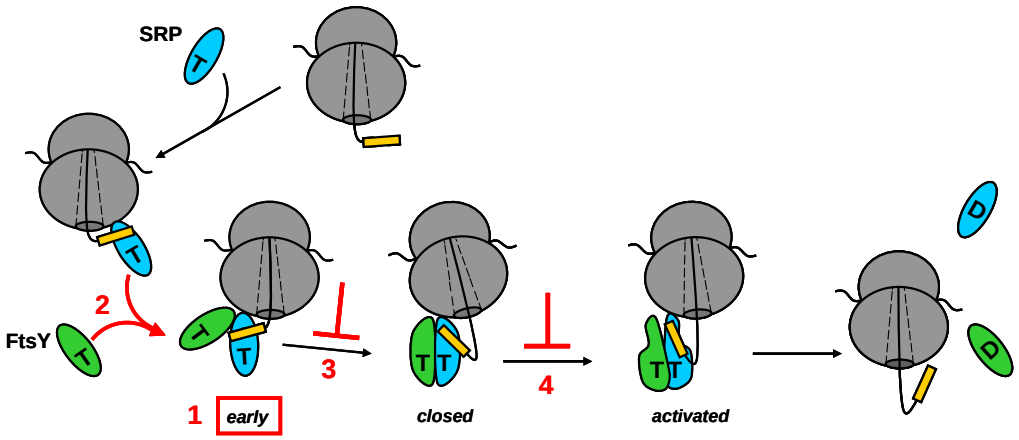

Figure 6. Effect of RNC on the SRP pathway. RNCs that are correct SRP substrates stabilize the early complex (1, red box) and increase the rate of formation of the stable complex (2). They also slow down the rearrangement of the early complex to the closed state (3). Further, the GTP hydrolysis from the targeting complex is inhibited in the presence of RNC (4). Overall, these effects, although increasing the lifetime of the SRP-RNC interaction and preventing premature disassembly of the targeting complex in the cytosol, pose a significant barrier for the subsequent handover of the cargo to the translocation machinery at the target membrane.

Such tight interaction of SRP with RNC is beneficial at the early stages of targeting as it prolongs the lifetime of the SRP-RNC association and allows the early complex to reach the target membrane without premature loss of RNC to the cytosol. However, it poses a significant challenge for subsequent release of the cargo to the translocon. To weaken this interaction, the early complex rearranges to the closed conformational state in which the affinity of SRP for RNC becomes ~ 3 nM. In the closed complex, SRP is in the cargo-releasing mode. Importantly, while RNC overall increases the rate of the closed complex ~ 100-fold, it slows the early→closed rearrangement, thus making the handover to the translocation channel unfavorable (Zhang, 2009). Further, RNC inhibits the formation of the activated complex indicated by ~8-fold reduction of the rate of GTP hydrolysis (Zhang, 2009). While GTP hydrolysis per se is not

required for the transfer of RNC to SecYEG, formation of the activated complex is critical for the handover (Shan, 2007). Such effect of RNC is intriguing. By favoring the early and disfavoring the late conformational states, RNC increases the chances of the targeting complex of reaching the target membrane, but makes the subsequent handover unfavorable. The effects of RNC alone, therefore, are insufficient to explain the efficient and timely manner in which the targeting reaction takes place.

The solution to this seemingly puzzling observation may be in the role of other regulatory factors in the SRP pathway that perhaps counteract the effect of RNC in a spatially and temporally controlled manner. The analysis of the effect of RNC on the FtsY•SRP complex described above was carried out in the absence of other potential biological cues, the lipid bilayer of the target membrane and the protein-conducting channel (Zhang, 2010, 2009, 2008). To fully explore how the GTPase cycle of the targeting complex is coupled to the efficient delivery of the cargo protein to the translocation channel, we examined the role of the target membrane itself by separately analyzing the contribution of the phospholipid bilayer and SecYEG on the SRP-mediated protein targeting pathway.

The first chapter of this thesis describes a thorough characterization of the effect of synthetic lipid vesicles, resembling the lipid composition of the *E. coli* inner membrane, on the SRP pathway. Earlier studies had shown that FtsY interacts with and is stimulated by anionic phospholipids (de Leeuw, 2000). However, for a long time, the physiological role of this interaction or its possible regulatory effects on cotranslational protein targeting remained unclear. Using a variety of biochemical and biophysical assays, we show that anionic phospholipids pre-organize FtsY into an active conformation, thus favoring the late conformational states of the targeting complex and facilitating the handover of RNC to SecYEG

(Lam, 2010). Unlike the FtsY•SRP complex formed in the cytosol, the targeting complex formed at the membrane is not likely to be trapped in the early intermediate since the lipid bilayer favors the closed/activated conformation of FtsY. The results of our studies further suggest that the fraction of the closed complex that forms in the cytosol as a result of an unfavorable rearrangement from the early intermediate is partitioned to the membrane due to its higher affinity for the lipid bilayer. Therefore, regardless of the route via which the targeting complex is formed, at the membrane or in the cytosol, the phospholipid bilayer makes the targeting reaction more efficient.

The effect of phospholipids alone, however, is insufficient to explain the efficient handover of RNC to SecYEG. While phospholipids favor the late conformational states of the targeting complex priming it for unloading its cargo, they do not remove the inhibitory effect of RNC on GTP hydrolysis (Figure 6). As mentioned earlier, formation of the activated conformational state is critical for the handoff of RNC to the translocation channel and completion of the targeting reaction. In the second chapter, we test the hypothesis that the trigger activating the targeting complex is provided by the translocation channel itself. We show that SecYEG solubilized in detergent and devoid of lipids and other protein factors is capable of removing the inhibitory effect of RNC on activation of the targeting complex and driving the cotranslational targeting reaction to completion (Akopian, 2013; Shen, 2012). We further explain the mechanism whereby this effect of SecYEG is achieved and propose an on-pathway SecYEG•FtsY•SRP•RNC transfer intermediate (Akopian 2013; Shen, 2012). Combined with previous observations, the results described in this chapter allow us to provide a high-resolution molecular picture of how the three biological cues – RNC, phospholipids, and SecYEG – sequentially regulate cotranslational protein targeting by modulating the conformation and

activity of the targeting complex, resulting in highly efficient delivery and transfer of RNC to SecYEG (Figure 7).

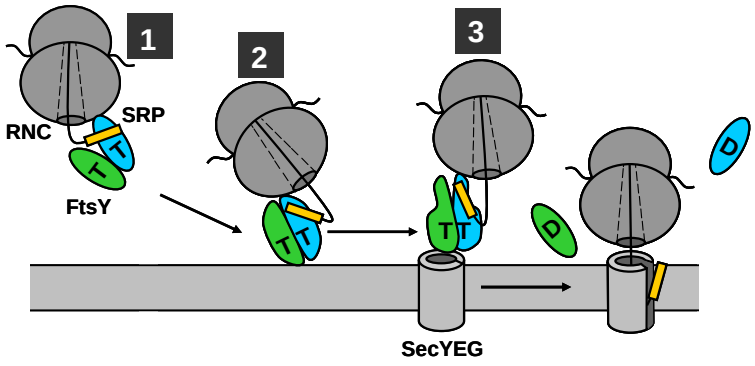

Figure 7. Coordinated action of RNC, phospholipid bilayer, and SecYEG temporally and spatially regulates SRP-mediated protein targeting. The boxed numbers indicate when in the pathway the three biological cues exert their effect on the targeting complex. See text below for description of the figure.

In the cytosol, RNC stabilizes the early complex and prevents its activation, prolonging its lifetime and thus increasing the time window for delivery of the complex to the target membrane without premature dissociation of the cargo (Figure 7, stage 1). The target membrane acts as a critical spatial cue that facilitates the rearrangement of the complex to the closed conformational state, weakening the affinity of SRP for RNC and priming the complex for unloading its cargo (Figure 7, stage 2). The final spatial cue is provided by SecYEG; it triggers the formation of the activated complex from which the handover of the cargo takes place (Figure 7, stage 3). Thus, the coordinated action of RNC, phospholipids, and SecYEG on the targeting complex ensures both efficient binding and efficient release of the cargo in the SRP pathway.

The handover of RNC from the targeting to the translocation machinery at the inner membrane is the least-understood step in the cotranslational protein targeting pathway. SRP and SecYEG bind the translating ribosome in a mutually exclusive manner as both form contacts with the nascent chain and the L23 protein at the ribosomal tunnel exit site (Fraunfeld, 2011; Menetret, 2007, 2000; Plath, 1998). Thus, in order to be transferred to SecYEG, RNC must first be released from the targeting complex, raising a question as to how the loss of the cargo from

the target membrane is avoided. The third chapter focuses on the detailed molecular mechanism of the transfer step using RNCs site-specifically labeled with a fluorescent probe, coumarin (Saraogi, 2011). Using a combination of FRET probes on RNC and SRP, as well as environmental sensitivity of coumarin-labeled RNCs to detergent-solubilized SecYEG, we show that the handoff of RNC takes place in a stepwise manner, with gradual dissolution of the contacts with SRP and formation of the contacts with SecYEG (Saraogi, 2014). The results in this chapter explain how the cargo loss from the target membrane is minimized during the transfer reaction. In addition to providing the insight into the final step of the SRP-pathway, we for the first time follow the fluorescently-labeled RNC in the pathway from the formation of the SRP•RNC complex to the final transfer of RNC to SecYEG and generate a detailed molecular picture of the SRP pathway.

The result of the cargo handover to SecYEG is formation of a stable SecYEG•RNC complex in which SecYEG interacts both with the large ribosomal subunit and the signal peptide or a TM (Fraunfeld, 2011; Becker, 2009; Menetret, 2007, 2000; Cheng, 2005; Raden, 2000; Plath 1998; Beckmann 1997). The latter contact involves association of the hydrophobic signal peptide (in the case of a secretory protein) or a TM (in the case of a nascent membrane protein) with a so-called lateral gate of SecYEG constituted by two of its hydrophobic α-helices, TM2a and TM7, (Driessen, 2008; van den Berg, 2004; Plath, 1998). The lateral gate acts as an important checkpoint distinguishing proteins destined for secretion/membrane integration from cytosolic proteins (du Plessis, 2009; Driessen, 2008; Rapoport, 2007; van den Berg, 2004; Flower, 1994; Derman, 1993). The early stages of this interaction remain unclear. Further, the dynamic changes undergone by the signal peptide or a TM as the nascent chain is elongated during translation have not been explored. In the fourth chapter, we describe a system to examine

the role of the nascent chain length and the signal peptide identity in SecYEG-RNC interaction. We use a highly sensitive FRET assay between RNC and SecYEG to map the orientation of the signal peptide in SecYEG and explore how the conformation of the signal peptide varies with its identity and the length of the nascent chain. The role that the nascent chain length plays in the affinity of RNC for SecYEG is also examined. The results of our studies suggest that SecYEG in detergent is capable of discriminating between RNCs bearing nascent chains of different lengths and can interact with a signal peptide in a well-defined Type II orientation. These studies, although preliminary, provide assays for exploring SecYEG-RNC interaction and lay the foundation for future investigation.

In vivo, SecYEG is a part of a holotranslocon complex that includes, among other membrane proteins, a novel insertase/foldase YidC (Schulze, 2014; Dalbey, 2014; Nouwen, 2002). The role of YidC in membrane protein biogenesis is only now beginning to emerge. A growing body of evidence suggests that YidC may cooperate with SecYEG to ensure proper biogenesis of a nascent membrane protein (Dalbey, 2014; Wagner, 2008; Facey, 2007; Yi, 2004). The last part of the fourth chapter examines the effect of YidC on the conformation of the signal peptide in SecYEG with an attempt to find how early in SecYEG-RNC interaction the role of YidC becomes important, and what features of the signal peptide/TM determine YidC-dependence. Taken together, the results described in this chapter provide insights into the early stages of translocation/membrane protein biogenesis and suggest further studies towards understanding SecYEG-signal peptide interaction and the role of YidC in it.

The chapter is concluded with a description of a cotranslational protein targeting assay involving SecYEG/YidC proteoliposomes.

References

Akopian, D., K. Dalal, K. Shen, F. Duong, Shan, S.-o. 2013. SecYEG activates GTPases to drive the completion of cotranslational protein targeting. *J. Cell Biol.* **200**, 397-405.

Akopian, D., Shen, K., Zhang, X., Shan, S.-o. 2013. Signal recognition particle: an essential protein-targeting machine. *Annu. Rev. Biochem.* **82**, 693-721.

Angelini, S., Boy, D., Schiltz, E., Koch, H. 2006. Membrane binding of the bacterial signal recognition particle receptor involves two distinct binding sites. *J. Cell Biol.* **174**, 715-724.

Angelini, S., Deitermann, S., Koch, H. 2005. FtsY, the bacterial signal-recognition particle receptor, interacts functionally and physically with the SecYEG translocon. *EMBO Rep.* **6**, 476-481.

Ataide, S.F., Schmitz, N., Shen, K., Ke, A., Shan, S.-o., Doudna, J.A., Ban, N. 2011. The crystal structure of the signal recognition particle in complex with its receptor. *Science* **331**, 881-886.

Becker, T., Bhushan, S., Jarasch, A., Armache, J., Funes, S., Jossinet, F., Gumbart, J., Mielke, T., Berninghausen, O., Schulten, K., Westhof, E., Gilmore, R., Mandon, E.C.,

Beckmann, R. 2009. Structure of monomeric yeast and mammalian Sec61 complexes interacting with the translating ribosome. *Science* **326**, 1369-1373.

Beckman, R., Bubeck, D., Grassucci, R., Penczek, P., Verschoor, A., Blobel, G., Frank, J. 1997. Alignment of conduits for the nascent polypeptide chain in the ribosome-Sec61 complex. *Science* **278**, 2123-2126.

Bradshaw, N., Neher, S.B., Booth, D.S., Walter, P. 2009. Signal sequences activate the catalytic switch of SRP RNA. *Science* **323**, 127-130.

Braig, D., Bar, C., Thumfart, J., Koch, H. 2009. Two cooperating helices constitute the lipid-binding domain of the bacterial SRP receptor. *J. Mol. Biol.* **390**, 401-413.

Brundage, L., Hendrick, J.P., Schiebel, E., Driessen, A.J.M., Wickner, W. 1990. The purified *E. coli* integral membrane protein SecY/E is sufficient for reconstitution of SecA-dependent precursor protein translocation. *Cell* **62**, 649-657.

Chatzi, K.E., Sardis, M.F., Economou, A., Karamanou, S. 2014. SecA-mediated targeting and translocation of secretory proteins. *Biochim. Biophys. Acta* Advance online publication. doi: 10.1016/j.bbamcr.2014.02.014

Cheng, Z., Jiang, Y., Mandon, E.C., Gilmore, R. 2005. Identification of cytoplasmic residues of Sec61p involved in ribosome binding and cotranslational translocation. *J. Cell Biol.* **168**, 67-77.

Connoly, T., Rapiejko, P., Gilmore, R. 1991. Requirement of GTP hydrolysis for dissociation of the signal recognition particle from its receptor. *Science* **252**, 1171-1173.

Cross, B.C.S., Sinning, I., Luirink, J., High, S. 2009. Delivering proteins for export from the cytosol. *Nat. Rev. Mol. Cell. Biol.* **10**, 255-264.

Dalbey, R.E., Kuhn, A., Zhu, L., Kiefer, D. 2014. The membrane insertase YidC. *Biochim. Biophys. Acta* Advance online publication. doi: 10.1016/j.bbamcr.2013.12.022

Derman, A.I., Puziss, J.W., Bassford, Jr. P.J., and J. Beckwith. 1993. A signal sequence is not required for protein export in *prlA* mutants of *Escherichia coli*. *EMBO J.* **12**, 879-888.

de Leeuw, E., te Kaat, K., Moser, C., Menestrina, G., Demel, R., de Kruijff, B., Oudega, B., Luirink, J., Sinning, I. 2000. Anionic phospholipids are involved in membrane association of FtsY and stimulate its GTPase activity. *EMBO J.* **19**, 531-541.

Driessen, A.J.M., Nouwen, N. 2008. Protein translocation across the bacterial cytoplasmic membrane. *Annu. Rev. Biochem.* **77**, 643-667.

du Plessis, D.J., Berrelkamp, G., Nouwen, N., Driessen, A.J. 2009. The lateral gate of SecYEG opens during protein translocation. *J. Biol. Chem.* **284**, 15805-15814.

Egea, P.F., Shan, S.-o., Napetschnig, J., Savage, D.F., Walter, P., Sroud, R.M. 2004. Substrate twinning activates the signal recognition particle and its receptor. *Nature* **427**, 215-221.

Eitan, A., Bibi, E. 2004. The core *Escherichia coli* signal recognition particle receptor contains only the N and G domains of FtsY. *J. Bacteriol.* **186**, 2492-2494.

Estrozi, L.F., Boehringer, D., Shan, S.-o., Ban, N., Schaffitzel, C. 2011. Cryo-EM structure of the *E. coli* translating ribosome in complex with SRP and its receptor. *Nat. Struct. Mol. Biol.* **18**, 88-90.

Facey, S.J., Neugebauer, S.A., Krauss, S., and A. Kuhn. 2007. The mechanosensitive channel protein MscL is targeted by the SRP to the novel YidC membrane insertion pathway of *Escherichia coli*. *J. Mol. Biol.* **365**, 995-1004.

Flower, A.M., Doebele, R.C., and T.J. Silhavy. 1994. PrlA and PrlG suppressors reduce the requirement for signal sequence recognition. *J. Bacteriol*. **176**, 5607-5614.

Focia, P.J., Shepotinovskaya, I.V., Seidler, J.A., Freyman, D.M. 2004. Heterodimeric GTPase core of the SRP targeting complex. *Science* **303**, 373-377.

Fraunfeld, J., Gumbart, J., Sluis, E.O., Funes, S., Gartmann, M., Beatrix, B., Mielke, T., Berninghausen, O., Becker, T., Schulten, K., Beckmann, R. 2011. Cryo-EM structure of the ribosome-SecYE complex in the membrane environment. *Nat. Struct. Mol. Biol.* **18**, 614-621.

Freyman, D.M., Keenan, R.J., Stroud, R.M., Walter, P. 1997. Structure of the conserved GTPase domain of the signal recognition particle. *Nature* **385**, 361-364.

Gilmore, R., Walter, P., Blobel, G. 1982. Protein translocation across the endoplasmic reticulum. II. Isolation and characterization of the signal recognition particle receptor. *J. Cell Biol.* **9**5, 470-477.

Gorlich, D., Prehn, S., Hartmann, E., Kalies, K., Rapoport, T.A. 1992. A mammalian homolog of Sec61 and SecYp is associated with ribosomes and nascent polypeptides during translocation. *Cell* **71**, 489-503.

Hainzl, T., Huang, S., Merilainen, G., Brannstrom, K., Sauer-Eriksson, A.E. 2011. Structural basis of signal-sequence recognition by the signal recognition particle. *Nat. Struct. Mol. Biol.* **18**, 389-391.

Hanada, M., Nishiyama, K., Mizushima, S., Tokuda, H. 1994. Reconstitution of an efficient protein translocation machinery comprising SecA and the three membrane proteins, SecY, SecE, and SecG (p12)*. *J. Biol. Chem.* **269**, 23625-23631.

Hartl, F., Lecker, S., Schiebel, E., Hendrick, J.P., Wickner, W. 1990. The binding cascade of SecB to SecA to SecY/E mediates preprotein targeting to the *E. coli* plasma membrane. *Cell* **63**, 269-279.

Janda, C.Y., Li, J., Oubridge, C., Hernandez, H., Robinson, C.V., Nagai, K. 2010. Recognition of a signal peptide by the signal recognition particle. *Nature* **465**, 507-510.

Kudva, R., Denks, K., Kuhn, P., Vogt, A., Muller, M., Koch, HG. 2013. Protein translocation across the inner membrane of Gram-negative bacteria: the Sec and Tat dependent protein transport pathways. *Res. Microbiol.* **164**, 505-534.

Lam, V.R., Akopian, D., Rome, M., Henningsen, D., Shan, S.-o. 2010. Lipid activation of the signal recognition particle receptor provides spatial coordination of protein targeting. *J. Cell Biol.* **190**, 623-635.

Lee, C., Beckwith, J. 1986. Cotranslational and posttranslational protein translocation in prokaryotic systems. *Annu. Rev. Cell Biol.* **2**, 315-336.

Luirink, J., ten Hagen-Jongman, C.M., van der Weijden, C.C., Oudega, B., High, S., Dobberstein, B., Kusters, R. 1994. An alternative protein targeting pathway in *Escherichia coli*: studies on the role of FtsY. *EMBO J.* **13**, 2289-2296.

Menetret, J., Neuhof, A., Morgan, D.G., Plath, K., Rademacher, M., Rapoport, T.A., Akey, C.W. 2000. The structure of ribosome-channel complexes engaged in protein translocation. *Mol. Cell* **6**, 1219-1232.

Menetret, J., Schaletzky, J., Clemons, Jr.W.M., Osborne, A.R., Skanland, S.S., Denison, C., Gygi, S.P., Kirkpatrick, D.S., Park, E., Ludtke, S.J., Rapoport, T.A., Akey, C.W. 2007. Ribosome binding of a single copy of the SecY compex: implications for protein translocation. *Mol. Cell* **28**, 1083-1092.

Miller, E.A., Schekman, R. 2013. COPII – a flexible vesicle formation system. *Curr. Opin. Cell Biol.* **25**, 1-8.

Montoya, G., Svensson, C., Luirink, J., Sinning, I. 1997a. Expression, crystallization and preliminary x-ray diffraction study of FtsY, the docking protein of the signal recognition particle of *E. coli*. *PROTEINS: Structure, Function, and Genetics* **28**, 285-288.

Montoya, G., Svensson, C., Luirink, J., Sinning, I. 1997b. Crystal structure of the NG domain from the signal-recognition particle receptor FtsY. *Nature* **385**, 365-368.

Neher, S.B., Bradshaw, N., Floor, S.N., Gross, J.D., Walter, P. 2008. SRP RNA controls a conformational switch regulating the SRP-SRP receptor interaction. *Nat. Struct. Mol. Biol*. **15**, 916-923.

Nouwen, N. and A.J. Driessen. 2002. SecDFyajC forms a heterotetrameric complex with YidC. *Mol. Microbiol.* **44**, 1397-1405.

Parlitz, R., Eitan, A., Stjepanovic, G., Bahari, L., Bange, G., Bibi, E., Sinning, I. 2007. *Escherichia coli* signal recognition particle receptor FtsY contains an essential and autonomous membrane-binding amphipathic helix. *J. Biol. Chem.* **282**, 32176-32184.

Peluso, P., Herschlag, D., Nock, S., Freyman, D.M., Johnson, A.E., Walter, P. 2000. Role of 4.5S RNA in assembly of the bacterial signal recognition particle with its receptor. *Science* **288**, 1640-1643.

Peluso, P., Shan, S., Nock, S., Herschlag, D., Walter, P. 2001. Role of SRP RNA in the GTPase cycles of Ffh and FtsY. *Biochemistry* **40**, 15224-15233.

Plath, K., Mothes, W., Wilkinson, B.M., Stirling, C.J., Rapoport, T.A. 1998. Signal sequence recognition in posttranslational protein transport across the yeast ER membrane. *Cell* **94**, 795-807.

Pool, M.R., 2005. Signal recognition particles in chloroplasts, bacteria, yeast and mammals. *Mol. Membr. Biol.* **22**, 3-15.

Pool, M.R., Stumm, J., Fulga, T.A., Sinning, I., Dobberstein. 2002. Distinct modes of signal recognition particle interaction with the ribosome. *Science* **297**, 1345-1348.

Poritz, M.A., Bernstein, H.D., Strub, K., Zopf, D., Wilhelm, H., Walter, P. 1990. An *E. coli* ribonucleoprotein containing 4.5S RNA resembles mammalian signal recognition particles. *Science* **250**, 1111-1117.

Raden, D., Song, W., Gilmore, R. 2000. Role of cytoplasmic segments of Sec61α in the ribosome-binding and translocation-promoting activities of the Sec61 complex. *J. Cell Biol.* **150**, 53-64.

Rapoport, T.A. 2007. Protein translocation across the eukaryotic endoplasmic reticulum and bacterial plasma membranes. *Nature* **450**, 663-669.

Saraogi, I., Akopian, D., Shan, S.-o. 2014. Regulation of cargo recognition, commitment, unloading drives cotranslational protein targeting. *J. Cell Biol*. In press

Saraogi, I., Shan, S.-o. 2013. Co-translational protein targeting to the bacterial membrane. *Biochim. Biophys. Acta* Advance online publication. doi: 10.1016/j.bbamcr.2013.10.013.

Saraogi, I., Zhang, D., Chandrasekaran, S., and Shan, S.-o. 2011. Site-specific fluorescent labeling of nascent proteins on the translating ribosome. *J. Am. Chem. Soc*. **133**, 14936-14939.

Schaffitzel, C., Oswald, M., Berger, I., Ishikawa, T., Abrahams, J.P., Koerten, H.K., Koning, R.I., Ban, N. 2006. Structure of the *E. coli* signal recognition particle bound to a translating ribosome. *Nature* **444**, 503-506.

Schulze, R.J., Komar, J., Botte, M., Allen, W.J., Whitehouse, S., Gold, V.A., Lycklama A Nijeholt, J.A., Huard, K., Berger, I., Schaffitzel, C., Collinson, I. 2014. Membrane protein insertion and proton-force-dependent secretion through the bacterial holo-translocon SecYEG-SecDF-YajC-YidC. *Proc. Natl. Acad. Sci. USA* Advance online publication. doi/10.1073/pnas/1315901111

Shan, S.-o., Chandrasekar, S., Walter, P. 2007. Conformational changes in the GTPase modules of the signal recognition particle and its receptor drive initiation of protein translocation. *J. Cell Biol.* **178**, 611-620.

Shan, S.-o., Schmid, S.L., Zhang, X. 2009. Signal recognition particle (SRP) and SRP receptor: a new paradigm for multistate regulatory GTPases. *Biochemistry* **48**, 6696-6704.

Shan, S.-o., Stroud, R.M., Walter, P. 2004. Mechanism of association and reciprocal activation of two GTPases. *PLOS Biology* **2**, 1572-1581.

Shan, S.-o., Walter, P. 2003. Induced nucleotide specificity in a GTPase. *Proc. Natl. Acad. Sci. USA* **100**, 4480-4485.

Shao, S., Hegde, R.S. 2011. Membrane protein insertion at the endoplasmic reticulum. *Rev. Cell Dev. Biol.* **27**, 25-56.

Shen, K., Arslan, S., Akopian, D., Ha. T., Shan, S.-o. 2012. Activated GTPase movement on an RNA scaffold drives co-translational protein targeting. *Nature* **492**, 271-275.

Ullers, R.S., Houben, E.N.G, Raine, A., ten Hagen-Jongman, C.M., Ehrenberg, M., Brunner, J., Oudega, B., Harms, N., Luirink, J. 2003. Interplay of signal recognition particle and trigger factor at L23 near the nascent chain exit site on the *Escherichia coli* ribosome. *J. Cell Biol.* **161**, 679-684.

van den Berg, B., Clemons, Jr. W.M., Collinson, I., Hartmann, E., Harrison, S.C., Rapoport, T.A. 2004. X-ray structure of a protein-conducting channel. *Nature* **427**, 36-44.

Voigts-Hoffman, F., Schmitz, N., Shen, K., Shan, S.-o., Ataide, S.F., Ban, N. 2013. The structural basis of FtsY recruitment and GTPase activation by SRP RNA. Mol. *Cell* **52**, 643-654.

Wagner, S., Pop, O.I., Haan, G.J., Baars, L., Koningstein, G., Klepsch, M.M., Genevaux, P., Luirink, J., and J.W. de Gier. 2008. Biogenesis of MalF and the MalFGK2 maltose transport complex in *Escherichia coli* requires YidC. *J. Biol. Chem*. **283**, 17881-17890.

Walter, P., Blobel, G. 1980. Purification of a membrane-associated complex required for protein translocation across the endoplasmic reticulum. *Proc. Natl. Acad. Sci. USA* **77**, 7112-7116.

Walter, P., Blobel, G. 1981. Translocation of protein across the endoplasmic reticulum. III. Signal recognition particle (SRP) causes signal sequence-dependent and site-specific arrest of chain elongation that is released by microsomal membranes. *J. Cell Biol*. **91**, 545-550.

Wang, S., Kaufman, R.J. 2012. The impact of the unfolded protein response on human disease. *J. Cell Biol.* **197**, 857-867.

Weiche, B., Burk, J., Angelini, S., Schiltz, E., Thumfart, J.O., Koch, H.G. 2008. A cleavable N-terminal membrane anchor is involved in membrane binding of the *Escherichia coli* SRP receptor. *J. Mol. Biol.* **377**, 761-773.

Yi. L., Celebi, N., Chen, M., and R.E. Dalbey. 2004. Sec/SRP requirement and energetics of membrane insertion of subunits a, b, and c of the *Escherichia coli* F_1F_0 ATP synthase. *J. Biol. Chem*. **279**, 39260-39267.

Zanetti, G., Pahuja, K.B., Studer, S., Shim, S., Schekman, R. 2012. COPII and the regulation of protein sorting in mammals. *Nat. Cell Biol.* **14**, 20-28.

Zhang, X., Schaffitzel, C., Ban, N., Shan, S.-o. 2009. Multiple conformational switches in a GTPase complex control cotranslational protein targeting. *Proc. Natl. Acad. Sci. USA* **106**, 1754-1759.

Zhang, X., Kung, S., Shan, S.-o. 2008. Demonstration of a multistep mechanism for assembly of the SRP•SR receptor complex: implications for the catalytic role of SRP RNA. *J. Mol. Biol.* **381**, 581-593.

Zhang, X., Lam, V.Q., Mou, Y., Kimura, T., Chung, J., Chandrasekar, S., Winkler, J.R., Mayo, S.L., Shan, S.-o. 2011. Direct visualization reveals dynamics of a transient intermediate during protein assembly. *Proc. Natl. Acad. Sci. USA* **108**, 6450-6455.

Zhang, X., Rashid, R., Wang, K. Shan, S.-o. 2010. Sequential checkpoints govern substrate selection during cotranslational protein targeting. *Science* **328**, 757-760.

Zopf, D., Bernstein, H.D., Johnson, A.E., Walter, P. 1990. The methionine-rich domain of the 54 kd protein subunit of the signal recognition particle contains an RNA binding site and can be crosslinked to a signal sequence. *EMBO J.* **9**, 4511-4517.

CHAPTER 1

Lipid Acivation of the Signal Recognition Particle Receptor Provides Spatial Coordination of Protein Targeting

This chapter has been published as:

*Lam, V., *Akopian, D., *Rome, M., Henningsen, D., Shan, SO. 2010. Journal of Cell Biology 190, 623. (*equal contribution).

Abstract

The Signal Recognition Particle (SRP) and SRP receptor comprise the major cellular machinery that mediates the co-translational targeting of proteins to cellular membranes. It remains unclear how the delivery of cargos to the target membrane is spatially coordinated. We show here that phospholipid binding drives important conformational rearrangements that activate the bacterial SRP receptor FtsY and the SRP•FtsY complex. This leads to accelerated SRP-FtsY complex assembly, and allows the SRP•FtsY complex to more efficiently unload cargo proteins. Likewise, formation of an active SRP•FtsY GTPase complex exposes FtsY's lipid binding helix and enables stable membrane association of the targeting complex. Thus, membrane binding, complex assembly with SRP, and cargo unloading are inextricably linked to each other via conformational changes in FtsY. These allosteric communications allow the membrane delivery of cargo proteins to be efficiently coupled to their subsequent unloading and translocation, thus providing spatial coordination during protein targeting.

Introduction

Co-translational protein targeting by the Signal Recognition Particle (SRP) is an evolutionarily conserved and essential pathway that mediates the localization of many membrane and secretory proteins to the eukaryotic endoplasmic reticulum, or the bacterial plasma membrane (Cross, 2009; Walter, 1994). As in other important cellular pathways, protein targeting is a complex process that requires exquisite spatial and temporal coordination. Targeting begins when SRP recognizes its cargo, ribosome-nascent chain complexes (RNC) carrying signal sequences that specify the cellular destination of the cargo protein (Pool, 2002; Walter, 1981). Cargo loading on the SRP triggers efficient complex assembly between the SRP and SRP receptor (SR) (Bradshaw, 2009; Zhang, 2009), and membrane localization of SR allows the cargo to be delivered to the target membrane. There, the SRP switches to a cargo-releasing mode and unloads the RNC to the protein translocation machinery, where the nascent polypeptide is either integrated into the membrane or translocated across the membrane to enter the secretory pathway (Rapoport, 2007; Simon, 1991).

Protein targeting is controlled by GTP-regulated dimerization between the SRP and SR. Both proteins contain a GTPase G-domain and a helical N-domain (Freymann, 2000), which together form a structural and functional unit called the NG-domain that mediates the interaction between SRP and SR (Egea, 2004; Focia, 2004; Montoya, 1997a). Previous work showed that the SRP-SR interaction is a highly dynamic process involving at least three discrete conformational stages (Shan, 2009; Shan, 2004; Zhang, 2008). Both GTPases by themselves are in an *open* conformation that exhibits low basal GTPase activity and is suboptimal for binding one another. In this state, they quickly associate to form a transient *early* intermediate independently of GTP (Zhang, 2008). This intermediate is characterized by loose interactions

between the two GTPases, but binds RNC with high affinity (Zhang, 2009). To unload the cargo and complete protein targeting, the *early* intermediate needs to undergo a series of GTP-dependent rearrangements to the more stable *closed* and *activated* conformations. Rearrangement to the *closed* complex involves readjustments at the N-G domain interface, so that the N-domains of both GTPases approach one another and form interface contacts that stabilize the heterodimer (Egea, 2004; Focia, 2004; Shan, 2004). A subsequent rearrangement of the catalytic loops positions multiple catalytic residues with respect to GTP, giving an *activated* complex that efficiently hydrolyzes GTP (Egea, 2004; Focia, 2004; Shan, 2004). Both of these rearrangements are essential for switching the SRP from a cargo-binding to a cargo-releasing mode, enabling the efficient unloading of cargo and initiation of protein translocation (Halic, 2006; Shan, 2007; Zhang, 2009). At the end of the targeting reaction, GTP hydrolysis from the *activated* complex drives the disassembly and recycling of SRP and SR (Connolly, 1991).

Intriguingly, cargo stabilizes the SRP•SR GTPase complex in the *early* conformational stage and disfavors its rearrangement into the *closed* and *activated* complexes (Zhang, 2009). In the absence of the target membrane, this could allow the SRP•SR complex to retain its cargo and prevent premature GTP hydrolysis, thus avoiding abortive targeting reactions. However, as described above, to complete the targeting reaction, the effect from cargo needs to be overcome to allow the GTPase complex to rearrange to its subsequent conformational states. Interaction of the SR with the target membrane provides an attractive molecular trigger to induce these rearrangements, thus driving the cargo handover and GTPase recycling events during late stages of protein targeting.

Eukaryotic SR is a heterodimeric complex comprised of the α and β subunits. SRα is a soluble protein, but it contains an X-domain that allows it to dimerize with SRβ, an integral

membrane protein, thus localizing the SRP receptor to the ER membrane (Schwartz, 2003). The bacterial SRP receptor is a single protein FtsY highly homologous to SRα, except that FtsY does not contain a transmembrane domain. Instead, FtsY is localized to the membrane through an N-terminal A-domain. An amphiphilic α-helix at the junction of the A- and N-domains provides an important lipid-binding motif (Parlitz, 2007). This helix is formed primarily by residues at the N-terminus of the N-domain (197–207), but α-helix formation requires Phe196 from the A-domain (Parlitz, 2007). Hence, a FtsY-NG+1 construct, in which only Phe196 from the A-domain was retained, exhibited lipid-binding activity (Parlitz, 2007) and could complement FtsY depletion *in vivo* (Eitan, 2004). Another amphiphilic helix at the N-terminus of the A-domain also contributes to lipid binding of FtsY (Weiche, 2008). Finally, FtsY also binds the SecYEG translocation machinery, which provides another membrane attachment for FtsY (Angelini, 2006; Angelini, 2005).

Although multiple membrane binding motifs have been identified, FtsY does not bind membrane as tightly as an integral membrane protein. In early cell fractionation studies, a substantial amount of FtsY was found in the cytosol (Luirink, 1994). A more recent microscopy study suggested that the amount of FtsY localized to the membrane is more substantial than previously suggested from fractionation studies, presumably because FtsY easily dissociated from the membrane during cell fractionation (Mircheva, 2009). In another fluorescence microscopy study in *Bacillus subtilis,* on the other hand, ~60% of FtsY was found in the cytosol (Rubio, 2005). Further, only a small fraction of FtsY associates with membranes in biochemical assays ((Parlitz, 2007) and results herein), suggesting that lipid binding of FtsY by itself is fairly weak. Together, these observations suggest that the association of FtsY with membrane is much more dynamic compared to that of integral membrane proteins.

Despite the progress towards understanding how FtsY binds the membrane, the molecular mechanisms by which membranes regulate FtsY's activity to ensure productive and efficient protein targeting remain to be elucidated. Many intriguing questions remain: How is the membrane localization of FtsY productively coupled to the protein targeting reaction? Can FtsY's GTPase cycle and its GTP-dependent interaction cycle with the SRP be regulated by the membrane to spatially coordinate protein targeting? Conversely, can FtsY's membrane binding activity be regulated by its unique GTPase cycles? Previous studies suggested that this could be the case. FtsY's basal GTPase reaction was stimulated by liposomes (de Leeuw, 2000), and studies of both the *E. coli* and chloroplast FtsY detected a ~two-fold lipid-stimulation of the GTPase reaction when both SRP and FtsY are present (Bahari, 2007; Marty, 2009). Nevertheless, a complete and rigorous mechanistic dissection of the functional consequences of FtsY's lipid binding on its conformational changes and its interactions with the SRP remains to be carried out, and the broader relationship between FtsY's lipid binding and the protein targeting reaction remains to be addressed.

Here, we show that interaction with phospholipids regulates multiple biochemical activities of FtsY, and drives the rearrangement of FtsY and the SRP•FtsY complex to the *activated* conformation. Reciprocally, formation of a stable and active SRP•FtsY complex exposes FtsY's lipid-binding motif and allows much stronger association with the membrane. These results demonstrate that the GTPase cycle of FtsY and the SRP•FtsY complex can be allosterically regulated in response to spatial cues such as membrane binding, and these allosteric regulations allow the targeting of cargo proteins to be efficiently coupled to their unloading and translocation.

Results

Phospholipids stimulate the basal GTPase activity of FtsY

Previous work showed that liposomes derived from a phospholipid mixture composed of 70% phosphatidylglycerol (PG) and 30% phosphatidylethanolamine (PE) stimulated the basal GTPase reaction of FtsY over 10^2-fold, whereas the NG-domain of FtsY (FtsY-NG) was stimulated to a much lesser extent (de Leeuw, 2000). These results were recapitulated in our experiments (Fig. 1A and supplementary Fig. 1). Further, quantitative analysis of the lipid concentration dependence of this stimulation provided additional insights. First, the lipid stimulation curve was cooperative, with a Hill coefficient of 2.9 (Fig. 1A, red), suggesting that the action of at least three lipid molecules is required for this stimulation, and that lipids induce conformational rearrangements in FtsY such that binding of the first lipid molecule enables stronger binding of additional lipid molecules. Second, the interaction of free FtsY with lipids is fairly weak, requiring a high concentration of liposomes (>3 mM) to reach saturation (Fig. 1A, red). Although the lipid concentrations in these experiments did not reflect the situation *in vivo* where the lipid distribution is heterogeneous, the apparent binding constants obtained from these analyses provided an operational measure of the ability of FtsY to bind phospholipids, allowing us to further probe the change in FtsY's lipid binding ability as the reaction components are varied (see below).

Phospholipids accelerate formation of the activated SRP•FtsY complex

Formation of a stable, GTP-dependent SRP•FtsY complex is slow because it requires extensive rearrangements of FtsY from the *open* to the *closed* and *activated* conformations (Shan, 2009; Shan, 2004). To test whether the interaction of FtsY with phospholipids helps

overcome this kinetic barrier, we used a well-established GTPase assay to measure the reciprocally stimulated GTPase reaction between SRP and FtsY. At sub-saturating FtsY concentrations, this assay measures the second-order reaction: ^{GTP}•SRP + FtsY•^{GTP} → products, which is rate-limited by the formation of a stable and active ^{GTP}•SRP•FtsY•^{GTP} complex (Peluso, 2001). This provides a convenient way to test the effect of phospholipids on the rate of stable SRP-FtsY complex assembly. Despite the stimulation of FtsY's basal GTPase activity by lipids, the basal GTPase rate was still significantly slower than that of the stimulated GTPase reaction (compare the Y-axis in Figs. 1A vs. 1B) and did not interfere with the analyses below.

Stable SRP-FtsY complex assembly was strongly stimulated by liposomes, with >100-fold rate acceleration observed at saturating lipid concentrations (Fig. 1B, red). The lipid concentration dependence of this stimulation was complex, with an initial inhibition at lipid concentrations below 0.3 mM followed by a cooperative stimulation at higher lipid concentrations (Fig. 1B, red). The same initial inhibitory effect was also observed with FtsY-NG, but FtsY-NG did not undergo substantial lipid-induced stimulation of complex assembly (Fig. 1B, black). SRP's activity was not significantly stimulated by lipids either (supplementary Fig. 2). Thus, this stimulation is specific to the interaction of lipids with the FtsY A-domain. To isolate this specific effect, we subtracted the liposome effects on the reaction of FtsY-NG from those of full-length FtsY (Fig. 1C, red). This yielded a highly cooperative lipid stimulation curve with a Hill coefficient of 4.4 (Fig. 1C, red), suggesting that the cooperative action of at least four lipid molecules is required to stimulate SRP-FtsY complex assembly.

An important lipid binding motif was identified at the junction between the A- and N-domains of FtsY (Parlitz, 2007), but it was unclear whether the remainder of the A-domain contributes to lipid binding or stimulation. To address this question, we compared the ability of

liposomes to stimulate full-length FtsY and FtsY-NG+1, in which only the lipid-binding helix at the A-N domain junction was retained. Both the basal GTPase activity of FtsY-NG+1 and its complex formation with SRP were strongly stimulated by liposomes (Fig. 1A & B, green). The magnitude of the lipid-stimulation with FtsY-NG+1 was ~two-fold smaller than that with full-length FtsY (Fig. 1A&B, green vs. red), but was still 50–100 fold compared to the rate in the absence of lipids. The lipid-stimulation curves for FtsY-NG+1 were also highly cooperative, giving Hill coefficients of 3.4 and 4.2 in the basal GTPase reaction and in complex assembly with SRP, respectively (Fig. 1A&B, green). Thus, the amphiphilic helix at the A-N domain junction provides the primary site for stimulation of FtsY by phospholipids, and the remainder of the A-domain modulates this effect by two-fold. These findings are consistent with the observation that expression of FtsY-NG+1 complements the defect of FtsY depletion *in vivo* (Eitan, 2004). Further in support of this notion, we performed *in vitro* protein targeting assays and found that FtsY-NG+1 was able to mediate efficient co-translational targeting of a model SRP substrate into membrane vesicles (Fig. 2). The efficiency of translocation was only 26% lower with FtsY-NG+1 than with full length FtsY (Fig. 2).

To provide direct evidence for a lipid-induced acceleration of complex assembly and to more accurately quantify the magnitude of this effect, we used a fluorescent probe, FtsY conjugated with acrylodan at residue C356, to directly measure SRP-FtsY complex formation. This probe monitors the final conformational stage of the SRP•FtsY complex, the *activated* state (Zhang, 2009). The presence of liposomes caused a large increase and a blue shift in the fluorescence emission spectrum of FtsY (Fig. 3A, open black vs. red circles), which was expected, as acrylodan is highly sensitive to changes in solvent polarity. In the presence of liposomes, formation of the SRP•FtsY complex in the presence of a GTP analogue, 5'-

guanylylimido-diphosphate (GppNHp), reduced the fluorescence intensity ~30% and induced a red shift in the emission spectrum of this probe, producing a spectrum that overlaps with that of the SRP•FtsY complex in the absence of liposomes (Fig. 3A, closed red and black circles). Thus, in the absence of liposomes, the increase in fluorescence of acrylodan-labeled FtsY C356 was used to monitor complex formation (Fig. 3A, open vs. closed black circles, and Fig. 3B) whereas in the presence of liposomes, the decrease in fluorescence was used (Fig. 3A, open vs. closed red circles, and Fig. 3C). The rate constant for formation of the *activated* SRP•FtsY complex was 3.0 $\times 10^6$ $M^{-1}s^{-1}$ in the presence of liposomes, 160-fold faster than that in the absence of liposomes (Fig. 3D). This provides direct evidence that phospholipids substantially accelerate formation of a stable and active SRP•FtsY complex.

Phospholipids stabilize the activated conformation of the SRP•FtsY complex

A possible mechanism to account for the stimulatory effects of phospholipids on FtsY's basal GTPase activity and on the kinetics of SRP-FtsY complex assembly is that interaction with phospholipids pre-organizes FtsY into the *closed* and *activated* conformations, which allows some of the unfavorable rearrangements during assembly of a stable, active SRP•FtsY complex to be bypassed. If this were true, then phospholipids should preferentially stabilize formation of the *closed/activated* SRP•FtsY complex. In contrast, the *early* intermediate, in which most of the GTPase rearrangements in FtsY have not taken place (Fig. 6 below and S.S., manuscript in preparation), should not be affected. To test this hypothesis, we determined the effect of phospholipids on the equilibrium stability of the SRP•FtsY complex at various conformational stages.

To measure the stability of the *early* intermediate, we used fluorescence energy transfer (FRET) between coumarin-labeled SRP C235 and BODIPY-fluorescein labeled FtsY C487. FRET allows us to detect early stages of complex formation before any conformational changes take place (Zhang, 2008). The *early* intermediate was isolated by leaving out GTP during complex assembly; this prevents its rearrangement to the subsequent conformational states and allows us to characterize its equilibrium properties. As the *early* intermediate has a weak stability and does not accumulate significantly unless it is stabilized by the cargo (Zhang, 2008; Zhang, 2009), we measured the stability of the *early* intermediate in the presence of the RNC. The RNC•SRP•FtsY *early* intermediate exhibited equilibrium dissociation constants (K_d) of 68 and 104 nM in the absence and presence of liposomes, respectively (Fig. 4A & D). Thus, phospholipids do not stabilize the *early* intermediate, but rather have a small destabilizing effect on this conformational state.

We also used FRET to measure the stability of the GTP-dependent *closed* and *activated* complexes, by carrying out complex assembly in the presence of GppNHp. This drives the rearrangement of the complex into these GTP-dependent conformational states, and the complex thus obtained and monitored by FRET is a mixture of the *closed* and *activated* conformations. In the absence of liposomes, the *closed/activated* complex had a K_d value of 68 nM, and this K_d value lowered to 7.2 nM in the presence of liposomes (Fig. 4B & D). To more specifically monitor the *activated* complex, we used acrylodan-labeled FtsY C356 (Fig. 4C). In the absence of liposomes, the *activated* complex had a K_d value of 145 nM (Fig. 4C, left), whereas in the presence of liposomes, the *activated* complex was much tighter, with an estimated K_d value of 4 nM or lower (Fig. 4C, right, and Fig. 4D), at least 40-fold lower than that in the absence of liposomes. Together, these results provide direct evidence that phospholipids specifically

stabilize the *closed* and *activated* complexes and thus drive the rearrangement of the SRP•FtsY complex from the *early* intermediate to the subsequent, GTP-stabilized conformational states.

FtsY binds more strongly to lipids when it forms an active complex with SRP

If phospholipids preferentially interact with FtsY in the *closed*/*activated* conformations, then formation of the SRP•FtsY complex in the presence of GTP, which drives FtsY into these conformations, would allow FtsY to bind phospholipids more strongly. To test this prediction, we measured FtsY-lipid binding using density gradient flotation (Fig. 5A). Free FtsY bound weakly to liposomes derived from *E. coli* lipids, with <2% FtsY co-fractionating with lipids to the top of the density gradient (Fig. 5A, left). In contrast, with the SRP•FtsY complex formed in the presence of GppNHp, the majority of both FtsY and the SRP protein Ffh co-fractionated with lipids to the top of the gradient (Fig. 5A, right). In contrast, with FtsY-NG that was not stimulated by lipids (Fig. 1), both the free protein and its complex with Ffh remained at the bottom fraction during centrifugation (Fig. 5B). These results, albeit qualitative in nature, directly demonstrated that FtsY binds more strongly to phospholipids when it forms the GTP-dependent *closed*/*activated* complex with SRP.

To provide additional evidence for this model and to more quantitatively determine how much stronger FtsY binds phospholipids upon complex formation with SRP, we determined the effect of lipids on the stimulated GTPase reaction at saturating protein concentrations. Under these conditions, GTP hydrolysis from a stable, active $^{GTP\bullet}$SRP•FtsY$^{\bullet GTP}$ complex (k_{cat}) was monitored. Liposomes accelerated this reaction ~two-fold but have a negligible effect on the reaction of the complex formed by FtsY-NG (Fig. 5C), consistent with previous observations (Bahari, 2007). Importantly, the lipid concentration dependence of this stimulation provided a

means to measure the apparent affinity of lipids to the ^{GTP}•SRP•FtsY•^{GTP} complex, as this complex was the predominant species in this reaction. Saturation could be reached at lipid concentrations above 65 μM for stimulation of the ^{GTP}•SRP•FtsY•^{GTP} complex, at least 50-fold lower than that for free FtsY (cf. Fig. 5C vs. Fig. 1A), demonstrating that formation of an active SRP•FtsY complex strengthens the FtsY-lipid interaction by almost two orders of magnitude.

GTP-dependent complex formation with SRP exposes the lipid binding helix of FtsY

To understand how the allosteric communications between FtsY and phospholipids occur, we probed the structural dynamics of the lipid binding helix at the A-N domain junction using electron paramagnetic resonance (EPR) spectroscopy. Individual residues in and adjacent to the lipid binding motif of FtsY-NG+1 (residues 195–209; Fig. 6A, *coral*), a FtsY construct strongly stimulated by phospholipids (Fig. 1), were replaced by cysteines for site-directed spin labeling with the nitroxide probe (1-oxyl-2,2,5,5,-tetramethyl-3-pyrroline-3-methyl) methanethiosulfonate (MTSSL). Only the sites where the nitroxide substitution did not substantially disrupt the activity of FtsY and its interaction with SRP were examined by EPR (supplementary Table 1). Information about the local mobility of the nitroxide probe at each position can be obtained from two features of the EPR spectra (Hubbell, 2003; Hubbell, 1996; Hustedt, 1999): (i) the line width of the central resonance (Fig. 6B, ΔH_0) and (ii) the overall breadth of the spectra along the magnetic field axis, especially the intensity of hyperfine splitting that arises from highly immobile populations of spin probes relative to the mobile population (Fig. 6B, 'im' vs. 'm').

As exemplified by residue 206, in apo-FtsY, the nitroxide probe exhibited broad EPR spectra with a significant population of immobile molecules and widened central line width (Fig.

6B, black). The extremely low mobility of this probe indicates that residue 206 is engaged in strong tertiary interactions with the remainder of the FtsY molecule. No significant spectral change was observed when FtsY formed an *early* intermediate with SRP in the presence of GDP (Fig. 6B, red). In contrast, the nitroxide probe exhibited significantly higher mobility when FtsY formed the *closed/activated* complex with SRP in the presence of GppNHp, as indicated by substantial reductions in both the central linewidth and the fraction of immobile population (Fig. 6B, green). The same pattern of nitroxide mobility changes was observed for other positions in the lipid binding helix (Fig. 6C & D, and supplementary Fig. 3). In apo-FtsY and in the *early* intermediate, there were significant position-dependent variations in nitroxide mobility (Fig. 6D, black and red), presumably reflecting periodic changes in the position of the probe along the solvent exposed vs. more buried surfaces of the helix. Despite these variations, the nitroxide probes at all of these positions underwent significant increases in mobility upon formation of the GTP-dependent complex (Fig. 6C & D, and supplementary Fig. 3). Together, these results demonstrate substantially reduced tertiary interactions and increased dynamics of FtsY's lipid binding helix upon formation of the *closed/activated* SRP•FtsY complex, and suggest that rearrangement of the GTPase complex to these conformational states disrupts intramolecular interactions of the lipid binding helix with the remainder of FtsY and allows this helix to become more accessible.

Anionic phospholipids specifically bind and stimulate FtsY

The stimulatory effects of lipids on FtsY's various activities described above or previously (de Leeuw, 2000) were primarily obtained with liposomes containing 70% PG and 30% PE. The inner membrane of *E. coli* is composed primarily of PE (~70%), with anionic

phospholipids PG and cardiolipin present at ~20% and ~5%, respectively. To determine whether FtsY has a preference for specific types of phospholipids, we tested the ability of various lipids to stimulate FtsY's basal GTPase reaction and to accelerate stable SRP-FtsY complex assembly. These two activities provided a sensitive and reliable readout for whether FtsY is stimulated by specific types of lipids, and could be conveniently measured with the GTPase assay. Liposomes derived from total *E. coli* lipids stimulated FtsY less efficiently than PG/PE: a higher lipid concentration was required to begin observe a stimulation for both the basal GTPase activity of FtsY and its complex assembly with SRP, and both activities were stimulated less than eight-fold at the highest liposome concentrations tested (Fig. 7A & B). Even less stimulation was observed with liposomes lacking anionic phospholipids (70% PE and 30% PC, Fig. 7C & D). Interestingly, an initial inhibitory effect of lipids was also observed with the *E. coli* and PE/PC liposomes during SRP-FtsY complex assembly with both FtsY and FtsY-NG (Fig. 7B & D), suggesting that this inhibition results from a highly nonspecific interaction of lipids either with SRP or with the FtsY-NG domain.

In contrast, liposomes comprised of anionic phospholipids strongly stimulated both activities of FtsY. Within experimental error, liposomes composed solely of PG stimulated FtsY with the same efficiency as PG/PE liposomes (Fig. 7E & F), suggesting that the PG contained in the PG/PE liposomes was responsible for the stimulations observed in Figures 1–4. Cardiolipin, which contains an additional negatively charged head group compared to PG, stimulated FtsY even more efficiently (Fig 7G & H). Comparison of the lipid concentration dependences of the stimulation indicates that roughly the same magnitude of lipid stimulation could be obtained with both PG and cardiolipin at saturating lipids, but saturation could be reached with cardiolipin at

much lower concentrations (Fig. 7G & H). Thus, FtsY binds more strongly to cardiolipin than to PG, but once bound, these two lipids induce the same amount of stimulation for FtsY.

The reduced stimulation of FtsY by *E. coli* and PE/PC lipids could arise from a weaker binding of FtsY to these lipids than to PG and cardiolipin, or from the inability of these lipids to activate FtsY even when it is membrane-bound. To distinguish between these possibilities, we directly measured the binding of FtsY to phospholipids using surface plasmon resonance (SPR). FtsY with a C-terminal His_6-tag was immobilized on CM5 biosensor chips coupled with anti-His_6 antibodies. Liposomes induced large changes in the surface plasmon resonance (Fig. 8A). The kinetics of lipid binding to or dissociation from FtsY was rapid but complex (Fig. 8A), as would be expected for a cooperative interaction. The resonance signals at 200 sec., when the binding reaction reaches a plateau, were used to monitor the equilibrium for FtsY-liposome binding. The values of K_d obtained from the SPR experiments were, in general, an order of magnitude lower than those observed from enzymatic assays, presumably due to differences between measurements in solution vs. those on a surface. Nevertheless, the following strongly suggest that SPR provides a reasonable comparison of the *relative* interactions of FtsY with different lipids: (i) In all cases, minimal or low lipid binding was observed with FtsY-NG (Figs. 8B-D, black), suggesting that the ability of the FtsY A-domain to interact with lipids was faithfully recapitulated in SPR measurements; (ii) FtsY-NG+1 bound liposomes ~3-fold weaker than full-length FtsY (supplementary Fig. 4), consistent with the two-fold difference observed in solution studies, indicating that the lipid binding helix at the A-N domain junction of FtsY was primarily responsible for lipid binding in SPR experiments; (iii) The FtsY-lipid binding curves were cooperative and exhibited Hill coefficients of 3 – 4 (Fig. 8 and supplementary Fig. 4), also consistent with observations from solution studies. Thus, although the values of K_d obtained

from SPR measurements were lower than those in solution, SPR provided a reasonable and semi-quantitative tool to compare the *relative* binding of FtsY to liposomes with different compositions.

FtsY bound to liposomes comprised of PE and PC weakly, with an apparent K_d value of 0.51 mM (Fig. 8B), whereas it bound PG/PE liposomes ~8-fold stronger (apparent K_d ~ 0.069 mM; Fig. 8C). Liposomes derived from *E. coli* phospholipids were bound by FtsY with an affinity intermediate between the anionic and PE/PC liposomes, presumably because they contain both types of phospholipids (Fig. 8D). The preference of FtsY to bind anionic phospholipids observed here was consistent with previous results using qualitative assays (de Leeuw, 2000). Nevertheless, these differences in binding affinity (~8-fold) were not sufficient to account for the ~100-fold higher activity of FtsY in the presence of PG/PE liposomes compared to PE/PC liposomes. These results suggest that anionic phospholipids not only bind FtsY more strongly, but are also more effective at stimulating the activities of FtsY after binding. Thus, the stimulatory effects of anionic phospholipids on FtsY are multimodal and can regulate bacterial protein targeting along different points in the reaction pathway.

Discussion

In this work, we demonstrate that multiple activities of the bacterial SRP receptor FtsY are allosterically regulated by its interaction with phospholipids, and vice versa. These include: (i) stimulation of FtsY's basal GTPase reaction; (ii) acceleration of stable SRP-FtsY complex assembly; (iii) preferential stabilization of the *closed* and *activated* SRP•FtsY complexes; and (iv) strengthening of FtsY's lipid binding affinity when it forms a stable SRP•FtsY complex. The simplest energetic model to explain these allosteric effects is that lipid binding shifts the conformational equilibrium of FtsY from the *open* to the *closed/activated* states (Fig. 9A). Pre-organization of FtsY towards these states would help bypass the substantial conformational rearrangement during stable complex assembly and thus accelerate the rate of this process (Fig. 7A, $\Delta G^{\ddagger}$, black vs. red). Pre-organization of FtsY also explains the acceleration of FtsY's basal GTPase activity and the specific stabilization of the SRP•FtsY complex in the *closed/activated* states (Fig. 9A, ΔG, black vs. red). Reciprocally, as phospholipids preferentially bind FtsY in the *closed/activated* conformation, FtsY will correspondingly bind phospholipids more strongly when it is driven into these conformational states upon GTP-dependent complex assembly with the SRP.

The ability of FtsY to be allosterically regulated by interaction with phospholipids suggests a simple and effective mechanism to spatially regulate protein targeting. The population of free FtsY molecules that are localized to the membrane (Fig. 9B, step 1) would be pre-organized into the *closed/activated* conformations and thus more efficient at forming a stable, GTP-dependent SRP•FtsY complex (Fig. 9B, step 2). This is consistent with the result from a recent study that suggested that membrane-bound FtsY is more efficient at targeting cargo-bound SRP to the membrane (Mircheva, 2009), and provides a molecular basis to explain

this observation. On the other hand, the population of free FtsY molecules in the cytosol exist primarily in the *open* conformation, in which it quickly forms an *early* targeting intermediate with cargo-bound SRP (Fig. 9B, step 3), but the equilibrium for rearrangement of the cargo•SRP•FtsY complex to the *closed* and *activated* states is not favorable in the cytosol (Zhang, 2009). Nevertheless, the fraction of targeting complexes that is in these late conformational states has a much higher affinity for phospholipids, and thus would preferentially localize to the membrane (Fig. 9B, step 5). In either pathway, the membrane-bound cargo•SRP•FtsY complex would be driven to the *closed/activated* states, in which the interaction between the SRP and the cargo is weakened (Halic, 2006; Zhang, 2009) so that the cargo would be primed for release and transfer to the translocon (Fig. 9B, step 6). Consistent with this model are the observations that PG/PE liposomes could induce significant FtsY-mediated release of SRP from the nascent chain (Scotti, 1999), and that FtsY-NG, which is not allosterically regulated by phospholipids, was compromised at late stages of targeting (Bahari, 2007). Thus the membrane targeting of the cargo can be efficiently coupled to its subsequent unloading and translocation through lipid-induced conformational changes in FtsY.

Although the *activated* state is significantly stabilized by phospholipids, phospholipids stimulate GTP hydrolysis from the SRP•FtsY complex by only two-fold. This effect, though reproducible from different laboratories (Bahari, 2007; Marty, 2009), is rather modest. Moreover, phospholipids did not significantly enhance GTP hydrolysis from the RNC•SRP•FtsY complex (Shan, unpublished results). Thus, phospholipids alone would not be able to completely reverse the inhibitory effect of cargo on the GTPase reaction of the SRP•FtsY complex (Zhang, 2009). Possibly, complete activation of GTP hydrolysis would require additional interaction of

FtsY with the SecYEG translocation machinery, or occurs only after the cargo has been unloaded from the SRP (Fig. 9B, step 6 or 7).

The results here also suggest an attractive model in which the GTPase cycle of SRP and FtsY could regulate the membrane binding of FtsY. Free FtsY and the SRP•FtsY *early* intermediate have weak affinities for and fast dissociation rates from phospholipids (Fig. 9B, step 1). In contrast, the affinity of FtsY for phospholipids increases over 50-fold when it forms the GTP-dependent *closed/activated* complex with SRP, thus enabling more stable association of FtsY with the membrane (Fig. 9B, step 5). After the cargo is unloaded, GTP hydrolysis drives the disassembly of the SRP•FtsY complex. This allows FtsY to go back to the *open* conformation in which its membrane binding becomes more dynamic (Fig. 9B, step 7). Regulation of a protein's membrane binding activity by nucleotide binding/hydrolysis cycles has also been observed for the ATPase MinD (Hu, 2002; Mileykovskaya, 2003). Intriguingly, although the eukaryotic SRP receptor is localized to the ER membrane through the transmembrane domain of SRβ, complex formation between the SRα and β subunits requires SRβ to be bound with GTP, suggesting that the GTPase cycle of SRβ could analogously regulate the association of SRα with the ER membrane (Schwartz, 2003).

What is the molecular mechanism by which phospholipid binding regulates conformational changes in FtsY? Previous work and the results here provided various pieces of clues that together suggest a cohesive model. Formation of a stable SRP•FtsY complex requires the removal of αN1, the first α-helix in the N-domains of Ffh and FtsY, which present steric blocks that would inhibit stable SRP-FtsY binding (Gawronski-Salerno, 2007; Neher, 2008; Shepotinovskaya, 2001). Here, we found that the lipid binding helix is highly restricted in motion and is most likely engaged in strong tertiary interactions in apo-FtsY and in the *early*

intermediate, but becomes substantially more mobile and exposed in the *closed/activated* complexes. We propose that movement of the αN1 helix during the *open* → *closed* rearrangement of FtsY exposes the lipid binding motif that immediately precedes the αN1 helix, thus leading to stronger lipid binding (Fig. 9C). Conversely, lipid binding to this motif would help promote movement of the αN1 helix, thus facilitating the rearrangement of FtsY into the *closed/activated* states and its GTP-dependent complex assembly with SRP (Fig. 9C). Consistent with this model are the observations that truncation of the αN1 helix led to the same phenotypes as those induced by lipid binding of FtsY: increase in FtsY's basal GTPase activity, acceleration of stable complex assembly, and stabilization of the GTP-dependent SRP•FtsY complex (Neher, 2008). The N-terminus of the FtsY N-domain became more protease-susceptible in the SRP•FtsY complex than in free FtsY (Neher, 2008), also supporting the model that the lipid binding motif of FtsY is more accessible in the SRP•FtsY complex. This lipid-induced conformational change of FtsY is also supported by the cooperative behavior of phospholipids observed in both the SPR measurements and biochemical assays. This cooperativity is consistent with a model in which binding of the first lipid molecule shifts the conformational equilibrium of FtsY and helps expose its lipid-binding helix, thus facilitating the binding of additional lipid molecules.

FtsY exhibits a strong preference for anionic phospholipids such as PG and cardiolipin ((de Leeuw, 2000) and this work). This is consistent with the abundance of basic residues on the amphiphilic lipid-binding helix of FtsY, and suggests a critical role of anionic phospholipids in co-translational protein targeting. Anionic phospholipids have also been found to preferentially interact with and stimulate the ATPase MinD that regulates cell division (Mileykovskaya, 2003), the SecA ATPase that drives the post-translational translocation of proteins (Hendrick, 1991;

Lill, 1990), and the integration of membrane proteins in Sec-independent pathways (Ridder, 2001). These biochemical observations are corroborated by *in vivo* experiments that showed that depletion of PG and cardiolipin in *E. coli* leads to severe defects in preprotein translocation, and that these defects can be rescued by restoring anionic phospholipids into membrane vesicles (de Vruje, 1988; Kusters, 1991). As PG and cardiolipin comprise a minor fraction of *E. coli* lipids, how do they stimulate protein function and targeting *in vivo*? Two speculative models could be envisioned. First, biophysical analyses showed that anionic phospholipids and PE are segregated in bacterial membrane with an extremely low extent of mixing, in contrast to model liposomes in which different phospholipids are well mixed (Fishov, 1999; Vanounou, 2003). It is possible that there are sites on *E. coli* membrane enriched in anionic phospholipids where FtsY could preferentially bind and be activated. Alternatively or in addition, the SecYEG machinery associates tightly with anionic phospholipids, cardiolipin and PG (Gold, 2010), which could provide sites for preferential FtsY binding and activation. Regardless of the molecular model, the results of this and previous work emphasize the crucial roles that anionic phospholipids play in the targeting and translocation of proteins across the bacterial inner membrane, and invite additional studies to delineate their precise distributions and mechanisms of action *in vivo*.

Materials and Methods

Material. Ffh, 4.5S RNA, FtsY and FtsY-NG were expressed and purified as described (Montoya, 1997b; Peluso, 2001). The expression plasmid for FtsY-NG+1 was based on pMal-c2X (New England Biosciences), in which the PCR fragment encoding FtsY-NG+1 was inserted between the BamHI and SalI restriction sites. The factor Xa cleavage site in pMal-c2X was replaced with a thrombin cleavage site using the QuikChange protocol (Stratagene). The MBP-fusion protein of FtsY-NG+1 was purified by affinity chromatography using Ni-NTA, digested with thrombin, MBP and uncleaved MBP-fusion proteins were removed using amylose resin (New England Biosciences), and FtsY-NG+1 was further purified by anion exchange chromatography over monoQ (GE Healthcare) using a linear gradient of 50 –300 mM NaCl. Large unilamellar vesicles were freshly prepared prior to each experiment by the extrusion method using 100 nm pore polycarbonate filters, as described previously (de Leeuw, 2000; Parlitz, 2007).

GTPase assay. GTP hydrolysis reactions were carried out in SRP buffer (50 mM KHEPES pH7.5, 150 mM potassium acetate, 1.5 mM magnesium acetate, 0.01 % nikkol, and 2 mM DTT) and were followed and analyzed as described (Peluso, 2001). Prior to initiation of the reaction, the proteins were pre-incubated with liposomes for at least 10 min. Varying this incubation time did not affect the reaction rate constants, suggesting that equilibrium binding between FtsY and liposomes has been reached. Michaelis-Menten analysis of FtsY's basal GTPase reaction was carried out using 0.5 μM FtsY and 2–100 μM GTP doped with γ-^{32}P-GTP. The GTP concentration dependence of the observed rate constants (k_{obsd}) was fit to Eq. 1,

$$k_{obsd} = k_{cat} \times \frac{[GTP]}{K_m + [GTP]} \qquad (1)$$

in which k_{cat} is the rate constant at saturating GTP concentrations, and K_m is the GTP concentration required to reach half-saturation.

The lipid concentration dependence of the basal GTPase reactions of FtsY were measured using 2 – 5 μM FtsY and 100 μM GTP doped with γ-^{32}P-GTP. To measure SRP-FtsY complex assembly rates, stimulated GTPase reactions were carried out at sub-saturating protein concentrations (100 nM SRP, 100–200 nM FtsY) in the presence of saturating GTP (100 μM), so that the second-order reaction: ^{GTP}•SRP + FtsY•^{GTP} → products was followed. To measure the effect of lipids on the GTPase rate of the ^{GTP}•SRP•FtsY•^{GTP} complex, stimulated GTPase reactions were carried out at saturating FtsY concentrations (10–25 μM). Varying the concentration of FtsY in this range did not affect the observed rate constant, confirming that FtsY is saturating and that the first-order reaction: ^{GTP}•SRP•FtsY•^{GTP} → products was followed. The lipid concentration dependences were fit to Eq 2,

$$k_{obsd} = k_0 \times \frac{K_d^n}{K_d^n + [\text{lipid}]^n} + k_1 \times \frac{[\text{lipid}]^n}{K_d^n + [\text{lipid}]^n} \qquad (2)$$

in which k_{obsd} is the observed rate constant, k_0 is the rate constant in the absence of lipids, k_1 is the rate constant at saturating lipid concentrations, n is the Hill coefficient, and K_d is the apparent equilibrium dissociation constant for FtsY-lipid binding. Note that the values of K_d from this analysis are only 'apparent' and do not represent the true binding constants, because FtsY-lipid interaction is cooperative, i.e., binding of the first lipid molecule strengthens the subsequent binding of additional lipid molecules to FtsY. The apparent K_d value from this analysis represents an average of these different lipid binding affinities. For example, if four lipid molecules bind to FtsY with K_d values of $K_{d,1}$, $K_{d,2}$, $K_{d,3}$ and $K_{d,4}$, then apparent $K_d^4 = K_{d,1} \times K_{d,2} \times K_{d,3} \times K_{d,4}$.

Fluorescence measurements. Fluorescence measurements were carried out as described previously (Zhang, 2008; Zhang, 2009). When labeled SRP was used and the concentration of FtsY was varied, equilibrium titrations were fit to eq 3,

$$F_{obsd} = F_1 \times \frac{[\mathrm{SRP}] + [\mathrm{FtsY}] + K_d - \sqrt{([\mathrm{SRP}] + [\mathrm{FtsY}] + K_d)^2 - 4 \times [\mathrm{SRP}][\mathrm{FtsY}]}}{2 \times [\mathrm{SRP}]} \qquad (3)$$

in which F_{obsd} is the observed FRET value or fluorescence change at a particular FtsY concentration, F_1 is the FRET value or fluorescence change at saturating FtsY concentrations, and K_d is the equilibrium dissociation constant of the complex being measured. An analogous quadratic equation was used in cases where the fluorescence of labeled FtsY was monitored and the concentration of SRP was varied, except that the denominator in eq 3 becomes 2×[FtsY].

Observed rate constants for assembly of the *activated* SRP•FtsY complex (k_{obsd}) were measured at varying SRP concentrations using a kintek stopped-flow apparatus. The SRP concentration dependence of k_{obsd} was fit to eq 4,

$$k_{obsd} = k_{on}\,[\mathrm{SRP}] + k_{off} \qquad (4)$$

in which k_{on} is the rate constant for complex assembly, and k_{off} is the rate constant for complex disassembly.

Co-translational protein targeting and translocation. A previously established heterologous protein targeting assay, based on the ability of *E. coli* SRP and FtsY to mediate the targeting of preprolactin (pPL) to microsomal membrane (Powers, 1997; Shan, 2007), was used in this study. 200 nM SRP and 4 equivalent of trypsin digested and salt washed microsomal membrane were used in the targeting reaction.

Density gradient floatation. Lipid flotation assays were performed as previously described (Parlitz, 2007; Valent, 1998) with slight modifications. For free FtsY, 100 nmol protein was incubated with *E. coli* liposomes (10 mg/ml) in SRP buffer at 37°C for 30 minutes. For the

SRP•FtsY complex, 20 μM FtsY and Ffh were pre-incubated with 5.3 mM GppNHp for 2 hr at 25 °C, and then incubated at 37°C for 30 minutes in the presence of 10 mg/ml liposomes. The protein-lipid mixture was overlaid with density gradients and ultracentrifuged as described (Parlitz, 2007; Valent, 1998). The gradient was collected in four fractions (600 μl, 400 μl, 400 μl, 600 μl) from the top, TCA precipitated, and analyzed by SDS-PAGE.

Site-directed spin labeling and EPR measurements

Spin-labeling reactions were carried out in 20 mM HEPES (pH 8.0), 300 mM NaCl, 2mM EDTA. Reduced and degassed single cysteine mutants of FtsY-NG+1 were labeled with a 3–5 fold molar excess of MTSSL (Toronto Research Chemicals) at room temperature in the dark for 2-3 hr. Excess MTSSL was removed by gel filtration, and the efficiency of spin-labeling (80–100%) was determined by EPR using a TEMPO calibration curve (Bruker user manual). EPR spectra were acquired using a 9.4 GHz (X-band) Bruker EMX EPR spectrometer equipped with an ER 4119HS cavity at 20–23 °C. The concentrations of spin-labeled samples were 30–100 μM for apo-FtsY and ~30 μM for the *early* and *closed/activated* complexes. Forty per cent glycerol was present in all samples to remove motions arising from the global tumbling of protein. 32–64 scans were accumulated and averaged using microwave power of 5 mW with modulation amplitude set at 1 G and magnetic field sweep width of 100 G. The central linewidth is the same from 0.2– 5 mW microwave power. Less than 2% background labeling was observed; background subtraction was therefore not necessary.

Surface Plasmon Resonance. Anti-His monoclonal antibody was immobilized onto the surface of CM5 chips at levels ranged from 12000 to 23000 RU. Changing the surface density of the antibody within this range had no effect on FtsY/lipid interaction. All the results here were obtained with a single IgG-derivatized biosensor chip in SRP buffer. Two IgG-derivatized flow

cells were used: the sample cell contained immobilized FtsY or FtsY-NG (at a surface density of ~250 RU), and the reference cell provided negative control whose changes in RU were subtracted from that of the sample cell. Liposomes at varying concentrations in SRP buffer were flowed in for 200–270 seconds at a rate of 30 μL/min. When equilibrium was reached, liposomes were allowed to dissociate for 60 seconds in SRP buffer. After each cycle of binding and dissociation, the surface was regenerated by 10 mM Glycine buffer (pH 2.5), and FtsY constructs were re-immobilized. To determine K_d, the RU values 5 seconds. before initiating dissociation of the liposomes were plotted against liposome concentration. The data were fit to Eq 5,

$$\mathrm{RU_{obsd}} = \mathrm{RU_0} \times \frac{K_d^n}{K_d^n + [\mathrm{lipid}]^n} + \mathrm{RU_1} \times \frac{[\mathrm{lipid}]^n}{K_d^n + [\mathrm{lipid}]^n} \qquad (5)$$

in which $\mathrm{RU_{obsd}}$ is the observed resonance units, $\mathrm{RU_0}$ is the resonance signal in the absence of lipids, $\mathrm{RU_1}$ is the resonance signal at saturating liposome concentrations, K_d is the apparent equilibrium dissociation constant for FtsY-lipid binding, and n is the Hill coefficient.

Acknowledgements

We thank Oded Lewinson in the Rees group for help and advice on liposome experiments, Jost Vielmetter at the Protein Expression Center (PEC) at Caltech and J. Van Deventer of the Tirrel group for help in SPR experiments and for providing the Biacore T100 instrument, Dr. W. Wintermeyer for the expression plasmid for full-length FtsY, and Ray Deshaies and members of the Shan laboratory for comments on the manuscript. This work was supported by NIH grant GM078024, and career awards from the Burroughs Welcome Foundation, the Henry and Camille Dreyfus foundation, the Beckman foundation, and the Packard foundation to S.S.. D. A. and M.R. were supported by NIH/NRSA training grant 5T32GM07616. The Biacore instrument at

the PEC is funded by the Moore Foundation grant for the “Center for Integrative Study of Cell Regulation” and in part by Caltech's Beckman Institute Funds.

References

Angelini, S., Boy, D., Schiltz, E., and Koch, H.-G. 2006. Membrane binding of the bacterial signal recognition particle receptor involves two distinct binding modes. *J. Cell Biol*. 174:715-724.

Angelini, S., Deitermann, S., and Koch, H.-G. 2005. FtsY, the bacterial signal recogntion particle receptor, interacts functionally and physically with the secYEG translocon. *EMBO Rep.* 6:476-481.

Bahari, L., Parlitz, R., Eitan, A., Stjepanovic, G., Bochkareva, E.S., Sining, I., Bibi, E. 2007. Membrane targeting of ribosomes and their release require distinct and separable functions of FtsY. *J. Biol. Chem.* 282:32168-75.

Bradshaw, N., Neher, S.B., Booth, D.S., and Walter, P. 2009. Signal sequences activate the catalytic switch of SRP RNA. *Science*. 323:127-130.

Connolly, T., Rapiejko, P. J., Gilmore, R. 1991. Requirement of GTP hydrolysis for dissociation of the signal recognition particle from its receptor. *Science*. 252:1171-1173.

Cross, B.C.S., Sinning, I., Luirink, J., High, S. 2009. Delivering proteins for export from the cytosol. *Nature Rev. Mol. Cell. Biol.* 10:255-264.

de Leeuw, E., te Kaat, K., Moser, C., Memestrina, G., Demel, R., de Kruijff, B., Oudegam B., Luirink, J., and Sinning, I. 2000. Anionic phospholipids are involved in membrane association of FtsY and stimulate its GTPase activity. *EMBO J.* 19:531-541.

de Vruje, T., de Swart, R.L., Dowhan, W., Tommassen, J., de Kruijff, B. 1988. Phosphotidylglycerol is involved in protein translocation across Escherichia coli inner membranes. *Nature*. 334:173-175.

Egea, P.F., Shan, S., Napetschnig, J., Savage, D.F., Walter, P., and Stroud, R.M. 2004. Substrate twinning activates the signal recognition particle and its receptor. *Nature*. 427:215-221.

Eitan, A., and Bibi, E. 2004. The core Escherichia coli signal recognition particle receptor contains only the N and G domains of FtsY. *J. Bacteriol.* 186:2492-2494.

Fishov, I., Woldringh, C.L. 1999. Visualization of membrane domains in Escherichia coli. *Molecular Microbiology*. 32:1166-1172.

Focia, P.J., Shepotinovskaya, I.V., Seidler, J.A., and Freymann, D.M. 2004. Heterodimeric GTPase Core of the SRP Targeting Complex. *Science*. 303:373-377.

Freymann, D.M., and Walter, P. 2000. GTPases in protein translocation and protein elongation. *In* Frontiers in Molecular Biology: GTPases. A. Hall, editor. Oxford University Press, London. 222-243.

Gawronski-Salerno, J., Freymann, D. M. 2007. Structure of the GMPPNP-stabilized NG domain complex of the SRP GTPases Ffh and FtsY. *J. Struct. Biol.* 158:122-128.

Gold, V.A.M., Robson, A., Bao, H., Romantsov, T., Duong, F., Collinson, I. 2010. The action of cardiolipin on the bacterial translocon. *Proc. Natl. Acad. Sci.* in press.

Halic, M., Gartmann, M., Schlenker, O., Mielke, T., Pool, M.R., Sinning, I., and Beckmann, R. 2006. Signal recognition particle receptor exposes the ribosomal translocon binding site. *Science*. 312:745-747.

Hendrick, J.P., Wickner, W. 1991. SecA protein needs both acidic phospholipids and secY/E protein for functional high affinity binding to the Escherichia coli plasma membrane. *J. Biol. Chem.* 266:24596-24600.

Hu, Z., Gogol, E.P., Lutkenhaus, J. 2002. Dynamic assembly of MinD on phospholipid vesicles regulated by ATP and MinE. *Proc. Natl. Acad. Sci. U. S. A.* 99:6761-6766.

Hubbell, W.L., Altenbach, C., Hubbell, C.M., Khorana, H.G. 2003. Rhodopsin structure dynamics, and activation: A perspective from crystallography, site-directed spin labeling, sulfhydryl reactivity, and disulfide cross-linking. . *Adv. Prot. Chem.* 63:243-286.

Hubbell, W.L., Mchaourab, H.S., Altenbach, C., Lietzow, M.A. 1996. Watching proteins move using site-directed spin labeling. *Structure*. 4:779-783.

Hustedt, E.J.a.B., A.H. 1999. Nitroxide spin-spin interactions: Applications to protein structure and dynamics. . *Ann. Rev. Biophys. Biomol. Struct.* 28:129-153.

Kusters, R., Dowhan, W., de Kruijff, B. 1991. Negatively charged phospholipids restore prePhoE translocation across phosphatidylglycerol-depleted Escherichia coli inner membranes. *J. Biol. Chem.* 266:8659-8662.

Lill, R., Dowhan, W., Wickner, W. 1990. The ATPase activity of secA is regulated by acidic phospholipids, secY, and the leader and mature domains of precursor proteins. *Cell*. 60:271-280.

Luirink, J., Hagen-Jongman, C. M. ten, Weijden, C., Oudega, B., High, S. Dobberstein, B., and Kusters, R. 1994. An alternative protein targeting pathway in *Escherichia coli*: studies on the role of FtsY. *EMBO J.* 13:2289-2296.

Marty, N., Rajalingam, D., Kight, A.D., Lewis, N., Fologea, D., Kumar, T.K.S., Henry, R., Goforth, R.L. 2009. The membrane binding motif of chloroplast signal recognition particle receptor (cpFtsY) regulates GTPase activity. *J. Biol. Chem.* 284:14891-14903.

Mileykovskaya, E., Fishov, I., Fu, X., Corbin, B.D., Margolin, W., Dowhan, W. 2003. Effects of phospholipid composition on MinD-membrane interactions in vitro and in vivo. *J. Biol. Chem.* 278:22193-22198.

Mircheva, M., Boy, D., Weiche, B., Hucke, F., Graumann, P., Koch, H.-G. 2009. Predominant membrane localization is an essential feature of the bacterial signal recognition particle receptor. *BMC Biology*. 7.

Montoya, G., Svensson, C., Luirink, J., and Sinning, I. 1997a. Crystal structure of the NG domain from the signal recognition particle receptor FtsY. *Nature*. 385:365-368.

Montoya, G., Svensson, C., Luirink, J., and Sinning, I. 1997b. Expression, crystallization and preliminary X-ray diffraction study of FtsY, the Docking protein of the signal recognition particle of E. coli. *PROTEINS: Structure, Function, and Genetics*. 28:285-288.

Neher, S.B., Bradshaw, N., Floor, S.N., Gross, J.D., Walter, P. 2008. SRP RNA controls a conformational switch regulating the SRP-SRP receptor interaction. *Nat. Struct. Mol. Biol.* 15:916-923.

Parlitz, R., Eitan, A., Stjepanovic, G., Bahari, L., Bange, G., Bibi, E., Sinning, I. 2007. Escherichia coli signal recognition particle receptor FtsY contains an essential and autonomous membrane-binding amphipathic helix. *J. Biol. Chem.* 282:32176-84.

Peluso, P., Shan, S., Nock, S., Herschlag, D., and Walter, P. 2001. Role of SRP RNA in the GTPase cycles of Ffh and FtsY. *Biochemistry*. 40:15224-15233.

Pool, M.R., Stumm, J., Fulga, T. A., Sinning, I., Dobberstein, B. 2002. Distinct modes of signal recognition particle interaction with the ribosome. *Science*. 297:1345-1348.

Powers, T., and Walter, P.w. 1997. Co-translational protein targeting catalyzed by the *Escherichia coli* signal recognition particle and its receptor. *EMBO J.* 16:4880-4886.

Rapoport, T.A. 2007. Protein translocation across the eukaryotic endoplasmic reticulum and bacterial plasma membranes. *Nature*. 450:663-669.

Ridder, A.N.J.A., Kuhn, A., Killian, J.A., de Kruijff, B. 2001. Anionic lipids stimulate Sec-independent insertion of a membrane protein lacking charged amino acid side chains. *EMBO Rep.* 2:403-408.

Rubio, A., Jiang, X., Pogliano, K. 2005. Localization of translocation complex components in Bacillus subtilis: enrichment of the signal recognition particle receptor at early sporulation septa. *J. Bacteriol.* 187:5000-5002.

Schwartz, T., Blobel, G. 2003. Structural basis for the function of the b-subunit of the eukaryotic signal recognition particle receptor. *Cell*. 112:793-803.

Scotti, P.A., Valent, Q., A., Manting, E. H., Urbanus, M. L., Driessen, A. J. M., Oudega, B., and Luiringk, B. O. 1999. SecA is not required for signal recognition particle-mediated targeting and initial membrane insertion of a nascent inner membrane protein. *J. Biol. Chem.* 274:29883-29888.

Shan, S., Chandrasekar, S., and Walter, P. 2007. Conformational changes in the GTPase modules of SRP and its receptor drive initiation of protein translocation. *J. Cell Biol.* 178:611-620.

Shan, S., Schmid, S.L., Zhang, X. 2009. Signal recognition particle (SRP) and SRP receptor: a new paradigm for multi-state regulatory GTPases. *Biochemistry*. 48:6696-6704.

Shan, S., Stroud, R., Walter, P. 2004. Mechanism of association and reciprocal activation of two GTPases. *Plos Biology*. 2:e320.

Shepotinovskaya, I.V., and Freymann, D. M. 2001. Conformational change of the N-domain on formation of the complex between the GTPase domains of *Thermus aquaticus* Ffh and FtsY. *Biochemica et Biophysica Acta*. 1597:107-114.

Simon, S.M., and Blobel, G. 1991. A protein-conducting channel in the endoplasmic reticulum. *Cell*. 65:371-380.

Valent, Q.A., Scotti, P.A., High, S., de Gier, J.W.L., von Heijne, G., Lentzen, G., Wintermeyer, W., Oudega, B., and Luirink, J. 1998. The *Escherichia coli* SRP and SecB targeting pathways converge at the translocon. *EMBO J.* 17:2504-2512.

Vanounou, S., Parola, A.H., Fishov, I. 2003. Phosphotidylethanolamine and phosphatidylglycerol are segregated into different domains in bacterial membrane. A study with pyrene-labelled phospholipids. *Molecular Microbiology*. 49:1067-1079.

Walter, P., and Johnson, A. E. 1994. Signal sequence recognition and protein targeting to the endoplasmic reticulum membrane. *Ann. Rev. Cell Biol.* 10:87-119.

Walter, P., Ibrahimi, I., and Blobel, G. 1981. Translocation of proteins across the endoplasmic reticulum I. Signal Recognition Protein (SRP) binds to *in vitro* assembled polysomes synthesizing secretory protein. *J. Cell. Biol.* 91:545-550.

Weiche, B., Burk, J., Angelini, S., Schiltz, E., Thumfart, J.O., Koch, H.-G. 2008. A cleavable N-terminal membrane anchor is involved in membrane binding of the Escherichia coli SRP receptor. *J Mol. Biol*. 377:761-773.

Zhang, X., Kung, S., Shan, S. 2008. Demonstration of a two-step mechanism for assembly of the SRP-SRP receptor complex: implications for the catalytic role of SRP RNA. *J. Mol. Biol.* 381 581-593.

Zhang, X., Schaffitzel, C., Ban, N., Shan, S. 2009. Multiple conformational changes in a GTPase complex regulate protein targeting. *Proc. Natl. Acad. Sci.* 106:1754-1759.

Figures

Figure 1

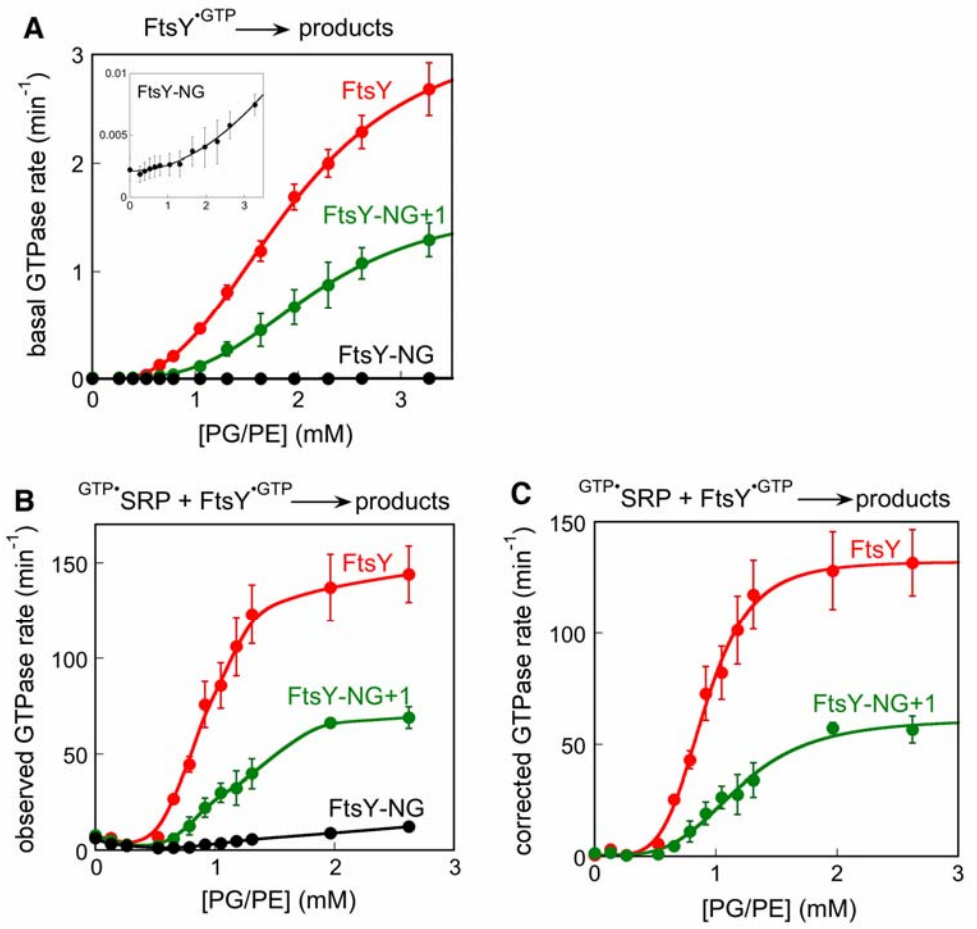

Figure 1. Phospholipids stimulate FtsY's basal GTPase activity and its complex assembly with SRP. (**A**) Effect of liposomes on the basal GTPase reaction of FtsY (red), FtsY-NG+1 (green) and FtsY-NG (black and inset). The data were fit to eq 2, and gave Hill coefficients of 2.9 and 3.4 for FtsY and FtsY-NG+1, respectively, and an apparent K_d value of 2.0 and 2.2 mM for lipid binding to FtsY and FtsY-NG+1, respectively. **(B)** Effect of liposomes on the reaction: ^{GTP}•SRP + FtsY$^{•GTP}$ → products for FtsY (red), FtsY-NG+1 (green), and FtsY-NG (black). (**C**) A-domain-specific lipid stimulation of complex assembly with FtsY (red) and FtsY-NG+1 (green), after subtraction of the rate constants from FtsY-NG. The data were fit to eq 2, and gave Hill coefficients of 4.4 and 3.8 for FtsY and FtsY-NG+1, respectively.

Figure 2

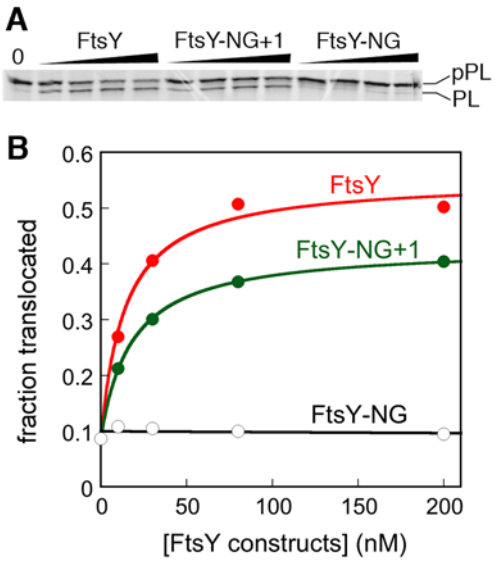

Figure 2. Role of the FtsY A-domain in preprotein targeting and translocation. (**A**) SDS-PAGE analysis of the translocation efficiency of preprolactin (pPL) mediated by FtsY, FtsY-NG+1, and FtsY-NG. (**B**) Quantitation of the results in part A.

Figure 3

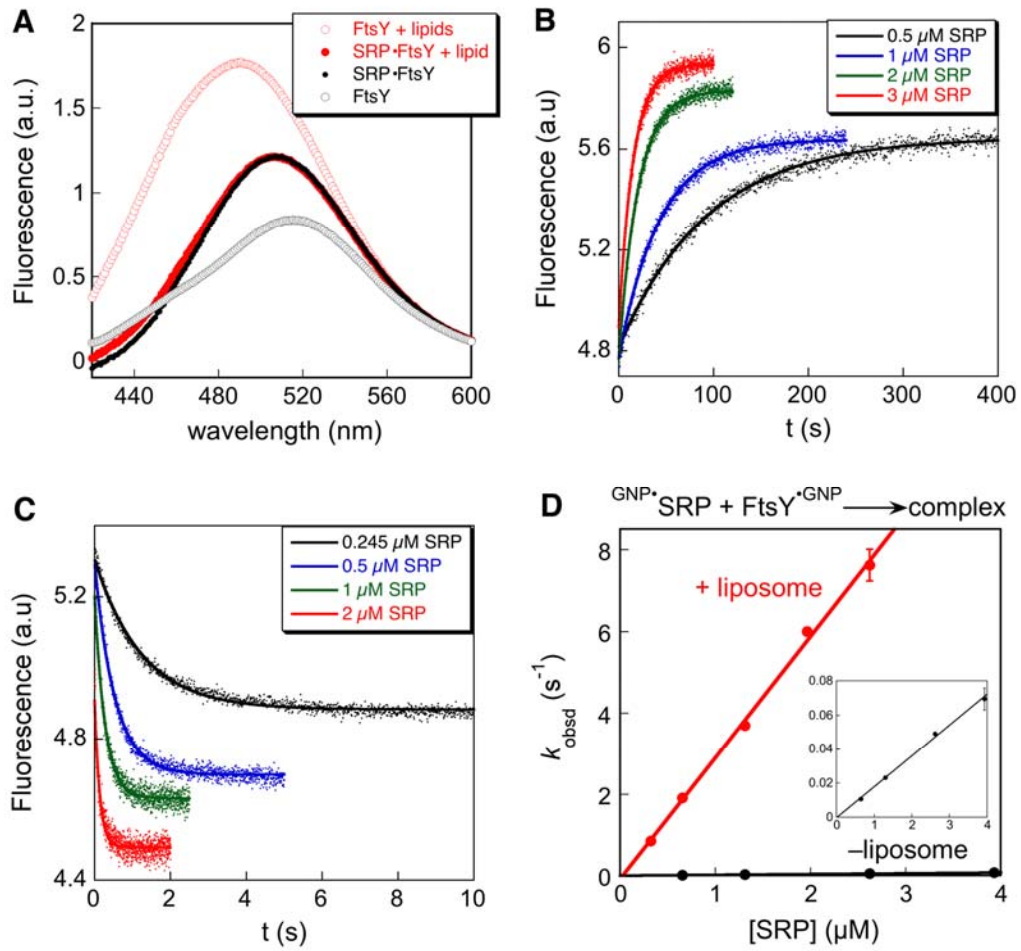

Figure 3. Phospholipids accelerate formation of the *activated* SRP•FtsY complex. (**A**) Fluorescence emission spectra of acrylodan-labeled FtsY C356 in the presence (closed circles) or absence (open circles) of SRP (5 μM), with (red) or without (black) 2 mM liposome present. The scattering from buffer, SRP, and liposomes have been subtracted from the respective spectra. (**B-C**) Time courses for complex assembly were measured in the presence of 200 nM acrylodan-labeled FtsY C356 and 200 μM GMPPNP without (part **B**) or with (part **C**) 2 mM liposome present. The data were fit to single exponential functions to yield the observed rate constants at individual SRP concentrations. (**D**) Liposomes accelerate formation of the *activated* SRP•FtsY complex. Observed rate constants for complex formation were from parts **B** and **C**. GNP denotes GppNHp. The inset shows the data in the absence of liposomes on an expanded scale. Linear fits of the data to eq 4 gave association rate constants of $k_{on} = 3.0 \times 10^6$ and 1.8×10^4 $M^{-1}s^{-1}$ in the presence and absence of liposomes, respectively. Error bars are standard deviations (SDs) from three or more measurements.

Figure 4

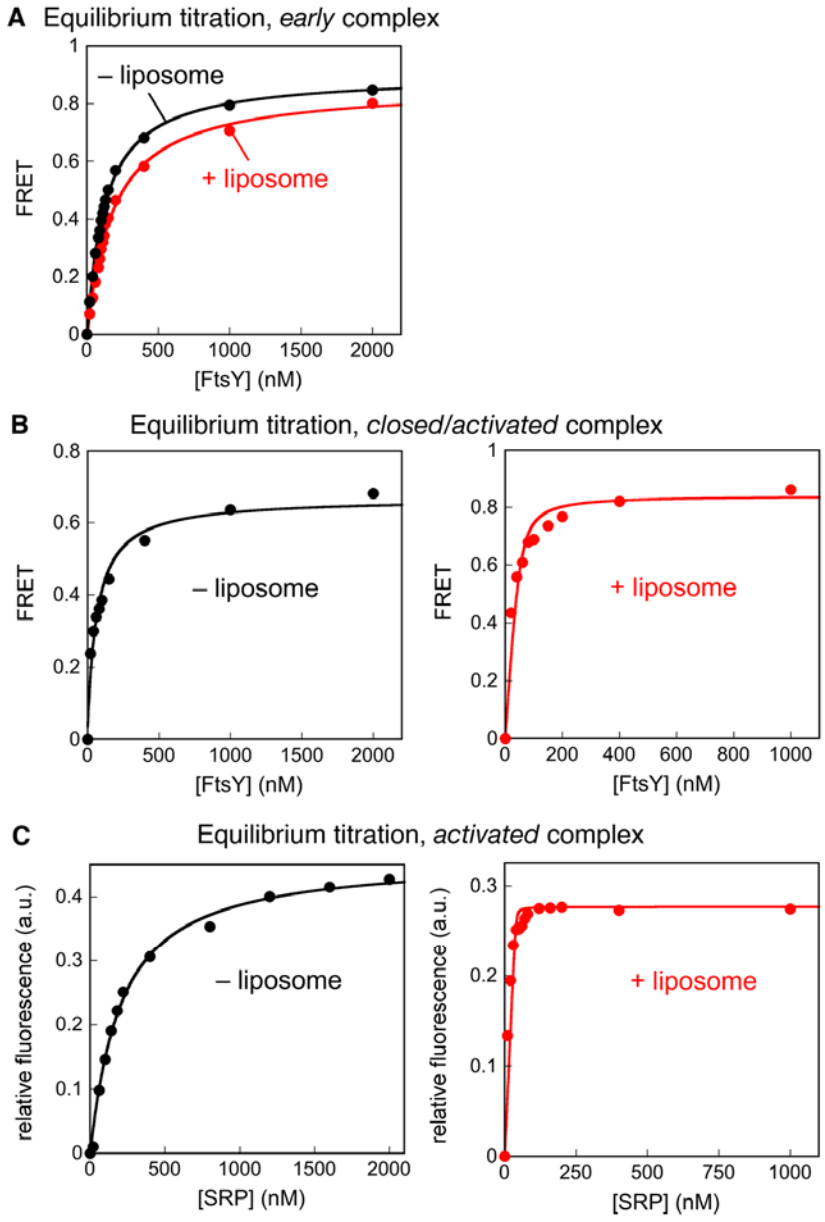

D

	K_d (nM)		
	early	*closed/activated*	*activated*
– liposome	68 ± 4	67 ± 13	145 ± 17
+ liposome	104 ±13	7.2 ± 3.5	≤ 4

Figure 4. FtsY preferentially stabilizes the SRP•FtsY complex in the *closed* and *activated* states. (**A**) Equilibrium titration of the *early* intermediate in the presence (red) and absence (black) of 2 mM liposomes. Titrations used 100 nM coumarin-labeled SRP C235, 200 nM RNC, and 200 μM GDP. (**B**) Equilibrium titration of the *closed/activated* complex in the absence (left) and presence (right) of 2 mM liposomes. Titrations used 50 nM coumarin-labeled SRP C235 and 200 μM GppNHp. (**C**) Equilibrium titration of the *activated* SRP•FtsY complex in the absence (left) and presence (right) of 2 mM liposomes. Titrations used 100 and 40 nM acrylodan-labeled FtsY C356 in the absence and presence of liposomes, respectively, and 200 μM GppNHp. The data were fit to eq. 3, and the values of K_d are summarized in (**D**). Representative fluorescence measurements were shown in **A**-**C**, and the K_d values reported in **D** are averaged from three or more measurements.

Figure 5

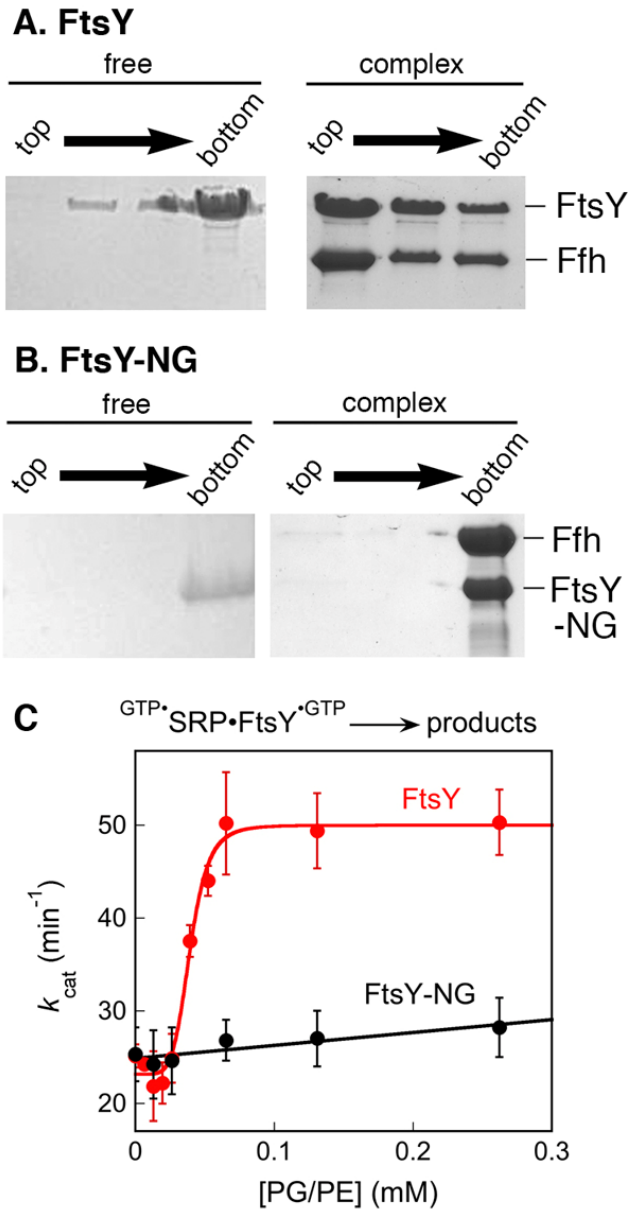

Figure 5. The stable SRP•FtsY complex binds more strongly to lipids than free FtsY. (**A**–**B**) Density gradient flotation analysis of the binding of FtsY (left) and the SRP•FtsY complex (right) to *E. coli* liposomes for full-length FtsY (part **A**) and FtsY-NG (part **B**). (**C**) Effect of liposomes on the reaction: ^{GTP}•SRP•FtsY$^{•GTP}$ → products with FtsY (red) and FtsY-NG (black). The data with FtsY was fit to eq 2, and gave a Hill coefficient of 4.8 and an apparent K_d value of 39 μM for FtsY-lipid binding in the complex. Error bars are SDs from two measurements.

Figure 6

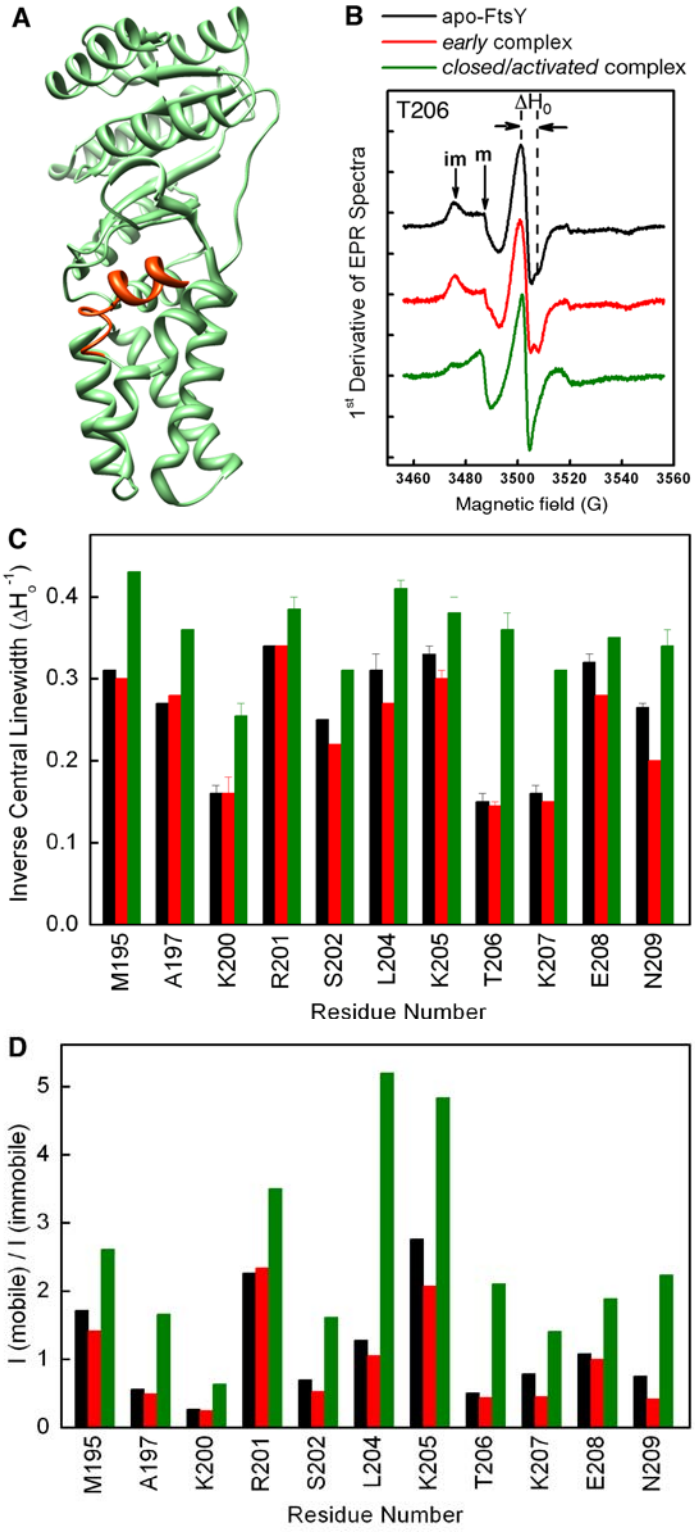
A
B
apo-FtsY
early complex
closed/activated complex
T206
ΔH0
im
m
1st Derivative of EPR Spectra
3460 3480 3500 3520 3540 3560
Magnetic field (G)
C
Inverse Central Linewidth (ΔH0-1)
0.0 0.1 0.2 0.3 0.4
M195 A197 K200 R201 S202 L204 K205 T206 K207 E208 N209
Residue Number
D
I (mobile) / I (immobile)
0 1 2 3 4 5
M195 A197 K200 R201 S202 L204 K205 T206 K207 E208 N209
Residue Number

Figure 6. Formation of the GTP-dependent SRP•FtsY complex exposes FtsY's lipid binding helix. **(A**) Crystal structure of *E. coli* FtsY-NG+1 (PDB ID: 2QY9). The amphiphilic lipid-binding helix at the A-N domain junction is highlighted in *coral*. (**B)** EPR spectra of the nitroxide spin probe at residue T206 of FtsY-NG+1 for apo-FtsY (black), the *early* intermediate formed in GDP (red), and the *closed/activated* complex formed in GppNHp (green). ΔH indicates the central line width, and 'im' and 'm' denote the population of immobile and mobile molecules, respectively. (**C**–**D**) Summary of the central linewidth (**C)** and fraction of mobile molecules (**D**) for nitroxide probes placed at different positions along FtsY's lipid binding helix. Color coding is the same as in (**B**). Error bars are SDs from two or more measurements.

Figure 7

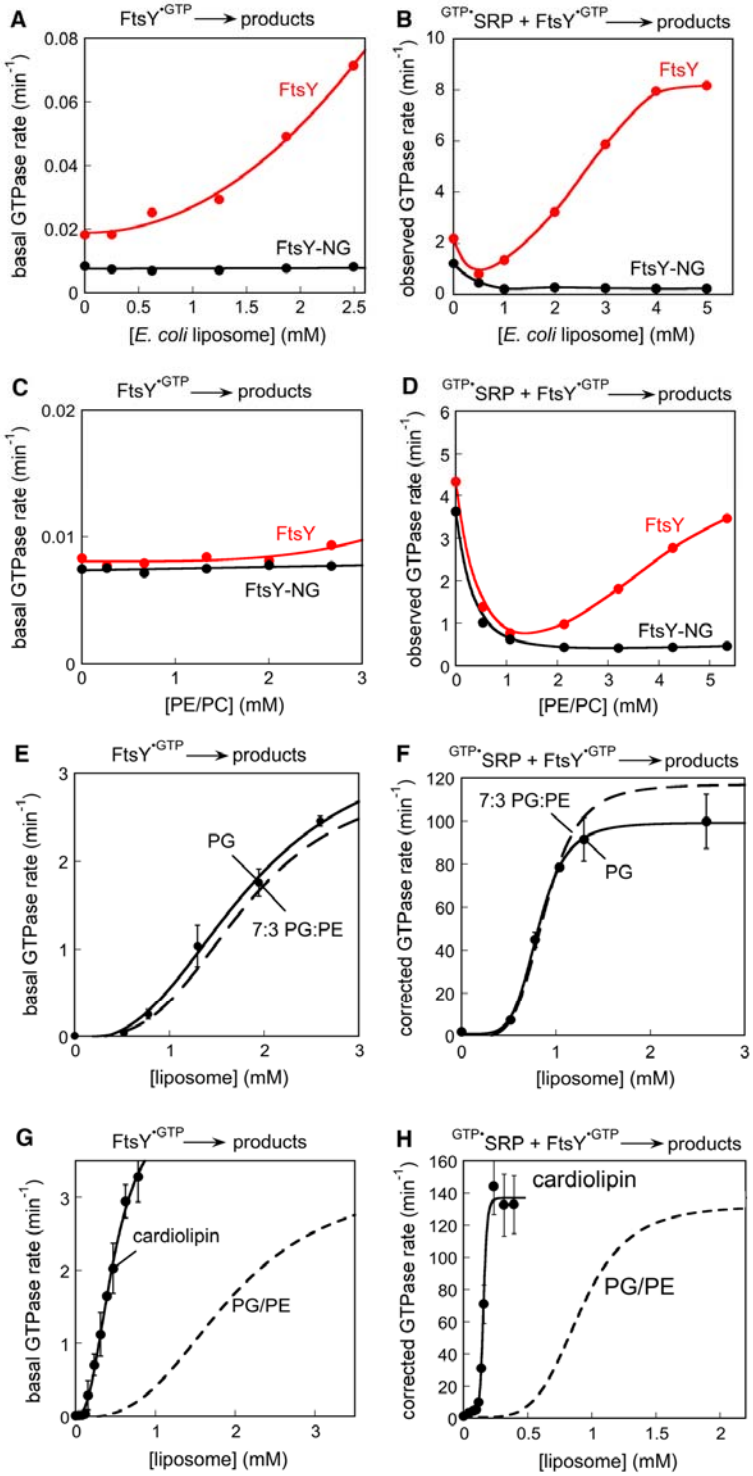
A
FtsY•GTP → products
basal GTPase rate (min-1)
FtsY
FtsY-NG
[E. coli liposome] (mM)
B
GTP•SRP + FtsY•GTP → products
observed GTPase rate (min-1)
FtsY
FtsY-NG
[E. coli liposome] (mM)
C
FtsY•GTP → products
basal GTPase rate (min-1)
FtsY
FtsY-NG
[PE/PC] (mM)
D
GTP•SRP + FtsY•GTP → products
observed GTPase rate (min-1)
FtsY
FtsY-NG
[PE/PC] (mM)
E
FtsY•GTP → products
basal GTPase rate (min-1)
PG
7:3 PG:PE
[liposome] (mM)
F
GTP•SRP + FtsY•GTP → products
corrected GTPase rate (min-1)
7:3 PG:PE
PG
[liposome] (mM)
G
FtsY•GTP → products
basal GTPase rate (min-1)
cardiolipin
PG/PE
[liposome] (mM)
H
GTP•SRP + FtsY•GTP → products
corrected GTPase rate (min-1)
cardiolipin
PG/PE
[liposome] (mM)

Figure 7. FtsY is specifically stimulated by anionic phospholipids. (**A–B**) Effects of *E. coli* liposomes on FtsY's basal GTPase rate (**A**) and on SRP-FtsY complex assembly (**B**). (**C**–**D**) Effect of 7:3 PE/PC liposomes on FtsY's basal GTPase reaction (**C**) and on SRP-FtsY complex assembly (**D**). (**E–F**) Effects of PG (circles) liposomes on FtsY's basal GTPase rate (**E**) and on SRP-FtsY complex assembly (**F**). (**G–H**) Effects of cardiolipin (solid circle) on FtsY's basal GTPase rate (**G**) and on SRP-FtsY complex assembly (**H**). The dashed lines depict the data for PG/PE liposomes and were shown for comparison. Error bars are SDs from two or more measurements.

Figure 8

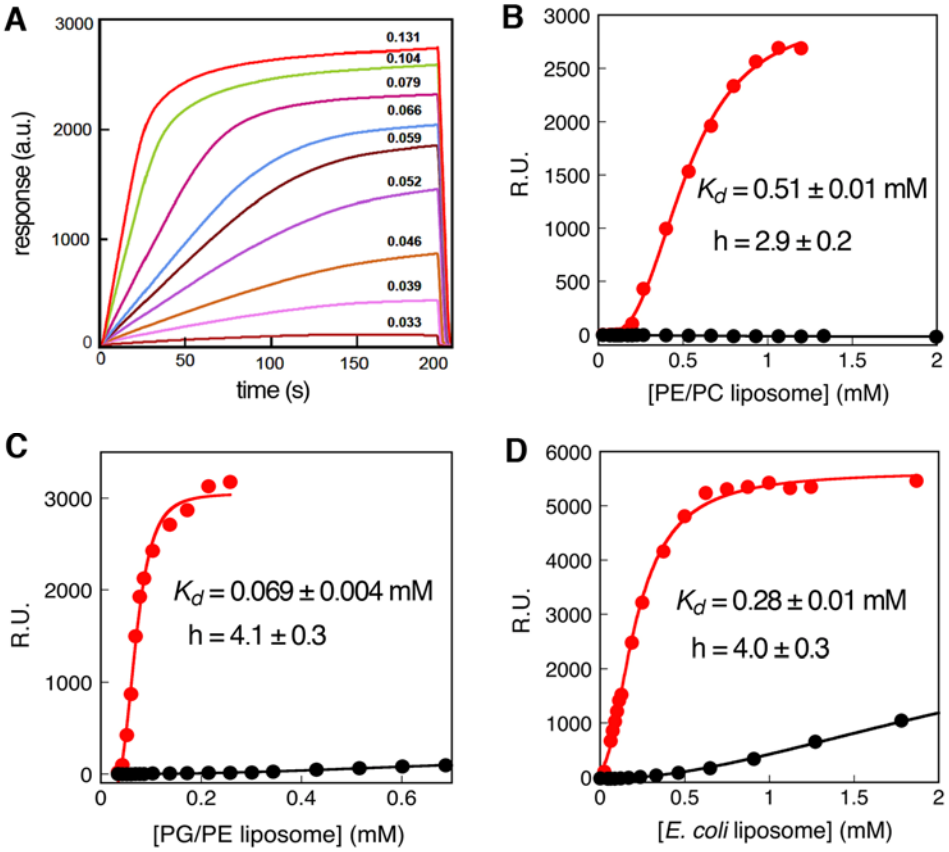

Figure 8. FtsY binds specifically to anionic phospholipids. (**A**) SPR traces depicting resonance changes on FtsY-immobilized biosensor chips due to liposome binding. The numbers above each line denote the corresponding liposome concentration. (**B**-**D**) Equilibrium binding curves of FtsY (red) or FtsY-NG (black) to liposomes composed of 7:3 PE/PC (**B**), 7:3 PG/PE (**C**), and *E. coli* (**D**) lipids. The data were fit to eq 5 to obtain the apparent K_d values and hill co-efficients (h) for FtsY-lipid binding.

Figure 9

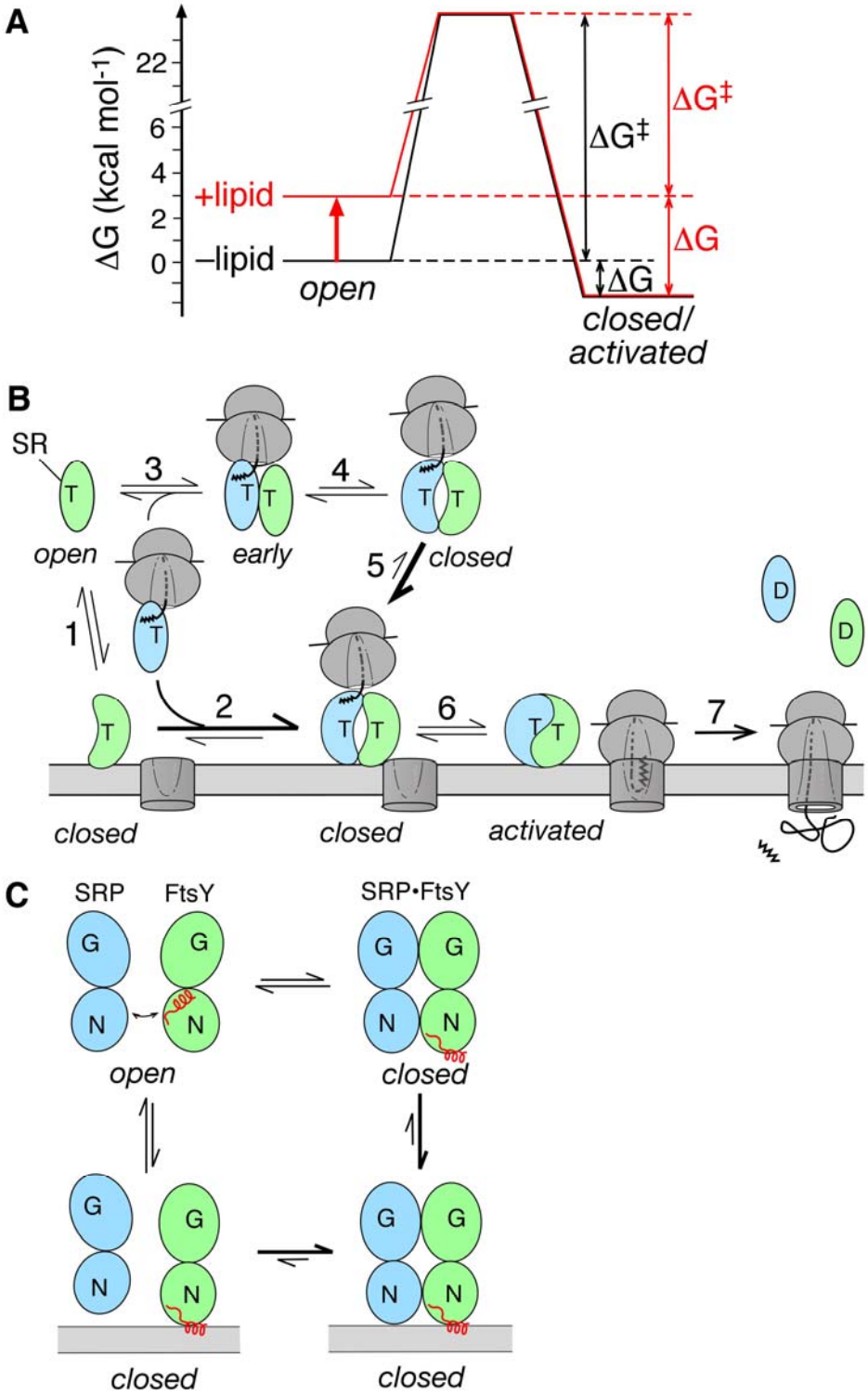
A
ΔG (kcal mol-1)
22
6
4
2
0
+lipid
–lipid
open
ΔG‡
ΔG‡
ΔG
ΔG
closed/
activated
B
SR
T
open
3
early
4
closed
5
1
2
6
7
D
D
closed
closed
activated
C
SRP
FtsY
SRP•FtsY
G
N
open
closed
closed
closed

Figure 9. Phospholipids drive conformational changes of FtsY to regulate protein targeting. (**A**) Free energy profile depicting the effect of phospholipids in shifting the conformational equilibrium of FtsY from the *open* to the *closed/activated* states by ~100-fold (~2.8 kcal/mol). A standard state of 1 μM FtsY was used to calculate the free energy differences and activation energy for GTP-dependent SRP-FtsY complex formation. (**B**) Model for how lipid binding of FtsY is coupled to the SRP-FtsY interaction and protein targeting. Step 1, dynamic association of free FtsY with the phospholipid membrane. Step 2, membrane-bound FtsY is more efficient at forming a stable *closed/activated* SRP•FtsY complex. Step 3, cytosolic FtsY forms an *early* complex with cargo-loaded SRP. Step 4, the cargo•SRP•FtsY complex shifts between the *early* and *closed* conformations with an equilibrium of ~1. Step 5, the *closed* complex binds more strongly to the membrane than free FtsY. Step 6, the *closed* complex rearranges to the *activated* state, during which it completes the transfer of cargo to the translocon. Step 7, GTP hydrolysis drives complex disassembly, returning a fraction of FtsY molecules to the cytosol. (**C**) Movement of the αN1 helix (red) accompanies the *open* → *closed* rearrangement and membrane binding of FtsY.

Figure S1

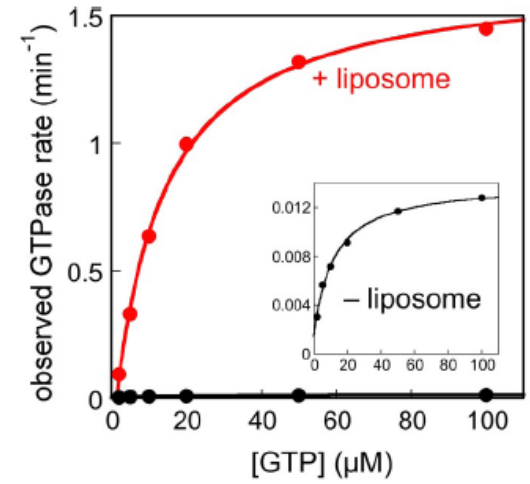

	k_{cat} (min^{-1})	K_m (μM)
– liposome	0.012	11.7
+ liposome	1.9	12.2

Figure S1. Phospholipids stimulate the basal GTP hydrolysis rate from the FtsY$^{\bullet GTP}$ but does not affect GTP binding to FtsY. Michaelis-Menten analysis of the basal GTPase reaction of FtsY was performed in the presence (red) and absence (black) of 2 mM liposomes. The inset shows the data in the absence of liposomes on an expanded scale. The data were fit to Eq. 1 as described in Materials and methods, and the kcat and Km values are summarized at the bottom. As the chemical step is rate-limiting for the basal GTPase reaction of FtsY (Peluso et al., 2001), K_m is equal to K_d, the equilibrium dissociation constant for FtsY binding to GTP, and k_{cat} is equal to the rate of GTP hydrolysis from the FtsY$^{\bullet GTP}$ complex.

Figure S2

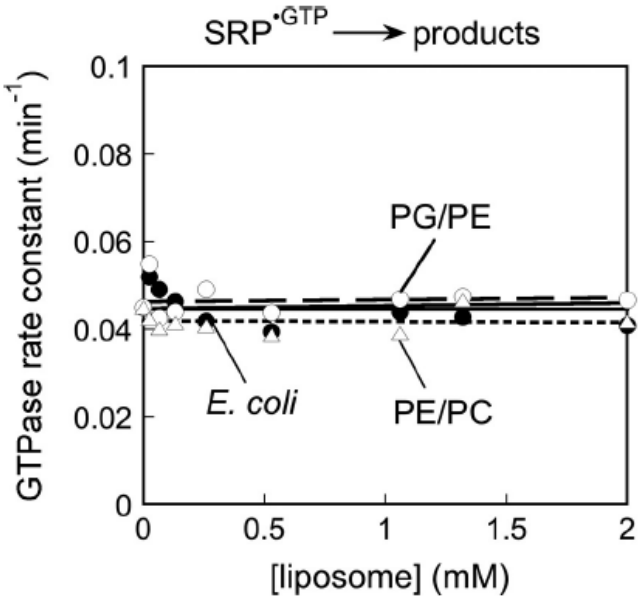

Figure S2. The GTPase activity of SRP was not affected by phospholipids. Basal GTPase reactions of SRP were performed under single turnover conditions using 2 μM SRP, as described previously (Peluso et al., 2001), in the presence of PG/PE (open circles), *E. coli* (closed circles), and PE/PC (triangles) liposomes.

Figure S3

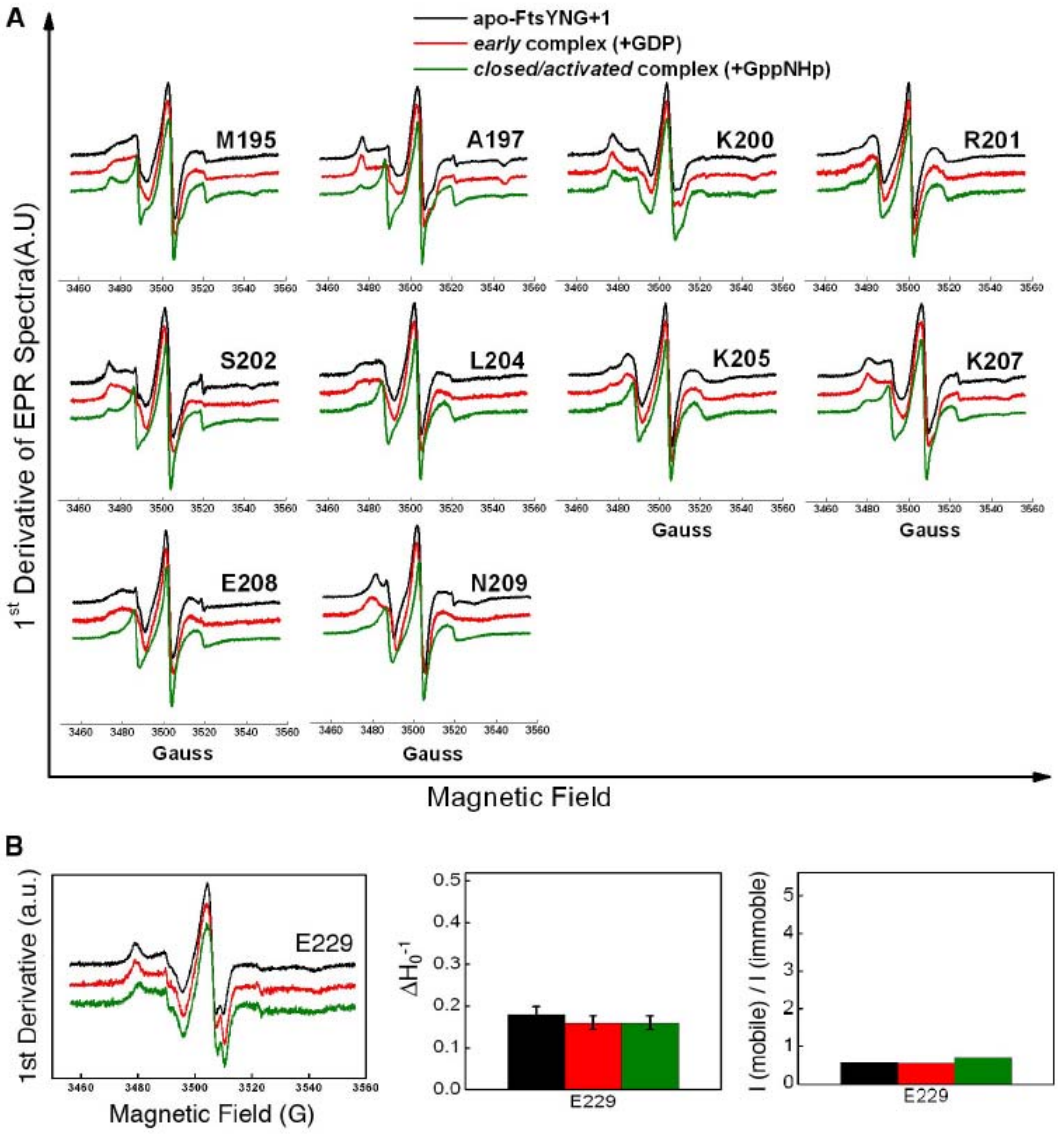

Figure S3. Mobility changes of nitroxide spin probes on the lipid binding helix of FtsY. (A) EPR spectra of nitroxide spin probes at residues 195-209 of FtsY-NG+1 for apo-FtsY (black), the early intermediate formed in GDP (red), and the closed/activated complex formed in GppNHp (green). The data are summarized in Fig. 6 (B and C). (B) EPR spectra of nitroxide spin probe at residue 229 (Fig. 6A, blue) in apo-FtsY and in its complexes with SRP (left). The middle and right panels summarize the central linewidth and fraction of mobile population, respectively, in the different conformational states of FtsY for this probe. The coclor notations are the same as in A. Error bars indicate SD.

Figure S4

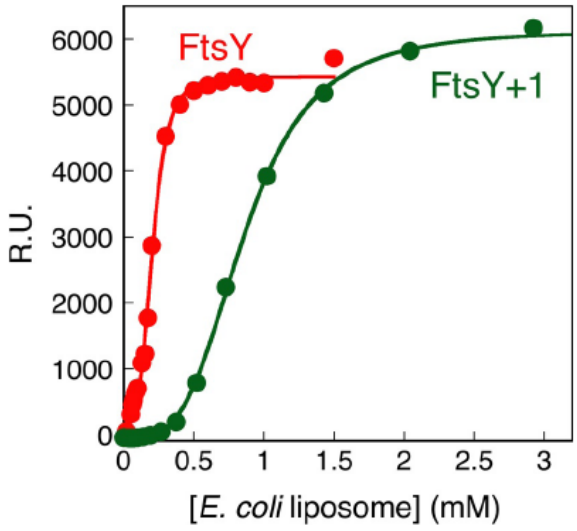

Figure S4. Binding of FtsY (red) or FtsY-NG+1 (green) to E. coli liposomes was determined by SPR. The data were fit to Eq. 5; they gave apparent K_d values of 0.28 and 0.78 mM, and Hill coefficients of 4.0 and 3.5 for lipid binding to FtsY and FtsY-NG+1, respectively.

Figure S5

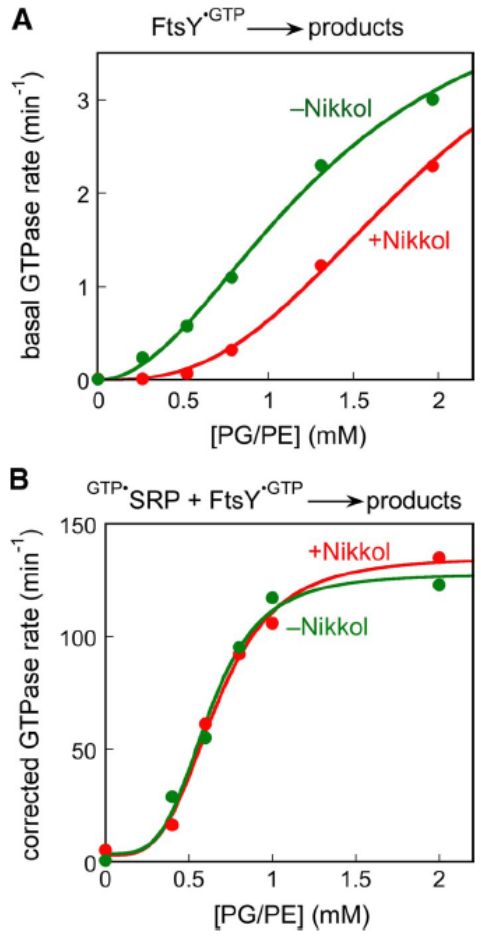

Figure S5. The presence of 0.01% Nikkol has a ≤30% effect on the lipid stimulation of FtsY. (A) The lipid concentration dependence of FtsY's basal GTPase activity. (B) The stimulated GTPase activity. The data were fit to Eq. 2 as described in Materials and methods; they gave apparent lipid-binding constants ($K_{d,app}$) of 1.9 and 1.5 mM, and Hill coefficients of 2.8 and 2.0 with and without Nikkol, respectively (A). The same analysis of the data in B gave $K_{d,app}$ values of 0.66 and 0.62 mM and Hill coefficients of 3.6 and 3.9 with and without Nikkol, respectively.

Table S1. **Rate constants of the stimulated GTPase reaction between SRP and spin-labeled (SL) FtsY-NG+1 used in the EPR measurements**

FtsY construct	k_{cat}	k_{cat}/K_M
	min^{-1}	$10^6\ M^{-1}min^{-1}$
Wild type	18 (1)	41 (1)
M195C-SL	11 (0.61)	20 (0.49)
A197C-SL	10 (0.56)	18 (0.44)
K200C-SL	15 (0.83)	12 (0.29)
R201C-SL	26 (1.4)	49 (1.2)
S202C-SL	26 (1.4)	90 (2.2)
L204C-SL	13 (0.72)	33 (0.80)
K205C-SL	27 (1.5)	53 (1.3)
T206C-SL	26 (1.4)	51 (1.0)
K207C-SL	25 (1.4)	51 (1.2)
E208C-SL	27 (1.5)	63 (1.5)
N209C-SL	25 (1.5)	83 (2.0)

The values in parenthesis denote the rate constant of the spin-labeled FtsY relative to that of the wild-type protein.

Supplemental References

Peluso, P., S.O. Shan, S. Nock, D. Herschlag, and P. Walter. 2001. Role of SRP RNA in the GTPase cycles of Ffh and FtsY. Biochemistry 40:15224-15233.

CHAPTER 2

SecYEG Activates GTPases to Drive the Completion of Cotranslational Protein Targeting

This chapter has been published as:

Akopian, D., Dalal, K., Shen, K., Duong, F., Shan, SO. 2013. Journal of Cell Biology 200, 397.

Abstract

Signal recognition particle (SRP) and its receptor (SR) comprise a highly conserved cellular machinery that cotranslationally targets proteins to a protein-conducting channel, the bacterial SecYEG or eukaryotic Sec61p complex, at the target membrane. Whether SecYEG is a passive recipient of the translating ribosome or actively regulates this targeting machinery remains unclear. Here, we show that SecYEG drives conformational changes in the cargo-loaded SRP•SR targeting complex that activate it for GTP hydrolysis and for handover of the translating ribosome. These results provide the first evidence that SecYEG actively drives the efficient delivery and unloading of translating ribosomes at the target membrane.

Introduction

Correct cellular localization of proteins is essential for the proper functioning of all cells. A universally conserved protein-conducting channel, SecYEG in bacteria or Sec61p in eukaryotes, is the point of convergence of many post- and cotranslational protein targeting pathways and mediates the translocation or integration of newly synthesized proteins (du Plessis, 2011; Cross, 2009; Driessen, 2008). In bacteria, the major post-translational pathway is mediated by the cytosolic chaperone SecB and the SecYEG-interacting ATPase SecA, which together deliver fully synthesized proteins to the periplasm (Driessen, 2008; Zhou, 2003; Hartl, 1990). The co-translational pathway is mediated by two GTPases, the SRP and SR, which target ribosome-nascent chain complexes (RNCs) to SecYEG (Cross, 2009; Walter, 1994; Walter, 1981).

Extensive work on the Sec pathway showed that SecYEG and pre-proteins stimulate SecA's ATPase activity and activate it to drive the translocation of pre-proteins into the periplasm (Duong, 2003; Karamonou, 2007; Kedrov, 2011; Deville, 2011; Gold, 2010; Dalal, 2012). Whether SecYEG analogously regulates the activity of the SRP and SR to drive cotranslational protein targeting is not known. The SecY subunit of SecYEG forms a stable complex with the translating ribosome by interacting with both the ribosome exit site and the signal sequence of the nascent protein (Frauenfeld 2011; Cannon, 2005; van den Berg, 2004). It is unclear, however, whether SecYEG is a passive recipient that simply binds RNCs released from the SRP, or actively regulates the activity of the RNC•SRP•SR targeting complex.

The functional core of SRP is the SRP54 GTPase (Ffh in bacteria) bound to the 4.5S RNA (Poritz, 1990). The bacterial SR, FtsY, has a GTPase domain highly homologous to that in Ffh (Montoya, 1997a). During targeting, SRP and FtsY form a heterodimer in which both

proteins undergo a series of conformational changes, including the early, closed, and activated states, that culminate in reciprocal GTPase activation (Fig. 1A) (Egea, 2004; Zhang; 2009; Shan, 2009, 2004). To ensure efficient and faithful delivery of cargo proteins to the target membrane, these GTPase rearrangements are actively regulated by the RNC (Zhang, 2009) and anionic phospholipids (Lam, 2010; Braig, 2011). RNC stabilizes the early intermediate but disfavors its rearrangement to the subsequent states. This generates a highly stable early targeting complex in which the RNC is predicted to bind SRP with picomolar affinity, and GTP hydrolysis is delayed (Zhang, 2009). Rearrangement of this complex to the closed/activated states, however, is required for the unloading of RNC (Shan, 2007; Zhang, 2009) and activating GTP hydrolysis. In part, these rearrangements could be driven by anionic phospholipids, which stabilize the closed/activated states of FtsY (Lam, 2010). Membranes, however, are insufficient to drive the release of RNC (Song, 2000) or reverse the RNC-induced delay of GTP hydrolysis (Fig. S1). What provides the missing element that drives these late events during the targeting reaction is unknown.

Here we show that SecYEG drives late conformational changes of the targeting complex and re-activates GTP hydrolysis. Our results demonstrate an active role of SecYEG in cotranslational protein targeting and suggest a concerted mechanism for handover of the RNC from the targeting to the translocation machinery.

Results and Discussion

SecYEG destabilizes the early targeting complex

We previously showed that RNCs stabilize the SRP•FtsY GTPase complex in the early conformational state, disfavor its rearrangement to subsequent conformations, and delay GTPase activation (Zhang, 2009, 2008). These allosteric regulations prevent abortive reactions and are beneficial at early stages of the pathway. However, they pose a barrier to the cargo unloading and GTPase activation events required at later stages of the pathway. To test whether SecYEG can help drive these late events, we purified SecYEG complexes (Fig S2A) and first showed that they are active for RNC binding (Fig. S2B). Furthermore, when reconstituted into synthetic lipid vesicles, SecYEG was active in SecA-dependent translocation of proOmpA (Fig. S2C) and capable of cotranslational translocation of a modified alkaline phosphatase containing an SRP-dependent signal sequence derived from DsbA (DsbA-phoA) (Fig. S2D). We focused on SecYEG solubilized in dodecyl-β-D-maltopyranoside (DDM) in this work, as DDM-solubilized SecYEG is fully functional in interacting with the RNC and translocating the nascent polypeptide (Mothes, 1998; and Fig. S2C & D) and activating the SecA ATPase (Duong, 2003; Gold, 2010; Deville, 2011). Further, since phospholipid membranes also exert stimulatory effects on the basal activity of FtsY and accelerate formation of the SRP•FtsY complex (Lam, 2010), the use of DDM-solubilized SecYEG allows us to distinguish its effects from those of phospholipids.

We asked whether and how SecYEG regulates the conformation of the SRP and FtsY GTPases in the RNC•SRP•FtsY targeting complex. We first tested the early intermediate formed between SRP and FtsY, which is stabilized ~10^2-fold by RNCs bearing highly hydrophobic signal sequences such as 1A9L (Zhang, 2009). As this intermediate can form with or without GTP, but its subsequent rearrangement is strictly GTP-dependent, it can be isolated by leaving

out GTP analogues (Zhang, 2008; Fig. 1A). FRET between coumarin-labeled SRP Cys235 and BODIPY-FL-labeled FtsY Cys487 was used to monitor formation of this intermediate (Zhang, 2008). Equilibrium titrations showed that SecYEG destabilized the RNC•SRP•FtsY early intermediate at least 15-fold, while DDM alone did not have any effect (Fig. 1B & F). This destabilizing effect of SecYEG increases linearly with the concentration of SecYEG (Fig. 1C), indicating strong antagonism between SecYEG and the early targeting intermediate. Importantly, SecYEG also lowered the FRET end point of the early intermediate (Fig. 1B & F), suggesting that it alters the conformation of the GTPases in this intermediate.

We next asked whether SecYEG can modulate the subsequent closed and activated states in the GTPase complex (Fig. 1A). To detect these states, we used an environmentally sensitive dye, acrylodan, conjugated to SRP Cys235. In the presence of a non-hydrolyzable GTP analogue, GppNHp, acrylodan at this position specifically changes fluorescence upon formation of the closed/activated complex (Zhang, 2009). Equilibrium titrations using this assay gave similar K_d values in the absence and presence of SecYEG (Fig. 1D & F). As the K_d value of this complex is over 20-fold below the concentration of SRP needed for reliable titrations, a possible effect of SecYEG on its stability might have escaped detection. To more specifically monitor the activated complex, we used acrylodan-labeled FtsY Cys356, which specifically detects movements of catalytic loops required for GTPase activation (Zhang, 2009). This assay revealed a 2–4 fold stabilization of the activated complex by SecYEG (Fig. 1E & F). Together, these results demonstrate that SecYEG drives conformational changes of the targeting complex by destabilizing the early intermediate and favoring the activated complex.

SecYEG re-activates GTP hydrolysis by the targeting complex

If SecYEG drives GTPase rearrangements to the activated state, it would reverse the RNC-induced delay of GTPase activation and re-activate GTP hydrolysis by the targeting complex. To test this hypothesis, we determined the effect of SecYEG on the GTP hydrolysis rate of the SRP•FtsY complex (k_{cat}). As observed previously, RNC_{1A9L} delays GTPase activation, reducing the k_{cat} value from 80 min^{-1} to 22 min^{-1}. SecYEG restored more efficient GTP hydrolysis in the RNC•SRP•FtsY complex and increased the k_{cat} value to 66 min^{-1}, approaching that of the SRP•FtsY complex alone (Fig. 2A). This stimulatory effect of SecYEG was saturable, with an apparent K_d value of ~2 μM (Fig. 2B), which could represent the affinity of SecYEG for the targeting complex. The stimulation was not an artifact of the detergent, as DDM concentrations up to 0.22% did not affect GTP hydrolysis from the RNC•SRP•FtsY complex (Fig. 2C). In comparison, the concentration of DDM introduced along with SecYEG was below 0.14%, as determined by a phenol-sulfuric acid reaction (Dubois, 1956). Indeed, even 0.02% DDM had an inhibitory effect on the stimulated GTPase activity in the absence of RNC (Fig. 2D), suggesting that the actual GTPase stimulation by SecYEG might be even greater than observed here.

As SecYEG was reported to interact with FtsY (Kuhn, 2011; Angelini, 2006), we asked if SecYEG affects the basal GTPase activity of FtsY or its stimulated GTPase reaction with SRP in the *absence* of RNC. No stimulation was observed in either case (Fig. 2E & F), indicating that SecYEG specifically exerts its stimulatory effect only when the SRP•FtsY complex is bound to the RNC.

SecYEG associates with the targeting complex via interaction with the ribosome

How does SecYEG re-activate GTP hydrolysis from the targeting complex? In the simplest model, SecYEG removes the RNC from the SRP, regenerating the SRP•FtsY complex

that hydrolyzes GTP faster. Release of RNC from SRP onto the Sec61p translocon was previously observed in reconstituted targeting reactions using components of the eukaryotic SRP pathway (Fulga, 2001; Song, 2000; Jungnickel, 1995; Gorlich, 1993). Alternatively, SecYEG forms a quaternary complex with RNC, SRP, and FtsY at steady state, in which GTP hydrolysis from the SRP•FtsY complex is activated. To distinguish between these possibilities, we analyzed the effect of SecYEG on the kinetics of formation of the closed SRP•FtsY complex. The most pronounced effect of the RNC is its ability to accelerate the assembly of this complex (Zhang, 2009), which provides a robust diagnostic for whether the RNC is bound to the SRP (Fig. 3A, red and green). If SecYEG did not remove the RNC from SRP, then the kinetics of closed complex formation in the presence of SecYEG would remain rapid. Consistent with this prediction, in the presence of SecYEG and RNC, the rate of closed complex assembly was similar to that with RNC-bound SRP and much faster than with free SRP (Fig. 3A). SecYEG itself does not affect complex assembly between SRP and FtsY (Fig. S3), indicating that it is not responsible for the fast assembly kinetics observed in Figure 3A. Further, in the presence of both SecYEG and RNC, the early $\rightarrow$ closed rearrangement of the SRP•FtsY complex occurred at the same rate, within error, as that with the RNC-loaded SRP and was significantly slower than with free SRP (Fig. 3B & C and Zhang, 2008).

Together, these results strongly suggest that restoration of efficient GTP hydrolysis by SecYEG was not simply due to the removal of RNC from the SRP. Instead, the results suggest the formation of a quaternary RNC•SRP•FtsY•SecYEG complex in which the GTPase activity of SRP and FtsY was stimulated. The K_d value of 2 μM observed earlier (Fig. 2B) likely represents the dissociation constant of SecYEG from this complex. We speculate that this quaternary complex is transient during protein targeting and translocation. It accumulated under our reaction

conditions either because the length of the nascent polypeptide used here (~85 residues) was optimized for interaction of the RNC with the SRP but is suboptimal for its transfer to SecYEG (Park, 2011; Mothes, 1998), or because phospholipid membranes or other components of the holotranslocon may be needed further to drive the efficient transfer of cargo. Regardless of the specific model, the observation of a quaternary complex suggests that the handover of RNC from the SRP to SecYEG could occur through a concerted mechanism, in which both the SRP and SecYEG are associated with the RNC.

How does SecYEG associate with the targeting complex? A large body of work shows that highly conserved basic residues in the cytosolic loops of SecYEG, R255 and R256 in the C4 loop and R357 in the C5 loop, serve as universal binding sites for cytosolic factors including the ribosome (Menetret, 2007), FtsY (Kuhn, 2011), and SecA (Kuhn, 2011; Alami, 2007). We therefore asked whether mutation of these residues abolishes the stimulatory effects of SecYEG. To this end, we purified SecYEG mutants containing charge reversal mutations either in C4 (R255E/R256E), C5 (R357E), or both loops (mtSecYEG) (Fig. S1A). In agreement with previous reports (Menetret, 2007), mtSecYEG was defective in ribosome binding (Fig. S1B). In contrast to wild-type SecYEG (wtSecYEG), none of the SecYEG mutants could restore efficient GTP hydrolysis from the targeting complex. A small amount of rescue could be detected with the R255E/R256E and R357E mutants, likely due to the remaining arginine residue(s) in the other cytosolic loop (Fig. 4A & B). We further tested the ability of mtSecYEG to destabilize the early intermediate and found that, relative to wtSecYEG, this activity was significantly impaired (Fig. 4C & D). Thus, the conserved basic residues in the cytosolic loops of SecYEG are essential for its ability to drive conformational changes in the targeting complex and to reactivate GTP hydrolysis. These results also support the specificity of the stimulatory activities observed with

wtSecYEG and suggest that the action of its cytosolic loops occurs prior to RNC docking, when the targeting machinery first contacts SecYEG.

SecYEG could use its basic cytosolic loops to contact either the ribosome (Menetret, 2007; Becker, 2009) or the A-domain of FtsY (Kuhn, 2011). To distinguish between these possibilities, we removed the N-terminal 196 residues comprising the A-domain of FtsY, generating mutant FtsY-NG (Parlitz, 2007). FtsY-NG could mediate the formation of the RNC-stabilized early intermediate with SRP, with a K_d value similar to that formed by full-length FtsY (Fig. 4E & F). SecYEG destabilized the early intermediate formed by FtsY-NG to the same extent, within error, as that formed by full-length FtsY (Fig. 4E & F). This result is not unexpected, and is in agreement with the poor conservation of the A-domain in bacteria (Eitan, 2004) and its dispensability *in vivo* (Parlitz, 2007; Eitan, 2004). Our results here indicate that the A-domain is not essential for the ability of SecYEG to drive conformational changes in the targeting complex. Instead, the basic cytosolic loops in SecYEG likely interact with the ribosomal protein L23 at the nascent polypeptide exit site (Menetret, 2007; Becker, 2009), thus exerting its stimulatory effects.

Collectively, the results here provide the first evidence that the SecYEG protein conducting channel actively modulates the conformation and activity of the targeting complex to drive completion of the cotranslational protein targeting reaction. Combined with previous work (Lam, 2010; Braig, 2011; Song, 2000; Gold,2010), these results suggest an attractive model in which SecYEG and anionic phospholipids serve overlapping functions in mediating the delivery of the targeting complex to sites of translocation at the target membrane. The targeting complex preferentially localizes to regions of the membrane enriched in anionic phospholipids (Vanounou, 2003; Fishov, 1999; Erez, 2010; Lam, 2010), with which SecYEG may also

preferentially associate (Gold, 2010; Campo, 2004; Shiomi, 2006). Although lipid interactions can induce rearrangements in FtsY to favor the closed/activated states (Lam, 2010), they are insufficient to overcome the stabilizing effect of RNC on the early complex (Lam, 2010) and reactivate the GTPase reaction of the RNC•SRP•FtsY targeting complex (Fig. S1). Association with SecYEG is required to overcome these 'stalling' effects of RNC and re-activate the GTPases. Together, phospholipids and SecYEG drive the rearrangement of the targeting complex to the activated conformation, which enables the unloading of RNC from the SRP to SecYEG and activates GTP hydrolysis, thus completing the targeting cycle. As discussed above, SecYEG likely exerts these effects by forming a transient quaternary intermediate with the targeting complex, in which it interacts directly with the ribosome exit site and displaces the SRP GTPase from this site (Fig. 5B; Halic, 2006). As the early SRP•FtsY complex is stabilized by interaction with the SRP RNA tetraloop (Shen, 2010), which is optimal only when the SRP NG-domain interacts with L23, displacement of the GTPase complex from the ribosome exit site would also explain the destabilizing effect of SecYEG on the early targeting complex. The fate of the signal sequence in the quaternary intermediate, what drives its transfer to SecYEG, and whether SecYEG interacts with FtsY's GTPase domain (Kuhn, 2011; Angelini, 2005, 2006) during these events remain intriguing questions for future investigations.

Materials and Methods

Materials. Full-length FtsY, FtsY-NG, Ffh, and 4.5S RNA were expressed and purified as described (Montoya, 1997b; Peluso, 2001). Single cysteine mutants of FtsY and Ffh were labeled with fluorescent dyes, N-(7-dimethylamino-4-methylcoumarin-3-yl) maleimide (DACM), the maleimide derivative of BODIPY-FL, or acrylodan (Invitrogen) as described (Zhang, 2009, 2008). RNCs bearing a hydrophobic signal sequence 1A9L were prepared as previously described (Zhang 2009; Schaffitzel, 2007). For GTPase assays, RNCs were further purified by sucrose gradient fractionation to collect monosomes free of GTPase contaminants as described (Zhang, 2009). Liposomes were prepared from *E. coli* polar lipid extract (Avanti Polar Lipids, inc.) as described (Lam, 2010; de Leeuw, 2000). n-Dodecyl-β-D-maltopyranoside (DDM) solid was from Anatrace.

4.5S RNA expression and purification. Expression and purification of 4.5S RNA was performed as described in Peluso, 2001. Briefly, DH5α cells transformed with pSN1 were grown in LB in the presence of 100 μg/ml and 1 mM IPTG for 10 h at 37°C. The cells were resuspended in 20 mM KOAc (pH 4.7) / 1 mM EDTA and extracted with acid phenol:chloroform. RNA was precipitated with isopropanol, dissolved in water, and further purified using gel filtration (TSK3000SW BAT). 4.5S RNA was precipitated with isopropanol, air dried, and stored as a pellet in ethanol at -20°C. The RNA was dissolved in the assay buffer (50 mM KHEPES, pH 7.5, 150 mM KOAc, 10 mM $Mg(OAc)_2$, 2 mM DTT) and quantitated using absorbance at 260 nm (1 A.U. = 40 μg/ml).

Fluorescence labeling. Site-specific labeling of FtsY and Ffh with fluorescent dyes was performed as described in Zhang, 2008, 2009. Single cysteine mutants of FtsY or Ffh were dialyzed in labeling buffer (50 mM KHEPES, pH 7.0, 300 mM NaCL, and 2 mM

ethylenediaminetetraacetic acid) and treated with 2 mM TCEP for 2 h. The reduced protein was incubated with 5-fold molar excess of the maleimide derivative of DACM or BodipyFL for 4 h, or with a 30-fold molar excess of acrylodan for 16h. The reaction was quenched with DTT, and the dye was separated from the labeled protein by gel filtration using Sephadex G-25 (Sigma). Labeling efficiency was determined using the following absorption co-efficients: DACM, $\varepsilon_{383} =$ 27, 000 $M^{-1}cm^{-1}$; BodipyFL, $\varepsilon_{504} =$ 79, 000 $M^{-1}cm^{-1}$; acrylodan, $\varepsilon_{391} =$ 20, 000 $M^{-1}cm^{-1}$.

Preparation of RNC. RNCs were generated and purified as described (Zhang 2009, Schafitzel 2007), using *in vitro* translation in a membrane-free extract from *E. coli* MRE600 cells. mRNA containing a truncated mature region of PhoA with 1A9L signal sequence and SecM stalling sequence was translated at 37°C for 25 min. Stalled RNCs were bound to a Strep-Tactin Sepharose column (IBA), eluted with desthiobiotin (Sigma), pelleted, and re-dissolved in the assay buffer. For GTPase assays, monosomes were purified using a 10-50% continuous sucrose gradient and untracentrifugation at 23 000 rpm 4°C for 15 h (SW-32, Beckman Coulter). The monosome fraction was pelleted at 55 000 rpm 4°C for 15 h (TLA 55, Beckman Coulter) and dissolved in assay buffer.

Expression and Purification of SecYEG. SecYEG containing N-terminally His_6-tagged SecY was expressed from plasmid pEK20 (du Plessis, 2009), a kind gift from Arnold Driessen. Triple charge reversal mutant of SecY (R255E, R256E, R357E) was generated based on pEK20 using the QuikChange mutagenesis protocol (Stratagene). SecYEG was expressed in BL21(DE3) cells and purified using previously described protocols (Dalal, 2010; van den Berg, 2004) with modifications. All steps were performed at 4 °C. Cells were lysed by sonication in KS300G buffer (50 mM KHEPES, pH 7.5, 300 mM NaCl, 10 % glycerol). After removal of intact cells (12,000 g, 20 min), membranes were collected by ultracentrifugation at 42,000 rpm for 45 min

(Ti45, Beckman Coulter), and extracted for 1 hour in KS100G buffer (50 mM KHEPES, pH 7.5, 100 mM NaCl, 10% glycerol) containing 1% DDM per 10 mg/mL total protein. The suspension was clarified by ultracentrifugation at 42,000 rpm for 32 min (Ti70, Beckman Coulter). The supernatant was purified by cation exchange on SP-Sepharose Fast Flow resin (GE Healthcare; 12 mL per 6 liters of cells) in KS100G/0.02% DDM, and eluted using a gradient of 100 – 1000 mM NaCl. Elution fractions containing SecYEG were further purified by affinity chromatography on Ni-NTA Agarose (Qiagen; 2 mL of resin per 6 L of cells). Protein was loaded and washed with KS300G/0.02% DDM/20 mM imidazole, and eluted with KS300G/0.02% DDM/300 mM imidazole. Purified SecYEG was dialyzed against 50 mM KHEPES, pH 7.5, 150 mM KOAc, 10% glycerol, 2 mM DTT, 0.02% DDM for 12 h. The concentration of SecYEG was determined using absorbance at 280 nm and the extinction coefficient of 71,000 $M^{-1}cm^{-1}$ (Kedrov, 2011).

Mutant SecYEG was purified by two rounds of immobilized metal affinity chromatography using Ni-Sepharose resin (GE Healthcare), using procedures similar to those described above except that 40 mM imidazole was used during binding and wash, and a 50 – 500 mM imidazole gradient was used during elution.

Fluorescence measurements. Fluorescence assays were performed as described (Zhang, 2009, 2008; Lam, 2010). All measurements were carried out at room temperature in assay buffer (50 mM KHEPES, pH 7.5, 150 mM KOAc, 10 mM $Mg(OAc)_2$, 2 mM DTT, and 0.01% Nikkol) supplemented with 0.02% DDM when necessary. Stability of the early complex was determined using FRET between DACM-labeled SRP Cys235 and BODIPY-FL-labeled FtsY Cys487. Equilibrium titrations were carried out with 40 nM SRP, 110 nM RNC where applicable, 100 μM GDP, with FtsY as a titrant. The data were fit to eq 1,

$$F_{obsd} = F_1 \times \frac{[\text{SRP}]+[\text{FtsY}]+K_d - \sqrt{([\text{SRP}]+[\text{FtsY}]+K_d)^2 - 4\times[\text{SRP}][\text{FtsY}]}}{2\times[\text{SRP}]} \qquad (1)$$

where F_{obsd} is the observed FRET, F_1 is the maximum FRET value at saturating FtsY concentrations, and K_d is the equilibrium dissociation constant of the early complex. Scattering due to SecYEG was subtracted before calculating the FRET values.

The stability of the closed/activated complex was determined using acrylodan-labeled SRP Cys235, with FtsY as the titrant. The stability of the activated complex was determined using acrylodan-labeled FtsY Cys356, with SRP as the titrant. Reactions were supplemented with 0.02% DDM. The data were fit to a quadratic equation similar to eq 1. When fluorescent FtsY was used, the denominator in eq 1 was replaced with 2×[FtsY].

The assembly kinetics of the closed complex from free SRP and FtsY was determined in the presence of GppNHp using FRET between DACM-labeled SRP Cys235 and BODIPY-FL-labeled FtsY Cys487, on a Fluorolog 3-22 (Jobin Yvon) as described (Zhang, 2009). The rate constant for association of SRP and FtsY (k_{on}) in the absence and presence of SecYEG was determined by measuring the observed rate of association (k_{obsd}) at varying FtsY concentrations as described above. The FtsY concentration dependence of k_{obsd} was fit to eq 2,

$$k_{obsd} = k_{on}[\text{FtsY}] + k_{off} \qquad (2)$$

in which k_{on} is the rate constant for complex assembly, and k_{off} is the rate constant for complex disassembly.

The rate of early $\rightarrow$ closed rearrangement was determined by pre-forming the early complex with 50 nM acrylodan-labeled SRP C235, 100 nM RNC, 5 μM FtsY in the absence or presence of SecYEG. Rearrangement to the closed complex was initiated by addition of 200 μM

GppNHp and monitored as an increase in acrylodan fluorescence on a Kintek stopped-flow apparatus. The data were fit to eq 3,

$$F_{obsd} = F_0 + (F_{max} - F_0)(1 - e^{-kt}) \quad (3)$$

in which F_0 and F_{max} are the initial and final fluorescence values, respectively, F_{obsd} is the observed fluorescence, and k is the rearrangement rate constant.

GTPase assay. GTP hydrolysis reactions were carried out in assay buffer, and were performed and analyzed as described (Peluso, 2001). Stimulated GTP hydrolysis of SRP with FtsY was determined using 40 nM SRP, 100 nM RNC where applicable, and increasing concentrations of FtsY as indicated. Wherever applicable, 8–12 μM SecYEG was added last and incubated with the reaction mixture for 10 min before initiation of reaction. The data were fit to eq 4,

$$k_{obsd} = k_{cat} \times \frac{[\text{FtsY}]}{K_m + [\text{FtsY}]} \quad (4)$$

in which k_{obsd} is the observed rate constant, k_{cat} is the rate constant at saturating FtsY and K_m is the concentration of FtsY required to reach the half-maximal rate.

Dose-dependent effects of SecYEG on GTP hydrolysis was measured using a pre-incubated mixture of 40 nM SRP, 100 nM RNC, and 3 or 8 μM of FtsY, to which increasing concentration of SecYEG was added before initiation of reaction. The data were fit to an equation analogous to eq 4, except that [FtsY] is replaced with [SecYEG], k_{cat} is replaced with k_{max}, and K_m is replaced with K_d.

Co-sedimentation assay. Interaction of SecYEG with RNC was determined using a co-sedimentation assay as described (Menetret, 2007; Fraunfeld, 2011) with modifications. 200 nM RNC was incubated with 1 μM SecYEG in assay buffer supplemented with 0.05% DDM for 35 min at room temperature. 35 μL of the solution were layered onto 200 μL of 30% sucrose solution in assay buffer supplemented with 0.05% DDM, and ultracentrifuged at 100,000 rpm for

12 min at 4 °C (TLA100, Beckman Coulter). The pellet was dissolved in SDS gel loading buffer and resolved on a 15% SDS gel.

Reconstitution of SecYEG into proteoliposomes. Purified SecYEG was reconstituted into *E.coli* liposomes as described (van der Does, 1998; Brundage, 1990; van der Does, 2003) with modifications. Before use, liposome suspension was activated in a bath sonicator until clear, and diluted with 0.5% Triton X-100 to 4 mg/mL. 200 μg of SecYEG (0.2 mg/ml in 10 mM TrisHCl, pH 8.0, 10% glycerol, 0.1% DDM, and 100 mM KCl) was mixed with 4 mg of liposomes and incubated for 30 min at 4 °C with gentle tumbling. 200 mg of Biobeads SM-2 (Bio-Rad Laboratories, Inc.), equilibrated in buffer A (50 mM TrisHCl, pH 8.0, 50 mM KCl, 1 mM DTT), was incubated with the SecYEG/liposome mixture with gentle stirring for 2 hours at 4 °C. The beads were removed by centrifugation at 500 g. The procedure was repeated with 200 mg of Biobeads and 4 hours of incubation in the second round, and 400 mg of Biobeads and overnight incubation in the third round. SecYEG proteoliposomes were collected by ultracentrifugation at 100,000 rpm for 30 min (TLA 100.3, Beckman Coulter) and dissolved in buffer A containing 10% glycerol. The concentration of SecYEG in proteoliposomes was determined using Coomassie staining on SDS-PAGE along with SecYEG standards of known concentration.

Post-translational translocation. Activity of SecYEG reconstituted into proteoliposomes was determined by examining SecA-dependent translocation of ^{35}S-labeled proOmpA and assayed using protection against proteinase K, as described (van der Does, 1998; Cunningham, 1989; van der Does, 2003). Briefly, *in vitro* translation of proOmpA was carried out in a wheat germ extract (Promega) in the presence of S^{35}-methionine at 26°C for 30 min and stopped by transferring to ice. Translocation of the substrate into SecYEG proteoliposomes was performed in the presence of SecA and ATP-regenerating system at 37°C for 15 minutes and stopped by

transferring the reaction to ice. Half of the reaction was treated with 0.02 mg/ml of proteinase K on ice for 15 min in the absence or presence of 1% Triton and quenched with phenylmethylsulfolyl fluoride (PMSF). Both reactions with and without PK treatment were precipitated with trichloroacetic acid (TCA), resolved on a denaturing gel, and quantified using autoradiography.

Cotranslational translocation assay. The coupled transcription/translation system used for cotranslational targeting assays was described previously (Saraogi, 2011). The signal sequence of PhoA was replaced with that of the SRP-dependent substrate DsbA and used as a model substrate. The coupled transcription/translation reaction containing ^{35}S-Met was supplemented with 5 mM GTP, 1 μM SRP, 1 μM FtsY, and either *E. coli* derived inner membrane vesicles (IMVs) or SecYEG proteoliposomes and carried out at 37°C for 30 min. The final concentration of SecYEG in the reaction was 2.2 μM. The reactions were quenched on ice, treated with 0.9 mg/mL of proteinase K for 15 min on ice in the absence or presence of 1% Triton and quenched with PMSF. The reaction was TCA precipitated and quantified as for the post-translational targeting reactions.

Acknowledgements

We thank Oded Lewinson in the Rees group for help and advice on liposome experiments. We would like to thank Ishu Saraogi for help in cotranslational targeting assays and valuable discussions, and members of the Shan laboratory for comments on the manuscript. This work was supported by NIH grant GM078024, and career awards from the Henry and Camille Dreyfus foundation and the David and Lucile Packard foundation to S.S. D. A. was supported by NIH/NRSA training grant 5T32GM07616.

References

Alami, M., Dalal, K., Lelj-Garolla, B., Sligar, S.G., and Duong, F. (2007). Nanodiscs unravel the interaction between the SecYEG channel and its cytosolic partner SecA. EMBO J. *26*, 1995-2004.

Angelini, S., Boy, D., Schiltz, E., and Koch, H.-G. (2006). Membrane binding of the bacterial signal recognition particle receptor involves two distinct binding sites. J. Cell Biol. *174*, 715-724.

Angelini, S., Deitermann, S., and Koch, H.-G. (2005). FtsY, the bacterial signal-recognition particle receptor, interacts functionally and physically with the SecYEG translocon. EMBO Rep. *6*, 476-481.

Becker, T., Bhushan, S., Jarasch, A., Armache, J.P., Funes, S., Jossinet, F., Gumbart, J., Mielke, T., Berninghausen, O., Schulten, K., Westhof, E., Gilmore, R., Mandon, E.C., and Beckmann, R. (2009). Structure of monomeric yeast and mammalian Sec61 complexes interacting with the translating ribosome. Science *326*, 1369-73.

Braig, D., Mircheva, M., Sachelaru, I., van der Sluis, E.O., Sturm, L., Beckman, R., and Koch, H.-G. (2011). Signal sequence-independent SRP-SR complex formation at the membrane suggests an alternative targeting pathway within the SRP cycle. Mol. Biol. Cell *22*, 2309-2323.

Brundage, L., Hendrick, J.P., Schiebel, E., Driessen, A.J., and Wickner, W. (1990). The purified *E. coli* integral membrane protein SecY/E is sufficient for reconstitution of SecA-dependent precursor protein translocation. Cell *62*, 649-657.

Campo, N., Tjalsma, H., Buist, G., Stepniak, D., Meijer, M., Veenhuis, M., Westermann, M., Muller, J.P., Bron, S., Kok, J., Kuipers, O.P., and Jongbloed, J.D. (2004). Subcellular sites for bacterial protein export. Mol. Microbiol. *53*, 1583-99.

Cannon, K.S., Or, E., Clemons, W. M., Jr., Shibata, Y., and Rapoport, T.A. (2005). Disulfide bridge formation between SecY and a translocating polypeptide localizes the translocation pore to the center of SecY. J. Cell Biol. *169*, 219-225.

Cross, B.C.S., Sinning, I., Luirink, J., and High, S. (2009). Delivering proteins for export from the cytosol. Nat. Rev. Mol. Cell. Biol. *10*, 255-264.

Cunningham, K., Lill, R., Crooke, E., Rice, M., Moore, K., Wickner, W., and Oliver, D. (1989). SecA protein, a peripheral protein of the *Escherichia coli* plasma membrane, is essential for the functional binding and translocation of proOmpA. EMBO J. *8*, 955-959.

Dalal, K., Chan, C.S., Sligar, S.G., and Duong, F. (2012). Two copies of SecY channel and acidic lipids are necessary to activate the SecA translocation ATPase. Proc. Natl. Acad. Sci. *109*, 4104-09.

Dalal, K., and Duong, F. (2010). Reconstitution of the SecY translocon in nanodiscs. Methods Mol. Biol. *619*, 145-156.

de Leeuw, E., te Kaat, K., Moser, C., Menestrina, G., Demel, R., de Kruijff, B., Oudega, B., Luirink, J., and Sinning, I. (2000). Anionic phospholipids are involved in membrane association of FtsY and stimulate its GTPase activity. EMBO J. *19*, 531-541.

Deville, K., Gold, V.A., Robson, A., Whitehouse, S., Sessions, R.B., Baldwin, S.A., Radford, S.E., and Collinson, I. (2011). The oligomeric state and arrangement of the active bacterial translocon. J. Biol. Chem. *286*, 4659-69.

Driessen, A.J.M., and Nouwen, N. (2008). Protein translocation across the bacterial cytoplasmic membrane. Annu. Rev. Biochem. *77*, 643-667.

Dubois, M., Gilles, K.A., Hamilton, J.K., Rebers, P.A., and Smith, F. (1956). Colorimetric method for determination of sugars and related substances. Anal. Chem. *28*, 350-356.

Duong, F. (2003). Binding, activation and dissociation of the dimeric SecA ATPase at the dimeric SecYEG translocase. EMBO J. *22*, 4375-84.

du Plessis, D.J., Berrelkamp, G., Nouwen, N., and Driessen, A.J. (2009). The lateral gate of SecYEG opens during protein translocation. J. Biol. Chem. *284*, 15805-14.

du Plessis, D.J., Nouwen, N., and Driessen, A.J. (2011). The Sec translocase. Biochim. Biophys. Acta *1808*, 851-865.

Egea, P.F., Shan, S., Napetschnig, J., Savage, D.F., Walter, P., and Stroud, R.M. (2004). Substrate twinning activates the signal recognition particle and its receptor. Nature *427*, 215-221.

Eitan, A., and Bibi, E. (2004). The core *Escherichia coli* signal recognition particle receptor contains only the N and G domains of FtsY. J. Bacteriol. *186*, 2492-2494.

Erez, E., Stjepanovic, G., Zelazny, A.M., Brugger, B., Sinning, I., and Bibi, E. (2010). Genetic evidence for functional interaction of the *Escherichia coli* signal recognition particle receptor with acidic lipids in vivo. J. Biol. Chem. *285*, 40508-14.

Fishov, I. and Woldringh, C.L. (1999). Visualization of membrane domains in *Escherichia coli*. Mol. Microbiol. *32*, 1166-72.

Fraunfeld, J., Gumbart, J., Sluis, E.O., Funes, S., Gartmann, M., Beatrix, B., Mielke, T., Berninghausen, O., Becker, T., Schulten, K., and Beckmann, R. (2011). Cryo-EM structure of the ribosome-SecYE complex in the membrane environment. Nat. Struct. Mol. Biol. *18*, 614-621.

Fulga, T.A., Sinning, I., Dobberstein, B., and Pool, M.R. (2001). SRβ coordinates sequence release from SRP with ribosome binding to the translocon. EMBO J. *20*, 2338-2347.

Gold, V.A., Robson, A., Bao, H., Romantsov, T., Duong, F., and Collinson, I. (2010). The action of cardiolipin on the bacterial translocon. Proc. Natl. Acad. Sci. USA *107*, 10044-9.

Gorlich, D., and Rapoport, T.A. (1993). Protein translocation into proteoliposomes reconstituted form purified components of the endoplasmic reticulum membrane. Cell *75*, 615-630.

Halic, M., Gartmann, M., Schlenker, O., Mielke, T., Pool, M.R., Sinning, I., and Beckman, R. (2006). Signal recognition particle receptor exposes the ribosomal translocon binding site. Science *312*, 745-7.

Hartl, F., Lecker, S., Schiebel, E., Hendrick, J.P., and Wickner, W. (1990). The binding cascade of SecB to SecA to SecY/E mediates preprotein targeting to the *E. coli* plasma membrane. Cell *63*, 269-279.

Jungnickel, B., and Rapoport, T.A. (1995). A posttargeting signal sequence recognition event in the endoplasmic reticulum membrane. Cell *82*, 261-270.

Karamanou, S., Gouridis, G., Papanikou, E., Sianidis, G., Gelis, I., Keramisanou, D., Vrontou, E., Kalodimos, C.G., and Economou, A. (2007). Preprotein-controlled catalysis in the helicase motor of SecA. EMBO J. *26*, 2904-2914.

Kedrov, A., Kusters, I., Krasnikov, V.V., and Driessen, A.J. (2011). A single copy of SecYEG is sufficient for preprotein translocation. EMBO J. *30*, 4387-97.

Kuhn, P., Weiche, B., Sturm, L., Sommer, E., Drepper, F., Warscheid, B., Sourjik, V., and Koch, H.-G. (2011). The bacterial SRP receptor, SecA and the ribosome use overlapping binding sites on the SecY translocon. Traffic *12*, 563-578.

Lam, V.Q., Akopian, D., Rome, M., Henningsen, D., and Shan, S. (2010). Lipid activation of the signal recognition particle receptor provides spatial coordination of protein targeting. J. Cell Biol. *190*, 623-635.

Menetret, J., Schaletzky, J., Clemons, Jr.W.M., Osborne, A.R., Skanland, S.S., Denison, C., Gygi, S.P., Kirkpatrick, D.S., Park, E., Ludtke, S.J., Rapoport, T.A., and Akey, C.W. (2007). Ribosome binding of a single copy of the SecY complex: implications for protein translocation. Mol. Cell *28*, 1083-1092.

Montoya, G., Svensson, C., Luirink, J., and Sinning, I. (1997a). Crystal structure of the NG domain from the signal-recognition particle receptor FtsY. Nature *385*, 365-368.

Montoya, G., Svensson, C., Luirink, J., and Sinning, I. (1997b). Expression, crystallization and preliminary x-ray diffraction study of FtsY, the docking protein of the signal recognition particle of *E. coli*. PROTEINS: Structure, Function, and Genetics *28*, 285-288.

Mothes, W., Jungnickel, B., Brunner, J., and Rapoport, T.A. (1998). Signal sequence recognition in cotranslational translocation by protein components of the endoplasmic reticulum membrane. J. Cell Biol. *142*, 355-364.

Park, E., and Rapoport, T.A. (2011). Preserving the membrane barrier for small molecules during bacterial protein translocation. Nature *473*, 239-42.

Parlitz, R., Eitan, A., Stjepanovic, G., Bahari, L., Bange, G., Bibi, E., and Sinning, I. (2007). *Escherichia coli* signal recognition particle receptor FtsY contains an essential and autonomous membrane-binding amphipathic helix. J Biol. Chem. *282*, 32176-84.

Peluso, P., Shan, S.O., Nock, S., Herschlag, D., and Walter, P. (2001). Role of SRP RNA in the GTPase cycles of Ffh and FtsY. Biochemistry *40*, 15224-33.

Poritz, M.A., Bernstein, H.D., Strub, K., Zopf, D., Wilhelm, H., and Walter, P. (1990). An *E. coli* ribonucleoprotein containing 4.5S RNA resembles mammalian signal recognition particles. Science *250*, 1111-1117.

Saraogi, I., Zhang, D., Chandrasekaran, S., and Shan, S. (2011). Site-specific fluorescent labeling of nascent proteins on the translating ribosome. J. Am. Chem. Soc. *133*, 14936-14939.

Schaffitzel, C., and Ban, N. (2007). Generation of ribosome nascent chain complexes for structural and functional studies. J. Struct. Biol. *158*, 463-71.

Shan, S., Chandrasekar, S., and Walter, P. (2007). Conformational changes n the GTPase modules of the signal recognition particle and its receptor drive initiation of protein translocation. J. Cell. Biol. *178*, 611-20.

Shan, S., Schmid, S.L., and Zhang, X. (2009). Signal recognition particle (SRP) and SRP receptor: a new paradigm for multistate regulatory GTPases. Biochemistry *48*, 6696-6704.

Shan, S., Stroud, R.M., and Walter, P. (2004). Mechanism of association and reciprocal activation of two GTPases. PLOS Biology *2*, 1572-1581.

Shen, K. and Shan, S. (2010). Transient tether between the SRP RNA and SRP receptor ensures efficient delivery during cotranslational protein targeting. Proc. Natl. Acad. Sci. USA *107*, 7698-703.

Shiomi, D., Yoshimoto, M., Homma, M., and Kawagishi, I. (2006). Helical distribution of the bacterial chemoreceptor via colocalization with the Sec protein translocation machinery. Mol. Microbiol. *60*, 894-906.

Song, W., Raden, D., Mandon, E.C., and Gilmore, R. (2000). Role of Sec61α in the regulated transfer of the ribosome-nascent chain complex from the signal recognition particle to the translocation channel. Cell *100*, 333-343.

van den Berg, B., Clemons, Jr. W.M., Collinson, I., Hartmann, E., Harrison, S.C., and Rapoport, T.A. (2004). X-ray structure of a protein-conducting channel. Nature *427*, 36-44.

van der Does, C., de Keyzer, J., van der Laan, M., and Driessen, A.J.M. (2003). Reconstitution of purified bacterial preprotein translocase in liposomes. Methods in Enzymology *372*, 86-98.

van der Does, C., Manting, E.H., Kaufmann, A., Lutz, M., and Driessen, A.J. (1998). Interaction between SecA and SecYEG in micellar solution and formation of the membrane-inserted state. Biochemistry *37*, 201-210.

Vanounou, S., Parola, A.H., and Fishov, I. (2003). Phosphatidylethanolamine and phosphatidylglycerol are segregated into different domains in bacterial membrane. A study with pyrene-labelled phospholipids. Mol. Microbiol. *49*, 1067-79.

Walter, P., and Blobel, G. (1981). Translocation of protein across the endoplasmic reticulum. III. Signal recognition particle (SRP) causes signal sequence-dependent and site-specific arrest of chain elongation that is released by microsomal membranes. J. Cell Biol. *91*, 545-550.

Walter, P., and Johnson, A.E. (1994). Signal sequence recognition and protein targeting to the endoplasmic reticulum membrane. Annu. Rev. Cell Biol. *10*, 87-119.

Zhang, X., Kung, S., and Shan, S. (2008). Demonstration of a multistep mechanism for assembly of the SRP•SR receptor complex: implications for the catalytic role of SRP RNA. J. Mol. Biol. *381*, 581-593.

Zhang, X., Schaffitzel, C., Ban, N., and Shan, S. (2009). Multiple conformational switches in a GTPase complex control co-translational protein targeting. Proc. Natl. Acad. Sci. USA *106*, 1754-1759.

Zhou, J., and Xu, Z. 2003. Structural determinants of SecB recognition by SecA in bacterial protein translocation. Nat. Struct. Biol. *10*, 942-947.

Figures

Figure 1

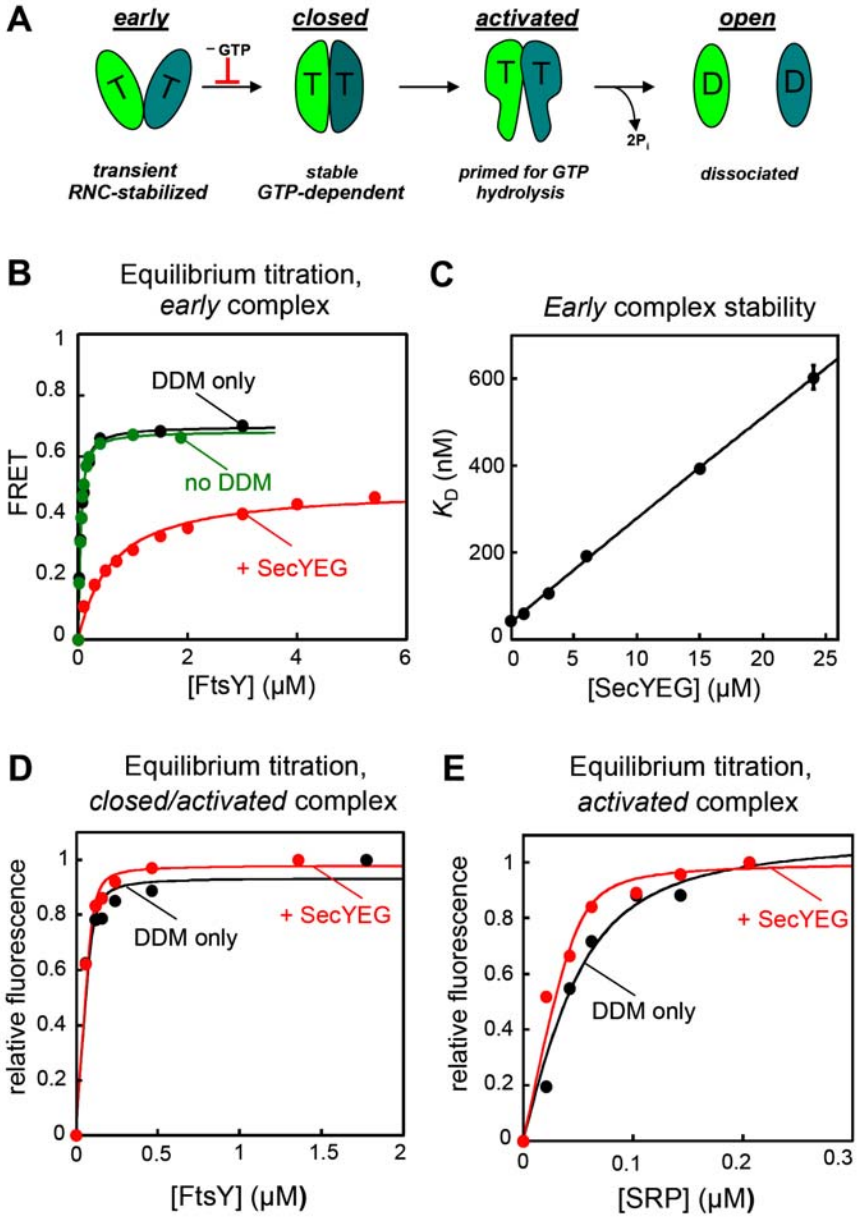

F

	K_D (nM)			FRET
	early	*closed/activated*	*activated*	*early*
DDM only	33 ± 7.3	5.3	25.4 ± 8.6	0.70 ± 0.02
+SecYEG	≥ 592 ± 28	6.5	6.6 ± 4.3	0.49 ± 0.06

Figure 1. SecYEG destabilizes the early intermediate in the RNC•SRP•FtsY complex. (**A**) Conformational states of the SRP•SR complex during its GTPase cycle. Blue denotes SRP, green denotes SR, and T and D denote GTP and GDP, respectively. (**B**) Equilibrium titration of the early complex in the absence (green) and presence of 0.05% DDM (black) or 24 μM SecYEG (red). Representative data out of four replicates are shown. The data were fit to eq 1 in the Methods, and gave K_d values and FRET end points reported in (E). (**C**) Effect of SecYEG on the stability of the early complex. The K_d values of the early complex were determined as in (A) at indicated concentrations of SecYEG. The line is a linear fit to the data. (**D**) Equilibrium titration of the closed/activated complex was performed in the presence of 0.02% DDM (black) or 12 μM SecYEG (red), using 100 nM acrylodan-labeled SRP, 230 nM RNC, and 200 μM GppNHp. Representative data out of two replicates are shown. The data were fit to eq 1 in the Methods and gave K_d values reported in (F). (**E**) Equilibrium titration of the activated complex was performed in the presence of 0.01% DDM (black) or 10 μM SecYEG (red), using 50 nM acrylodan-labeled FtsY C356, 300 nM RNC, and 200 nM GppNHp. Representative data from two replicates are shown. The data points of the two titrations overlapped at 0.2 μM SRP, which may render this data point for the –SecYEG titration less visible. The data were fit to eq 1 and gave K_d values reported in (F). (**F**) Summary of the K_d values and FRET end points from the experiments in panels A-D. The values are averages of 2–4 experiments ± standard deviation.

Figure 2

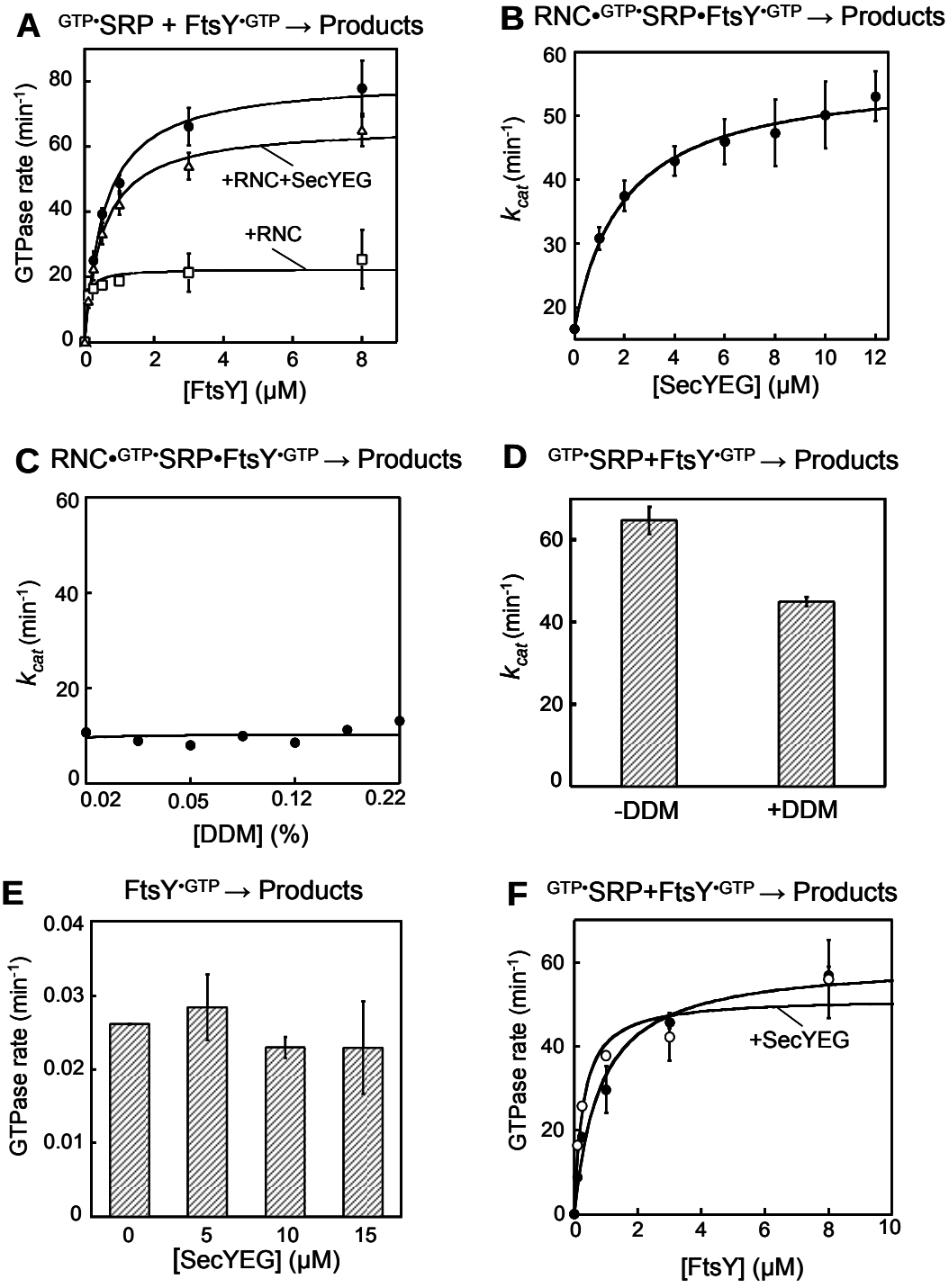
A GTP•SRP + FtsY•GTP → Products
GTPase rate (min-1)
+RNC+SecYEG
+RNC
[FtsY] (μM)
B RNC•GTP•SRP•FtsY•GTP → Products
kcat (min-1)
[SecYEG] (μM)
C RNC•GTP•SRP•FtsY•GTP → Products
kcat (min-1)
[DDM] (%)
D GTP•SRP+FtsY•GTP → Products
kcat (min-1)
-DDM
+DDM
E FtsY•GTP → Products
GTPase rate (min-1)
[SecYEG] (μM)
F GTP•SRP+FtsY•GTP → Products
GTPase rate (min-1)
+SecYEG
[FtsY] (μM)

Figure 2. SecYEG re-activates GTP hydrolysis from the RNC•SRP•FtsY complex. (**A**) Stimulated GTP hydrolysis of SRP with FtsY in the absence (circles) and presence (squares) of RNC, and in the presence of both RNC and SecYEG (triangles). The data are the average of three experiments ± standard deviation. The data were fit to eq 4 in the Methods and gave k_{cat} values of 80, 22 and 66 min^{-1} for the SRP•FtsY, RNC•SRP•FtsY, and RNC•SRP•FtsY•SecYEG complexes, respectively. (**B, C**) Effect of SecYEG (B) or DDM (C) on GTP hydrolysis from the RNC•SRP•FtsY complex. The data in (B) were fit to eq 4 in Methods and gave a K_d value of 2 μM and a k_{max} value of 57 min^{-1}. The data in (B) are the average of two experiments ± standard deviation. (**D**) DDM reduces GTP hydrolysis rate from the SRP•FtsY complex. k_{cat} values were determined as in (A) in the absence and presence of 0.02% DDM. The data are the average of two experiments ± standard deviation. (**E**) SecYEG does not affect the basal GTPase activity of FtsY. Reactions were performed in the presence of 4 μM FtsY, 100 μM GTP, and indicated concentrations of SecYEG. The data are the average of two experiments ± standard deviation. (**F**) In the absence of RNC, SecYEG does not significantly affect GTP hydrolysis from the SRP•FtsY complex. The data are the average of two experiments ± standard deviation. The data were fit to eq 2 in the Methods, and gave k_{cat} values of 60 and 51 min^{-1} in the absence (closed) and presence (open) of 12 μM SecYEG, respectively.

Figure 3

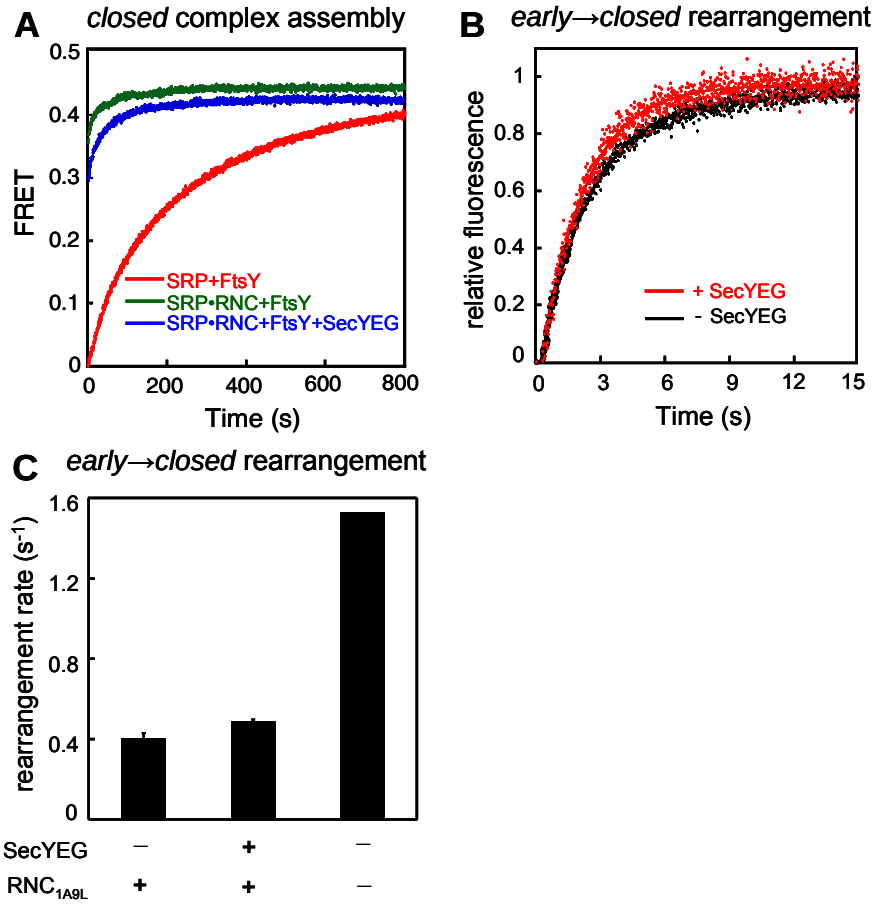

Figure 3. SecYEG forms a quaternary complex with RNC, SRP and FtsY. (**A**) Kinetics of closed complex assembly was measured in the absence (red) and presence of 100 nM RNC (green), and in the presence of 100 nM RNC and 7 μM SecYEG (blue). Reactions contained 40 nM DACM-labeled SRP, 100 nM BODIPY-FL-labeled FtsY, and 200 μM GppNHp. Representative data from three replicates are shown. (**B**) Kinetics of rearrangement of the RNC•SRP•FtsY complex from the early to the closed conformation, in the absence (black) and presence (red) of 12 μM SecYEG. Representative data from two replicates are shown. Single exponential fits to the data gave the rearrangement rate constants of 0.403 ± 0.027 s^{-1} and 0.489 ± 0.008 s^{-1} with and without SecYEG, respectively. (**C**) Summary of the *early* → *closed* rearrangement rate constants. The value of 1.5 s^{-1} was obtained in the absence of SecYEG and RNC and is shown for comparison.

Figure 4

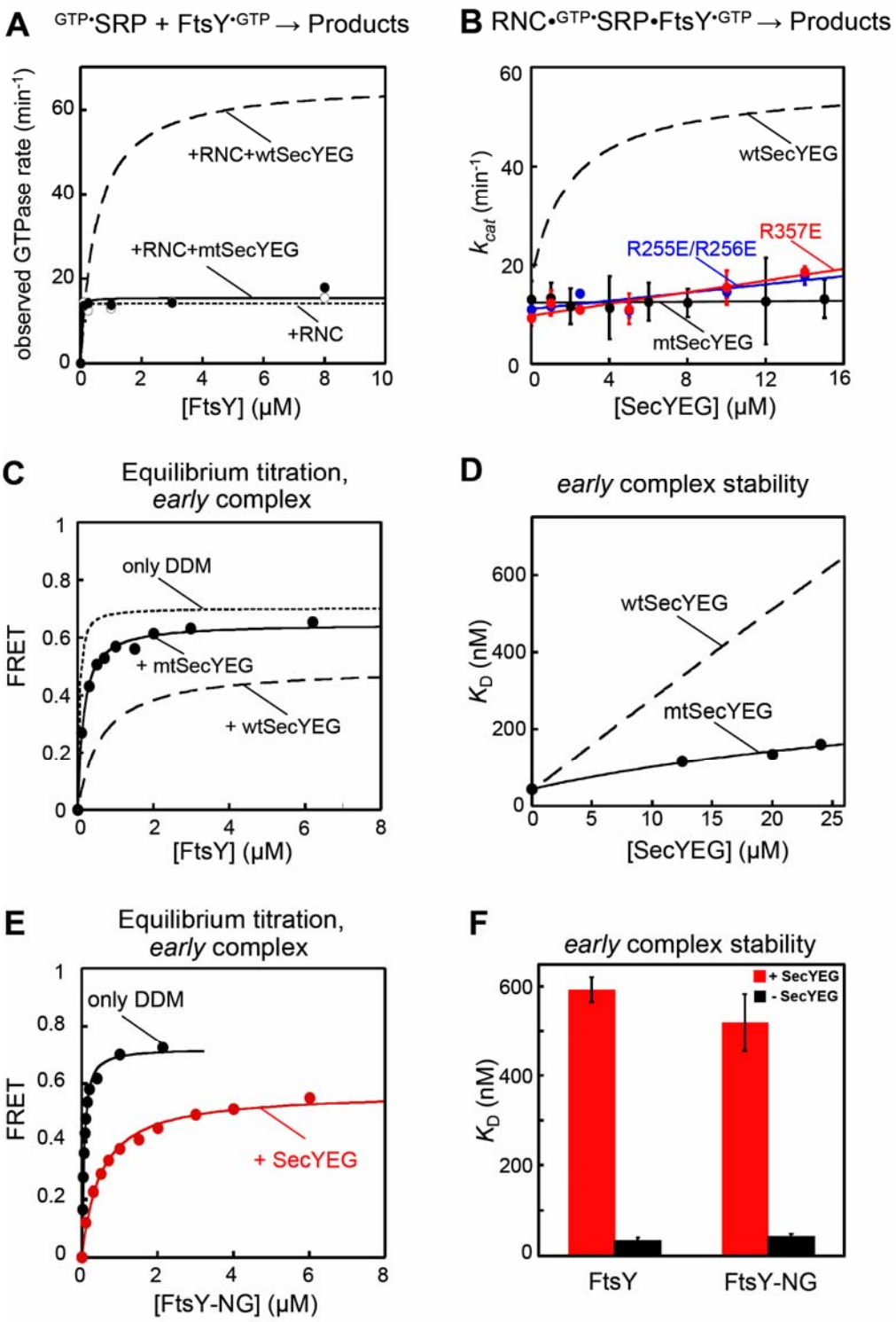
A
GTP•SRP + FtsY•GTP → Products
observed GTPase rate (min-1)
+RNC+wtSecYEG
+RNC+mtSecYEG
+RNC
[FtsY] (μM)
B
RNC•GTP•SRP•FtsY•GTP → Products
kcat (min-1)
wtSecYEG
R357E
R255E/R256E
mtSecYEG
[SecYEG] (μM)
C
Equilibrium titration, early complex
FRET
only DDM
+ mtSecYEG
+ wtSecYEG
[FtsY] (μM)
D
early complex stability
KD (nM)
wtSecYEG
mtSecYEG
[SecYEG] (μM)
E
Equilibrium titration, early complex
FRET
only DDM
+ SecYEG
[FtsY-NG] (μM)
F
early complex stability
KD (nM)
+ SecYEG
- SecYEG
FtsY
FtsY-NG

Figure 4. Mutations in basic cytosolic loops of SecYEG abolish its stimulatory effects. (**A**) Stimulated GTP hydrolysis between the RNC-bound SRP and FtsY in the absence (open circles) and presence (closed circles) of 12 μM mtSecYEG. The data were fit to eq 4. The dashed line is the data for wild type SecYEG from Figure 2A and is shown for comparison. Representative data from two replicates are shown. (**B**) Effect of SecYEG charge reversal mutants on GTP hydrolysis from the RNC•SRP•FtsY complex. Solid black, R255E/R256E/R357 (mtSecYEG); red, R357E; blue, R255E/R256E. Representative data from two or more replicates are shown. The dashed line is the data for wild type SecYEG from Figure 2B and is shown for comparison. (**C**) Equilibrium titration of the early complex in the presence of 24 μM mtSecYEG (solid circles). Representative data from three replicates are shown. The data were fit to eq 1 and gave a K_d value of 162 ± 4 nM. Titration in the presence of DDM (dotted) and wild type SecYEG (dashed) are from Figure 1 and are shown for comparison. (**D**) Effect of mtSecYEG on the stability of the early complex. K_d values were determined as described in (C). The data with wild type SecYEG (dashed line) from Figure 1B is shown for comparison. (**E**) Equilibrium titration of the early targeting complex formed by FtsY-NG in the presence of 0.05% DDM (black) or 24 μM SecYEG (red). Representative data from two replicates are shown. The data were fit to Eq 1 in Methods, and K_d values are reported in (F). (**F**) Summary of the effects of SecYEG on the stability of the early targeting complex formed with full-length FtsY and FtsY-NG. The values with full-length FtsY are from Figure 1 and are shown for comparison. Error bars denote standard deviation from 2-3 experiments.

Figure 5

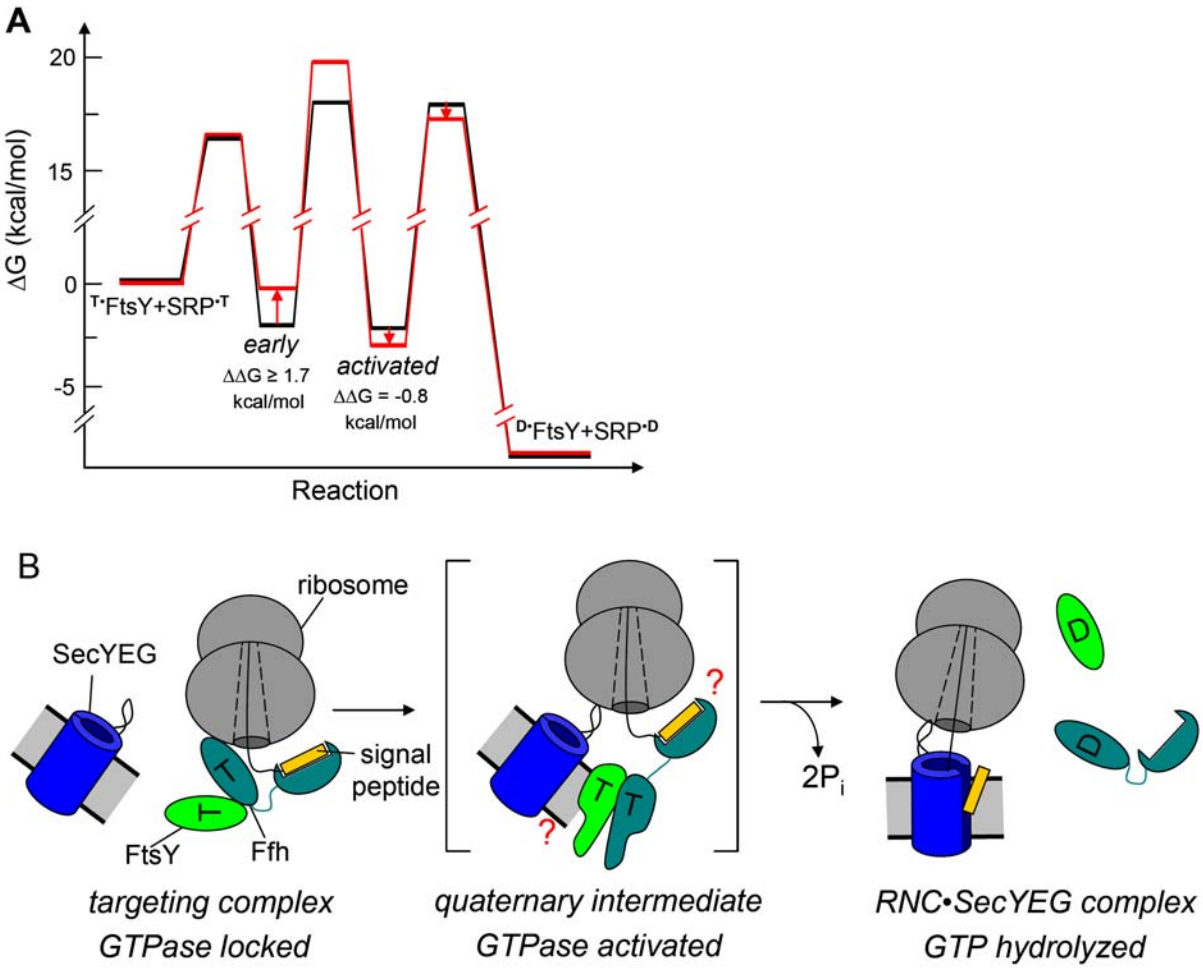

Figure 5. SecYEG drives conformational changes in the RNC•SRP•FtsY complex. (**A**) Free energy profile for the FtsY-SRP interaction in the absence (black) and presence (red) of SecYEG. The red arrows denote the effect of SecYEG on the conformational states. Activation energies were calculated from the determined rate constants using $\Delta G^{\ddagger} = -RT\ln[kh/(k_BT)]$, where R = 1.987 cal•K^{-1}•mol^{-1}, $h = 1.58 \times 10^{-37}$ kcal•s, $k_B = 3.3 \times 10^{-27}$ kcal•K^{-1}, and T = 298 K. The relative free energies of the conformational states were calculated from the equilibrium stability of the complexes using $\Delta G = -RT\ln K$, where K is the equilibrium constant. A standard state of 1 μM was used. T denotes GTP, D denotes GDP. (**B**) Model for the role of SecYEG in driving GTPase rearrangements in the targeting complex and completing cotranslational protein targeting, as described in the text. The M-domain of Ffh that binds the signal sequence is also shown. The SRP RNA is not depicted for clarity. ? denotes unanswered questions regarding the fate of the signal sequence and the interaction of SecYEG with FtsY in the putative quaternary intermediate.

Figure S1

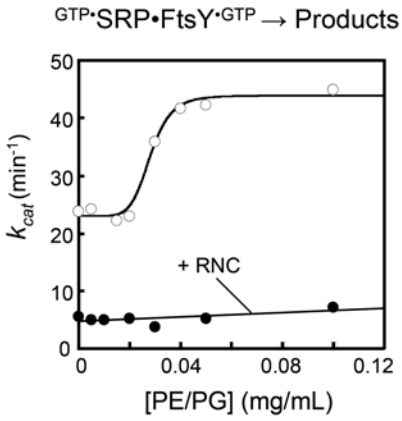

Figure S1. Liposomes do not re-activate GTPase activity of the targeting complex in the presence of RNC. The effect of increasing lipid concentration on the rate of GTP hydrolysis from the FtY•SRP complex was measured using 50 nM SRP, 10 μM FtsY, and saturating GTP in the absence (open circles) and presence of (solid circles) of 100 nM RNC_{1A9L}.

Figure S2

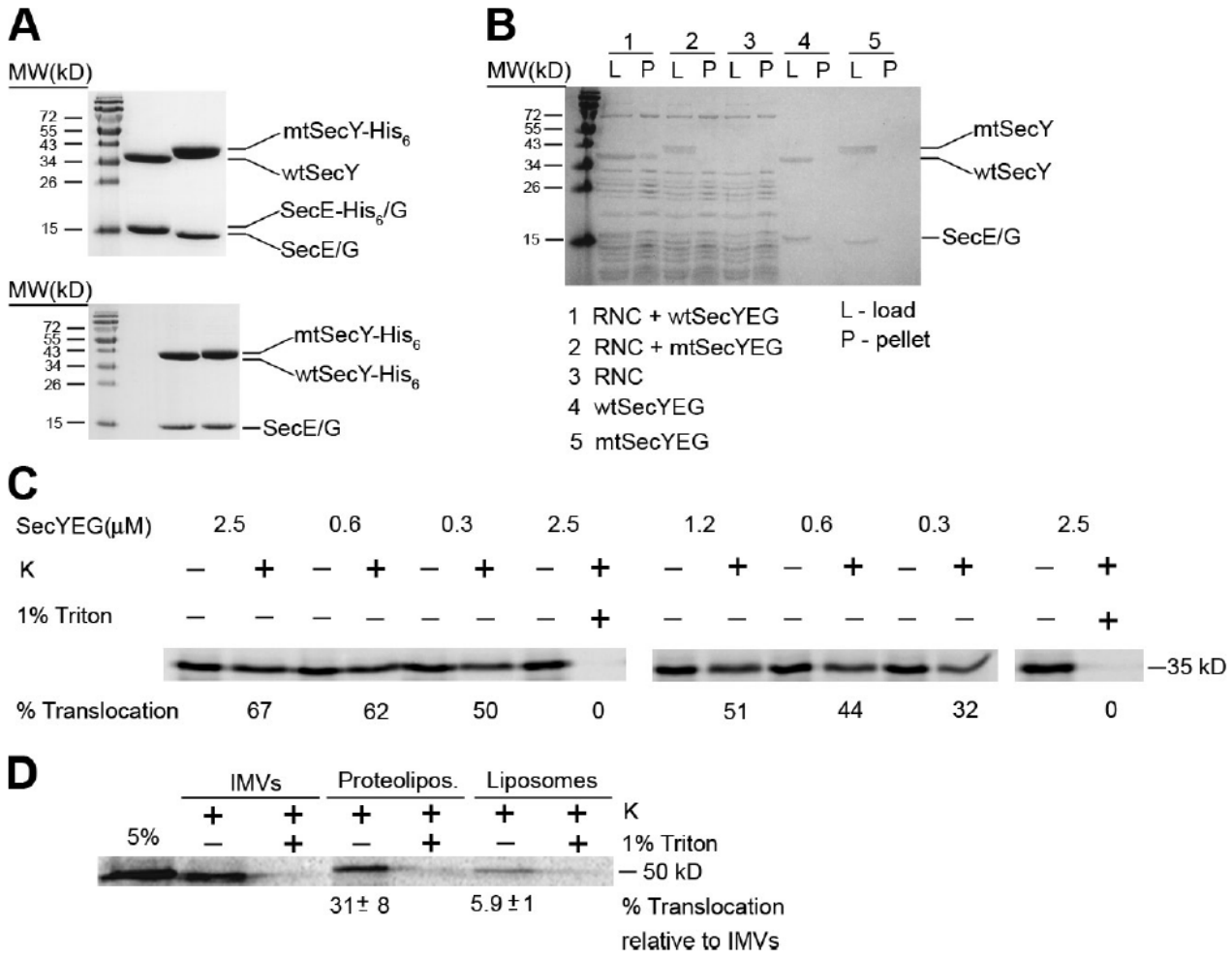
A
MW(kD)
72
55
43
34
26
15
mtSecY-His6
wtSecY
SecE-His6/G
SecE/G
MW(kD)
mtSecY-His6
wtSecY-His6
SecE/G
B
1 2 3 4 5
MW(kD)
L P L P L P L P L P
mtSecY
wtSecY
SecE/G
1 RNC + wtSecYEG
2 RNC + mtSecYEG
3 RNC
4 wtSecYEG
5 mtSecYEG
L - load
P - pellet
C
SecYEG(μM) 2.5 0.6 0.3 2.5 1.2 0.6 0.3 2.5
K
1% Triton
35 kD
% Translocation 67 62 50 0 51 44 32 0
D
IMVs
Proteolipos.
Liposomes
K
5%
1% Triton
50 kD
31± 8
5.9 ± 1
% Translocation
relative to IMVs

Figure S2. Purification and activity of SecYEG. (**A**) Wild-type (wt) and the triple charge reversal mutant (mt) SecYEG were expressed and purified as described in Methods and resolved on a 15% SDS gel. SecY- and SecE-His_6 tagged constructs were used to ensure that the affinity tag does not contribute to ribosome binding. The first panel shows wtSecYE_{His6}G and mtSecY$_{His6}$EG resolved on a denaturing gel. In the second panel, both wtSecYEG and mtSecYEG are tagged at SecY. Charge reversal of basic residues slightly reduces the mobility of SecY. (**B**) Co-sedimentation assay examining the binding of wtSecYEG and mtSecYEG to RNC, performed as described in the Methods. L denotes the load before centrifugation, P denotes the pellet. (**C**) SecYEG-proteoliposomes mediate SecA-catalyzed translocation of proOmpA. The concentrations of SecYEG in proteoliposomes are indicated above the gel. K denotes proteinase K. '–' denotes equivalent amount of proOmpA prior to proteinase K treatment. Where indicated, 1% Triton X-100 was added before treatment with proteinase K. Gels from two independent experiments are shown. (**D**) SecYEG proteoliposomes mediate SRP-dependent translocation of DsbA-PhoA substrate. Combined transcription/translation/translocation of DsbA-PhoA was carried out in the presence of either *E. coli* inner membrane vesicles (IMVs), SecYEG proteoliposomes (3.7 μM SecYEG), or empty liposomes. The reactions were treated with proteinase K in the absence and presence of 1% Triton to assess the extent of translocation. Five percent of the translation reaction were loaded as reference. Representative data from two replicate experiments are shown.

Figure S3

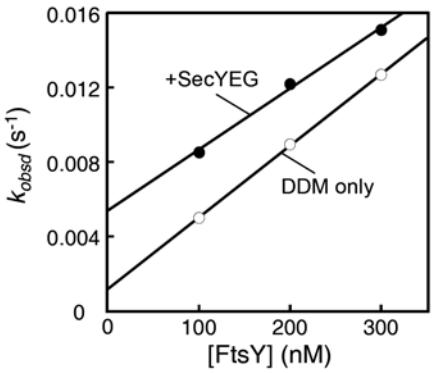

Figure S3. SecYEG does not affect SRP-FtsY complex assembly kinetics in the absence of RNC. Observed complex formation rate constants are determined as described in Methods. Linear fits of the data gave k_{on} values of 3.85×10^4 $M^{-1}s^{-1}$ and 3.28×10^4 $M^{-1}s^{-1}$ in the absence and presence of SecYEG, respectively.

CHAPTER 3

Regulation of Cargo Recognition, Commitment, and Unloading Drives Cotranslational Protein Targeting

This chapter has been published as:

*Saraogi, I., *Akopian, D., Shan, SO. 2014. Journal of Cell Biology

(*equal contribution)

Abstract

Efficient and accurate protein localization is essential to cells and requires protein-targeting machineries to both effectively capture the cargo in the cytosol and productively unload the cargo at the membrane. To understand how these challenges are met, we followed the interaction of translating ribosomes during their targeting by the signal recognition particle (SRP) using a site-specific fluorescent probe in the nascent protein. We show that initial recruitment of SRP receptor (SR) selectively enhances the affinity of SRP for correct cargos, thus committing SRP-dependent substrates to the pathway. Real time measurement of cargo transfer from the targeting to translocation machinery reveals multiple factors that drive this event, including GTPase rearrangement in the SRP•SR complex, stepwise displacement of SRP from the ribosome and signal sequence by SecYEG, and elongation of the nascent polypeptide. Our results elucidate how active and sequential regulation of the SRP-cargo interaction drives efficient and faithful protein targeting.

Introduction

To ensure proper biogenesis of proteins in the crowded cellular environment, cells have evolved sophisticated molecular machineries that are recruited to the polypeptide exit site of the ribosome early in translation (Kramer et al., 2009). An example is the universally conserved Signal Recognition Particle (SRP), which delivers ~30% of the proteome to the eukaryotic endoplasmic reticulum (ER) or the bacterial plasma membrane (Keenan et al., 2001). SRP recognizes the N-terminal signal sequence of a protein as it emerges from the translating ribosome (Fig. 1A, Recognition). The ribosome nascent chain complex (RNC or cargo) is delivered to the target membrane via interactions of SRP with its receptor (SR) (Fig. 1A, Targeting). At the membrane, RNC is transferred to the Sec61p or SecYEG translocation machinery (Rapoport, 2007), where the nascent protein is either integrated into or translocated across the membrane (Cross et al., 2009). GTP hydrolysis disassembles SRP and SR and recycles them for additional rounds of targeting (Fig. 1A, last step).

Co-translational protein targeting involves a series of molecular events that present conflicting requirements for the targeting machinery. In the cytosol, SRP must efficiently select its substrates from ~100-fold excess of translating ribosomes. SRP does so by interacting with RNC via two domains in the universally conserved SRP54 protein (Ffh in bacteria) (Poritz et al., 1990). The Ffh M-domain binds the signal sequence of the nascent protein (Hainzl et al., 2011; Janda et al., 2010; Keenan et al., 1998) while its N-domain interacts with L23 and L29 at the polypeptide exit site of the ribosome (Gu et al., 2003; Halic et al., 2006a; Pool et al., 2002; Schaffitzel et al., 2006). How this bidentate interaction enables effective and accurate substrate selection by SRP remains unclear.

Cargo-bound SRP is targeted to the membrane through the binding of its NG-domain, composed of the N-domain and a GTPase, G-domain, to a homologous NG-domain in the SRP receptor (FtsY in bacteria) (Egea et al., 2004; Focia et al., 2004). SRP and FtsY belong to a novel class of GTPases regulated by GTP-dependent dimerization (Gasper et al., 2009; Shan et al., 2009). Discrete conformational changes, from a transient '*early*' intermediate upon initial FtsY binding, to a GTP-stabilized '*closed*' complex and finally an '*activated*' complex, occur in the SRP•SR dimer that culminate in their GTPase activation (Shan et al., 2004; Zhang et al., 2011; Zhang et al., 2009). These rearrangements are strongly regulated by the cargo, anionic phospholipids and the SecYEG translocon, and thus couple the recognition of cargo by SRP to its delivery to the membrane (Akopian et al., 2013; Braig et al., 2009; Lam et al., 2010; Stjepanovic et al., 2011; Zhang et al., 2009). For example, the cargo for SRP strongly stabilizes the otherwise labile *early* intermediate, and thus accelerates formation of the *closed* targeting complex (Zhang et al, 2009). Whether and how the SRP/SR GTPases reciprocally regulate the SRP-cargo interaction is poorly understood. This regulation would be particularly important at the target membrane, where SRP must switch from a 'cargo-binding' mode to a 'cargo-releasing' mode.

Handover of the cargo to the SecYEG translocon remains one of the least understood aspects of the pathway. SecYEG binds the translating ribosome via its cytosolic loops c4 and c5 (Cheng et al., 2005; Menetret et al., 2007). A lateral gate formed by two transmembrane helices (TM2 and TM7) of SecY binds signal sequence (du Plessis et al., 2009; van den Berg et al., 2004). As both SRP and SecYEG bind RNC via L23 on the ribosome and the signal sequence, the transfer of RNC to SecYEG (Jungnickel and Rapoport, 1995; Song et al., 2000) would require RNC to first detach from SRP. How the loss of cargo during this handover is prevented remains unclear. Recent studies suggest that such abortive events are minimized by formation of a

RNC•SRP•SR•SecYEG quaternary intermediate (Akopian et al., 2013; Shen et al., 2012); however the precise molecular mechanism of cargo transfer is not understood.

A major limitation in addressing these questions has been the lack of quantitative assays that directly and quantitatively report on the interaction of the translating ribosome with SRP and SecYEG. Recently, we developed an efficient method to site-specifically label the nascent protein on a translating ribosome using a fluorescent non-natural amino acid (Saraogi et al., 2011). Close to 100% incorporation efficiency was achieved, yielding milligram quantities of purified fluorescent RNC (Saraogi et al., 2011). This allowed us, for the first time, to quantitatively measure the dynamic changes in the interaction of the translating ribosome with SRP and SecYEG at discrete stages of the targeting reaction, and generate a detailed molecular picture of the SRP pathway. We found that the targeting and translocation machineries actively regulate the conformation, energetics, and dynamics of the cargo-SRP interaction, thereby ensuring the efficient capture, delivery, and coordinated unloading of the cargo.

Results

General experimental design

To analyze the interaction of SRP with the nascent protein, we used Förster Resonance Energy Transfer (FRET) between a donor fluorophore on the nascent protein (Fig 1B, green star) and an acceptor fluorophore on SRP (Fig 1B, red star). We generated stalled RNCs of 85 residues with a fluorescent probe, 7-hydroxycoumaryl ethylglycine (Cm), incorporated at the signal sequence (Fig 1C, asterisk) (Saraogi et al., 2011). BODIPY-FL, a FRET acceptor for Cm, was introduced in the SRP M-domain at residue 421 (Fig. 1B, M-domain pair) or the SRP N-domain at residue 11 (Fig. 1B, N-domain pair). Structural data (Halic et al., 2006a) suggests that both positions lie within < 30 Å of the signal sequence in the RNC•SRP complex, well within the estimated Förster radius of this dye-pair (Saraogi et al., 2011).

Using both FRET pairs, we measured and compared the energetics, dynamics and conformation of SRP-RNC interactions at every stage of the SRP pathway, from the RNC•SRP complex to the *early* and *closed* RNC•SRP•SR targeting complexes. Finally, the transfer of cargo from the SRP•SR to SecYEG complex was measured using a combination of the FRET probes (Fig. 1B) and the increase in Cm fluorescence upon binding SecYEG, which reports on a functional interaction of the signal sequence with the translocon.

As model SRP substrates we used two engineered signal sequences, 1A9L and 3A7L (Fig 1C), shown to direct efficient co-translational protein targeting (Doud et al., 1993; Zhang et al., 2010). To understand how SRP rejects borderline substrates, we used the alkaline phosphatase (phoA) signal sequence (Doud et al., 1993; Zhang et al., 2010), which is primarily targeted via the Sec pathway. A mutant signal sequence, in which two leucine residues in 3A7L are replaced by arginine, serves as a negative control (Fig. 1C, 3A5L2R).

Ribosomes bearing SRP substrates are selectively retained by SRP

We first asked if SRP could effectively discriminate between signal sequences during cargo recognition (Fig 2A, boxed). Equilibrium titrations based on the M-domain FRET pair (Fig. 1B, left) showed that RNC_{3A7L} bound to SRP with a dissociation constant (K_d) of 3 nM, whereas the binding of RNC_{PhoA} was 7-fold weaker (Fig 2B). RNC_{3A5L2R} did not induce a significant FRET signal, supporting specificity of the assay (Fig 2B, green and Fig S1A).

To more accurately determine the binding affinity between RNC and SRP and to gain information into the dynamics of this interaction, we measured the association (k_{on}) and dissociation (k_{off}) rate constants for their binding. SRP bound to RNC_{3A7L} with a k_{on} value of 2.1 $x10^6$ $M^{-1}s^{-1}$ (Fig 2C & F and Fig S1B), similar to that of the more hydrophobic RNC_{1A9L} (Fig 1C; Fig 2C, dotted line & Fig 2F) (Saraogi et al., 2011). RNC_{PhoA} bound SRP three-fold more rapidly (Fig 2C, F & Fig S1C). Nevertheless, SRP dissociated from RNC_{PhoA} at a rate comparable to non-translating ribosomes (Fig 2D, E, F and Fig S1D). In contrast, the dissociation of RNC_{3A7L} and RNC_{1A9L} was 20- and 1000-fold slower, respectively (Fig 2D, F). These findings are consistent with a recent report (Holtkamp et al., 2012) (see Fig S1E and Discussion for a detailed explanation). Thus, SRP binds quickly to ribosomes with or without SRP substrates, but RNCs bearing strong signal sequences form kinetically more stable complexes with SRP and hence persist much longer.

FtsY actively regulates the SRP-cargo interaction

In the next step, RNC is targeted to the membrane via the SRP-SR interaction (Fig 3A, boxed), which proceeds through an *early* intermediate (Zhang et al., 2008). This intermediate is strongly stabilized by the RNC (Zhang et al., 2009), and its stability directly correlates with the rate of formation of the *closed* SRP•SR complex (Shen and Shan, 2010; Shen et al., 2011; Zhang et al.,

2008; Zhang et al., 2010; Zhang et al., 2009) and with co-translational protein targeting (Zhang et al., 2008). As the *early* complex can form with or without GTP, but its subsequent rearrangements are strictly GTP-dependent (Zhang et al., 2008; Zhang et al., 2009), a homogenous *early* targeting complex can be isolated by incubating RNC, SRP and SR in the absence of GTP. We tested how the initial recruitment of SR modulates the dynamics and stability of the RNC-SRP interaction. Compared to free SRP, the SRP•SR *early* complex bound to RNC_{3A7L} 6-fold faster (Figs 3B & S2) and dissociated from it 10-fold slower (Fig 3C). Overall, the interaction of RNC_{3A7L} with SRP was stabilized 80-fold upon formation of the *early* targeting complex, bringing the K_d value to the picomolar range (Fig 3F). In contrast, the corresponding stabilization for RNC_{PhoA} was less than 4-fold (Fig 3B, C, & F). Thus, the initial recruitment of FtsY increases the specificity of SRP for correct substrates from 7-fold in the RNC•SRP complex to >100-fold in the *early* targeting complex (Fig 3F).

While a strong SRP-RNC interaction is beneficial in the cytosol, it will render cargo release at the target membrane difficult. Notably, anionic phospholipids strongly stabilizes the *closed* SRP•SR complex and reciprocally, formation of the *closed* complex exposes a lipid binding helix of FtsY and allows the targeting complex to associate much more stably with the membrane (Braig et al., 2011; Lam et al., 2010; Stjepanovic et al., 2011). We therefore asked whether rearrangement of the RNC•SRP•SR complex from the *early* to the *closed* state (Fig 3A), which is coupled to stable membrane attachment of the targeting complex, could help overcome this barrier. Interestingly, in a *closed* targeting complex assembled using the non-hydrolyzable GTP analogue GppNHp, RNC-SRP association was 3–4 fold slower and their dissociation was 10-fold faster compared to the *early* targeting complex (Fig 3D, E, F & Fig S2). Overall, the affinity of RNC_{3A7L} for SRP was weakened 30-fold in the *closed* state (Fig 3F), suggesting that

the *early* $\rightarrow$ *closed* rearrangement primes the cargo for subsequent unloading. This regulation was not observed with RNC_{PhoA} (Fig 3F). Collectively, the results in this section show that FtsY assists SRP in sensing distinct stages of targeting, and it does so only for the correct substrates.

Molecular basis for FtsY-regulated SRP-RNC interaction

To understand how FtsY alters the energetics of the SRP-RNC interaction, we examined the interaction of SRP with the ribosome and signal sequence. To probe the interaction of the signal sequence with the SRP M-domain, we measured maximal FRET efficiencies between Cm at 3A7L signal sequence and BODIPY-FL at residues 415, 421, 425 or 429 along helix M4, which lines the signal sequence-binding groove (Fig 4A, red). The cysteine mutations and BODIPY labeling do not affect RNC-SRP binding (Fig S3A) or protein targeting (Fig S3B). Upon formation of the *early* targeting complex, the FRET efficiency between Cm at the signal sequence C-terminus and residues 425 and 429 in helix M4 increased (Fig 4B, pink vs dark red). A similar trend was observed with Cm at the signal sequence N-terminus (Fig S3C). The anisotropy of the dyes was low and comparable in all constructs, indicating no significant contribution of dye orientation to the observed FRET (Table S1), and the position of Cm on the signal sequence did not significantly affect RNC-SRP binding (Fig S3D). These results suggest that formation of the *early* targeting complex allow the signal sequence to pack more tightly against the signal peptide-binding groove.

To probe the interaction of the Ffh N-domain with the ribosome, we looked for an Ffh mutant defective in ribosome binding. Based on the cryo-EM model of SRP bound to an RNC (Halic et al., 2006a), sequence conservation (Fig S4A), previous cross-linking (Gu et al., 2003; Ullers et al., 2003), and the electrostatic nature of the interaction of Ffh with acidic residues in L23 (del Alamo et al., 2011; Schaffitzel et al., 2006), we introduced charge reversal mutations at two

highly conserved basic residues of Ffh, R19 and R21 (Fig 4C, gold). Mutant SRP19/21E was defective in SRP-dependent targeting (Fig S4A, right panel), supporting the importance of these residues in SRP function.

We measured the extent to which the SRP19/21E mutations weaken the binding between SRP and RNC_{3A7L} (Fig S4B, C & Fig 4D). This provides an empirical measure for the energetic contribution of the ribosomal contacts with R19/21 at different stages of targeting. In the RNC•SRP complex, the SRP19/21E mutations weakened SRP-RNC binding 24-fold (Fig 4E, pink and Fig S4B, C). In the *early* complex, these mutations caused >300-fold defect (Fig 4E, dark red and Fig S4D, E), suggesting that the interaction of R19/21 with the ribosome becomes stronger. Together, these results show that tighter RNC-SRP binding in the *early* targeting complex arises from stronger interactions of both the signal sequence and the ribosome with the M- and N-domains of SRP, respectively.

We then asked whether these contacts were reorganized in the *closed* targeting complex to result in weaker RNC-SRP interaction (Fig 3F). To test if the signal sequence rearranged in the M-domain in the *closed* complex, we measured FRET efficiencies between Cm at the signal sequence and acceptor dyes in helix M4 of Ffh as described earlier (Fig 4A). The FRET efficiencies with residues 415, 421, and 425 were reduced upon the *early* → *closed* rearrangement (Fig 4B, green), suggesting re-positioning of the signal sequence in the M-domain.

To test whether the contact of SRP N-domain with the ribosome is altered in the *closed* targeting complex, we measured the effect of the SRP19/21E mutations on the RNC-SRP interaction. In the *closed* complex, these mutations caused only a 6-fold weaker binding (Fig 4E, green and Fig S4F, G). The actual mutational defect is likely smaller because even in the presence of GppNHp,

a significant fraction of the RNC•SRP•SR complex remains in the *early* state (Zhang et al., 2009) in which these mutations are highly destabilizing. The rescue of the SRP19/21E mutant in the *closed* targeting complex strongly suggests that the interaction of the SRP N-domain with the ribosome is substantially weakened at this stage.

Recent studies show that at late stages of protein targeting, the SRP•SR NG-domain complex localizes to the distal end of the SRP RNA (Ataide et al., 2011; Shen et al., 2012). This large-scale movement would vacate L23 at the ribosome exit site for interaction with SecYEG. We therefore asked if this movement had occurred in the *closed* targeting complex. To probe for the proximity of the N-domain to the signal sequence at the ribosome exit site, we used the N-domain FRET pair (Figs. 1B & 4C). Consistent with structural data (Halic et al., 2006a), we observed efficient FRET (~ 0.5) in the RNC•SRP complex (Fig 4F, pink). The FRET value, albeit slightly lower, persisted in the *closed* targeting complex (Fig 4F, green). Thus, although previous work (Halic et al., 2006b; Pool et al., 2002) and our mutational analysis suggest that the SRP N-domain interacts weakly with the ribosome at this stage, the NG-domain complex remains in the vicinity of the nascent polypeptide exit site.

Cm labeled signal sequence reports on RNC-SecYEG interaction

At the membrane, SecYEG must engage RNC. To monitor these late events in targeting, we first tested whether the Cm dye can be used to detect the interaction of a signal sequence with SecYEG (Fig 5A). Indeed, addition of SecYEG, solubilized in 0.02% DDM (Akopian et al., 2013; Dalal and Duong, 2010), induced ~2-fold increase in the fluorescence of Cm-labeled RNC_{3A7L} (Fig 5B, green). Equilibrium titrations based on this fluorescence change showed that RNC_{3A7L} bound tightly to wt-SecYEG (K_d = 3 ± 2 nM; Fig 5C), in agreement with previous reports (Wu et al., 2012). The following observations demonstrate the specificity of this assay.

First, a SecYEG c4/c5 mutant harboring charge reversal mutations (R255/256/357E) in two cytosolic loops critical for ribosome binding (Akopian et al., 2013; Cheng et al., 2005; Menetret et al., 2007) showed no detectable binding to RNC_{3A7L} (Fig 5B and C, grey). Second, introduction of two arginines into the signal sequence (RNC_{3A5L2R} or mt-RNC) weakened RNC-SecYEG binding 46-fold (Fig 5C, light green), showing that the interaction is specific to a functional signal sequence. Third, when Cm-labeled RNC_{3A7L} is bound to SecYEG labeled with BODIPY-FL at residue 180, efficient FRET was observed (Fig S5A). These results support the specificity of the Cm probe in detecting a functional RNC-SecYEG interaction.

SecYEG effectively displaces the SRP•SR complex from RNC

As SecYEG enhances Cm fluorescence upon RNC binding, whereas BODIPY-labeled SRP reduces Cm fluorescence due to FRET, this provides a sensitive assay to monitor the transfer of RNC from the targeting complex to SecYEG (Fig 6A, boxed). To test whether SecYEG can displace the SRP•SR complex from RNC in this minimal system, we added SecYEG to a pre-formed *closed* targeting complex containing Cm-labeled signal sequence. The transfer reaction was carried out either with the N-domain FRET pair (Fig. 1B) to monitor displacement of the NG-domain complex from the ribosome exit site (Fig 6B, C), or with the M-domain FRET pair to monitor the transfer of the nascent chain from the signal sequence binding site (Fig 6D, E). In both cases, addition of SecYEG induced a similar dose-dependent increase in the fluorescence of Cm-labeled RNC (Fig 6B, C, magenta and Fig 6D, E; blue; see also Fig S5B). The SecYEG-induced increase in Cm fluorescence far exceeded that expected from loss of FRET due to dissociation of the RNC•SRP complex (Fig 6B, D and Fig 6F, cf. blue or magenta vs. black), indicating engagement of the signal sequence with SecYEG (see next paragraph). The effect of SecYEG during the transfer reaction was saturable, with an EC_{50} value of 39 ± 26 nM (Fig 6E),

indicating that SecYEG efficiently displaces SRP from the RNC. The c4/c5 mutations abolished this reaction (Fig 6C and E, grey, and Fig S5B), indicating that functional cytosolic loops are required for the observed cargo transfer reaction.

If complete transfer of RNC to SecYEG occurred, FRET between Cm-labeled signal sequence and SRP should be abolished. Hence, the Cm fluorescence after the transfer reaction would be the same for targeting complexes containing labeled or unlabeled SRP. When we repeated the transfer reaction using unlabeled SRP, this was indeed the case (Fig 6F, cf. blue and magenta vs. brown). The Cm fluorescence at the end of the transfer reaction is similar to that from direct addition of saturating SecYEG to RNC (Fig 5B and 6F; green), indicating that close to complete cargo transfer was achieved. These results demonstrate for the first time that detergent-solubilized SecYEG can drive the transfer of cargo from SRP.

Step-wise transfer of RNC from SRP to SecYEG

To probe the mechanism of the molecular relay between SRP and SecYEG, we analyzed the kinetics of the transfer reaction monitored using either the M- or N-domain FRET pair (Fig. 1B). As the nascent protein continues to elongate during targeting, we examined the transfer reaction using RNCs with different nascent chain length. Several intriguing observations suggest that the transfer occurs in a stepwise mechanism. First, the SecYEG-driven release of the SRP N-domain from the RNC-85 was 3-fold faster than that of signal sequence release from the SRP M-domain (Fig 7A, magenta vs. blue and 7D). Second, when we repeated the transfer reaction with RNC_{3A7L} containing 50 additional residues (RNC-135), the initial release of the SRP N-domain was 4-fold faster than that of signal sequence from the M-domain (Fig 7B-D). Significantly, the transfer reaction of RNC-135 monitored with the N-domain FRET pair exhibited bi-phasic kinetics with a pronounced burst, indicating at least two steps during this transfer (Fig. 7C). The

magnitude of rise in Cm fluorescence during the burst phase agrees well with the loss of FRET with the acceptor dye in the SRP N-domain (Fig. 7C), providing additional evidence that displacement of SRP N-domain from the ribosome precedes docking of the signal sequence into SecYEG.

To explain the experimentally observed kinetics of the transfer reaction and to better understand its underlying mechanism, we carried out numerical simulations. In the simplest model (Fig 7E, model (i)), the binding of SecYEG first results in the displacement of the SRP N-domain from the ribosome. This generates a transfer intermediate, from which the signal sequence is transferred to SecYEG. To validate this model, we simulated the expected rise in Cm fluorescence based on the experimentally observed rate and equilibrium constants of the transfer reaction (for details, see Supplemental Methods). Simulations based on model (i) predict pronounced biphasic increase in Cm fluorescence during the transfer reaction with N-domain labeled SRP (Fig 7F, magenta). This is because assembly of SecYEG with the targeting complex to form the transfer complex would occur rapidly at saturating SecYEG concentrations. The resultant loss of FRET between the signal sequence and SRP N-domain would far precede the additional increase in Cm fluorescence caused by the slower docking of the signal sequence into SecYEG. Such biphasic kinetics was observed with RNC-135 (Fig 7C) but was barely detectable with RNC-85 (Fig 7A, magenta), suggesting that model (i) is insufficient to explain all the experimental data.

The absence of a burst expected for formation of the transfer complex indicates that such a complex is transient during the transfer reaction, and cannot be formed simply by bi-molecular association between SecYEG and the targeting complex. We therefore considered the possibility that formation of transfer complex with RNC-85 is preceded by and in unfavorable equilibrium

with an initial encounter complex, in which the SRP N-domain is not yet removed from the ribosome (Fig 7E, model (ii)). Kinetic simulations based on this model showed that indeed, as the equilibrium to form the transfer complex from the encounter complex (Fig 7E, $K_4 = k_4/k_{-4}$) was made less favorable (Fig 7G, red arrow), the burst associated with release of the N-domain labeled SRP from RNC was progressively removed. At values of $K_4 \leq 0.2$, the burst expected for removal of the SRP N-domain from RNC was barely detectable, and the simulated results closely matched experimental data with RNC-85. A more favorable equilibrium to form the transfer complex ($K_4 \sim 5$) generated curves that better matched the results obtained with RNC-135 (Fig 7G). These simulations strongly suggest that formation of the productive transfer complex required for efficient cargo transfer is more favorable with RNC-135, whereas the shorter nascent chain in RNC-85 does not provide a strong cue for fast removal of the N-domain (Park and Rapoport, 2011). In agreement with this, an overall faster rate of cargo transfer was observed with RNC-135 than RNC-85 (Fig. 7D). The slow kinetics of RNC-85 transfer to SecYEG could also be explained, in part, by the unfavorable equilibrium to generate the transfer complex.

Discussion

Proper localization of membrane and secretory proteins requires the efficient and accurate execution of a series of molecular events including capture of the cargo protein, its delivery to the membrane, and its productive handover from the targeting to the translocation machinery (Saraogi and Shan, 2011). Here, we address the molecular mechanisms underlying these events in the SRP pathway, which has served as a paradigm for understanding the molecular basis of protein localization. For the first time, non-natural amino acid technology has allowed us to study, at an unprecedented resolution, the dynamic interaction of the translating ribosome with SRP as it enters, progresses along, and finally exits the SRP pathway.

How does SRP identify the correct substrates in the crowded cytosol, given a 10 – 100 fold excess of ribosomes that bind to SRP with substantial affinity (80-100 nM) (Bornemann et al., 2008; Flanagan et al., 2003; Zhang et al., 2010)? Our results show that SRP binds quickly to ribosomes with or without an SRP signal sequence (Fig 8, step 1), but the kinetic stability of the RNC•SRP complex increases significantly with stronger signal sequences. A recent paper (Holtkamp et al., 2012) reached similar conclusions using FRET between L23 and the SRP M-domain. Triphasic RNC-SRP binding kinetics was observed in Holtkamp et al., which could arise from multiple factors. The fluorescent probes placed on L23 likely reported on transient SRP-ribosome interactions prior to signal sequence docking into the M-domain. In contrast, our assay specifically reports on the engagement of the signal sequence with the SRP M-domain when a stable RNC•SRP complex is formed. The specificity of the probe allowed us to obtain more straightforward kinetic data in most cases (see Materials and Methods).

Holtkamp et al. further postulate that the SRP rapidly ‘scans’ translating ribosomes for the presence of signal sequences, based on rapid RNC-SRP binding and dissociation rate constants.

However, the reported 'rapid' binding ($k_1 \sim 10^8$ $M^{-1}s^{-1}$) refers to the formation of a highly labile intermediate that forms independently of the signal sequence. Formation of the final RNC•SRP complex, in which the correct and incorrect RNCs are distinguished, requires this intermediate to undergo two additional slow rearrangements and hence proceeds at much slower rates. Holtkamp et al. also reported rapid 'k_{off} ' values because, rather than treating SRP dissociation as a sequential process as proposed in the same paper, their 'k_{off}' values were obtained from averaging the rate constants of three steps during dissociation. Hence, the rapid dissociation rate from <10% of highly labile complexes dominated the calculation. This led to overall 'k_{off}' values for a sequential reaction that are much faster than sub-steps in the reaction sequence, which is physically impossible. A kinetic simulation based solely on the 3-step model and individual rate constants reported by Holtkamp et al. predicts that SRP dissociates from the final stable RNC•SRP complex at a rate constant of 0.0058 s^{-1} for RNCs bearing a model SRP substrate Lep, and 0.36 s^{-1} from the 70S ribosome (Fig S1E). These values are in good agreement with our measurements (Fig 2F). Thus, although it remains possible that SRP rapidly 'scans' translating ribosomes*,* such a mechanism would have to be enabled by additional components *in vivo*, rather than by the intrinsic property of SRP-RNC interaction.

Indeed, our results indicate that the intrinsic difference in binding between an SRP-dependent substrate, 3A7L, and a Sec-dependent substrate, phoA, is fairly modest, only 7-fold. Importantly, the interaction of SRP with RNC_{3A7L} is strongly enhanced upon initial recruitment of FtsY to form the *early* targeting complex (Fig 8, step 2), whereas that with RNC_{phoA} is marginally affected. This stabilization was predicted by Zhang *et al.* from a thermodynamic analysis of the SRP-SR GTPase cycle (Zhang et al., 2009). Our data fulfill this prediction and provide direct evidence that the SRP/SR GTPases regulate the cargo~SRP interaction. Further, we show that this

stabilization arises from stronger interactions of both the SRP M- and N-domains with the signal sequence and the ribosome, respectively. This gives the *early* targeting complex, in which the lipid binding helix of FtsY is not yet exposed (Lam et al., 2010), an extended time window to search for the membrane. The residence time of SRP on RNCs bearing correct signal sequences is 3000–5000 seconds, much longer than the 3–5 seconds time window estimated for the SRP to complete targeting (Zhang et al., 2010). Thus, once a correct cargo binds SRP, it likely undergoes subsequent steps in the pathway without dissociating from it. In contrast, the *early* targeting complex formed by incorrect cargos, in which neither the RNC-SRP interaction (this work) nor the SRP-FtsY interaction (Zhang et al., 2009) is stabilized, is more likely to disassemble prematurely in the cytosol. These results demonstrate that formation of the RNC•SRP•FtsY *early* targeting complex is a major commitment step at which the correct substrates selectively enter the SRP pathway.

However, a strong interaction between SRP and RNC poses a challenge to its subsequent release at the membrane. How is this barrier overcome? Notably, anionic phospholipids drive the rearrangement of the GTPases from the *early* to the *closed* conformation, which associates with the membrane more stably (Braig et al., 2011; Lam et al., 2010). Here, we demonstrate that this conformational switch (Fig 8, step 3) also weakens the affinity of SRP for its cargo 30-fold, thus coupling the membrane localization of the targeting complex to the release of cargo. The reduction in binding affinity arises from substantially weaker interaction of the SRP N-domain with the ribosome and possibly a repositioning of the signal sequence in the M-domain. These results agree with earlier studies of eukaryotic SRP, which showed loss of electron density of the SRP NG-domain (Halic et al., 2006b) and loss of SRP-L23a crosslink (Pool et al., 2002) upon assembly of a stable GTP-dependent complex between RNC, SRP and SR.

Nevertheless, in the *closed* targeting complex, the SRP NG-domain remains adjacent to the ribosome exit site, and the signal sequence is still bound to the M-domain, indicating that the GTPase rearrangements are insufficient to drive the complete release of cargo. The targeting cycle is completed by SecYEG, which displaces the SRP•SR complex from the RNC to drive cargo unloading. Two recent studies show that SecYEG induces relocalization of the SRP•SR NG domains away from the ribosome exit site, to the distal end on SRP RNA, where GTP hydrolysis can be activated (Shen et al, 2012; Akopian et al, 2013). Under these conditions, the RNC remain attached to the SRP•SR complex. In this work, we observed that detachment of the SRP N-domain from the ribosome is faster and precedes the release of signal sequence from the SRP M-domain and signal sequence docking into SecYEG. Collectively, these data suggest a highly coordinated, step-wise mechanism of cargo transfer (Fig 8): after initial encounter with the targeting complex (step 4, encounter complex), SecYEG first displaces the SRP NG-domain from the ribosome exit site via interaction of its cytosolic loops with L23 (step 5, transfer complex). This is followed by transfer of the signal sequence from the SRP M-domain to SecYEG (step 6). The step-wise transfer prevents abortive loss of RNC from the membrane. During the transfer process, the SRP•SR NG-domain complex relocalizes to the distal site of the SRP RNA, where GTP hydrolysis is activated (Ataide et al., 2011; Shen et al., 2012) to reset the targeting cycle (Fig 8, step 6).

The RNC transfer reactions observed here proceed with a halftime ($t_{1/2} = \ln 2/k$) of 70 – 140 seconds. This is slower than those expected physiologically, but is not unexpected for a reaction reconstituted with minimal components and suggests that additional *in vivo* factors could allosterically regulate SRP, SR, or SecYEG to accelerate transfer. Quantitative analysis of cargo transfer coupled with kinetic simulations in this minimal system helps define the rate-limiting

barriers that can be facilitated by these additional factors. A major barrier arises from an unfavorable equilibrium to form the transfer complex (Fig 8, step 5). This is consistent with observations in single molecule experiments, in which only ~30% of the SRP•SR NG-domain complex relocalizes to the SRP RNA distal site in the presence of RNC-85 and SecYEG (Shen et al., 2012). Indeed, elongation of the nascent polypeptide facilitates the transfer reaction, and this stimulation appears to arise from more facile release of the NG-domain from the ribosome to form the transfer complex. A low probability of signal sequence docking into SecYEG (Fig 8, step 6), which requires opening of the lateral gate, could present an additional barrier. We speculate that under physiological conditions, both formation of the transfer complex and gate opening in SecYEG could be stimulated by additional factors, including anionic phospholipid membranes and other components of the holo-translocon (Duong and Wickner, 1997).

In summary, we show that the SRP/SR GTPase cycle and the SecYEG translocon actively regulate the conformation, energetics and dynamics of the SRP-cargo interaction, giving rise to highly coordinated assembly, commitment, and disassembly of the targeting complex. The challenges faced by SRP are general to targeting machineries. Hence, the active regulation of cargo interactions and the stepwise mechanism of cargo transfer observed here could represent general phenomena in protein targeting pathways. The bidentate nature of RNC's interactions with SRP and SecYEG plays a key role in this regulatory mechanism since the individual contacts can be sequentially formed, dissolved and exchanged, thus ensuring productive 'relay' between upstream and downstream factors in the pathway. In addition to SRP and SecYEG, numerous other cellular machineries contact the ribosome exit site (e.g. chaperones, maturation and quality control enzymes etc), many of which recognize both the ribosome and sequence motifs on the nascent protein. These multi-dentate interactions may provide an effective handling

of the translating ribosome during the biogenesis of nascent proteins. The use of fluorescently-labeled RNCs will be a powerful tool for a detailed molecular understanding of the multiplicity of fates that await the nascent protein as it exits the ribosome (Kramer et al., 2009).

Materials and Methods

Materials: Ribosome nascent chain complexes labeled with L-(7-hydroxycoumarin-4-yl)ethylglycine were generated as described before (Saraogi et al., 2011). *E. coli* SRP (Ffh and 4.5S RNA component) and full-length FtsY were expressed and purified according to published protocol (Peluso et al., 2001). Ffh mutants were constructed using the QuikChange mutagenesis procedure (Stratagene) and were expressed and purified using the same protocol as the wild-type protein. The SRP mutants were tested for their ability to translocate preprolactin in a heterologous protein translocation assay as described (Shan et al., 2007). Single cysteine mutants of Ffh were labeled using the fluorescent dye BODIPY-Fluorescein-N-(2-aminoethyl)-maleimide (BODIPY-FL, Invitrogen) as described previously (Zhang et al., 2008; Zhang et al., 2009). 70S ribosomes were purified from *E. coli* MRE600 cells using published protocol (Moazed and Noller, 1989; Zhang et al., 2009). SecYEG was purified as described (Akopian et al., 2013). For SecYEG labeling, a unique cysteine residue was introduced at position 180 of cysteine-less SecYEG and labeled according to published protocol with modifications (Kedrov et al., 2011). Briefly, SecYEG purified via Ni-NTA agarose was rebound to Ni-NTA agarose and labeled on beads with BODIPY-FL. The labeled protein was dialyzed in the assay buffer and quantified using absorbance at 280 nm.

Fluorescence measurements: All steady-state fluorescence measurements were carried out at 25°C in assay buffer (50 mM KHEPES, pH 7.5, 150 mM KOAc, 10 mM $Mg(OAc)_2$, 2 mM DTT, 10% glycerol; supplemented with 0.02% DDM in assays with SecYEG) on a Fluorolog-3-22 spectrofluorometer (Horiba Jobin Yvon, Edison, NJ). Fast reactions were measured on a Kintek stopped flow apparatus at 25°C. FRET experiments were carried out using an excitation wavelength of 360 nm and an emission wavelength of 453 nm. All FRET measurements were

performed with RNCs labeled 2 residues downstream of the signal sequence. FRET efficiency (E) was calculated according to Eq S1:

$$E = 1 - \frac{F_{DA}}{F_D} \quad [S1]$$

in which F_{DA} and F_D are the fluorescence intensities of the donor measured in the presence and absence of the acceptor, respectively. Background fluorescence due to light scattering was subtracted from the fluorescence spectra. The details of the kinetic and equilibrium measurements are described in Supplemental Methods.

Online Supplemental Material

Supplemental Methods describes the details of kinetic and equilibrium measurements and kinetic simulations. Figs S1 show additional data for RNC binding and dissociation from SRP. Fig S2 shows the time courses for RNC binding to the SRP•SR early and closed complexes. Fig S3 shows signal sequence binding to the SRP M-domain. Fig S4 describes the SRP 19/21E mutant. Fig S5 shows the interaction of the Cm probe with SecYEG. Table S1 lists the anisotropy of the Cm and BODIPY-FL fluorophores.

Online Supplemental Methods

Equilibrium titrations: The equilibrium binding affinity of RNCs for SRP was measured as described (Saraogi et al., 2011). Briefly, aliquots of SRP labeled with BODIPY-FL were added to 20 nM of Cm-labeled RNC and the decrease in donor fluorescence was noted. The FRET values obtained from Eq S1 were plotted against SRP concentration and the data were fit to Eq S2:

$$E = E_{max} \frac{K_d + [RNC] + [SRP] - \sqrt{(K_d + [SRP] + [RNC])^2 - 4[SRP][RNC]}}{2[RNC]} \quad [S2]$$

in which E_{max} is the FRET efficiency at saturating SRP concentration, and K_d is the dissociation constant of the RNC•SRP complex.

Association rate constants: Rate constants for RNC-SRP binding were measured on a Kintek stopped-flow apparatus at 25°C. The observed rate constants for formation of the RNC•SRP complex (k_{obsd}) at different stages of targeting were measured by mixing 40-50 nM Cm-labeled RNC with varying concentrations of BODIPY-FL labeled SRP or a preformed *early*/*closed* complex. Unlabeled full-length FtsY and 100 μM GDP or GppNHp were used to form the required complexes. The time course for change in donor fluorescence was fit to Eq S3,

$$F_{obsd} = F_0 - \Delta F_1(1-e^{-k_{obsd}t}) - k_{lin}t \qquad [S3]$$

in which k_{obsd} is the observed rate constant, F_{obsd} is the observed fluorescence, F_0 is the initial fluorescence, ΔF_1 is the amplitude of fluorescence change, and k_{lin} represents a very slow linear term that was required to obtain the best fitting. As the significance of this term was not apparent, and its contribution to the fitting was very small, we did not pursue this further.

The dependence of k_{obsd} on SRP concentration was fit to Eq S4,

$$k_{obsd} = k_{on}[SRP] + k_{off} \qquad [S4]$$

in which k_{on} and k_{off} are the association and dissociation rate constants, respectively, for the RNC•SRP complex. As k_{off} values obtained from this fit may not be very accurate, these were measured directly as described below.

Dissociation rate constants: The rate of dissociation of RNCs from SRP, *early* or *closed* targeting complex was measured independently by a pulse-chase experiment. Cm-labeled RNC (20 nM) and BODIPY-FL labeled SRP (40 nM), *early* or *closed* complexes were incubated for 15 min to form the respective targeting complexes. The solution was then mixed with an equal volume of 1.5 – 2 μM unlabeled SRP to initiate irreversible dissociation of the complex. The

time course for change in donor fluorescence was fit to a single (Eq S5a) or double exponential (Eq S5b), in which F_{obsd} is the observed fluorescence, F_0 is the initial fluorescence, ΔF_1 and ΔF_2 are the amplitudes of fluorescence changes, and k_1 and k_2 are the dissociation rate constants.

$$F_{obsd} = F_0 + \Delta F_1(1 - e^{-k_1 t}) \qquad [S5a]$$

$$F_{obsd} = F_0 + \Delta F_1(1 - e^{-k_1 t}) + \Delta F_2(1 - e^{-k_2 t}) \qquad [S5b]$$

Eq. S5b was needed for analysis of the dissociation kinetics of RNC_{phoA} from SRP, during which we observed two kinetic phases that differed by ~5-fold in rate constants (Fig 2F and Fig S1D). This phenomenon could arise from different populations of RNC_{phoA}-SRP complexes in which SRP is bound in distinct conformations, or from multi-step dissociation of SRP from the RNC that becomes more apparent with RNC_{phoA}. Although this biphasic kinetics with RNC_{phoA} persists as the targeting reaction progresses, the two phases responded similarly to FtsY (Fig 3F). Therefore, only the rate constants from the faster dissociating phase are reported in the main text. To determine the dissociation rate constant of SRP from 70S ribosomes, a pre-incubated solution of 100 nM BODIPY-labeled SRP and 500 nM 70S ribosomes was chased with 120 nM or 300 nM Cm-labeled RNC_{1A9L}. Under these conditions, RNC_{1A9L}-SRP association is much faster than SRP•ribosome complex dissociation. Thus, the appearance of the FRET signal is rate-limited by, and reflects the dissociation rate of, the SRP-ribosome complex. The reaction time course was fit to Eq S5b to obtain the dissociation rate constants.

***Equilibrium measurements with SecYEG*:** The binding of SecYEG (wt or mutant) to Cm-labeled RNC was measured by titrating aliquots of SecYEG into 20 nM Cm-labeled RNC. A parallel titration of SecYEG into buffer was used to correct for light scattering from SecYEG. The fluorescence values obtained were plotted against SecYEG concentration, and the data were fit to Eq S6 to obtain the respective K_d values.

$$F = F_0 + \Delta F \times \frac{K_d + [RNC] + [YEG] - \sqrt{(K_d + [YEG] + [RNC])^2 - 4[YEG][RNC]}}{2[RNC]} \qquad [S6]$$

in which F is the observed fluorescence at a given SecYEG concentration, F_0 is the fluorescence of RNC in the absence of SecYEG, ΔF is the maximum change in fluorescence at saturating SecYEG concentration, and K_d is the dissociation constant for SecYEG-RNC binding.

RNC-SecYEG FRET: A unique cysteine residue introduced into cysteine-less SecYEG at position 180 was labeled with BODIPY-FL. For the FRET assay, 30 nM labeled SecYEG was incubated with 40 nM Cm-labeled RNC. Since addition of SecYEG (labeled or unlabeled) induces a strong environmental sensitivity in Cm fluorescence, unlabeled SecYEG was added to RNC to obtain the donor only signal and allow us to quantify FRET.

Kinetics of transfer reaction: To measure the equilibrium of the transfer reaction, SecYEG (wt or mutant) was titrated into a complex preincubated with 20 nM Cm-labeled RNC, 40 nM BODIPY-FL labeled SRP, 500 nM FtsY, and 100 μM GppNHp. The increase in fluorescence was plotted against SecYEG concentration and fit to Eq S6, in which K_d was replaced by EC_{50} and denotes the amount of SecYEG needed for 50% transfer of RNC to SecYEG.

To measure the rate of transfer of RNC from the SRP•FtsY complex to SecYEG, a closed targeting complex was preformed using 20 nM Cm-labeled RNC, 40 nM BODIPY-FL labeled SRP, 500 nM FtsY, 100 μM GppNHp. RNC transfer was initiated by addition of 1 μM SecYEG. The increase in fluorescence over time was fit to Eq S5a or b to give the observed rate constant (k_{obs}).

Kinetic Simulations: The software Berkeley Madonna was used to perform kinetic simulations. For the SecYEG driven release of RNC from the *closed* targeting complex (Fig 7F, G) according to model (i), the following reactions were used:

$$RNC\bullet SRP\bullet SR + SecYEG \underset{k_{-1}}{\overset{k_1}{\rightleftharpoons}} RNC\bullet SRP\bullet SR\bullet SecYEG \quad [S7a]$$

$$RNC\bullet SRP\bullet SR\bullet SecYEG \underset{k_{-2}}{\overset{k_2}{\rightleftharpoons}} RNC\bullet SecYEG + SRP\bullet SR \quad [S7b]$$

$$RNC + SRP\bullet SR \underset{k_{-5}}{\overset{k_5}{\rightleftharpoons}} RNC\bullet SRP\bullet SR \quad [S7c]$$

For transfer reaction with acceptor in the SRP M domain, the change in Cm fluorescence was determined by the following equation:

F(M) = 50[RNC] + 25[RNC•SRP•SR] + 25[RNC•SRP•SR•SecYEG] + 90 [RNC•SecYEG]

For transfer reaction with acceptor in the SRP N domain, the change in Cm fluorescence was determined by the following equation:

F(N) = 50[RNC] + 30[RNC•SRP•SR] + 60[RNC•SRP•SR•SecYEG] + 90 [RNC•SecYEG]

Each of the coefficients indicates the relative fluorescence contribution of the corresponding species during the transfer reaction (Fig 6F).

For model (ii), the following reactions were used: (* represents encounter complex)

$$RNC\bullet SRP\bullet SR + SecYEG \underset{k_{-3}}{\overset{k_3}{\rightleftharpoons}} RNC\bullet SRP\bullet SR\bullet SecYEG^* \quad [S8a]$$

$$RNC\bullet SRP\bullet SR\bullet SecYEG^* \underset{k_{-4}}{\overset{k_4}{\rightleftharpoons}} RNC\bullet SRP\bullet SR\bullet SecYEG \quad [S8b]$$

$$RNC\bullet SRP\bullet SR\bullet SecYEG \underset{k_{-2}}{\overset{k_2}{\rightleftharpoons}} RNC\bullet SecYEG + SRP\bullet SR \quad [S8c]$$

$$RNC + SRP\bullet SR \underset{k_{-5}}{\overset{k_5}{\rightleftharpoons}} RNC\bullet SRP\bullet SR \quad [S8d]$$

For transfer reaction with acceptor in the SRP M domain, the change in Cm fluorescence was determined by the following equation:

F(M) = 50[RNC] + 25[RNC•SRP•SR] + 25[RNC•SRP•SR•SecYEG*]+ 25 [RNC•SRP•SR•SecYEG] + 90[RNC•SecYEG]

For transfer reaction with acceptor in the SRP N domain, the change in Cm fluorescence was determined by the following equation:

F(N) = 50[RNC] + 30[RNC•SRP•SR] + 30[RNC•SRP•SR•SecYEG*] + 60 [RNC•SRP•SR•SecYEG] + 90[RNC•SecYEG]

For model (ii), multiple curves were generated for the SRP N-domain by constraining the equilibrium between the transfer complex and encounter complex ($K_4=k_4/k_{-4}$) to values ranging from 25 to 0.1.

The concentrations used for the simulations were: 20 nM RNC_{3A7L} pre-incubated with 40 nM SRP•SR *closed* complex, and 1 μM SecYEG. The following information was used to constrain values of rate constants:

$k_5 = 3.4\ \mu M^{-1}s^{-1}$; $k_{-5} = 0.003\ s^{-1}$; $k_2 = 0.005\ s^{-1}$; $K_4=k_4/k_{-4} = 25, 5, 1, 0.2, 0.1$

$\frac{k_{-1}}{k_1} \times \frac{k_{-2}}{k_2} = 0.039\ \mu M$ (EC_{50} of transfer under these conditions)

To generate the curves in Fig 7F and G, the following values of the rate constants were used: k_1 = $1.2\ \mu M^{-1}s^{-1}$; $k_{-1} = 0.363\ s^{-1}$; $k_3 = 1\ \mu M^{-1}s^{-1}$; $k_{-3} = 0.08\ s^{-1}$; $k_{-2} = 0.0006\ s^{-1}$.

For simulation of the dissociation rate constant of a stable RNC•SRP or ribosome•SRP complex according to the three-step model of Holtkamp et al (Holtkamp et al., 2012), the following equations (Eq S9a-f) were used, in which R denotes the RNC or ribosome, I1 and I2 denote the intermediates described by Holtkamp et al, chase refers to the unlabeled SRP used to trap dissociated 'R' in the measurement of k_{off} values, and I1chase and I2chase refer to the corresponding intermediates formed between 'R' and the chase molecules.

$$R\bullet SRP \underset{k_3}{\overset{k_{-3}}{\rightleftharpoons}} I2 \qquad [S9a]$$

$$I2 \underset{k_2}{\overset{k_{-2}}{\rightleftharpoons}} I1 \qquad [S9b]$$

$$I1 \underset{k_1}{\overset{k_{-1}}{\rightleftharpoons}} R + SRP \qquad [S9c]$$

$$R + chase \underset{k_{-1}}{\overset{k_1}{\rightleftharpoons}} I1chase \qquad [S9d]$$

$$I2chase \underset{k_{-2}}{\overset{k_2}{\rightleftharpoons}} I2chase \qquad [S9e]$$

$$I2chase \underset{k_{-3}}{\overset{k_3}{\rightleftharpoons}} R\bullet chase \qquad [S9f]$$

Assuming that our fluorescence assay reports specifically on the final stable complex (R•SRP), the normalized fluorescence change is denoted as 1x [R•SRP]. The values of k_1, k_{-1}, k_2, k_{-2}, k_3 and k_{-3} were those reported by (Holtkamp et al., 2012). The initial concentrations of each species were calculated based on the experimental conditions used by Holtkamp *et al* (0.05 μM R, 0.1 μM SRP, 2 μM chase) and the equilibrium constants reported in the same article. As expected for exponential functions, varying the initial concentration of R•SRP or the fluorescence value assigned to it does not affect the simulated time course and the resulting k_{off} values.

Acknowledgements

We thank Tom Miller and Connie Wang for discussions and members of the Shan group for comments on the manuscript. This work was supported by NIH grant GM078024 to S.S. S.S. was supported by the Henry Dreyfus teacher-scholar award and the Packard and Lucile Fellowship in science and engineering.

References

Akopian, D., K. Dalal, K. Shen, F. Duong, and S.-o. Shan. 2013. SecYEG activates GTPases to drive the completion of cotranslational protein targeting. *J. Cell Biol.* 200:397-405.

Angelini, S., D. Boy, E. Schiltz, and H.-G. Koch. 2006. Membrane binding of the bacterial signal recognition particle receptor involves two distinct binding sites. *J. Cell Biol.* 174:715-724.

Ataide, S.F., N. Schmitz, K. Shen, A. Ke, S. Shan, J.A. Doudna, and N. Ban. 2011. The Crystal Structure of the Signal Recognition Particle in Complex with Its Receptor. *Science*. 331:881-886.

Bornemann, T., J. Jockel, M.V. Rodnina, and W. Wintermeyer. 2008. Signal sequence-independent membrane targeting of ribosomes containing short nascent peptides within the exit tunnel. *Nat. Struct. Mol. Biol.* 15:494-499.

Braig, D., C. Baer, J.-O. Thumfart, and H.-G. Koch. 2009. Two Cooperating Helices Constitute the Lipid-binding Domain of the Bacterial SRP Receptor. *J. Mol. Biol.* 390:401-413.

Braig, D., M. Mircheva, I. Sachelaru, E.O. van der Sluis, L. Sturm, R. Beckmann, and H.-G. Koch. 2011. Signal sequence-independent SRP-SR complex formation at the membrane suggests an alternative targeting pathway within the SRP cycle. *Mol. Biol. Cell*. 22:2309-2323.

Cheng, Z.L., Y. Jiang, E.C. Mandon, and R. Gilmore. 2005. Identification of cytoplasmic residues of Sec61p involved in ribosome binding and cotranslational translocation. *J. Cell Biol.* 168:67-77.

Cross, B.C.S., I. Sinning, J. Luirink, and S. High. 2009. Delivering proteins for export from the cytosol. *Nat. Rev. Mol. Cell. Biol.* 10:255-264.

Dalal, K., and F. Duong. 2010. Reconstitution of the SecY translocon in nanodiscs. *Methods Mol. Biol.* 619:145-56.

del Alamo, M., D.J. Hogan, S. Pechmann, V. Albanese, P.O. Brown, and J. Frydman. 2011. Defining the Specificity of Cotranslationally Acting Chaperones by Systematic Analysis of mRNAs Associated with Ribosome-Nascent Chain Complexes. *PLOS Biol.* 9:e1001100.

Doud, S.K., M.M. Chou, and D.A. Kendall. 1993. Titration of protein-transport activity by incremental changes in signal peptide hydrophobicity. *Biochemistry*. 32:1251-1256.

du Plessis, D.J.F., G. Berrelkamp, N. Nouwen, and A.J.M. Driessen. 2009. The Lateral Gate of SecYEG Opens during Protein Translocation. *J. Biol. Chem.* 284:15805-15814.

Duong, F., and W. Wickner. 1997. Distinct catalytic roles of the SecYE, SecG and SecDFyajC subunits of preprotein translocase holoenzyme. *EMBO J.* 16:2756-2768.

Egea, P.F., S.O. Shan, J. Napetschnig, D.F. Savage, P. Walter, and R.M. Stroud. 2004. Substrate twinning activates the signal recognition particle and its receptor. *Nature*. 427:215-221.

Flanagan, J.J., J.C. Chen, Y.W. Miao, Y.L. Shao, J.L. Lin, P.E. Bock, and A.E. Johnson. 2003. Signal recognition particle binds to ribosome-bound signal sequences with fluorescence-detected subnanomolar affinity that does not diminish as the nascent chain lengthens. *J. Biol. Chem.* 278:18628-18637.

Focia, P.J., I.V. Shepotinovskaya, J.A. Seidler, and D.M. Freymann. 2004. Heterodimeric GTPase core of the SRP targeting complex. *Science*. 303:373-377.

Freymann, D., R. Keenan, R. Stroud, and P. Walter. 1997. Crystal structure of the 'NG' GTPase of the prokaryotic SRP54 homolog Ffh. *FASEB Journal*. 11:A1063-A1063.

Gasper, R., Meyer, S., Gotthardt, K., Sirajuddin, M., and Wittinghofer, A. 2009. It takes two to tango: regulation of G proteins by dimerization. *Nature Rev. Mol. Cell. Biol.* 10:423-429.

Gu, S.Q., F. Peske, H.J. Wieden, M.V. Rodnina, and W. Wintermeyer. 2003. The signal recognition particle binds to protein L23 at the peptide exit of the Escherichia coli ribosome. *RNA*. 9:566-573.

Hainzl, T., S.H. Huang, G. Merilainen, K. Brannstrom, and A.E. Sauer-Eriksson. 2011. Structural basis of signal-sequence recognition by the signal recognition particle. *Nat. Struct. Mol. Biol.* 18:389-391.

Halic, M., M. Blau, T. Becker, T. Mielke, M.R. Pool, K. Wild, I. Sinning, and R. Beckmann. 2006a. Following the signal sequence from ribosomal tunnel exit to signal recognition particle. *Nature*. 444:507-511.

Halic, M., M. Gartmann, O. Schlenker, T. Mielke, M.R. Pool, I. Sinning, and R. Beckmann. 2006b. Signal recognition particle receptor exposes the ribosomal translocon binding site. *Science*. 312:745-747.

Holtkamp, W., S. Lee, T. Bornemann, T. Senyushkina, M.V. Rodnina, and W. Wintermeyer. 2012. Dynamic switch of the signal recognition particle from scanning to targeting. *Nat. Struct. Mol. Biol.* 19:1332-7.

Janda, C.Y., J. Li, C. Oubridge, H. Hernandez, C.V. Robinson, and K. Nagai. 2010. Recognition of a signal peptide by the signal recognition particle. *Nature*. 465:507-510.

Jungnickel, B., and T.A. Rapoport. 1995. A posttargeting signal sequence recognition event in the endoplasmic-reticulum membrane. *Cell*. 82:261-270.

Kedrov, A., I. Kusters, V.V. Krasnikov, and A.J.M. Driessen. 2011. A single copy of SecYEG is sufficient for preprotein translocation. *EMBO J.* 30:4387-4397.

Keenan, R.J., D.M. Freymann, R.M. Stroud, and P. Walter. 2001. The signal recognition particle. *Ann. Rev. Biochem.* 70:755-775.

Keenan, R.J., D.M. Freymann, P. Walter, and R.M. Stroud. 1998. Crystal structure of the signal sequence binding subunit of the signal recognition particle. *Cell*. 94:181-191.

Kramer, G., D. Boehringer, N. Ban, and B. Bukau. 2009. The ribosome as a platform for co-translational processing, folding and targeting of newly synthesized proteins. *Nat. Struct. Mol. Biol.* 16:589-597.

Lam, V.Q., D. Akopian, M. Rome, D. Henningsen, and S. Shan. 2010. Lipid activation of the signal recognition particle receptor provides spatial coordination of protein targeting. *J. Cell Biol.* 190:623-635.

Luirink, J., C.M. Tenhagenjongman, C.C. Vanderweijden, B. Oudega, S. High, B. Dobberstein, and R. Kusters. 1994. An alternative protein targeting pathway in Escherichia-coli - studies on the role of FtsY. *EMBO J.* 13:2289-2296.

Menetret, J.-F., J. Schaletzky, W.M. Clemons, Jr., A.R. Osborne, S.S. Skanland, C. Denison, S.P. Gygi, D.S. Kirkpatrick, E. Park, S.J. Ludtke, T.A. Rapoport, and C.W. Akey. 2007. Ribosome binding of a single copy of the SecY complex: Implications for protein translocation. *Mol. Cell*. 28:1083-1092.

Moazed, D., and H.F. Noller. 1989. Interaction of transfer-RNA with 23S ribosomal-RNA in the ribosomal A-sites, P-sites, and E-sites. *Cell*. 57:585-597.

Park, E., and T.A. Rapoport. 2011. Preserving the membrane barrier for small molecules during bacterial protein translocation. *Nature*. 473:239-+.

Parlitz, R., A. Eitan, G. Stjepanovic, L. Bahari, G. Bange, E. Bibi, and I. Sinning. 2007. Escherichia coli signal recognition particle receptor FtsY contains an essential and autonomous membrane-binding amphipathic helix. *J. Biol. Chem.* 282:32176-32184.

Peluso, P., S.O. Shan, S. Nock, D. Herschlag, and P. Walter. 2001. Role of SRP RNA in the GTPase cycles of ffh and FtsY. *Biochemistry*. 40:15224-15233.

Pettersen, E.F., T.D. Goddard, C.C. Huang, G.S. Couch, D.M. Greenblatt, E.C. Meng, and T.E. Ferrin. 2004. UCSF chimera - A visualization system for exploratory research and analysis. *J. Comput. Chem.* 25:1605-1612.

Pool, M.R., J. Stumm, T.A. Fulga, I. Sinning, and B. Dobberstein. 2002. Distinct modes of signal recognition particle interaction with the ribosome. *Science*. 297:1345-1348.

Poritz, M.A., H.D. Bernstein, K. Strub, D. Zopf, H. Wilhelm, and P. Walter. 1990. An Escherichia-coli ribonucleoprotein containing 4.5S RNA resembles mammalian Signal Recognition Particle *Science*. 250:1111-1117.

Powers, T., and P. Walter. 1996. The nascent polypeptide-associated complex modulates interactions between the signal recognition particle and the ribosome. *Curr. Biol.* 6:331-338.

Rapoport, T.A. 2007. Protein translocation across the eukaryotic endoplasmic reticulum and bacterial plasma membranes. *Nature*. 450:663-669.

Saraogi, I., and S. Shan. 2011. Molecular Mechanism of Co-translational Protein Targeting by the Signal Recognition Particle. *Traffic*. 12:535-542.

Saraogi, I., D. Zhang, S. Chandrasekaran, and S. Shan. 2011. Site-specific fluorescent labeling of nascent proteins on the translating ribosome. *J. Amer. Chem. Soc.* 133:14936-14939.

Schaffitzel, C., M. Oswald, I. Berger, T. Ishikawa, J.P. Abrahams, H.K. Koerten, R.I. Koning, and N. Ban. 2006. Structure of the E-coli signal recognition particle bound to a translating ribosome. *Nature*. 444:503-506.

Shan, S., S. Chandrasekar, and P. Walter. 2007. Conformational changes in the GTPase modules of the signal recognition particle and its initiation of protein translocation. *J. Cell Biol.* 178:611-620.

Shan, S., Schmid, S.L., and Zhang, X. 2009. Signal recognition particle (SRP) and SRP receptor: a new paradigm for multi-state regulatory GTPases. *Biochemistry*. 48:6696-6704.

Shan, S.O., R.M. Stroud, and P. Walter. 2004. Mechanism of association and reciprocal activation of two GTPases. *PLOS Biol.* 2:1572-1581.

Shen, K., S. Arslan, D. Akopian, T. Ha, and S.-o. Shan. 2012. Activated GTPase movement on an RNA scaffold drives co-translational protein targeting. *Nature*. 492:271-275.

Shen, K., and S. Shan. 2010. Transient tether between the SRP RNA and SRP receptor ensures efficient cargo delivery during cotranslational protein targeting. *Proc. Nat. Acad. Sci. USA*. 107:7698-7703.

Shen, K., X. Zhang, and S. Shan. 2011. Synergistic actions between the SRP RNA and translating ribosome allow efficient delivery of the correct cargos during cotranslational protein targeting. *RNA*. 17:892-902.

Song, W.Q., D. Raden, E.C. Mandon, and R. Gilmore. 2000. Role of Sec61 alpha in the regulated transfer of the ribosome-nascent chain complex from the signal recognition particle to the translocation channel. *Cell*. 100:333-343.

Stjepanovic, G., K. Kapp, G. Bange, C. Graf, R. Parlitz, K. Wild, M.P. Mayer, and I. Sinning. 2011. Lipids trigger a conformational switch that regulates signal recognition particle (SRP)-mediated protein targeting. *J. Biol. Chem.* 286:23489-23497.

Ullers, R.S., E.N.G. Houben, A. Raine, C.M. ten Hagen-Jongman, M. Ehrenberg, J. Brunner, B. Oudega, N. Harms, and J. Luirink. 2003. Interplay of signal recognition particle and trigger factor at L23 near the nascent chain exit site on the Escherichia coli ribosome. *J. Cell Biol.* 161:679-684.

van den Berg, B., W.M. Clemons, I. Collinson, Y. Modis, E. Hartmann, S.C. Harrison, and T.A. Rapoport. 2004. X-ray structure of a protein-conducting channel. *Nature*. 427:36-44.

Wu, Z.C., J. de Keyzer, A. Kedrov, and A.J.M. Driessen. 2012. Competitive Binding of the SecA ATPase and Ribosomes to the SecYEG Translocon. *J. Biol. Chem.* 287:7885-95.

Zhang, X., S. Kung, and S.O. Shan. 2008. Demonstration of a multistep mechanism for assembly of the SRP.SRP receptor complex: Implications for the catalytic role of SRP RNA. *J. Mol. Biol.* 381:581-593.

Zhang, X., V.Q. Lam, Y. Mou, T. Kimura, J. Chung, S. Chandrasekar, J.R. Winkler, S.L. Mayo, and S. Shan. 2011. Direct visualization reveals dynamics of a transient intermediate during protein assembly. *Proc. Nat. Acad. Sci. USA*. 108:6450-6455.

Zhang, X., R. Rashid, K. Wang, and S.O. Shan. 2010. Sequential checkpoints govern substrate selection during cotranslational protein targeting. *Science*. 328:757-760.

Zhang, X., C. Schaffitzel, N. Ban, and S.O. Shan. 2009. Multiple conformational switches in a GTPase complex control co-translational protein targeting. *Proc. Nat. Acad. Sci. USA*. 106:1754-1759.

Figures

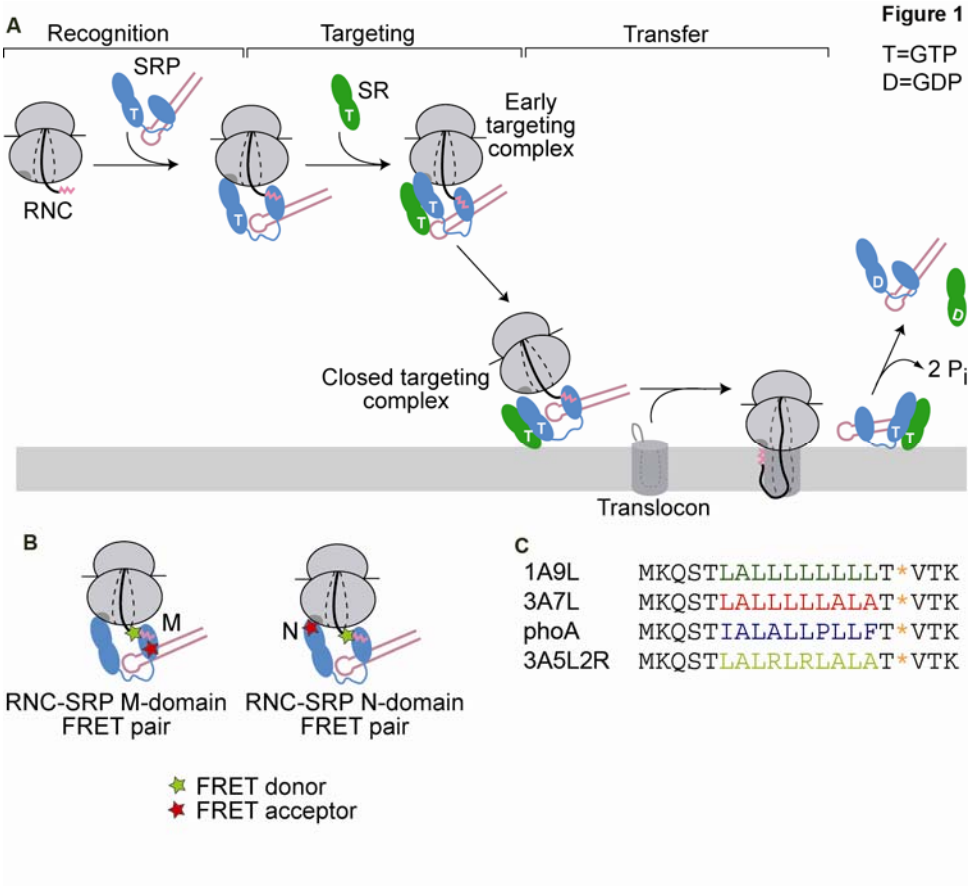

Figure 1. **Co-translational protein targeting by SRP.** (A) The targeting of ribosomes carrying SRP signal sequences (magenta) to the membrane requires three sequential steps: cargo recognition by SRP, cargo targeting to the membrane via interaction of SRP with SR, and cargo transfer to the SecYEG translocon. Ffh is in blue, FtsY is in green, and the SRP RNA is in pink. 'T' and 'D' denote GTP and GDP, respectively. (B) Scheme of the FRET probes used. The nascent chain was labeled with a donor dye (green star) at the signal sequence. SRP was labeled with an acceptor dye (red star) in the M- or N-domain. (C) The signal sequences of substrates used in this study. The position of the donor dye is denoted with an asterisk.

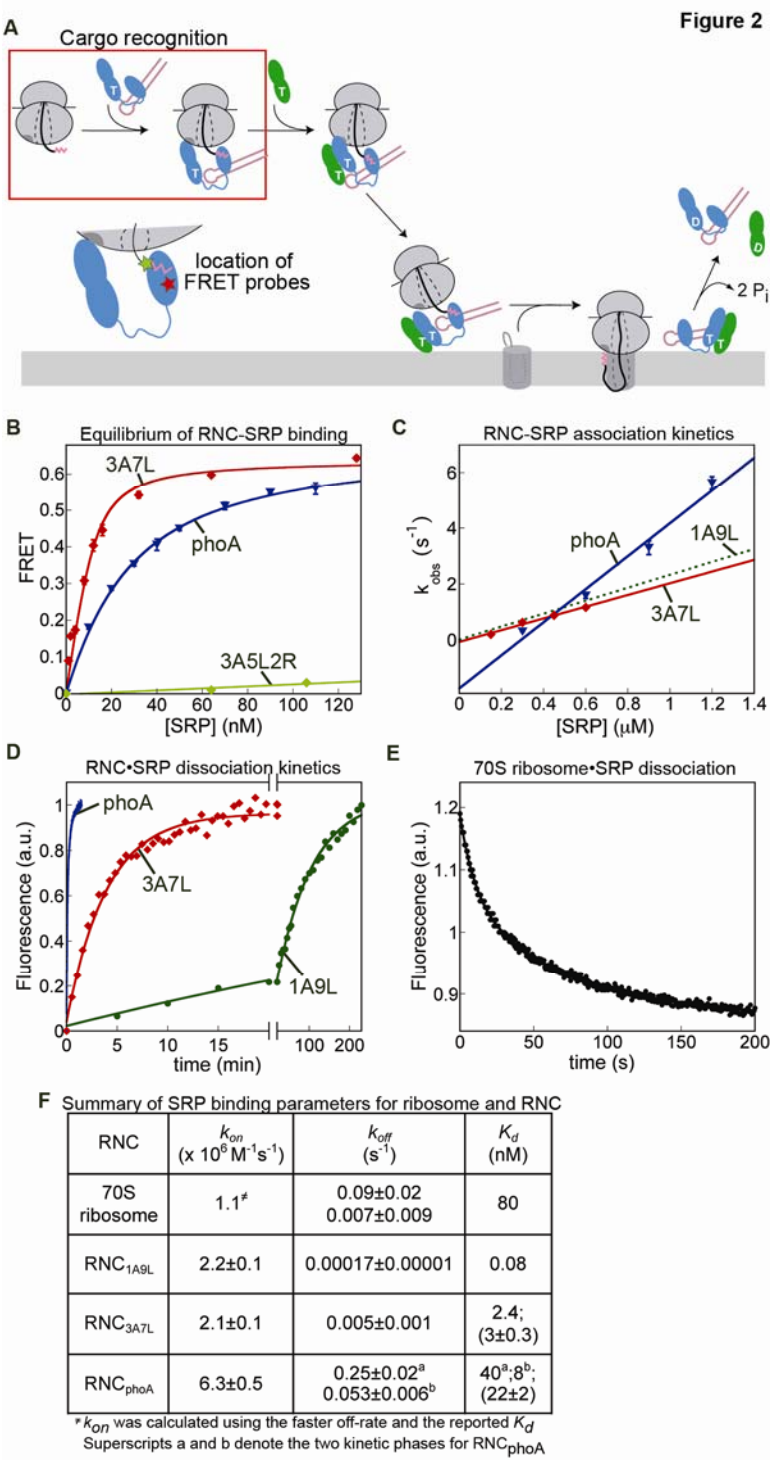

F Summary of SRP binding parameters for ribosome and RNC

RNC	k_{on} (x 10^6 $M^{-1}s^{-1}$)	k_{off} (s^{-1})	K_d (nM)
70S ribosome	1.1[≠]	0.09±0.02 0.007±0.009	80
RNC_{1A9L}	2.2±0.1	0.00017±0.00001	0.08
RNC_{3A7L}	2.1±0.1	0.005±0.001	2.4; (3±0.3)
RNC_{phoA}	6.3±0.5	0.25±0.02[a] 0.053±0.006[b]	40[a];8[b]; (22±2)

[≠] k_{on} was calculated using the faster off-rate and the reported K_d
Superscripts a and b denote the two kinetic phases for RNC_{phoA}

Figure 2. **Ribosomes bearing SRP substrates are selectively retained by SRP.** (A) Highlight of the cargo recognition step (box) measured in this figure and the FRET probes used. (B) Equilibrium titration for SRP binding to RNC_{3A7L} (red) and RNC_{PhoA} (blue). The data were fit to Eq. S2, and obtained K_d values are summarized in Fig. 2F in parentheses. The FRET signal with RNC_{3A5L2R} (light green) was too small to be quantified (See also Fig S1A). (C) Observed rate constants (k_{obsd}) for RNC-SRP association plotted against SRP concentration. Values of k_{on} were obtained from fit of the data to Eq. S4 and summarized in Fig 2F. The data for RNC_{1A9L} (dotted line) is from Saraogi *et al.* 2011 and shown for comparison. See Fig S1B, C for representative time courses. (D) Rate constants of SRP dissociation from RNC. The data were fit to Eq S5a for RNC_{1A9L} and RNC_{3A7L}, and Eq S5b for RNC_{PhoA} (see Fig S1D). The k_{off} values are summarized in Fig 2F. (E) Kinetics of SRP dissociation from the 70S ribosome. These data were fit to Eq S5b and k_{off} values arereported in Fig 2F. (F) Summary of the rate constants obtained in (C)-(E). The K_d values were calculated from measured rate constants using $K_d = k_{off}/k_{on}$, or from equilibrium titrations (values in parentheses). For RNC_{PhoA}, the measured K_d was the same, within error, as the weighted average of the K_d values for the two kinetic phases (indicated by superscripts a and b). See Supplemental Methods and Fig S1D for a discussion of the biphasic behavior of $RNC_{PhoA.}$ The k_{on} value for SRP-70S ribosome association was calculated from $k_{on} = k_{off}/K_d$ (Zhang et al., 2010). Error bars are depicted but may not be visible in panels (B) and (C). Values are averages of 2-3 experiments ± SD.

Figure 3

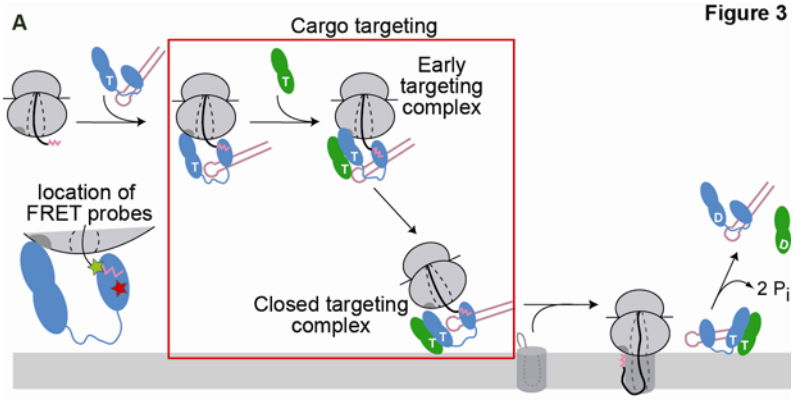

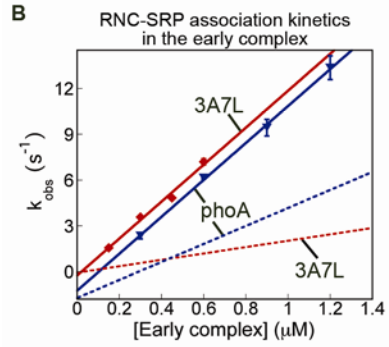

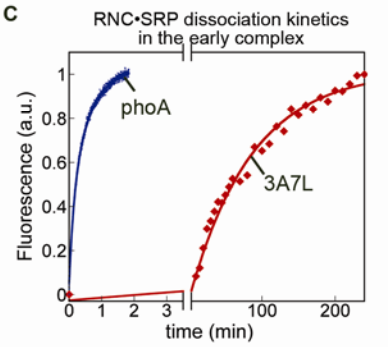

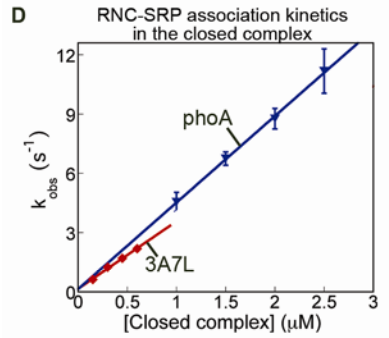

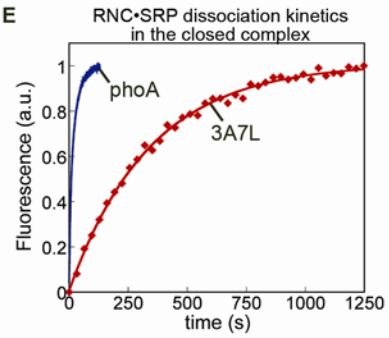

F

Summary of RNC binding to SRP during targeting

RNC	Complex with	k_{on} (x 10^6 $M^{-1}s^{-1}$)	k_{off} (s^{-1})	K_d (nM)
RNC_{3A7L}	SRP-only	2.1±0.1	0.005±0.001	2.4
	SRP-SR *Early*	12.1±0.5	0.0003±0.0001	0.03
	SRP-SR *Closed*	3.4±0.2	0.0031±0.0004	0.9
RNC_{phoA}	SRP-only	6.3±0.5	0.25±0.02[a] 0.053±0.006[b]	40[a] 8[b]
	SRP-SR *Early*	12.1±0.8	0.13±0.03[a] 0.033±0.006[b]	11[a] 3[b]
	SRP-SR *Closed*	4.4±0.5	0.19±0.04[a] 0.040±0.004[b]	43[a] 9[b]

Superscripts a and b denote the two kinetic phases for RNC_{phoA}

Figure 3. **FtsY actively regulates the interaction of SRP with its substrates.** (A) Highlight of the targeting step (box) measured in this figure and the FRET probes used. (B, D) Kinetics of RNC binding to the SRP•FtsY *early* complex (panel B) or *closed* complex (panel D) with RNC_{3A7L} (red) and RNC_{PhoA} (blue). The data were fit to Eq S4, and the k_{on} values obtained are summarized in Fig 3F. See Fig S2 for representative time courses. The dotted lines indicate the corresponding binding kinetics in the absence of FtsY (from Fig 2C) and are shown for comparison. (C, E) Kinetics of RNC dissociation from the *early* (C) or *closed* (E) targeting complex. The data were fit to Eq S5a or Eq S5b, and the obtained k_{off} values are summarized in Fig 3F. (F) Summary of the RNC-SRP binding affinity at different stages of the targeting pathway. The values for SRP only are from Fig 2F and are shown for comparison. K_d values were calculated from $K_d = k_{off}/k_{on}$. The two kinetic phases for RNC_{PhoA} are indicated by superscripts a and b. Values are averages of 2-3 experiments ± SD.

Figure 4

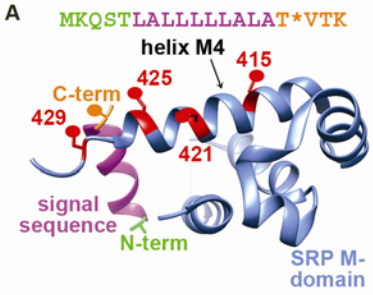

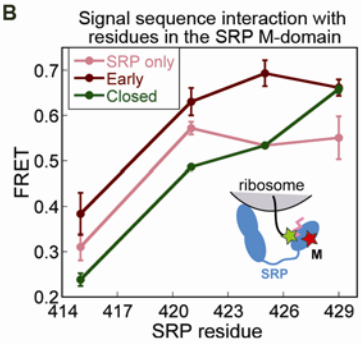

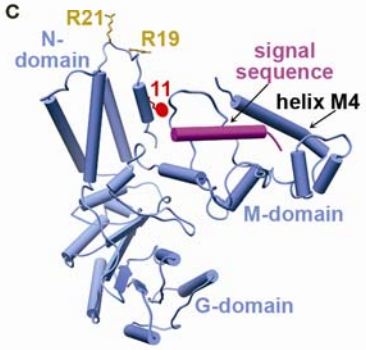

D

Binding parameters for RNC-SRP19/21E interaction during targeting

RNC_{3A7L} complex with	k_{on} (x 10^6 $M^{-1}s^{-1}$)	k_{off} (s^{-1})	K_d (nM)
SRP19/21E only	0.7±0.1	0.041±0.004	59
SRP19/21E-SR (*Early*)	3.0±0.3	0.034±0.004	11
SRP19/21E-SR (*Closed*)	2.1±0.1	0.013±0.002	6

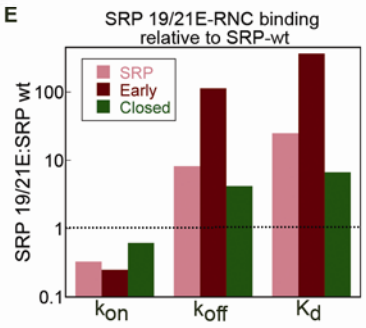

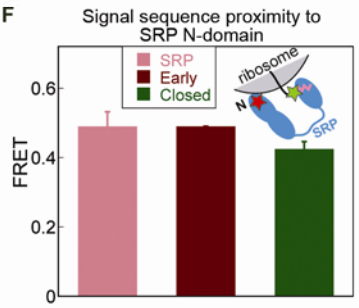

Figure 4. **Molecular basis for FtsY-induced changes in SRP-RNC binding affinity.** (A) Crystal structure of a signal sequence (magenta) bound to the *M. jannaschii* Ffh M-domain (blue) (PDB ID: 3NDB (Hainzl et al., 2011)). The donor dye at the signal sequence N- and C-terminus are in green and orange, respectively. The acceptor dyes on Ffh helix M4 are in red. Residue numbering is for homologous residues in *E. coli* Ffh. (B) FRET efficiency between Cm at the signal sequence C-terminus and BODIPY-FL at indicated residues in SRP helix M4 in the RNC•SRP complex (pink) and the *early* (dark red) and *closed* (green) targeting complexes. Inset shows a cartoon of the FRET pair used for this experiment. (C) Crystal structure of Ffh (blue) modeled into the cryo-EM density (PDB ID: 2J28 (Halic et al., 2006a)) for the SRP•RNC complex. The signal sequence is in magenta. Conserved residues 19 and 21 in the Ffh N-domain are shown in gold. Red denotes the FRET acceptor labeled at C11 in the N-domain. For clarity, the ribosome, which sits directly above R19 and R21, is not shown. (D) A summary of the kinetic parameters for SRP19/21E mutant binding to RNC_{3A7L} at various stages of targeting (see Fig S4B-G for time courses). (E) The defect displayed by mutant SRP19/21E in binding RNC_{3A7L} at different stages of targeting. The ratios of the rate or equilibrium constants for RNC_{3A7L} binding to SRP19/21E relative to wild-type SRP are plotted. The dotted line indicates the expected ratio of 1 if the mutant displays no defect (see Fig 4D and Fig S4). (F) Maximal FRET efficiency between Cm-labeled RNC_{3A7L} and BODIPY-labeled SRP C11 (panel C) during the targeting cycle. Inset shows a cartoon of the FRET pair used for this experiment. Molecular graphics were generated using UCSF Chimera (Pettersen et al., 2004). Values in (B) are averages of 4 experiments ± SEM. Values in (D) are averages of 2-3 experiments ± SD.

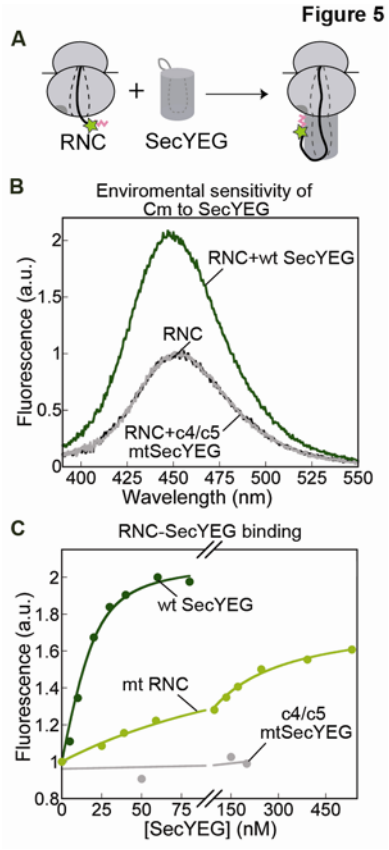

Figure 5. **Cm-labeled signal sequence reports on RNC binding to SecYEG.** (A) A scheme of RNC binding to SecYEG. The green star denotes the Cm dye. (B) Fluorescence spectra of 20 nM Cm-labeled RNC_{3A7L} in the absence (black) and presence of 300 nM wild-type (green) or c4/c5 mutant SecYEG (grey). (C) Equilibrium titration of 20 nM RNC_{3A7L} with wt-SecYEG (green) or c4/c5 mutant SecYEG (grey) and of 30 nM RNC_{3A5L2R} (mt-RNC) with wt-SecYEG (light green). The data were fit to Eq S6 and gave K_d values of 3 ± 2 nM (average ± SD, with n = 20) and 140 nM with RNC and mt-RNC, respectively.

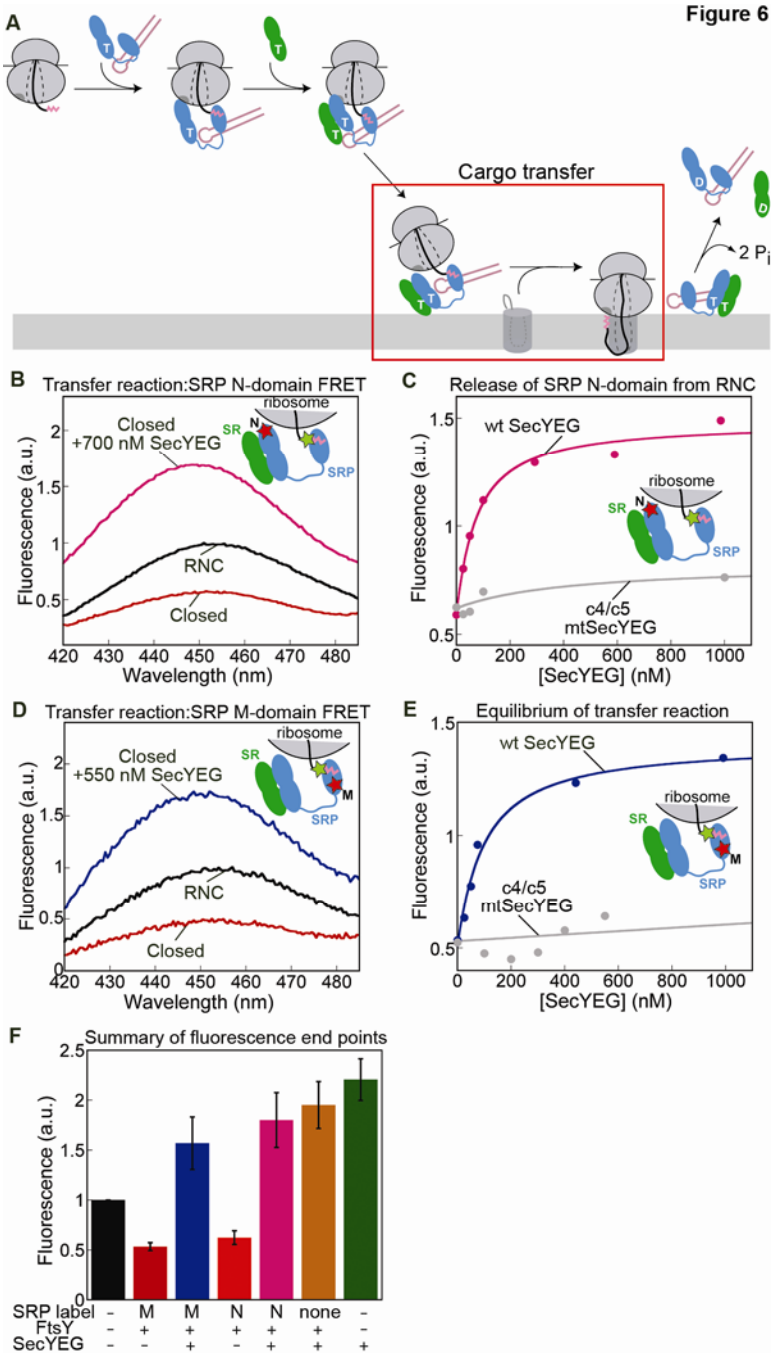
Figure 6
A
Cargo transfer
2 Pi
B
Transfer reaction:SRP N-domain FRET
Closed
+700 nM SecYEG
RNC
Closed
Fluorescence (a.u.)
Wavelength (nm)
ribosome
SR
SRP
C
Release of SRP N-domain from RNC
wt SecYEG
c4/c5
mtSecYEG
[SecYEG] (nM)
D
Transfer reaction:SRP M-domain FRET
Closed
+550 nM SecYEG
RNC
Closed
E
Equilibrium of transfer reaction
F
Summary of fluorescence end points
SRP label - M M N N none -
FtsY - + + + + + -
SecYEG - - + - + + +

Figure 6. SecYEG effectively unloads cargo from the *closed* targeting complex. (A) Highlight of the cargo transfer step in the targeting pathway. (B) Fluorescence spectra of Cm-labeled RNC3A7L by itself (black), in the *closed* targeting complex with SRP labeled with BODIPY-FL at C11 (N-domain) (red), and upon addition of SecYEG to the *closed* targeting complex (pink). Inset shows a cartoon of the FRET pair used for this experiment. (C) Titration of wildtype (pink) or mutant (grey) SecYEG into the *closed* targeting complex formed with BODIPY-labeled SRP (C11) (also see Fig S5B). (D) As in B, except that the M-domain FRET pair (inset and Fig. 1B) was used. (E) As in C, except that the M-domain FRET pair was used. The data were fit to Eq S6 to give an EC_{50} for transfer of 39 ± 26 nM. (F) Summary of the changes in fluorescence end points upon addition of saturating SecYEG to the *closed* targeting complex, formed with unlabeled SRP (brown) or with SRP labeled at the M- (blue) or N- (magenta) domain. The fluorescence signal upon direct addition of RNC to SecYEG is in green. All experiments were performed with 20 nM RNC_{3A7L} labeled with Cm at the C-terminus of the signal sequence, 40 nM SRP, 500 nM FtsY, and 100 μM GppNHp. All fluorescence values are normalized relative to that of RNC (black). Values are averages of >3 experiments ± SD.

Figure 7

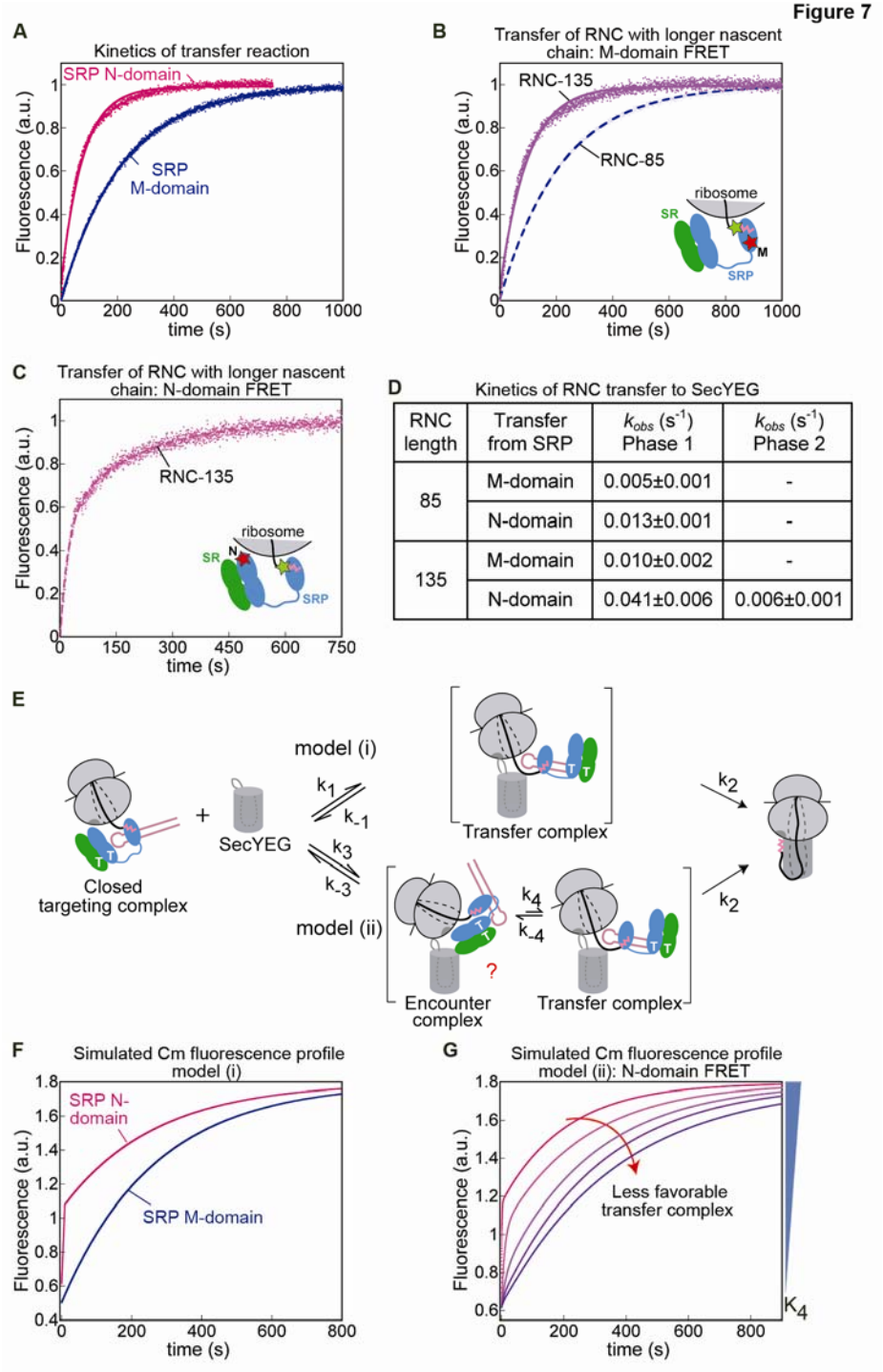

RNC length	Transfer from SRP	k_{obs} (s^{-1}) Phase 1	k_{obs} (s^{-1}) Phase 2
85	M-domain	0.005±0.001	-
	N-domain	0.013±0.001	-
135	M-domain	0.010±0.002	-
	N-domain	0.041±0.006	0.006±0.001

Figure 7. **Kinetics of cargo transfer to SecYEG.** (A) Kinetics of transfer of RNC_{3A7L}-85 upon addition of 1μM SecYEG to the *closed* targeting complex formed by SRP labeled with BODIPY-FL at the M- (blue) or N-domain (pink). The data were fit to Eq S5a to obtain the observed rate constants listed in D. (B) Kinetics of transfer of RNC_{3A7L}-135 upon addition of SecYEG to the *closed* targeting complex formed by SRP labeled with BODIPY-FL at the M-domain (purple). Data for RNC_{3A7L}-85 (blue) is shown for comparison. (C) As in B, except that the *closed* targeting complex was formed fby SRP labeled with BODIPY-FL at the N-domain (magenta). (D) Summary of the observed rate constants for RNC transfer from (A)-(C). (E) Alternative models for transfer of signal sequence from SRP to SecYEG. (F) Simulated kinetic behavior of the transfer reaction according to model (i), monitored using FRET acceptor labeled at the SRP M- (blue) or N- (pink) domain. (G) Simulated kinetic behavior of the transfer reaction according to model (ii) as the equilibrium to form the transfer complex was progressively less favorable (top to bottom). The value of $K_4 = k_4/k_{-4}$ was set to 25, 5, 1, 0.2, 0.1 respectively. For clarity, only results with the SRP N-domain are shown (see Supplemental Methods for details). Values are averages of 2-3 experiments ± SD.

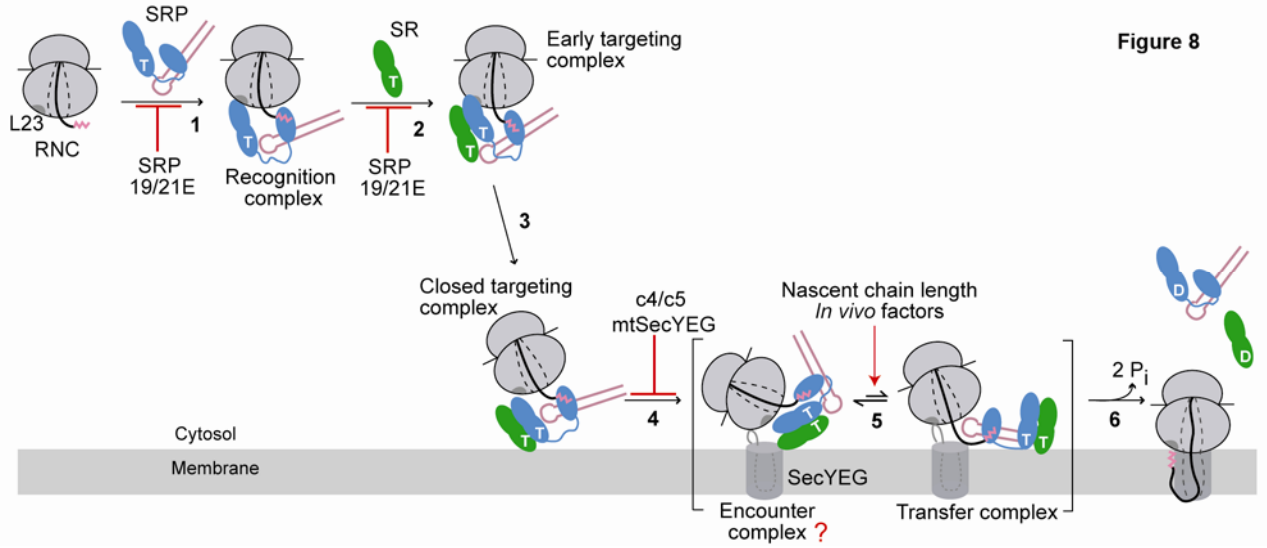

Figure 8. **A model for highly coordinated delivery of RNC from the cytosol to the translocon, driven sequentially by the SRP/SR GTPases and SecYEG at different stages of the targeting cycle.** See text for description of the model. Color notations are the same as in Figure 1A. The question mark indicates the unknown nature and structure of the encounter complex.

Figure S1

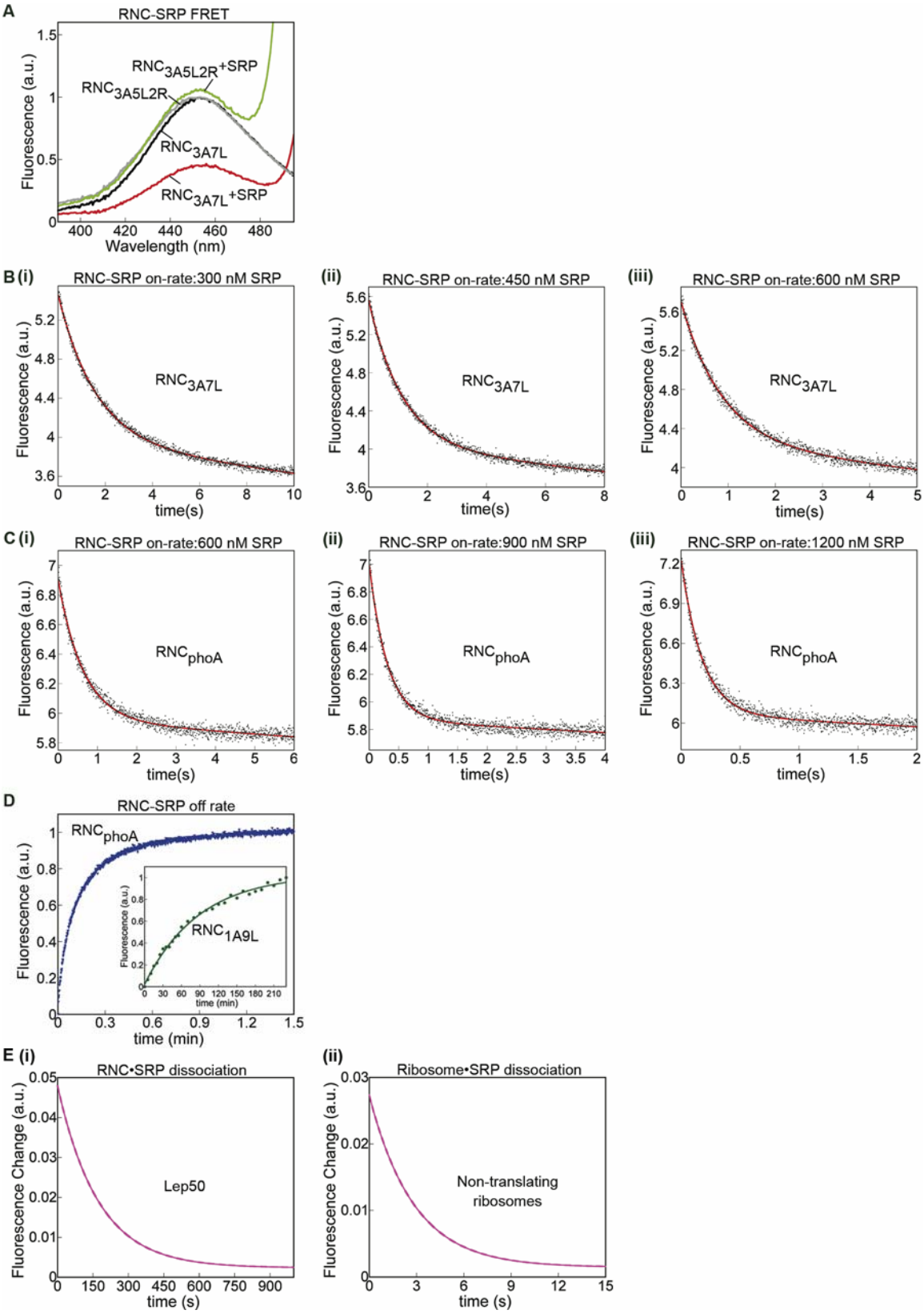
A
RNC-SRP FRET
Fluorescence (a.u.)
Wavelength (nm)
RNC3A5L2R+SRP
RNC3A5L2R
RNC3A7L
RNC3A7L+SRP
B (i)
RNC-SRP on-rate:300 nM SRP
(ii)
RNC-SRP on-rate:450 nM SRP
(iii)
RNC-SRP on-rate:600 nM SRP
RNC3A7L
time(s)
C (i)
RNC-SRP on-rate:600 nM SRP
(ii)
RNC-SRP on-rate:900 nM SRP
(iii)
RNC-SRP on-rate:1200 nM SRP
RNCphoA
D
RNC-SRP off rate
RNC1A9L
time (min)
E (i)
RNC•SRP dissociation
Lep50
(ii)
Ribosome•SRP dissociation
Non-translating ribosomes
Fluorescence Change (a.u.)
time (s)

Figure S1. Equilibrium and dynamics of RNCs binding to SRP. (A) Change in donor fluorescence when 25 nM Cm-labeled wt-RNC (RNC_{3A7L}) or mt-RNC (RNC_{3A5L2R} containing two arginines into the signal sequence) was treated with 50 nM or 424 nM respectively of BODIPY-FL labeled SRP 421. (B) Time courses for association of RNC_{3A7L} with 300, 450 and 600 nM SRP. (C) Time courses for association of RNC_{phoA} with 600, 900 and 1200 nM SRP. For B and C, the observed rate constants obtained from Eq S3 were used to generate Fig 2C. (D) A magnification of the plot for dissociation of RNC_{phoA} from SRP (Fig 2D) showing the biphasic behavior of RNC_{phoA}. The time course for phoA was fit to a double exponential (Eq S5b) to give dissociation rate constants of 0.25 ± 0.023 s^{-1} and 0.053 ± 0.006 s^{-1}. The amplitudes for the two phases were 40% and 60%, respectively. Although the biphasic nature of SRP•RNC_{phoA} dissociation persisted as the targeting reaction progressed, the two phases responded similarly to FtsY. Therefore, only the rate constants from the faster-dissociating phase are plotted in the main text. Inset shows the complete plot for SRP•RNC_{1A9L} dissociation (Fig 2D). (E) Kinetic simulations of SRP dissociation from (i) Lep50 and (ii) non-translating ribosomes based on the 3-step model and individual rate constants reported by Holtkamp et al. (Holtkamp et al., 2012). These simulations show that SRP dissociates from the final, stable RNC•SRP complex at a rate constant (k_{off}) of 0.0058 s^{-1} for RNC bearing a model SRP substrate Lep, and at a k_{off} value of 0.36 s^{-1} from the 70S ribosome. See Materials and Methods for details.

Figure S2

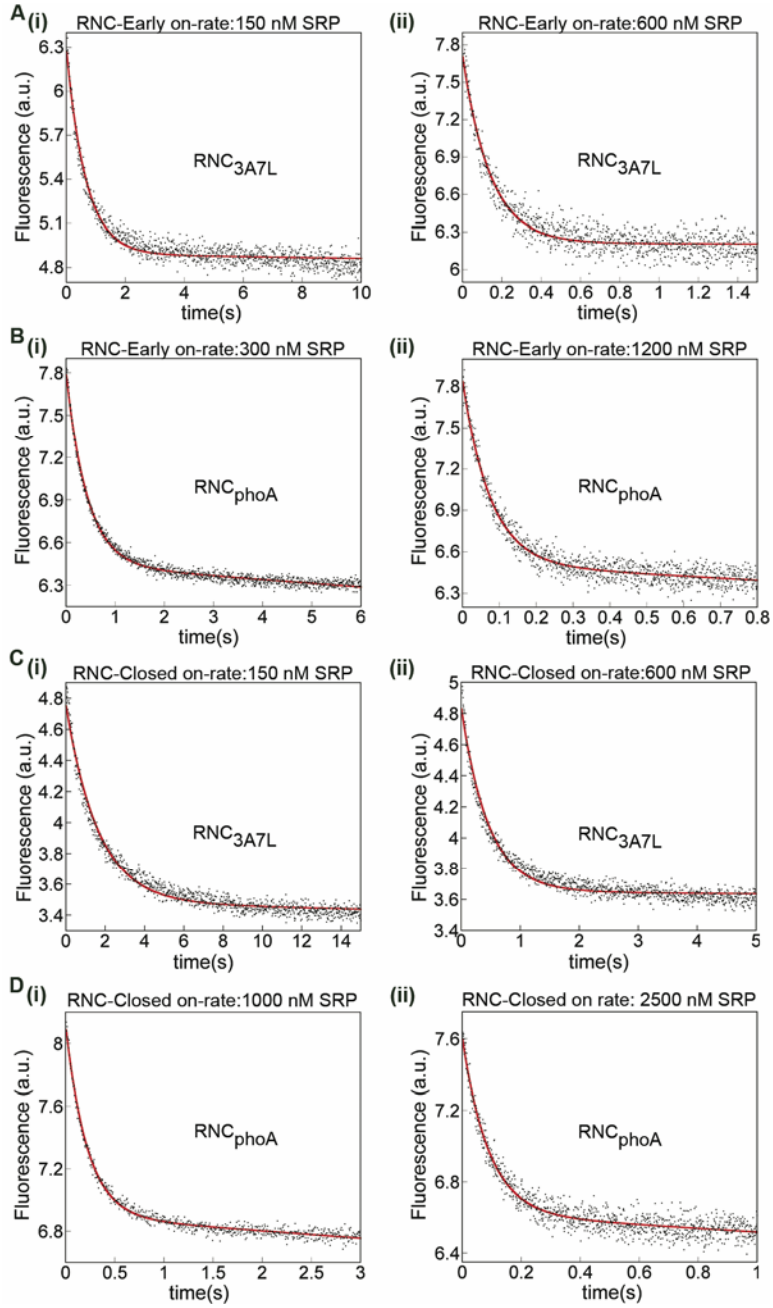

Figure S2. **Kinetics of RNC binding to early and closed complexes.** Representative curves showing the time courses for association of RNCs with the SRP•SR early (A-B) or closed complex (C-D) for RNC_{3A7L} (A, C) and RNC_{phoA} (B, D). The observed rate constants obtained from Eq S3 were used to generate Figs 3B and 3D.

Figure S3

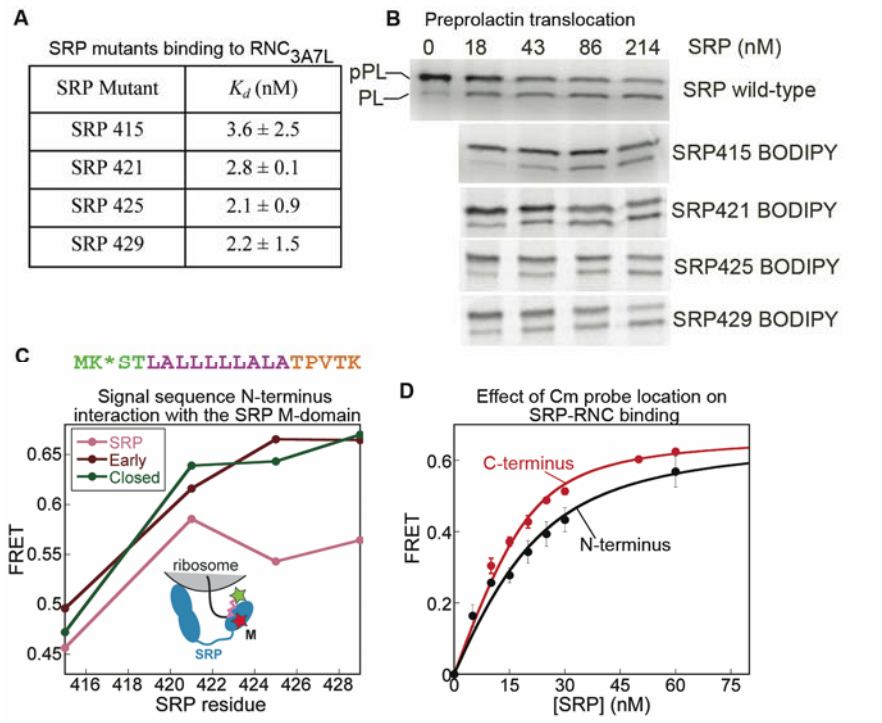

Figure S3. Signal sequence binding to the SRP M-domain. (A) A summary of the binding dissociation constants obtained for BODIPY-FL-labeled single cysteine mutants of SRP at residues 415, 421, 425 and 429 in the SRP M-domain binding to fluorescently labeled RNC_{3A7L}. (B) The activity of BODIPY-FL-labeled single cysteine mutants of SRP was tested in a protein translocation assay (Shan et al., 2007). (C) Maximal FRET efficiency between Cm at the N-terminus of signal sequence and BODIPY-FL at indicated residues in SRP helix M4 upon RNC binding to SRP (pink), and the *early* (dark red) and *closed* (green) targeting complexes. Inset shows a cartoon of the FRET pair used for this experiment. For clarity, only a part of the ribosome is shown. The location of the donor fluorophore at the N-terminus of the signal sequence is shown with an asterisk (top). (D) The binding affinity of SRP, labeled with BODIPY-FL at residue 421, for RNC_{3A7L} labeled with Cm at either the C- or N-terminus of the signal sequence. The data were fit to Eq. S2 and gave K_d values of 3.7 and 8.4 nM for RNC_{3A7L} labeled at the C- and the N-terminus, respectively.

Figure S4

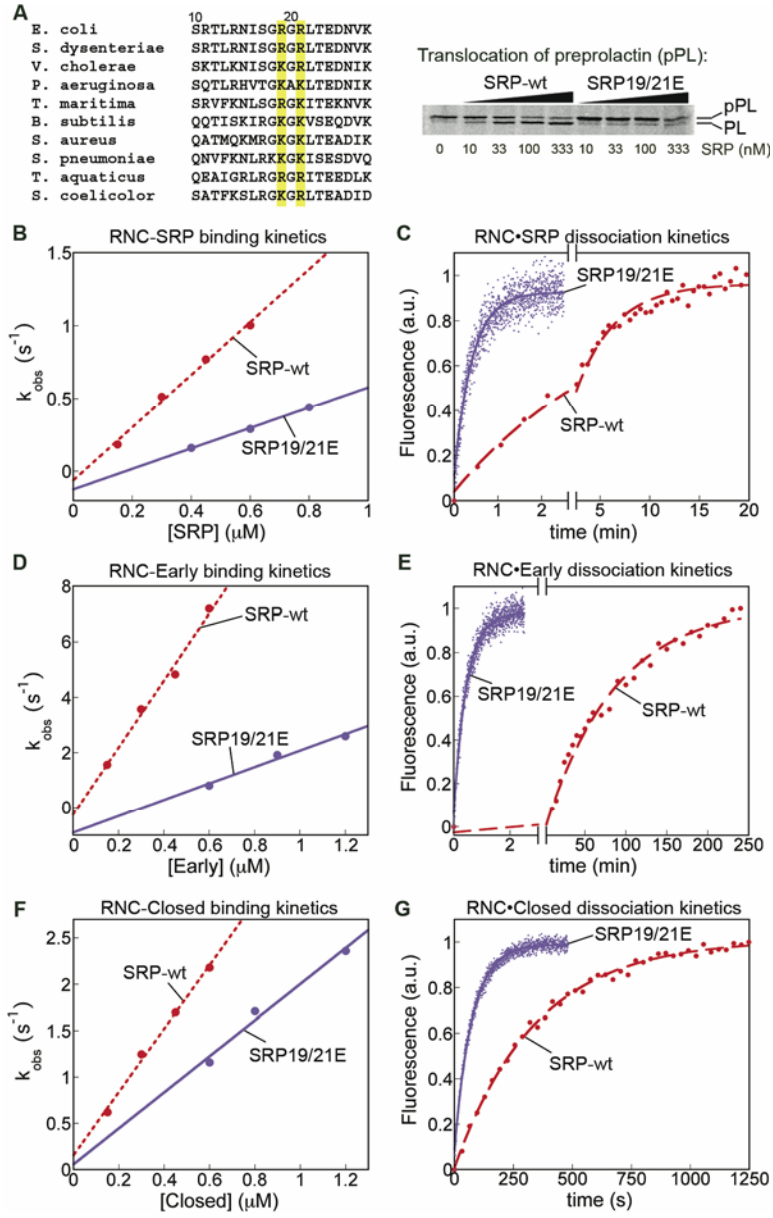

Figure S4. Sequence information and kinetic data for SRP 19/21E mutant. (A) Sequence alignment of Ffh homologues with the two conserved basic residues highlighted. Numbering is for *E. coli* Ffh. The right panel shows the activity of the SRP 19/21E mutant in a protein translocation assay (Shan et al., 2007). (B-G) Kinetic measurements for SRP19/21E association with (B, D, F) and dissociation from RNC_{3A7L} (C, E, G) at different stages of the targeting pathway. (B), (C) SRP only; (D), (E) *Early* and (F), (G) *Closed* targeting complex. The data for wild-type SRP (dashed lines) are shown for comparison. The rate constants obtained from these data are tabulated in Fig 4D.

Figure S5

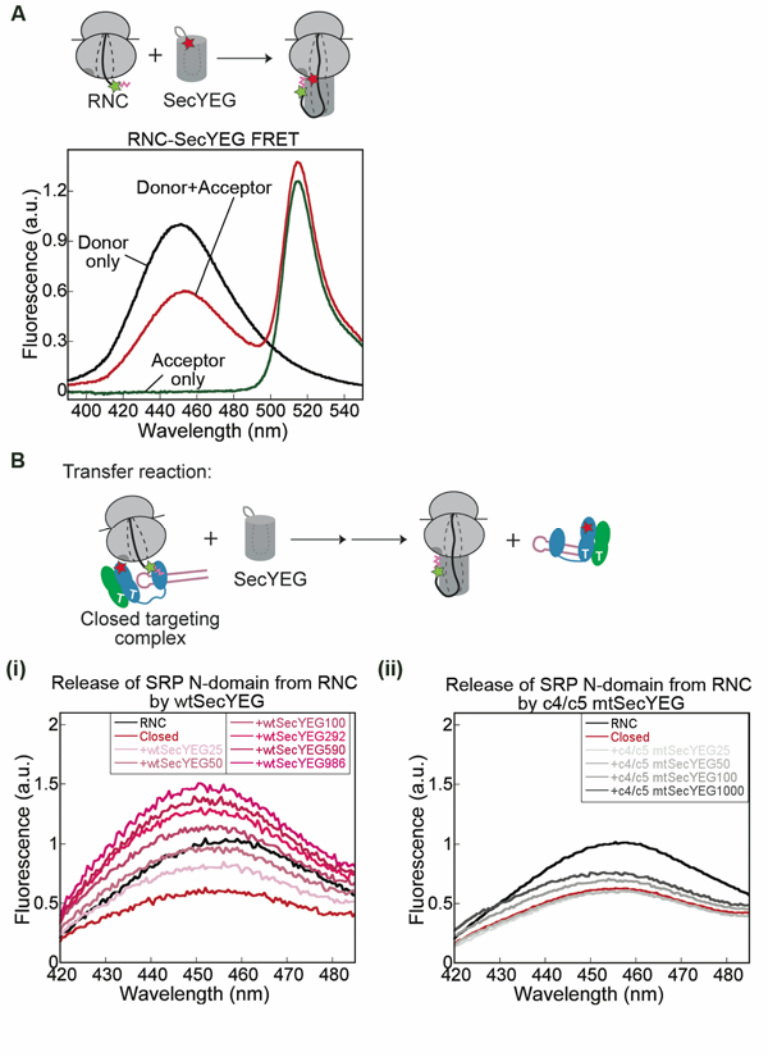

Figure S5. Cm probe incorporated into the signal sequence reports on RNC-SecYEG binding. (A) FRET between Cm–labeled RNC and BODIPY-labeled SecYEG. 30 nM SecYEG labeled with BODIPY-FL at residue 180 was added to 40 nM RNC_{3A7L} labeled with Cm at the C-terminus. (B) Titration of the *closed* targeting complex with SecYEG. Wt-SecYEG (i) or c4/c5 mtSecYEG (ii) was titrated into the *closed* targeting complex containing 20 nM RNC_{3A7L} labeled with Cm at the C-terminus, 40 nM SRP labeled with BODIPY-FL at position 11 (N-domain), 500 nM FtsY, 100 μM GppNHp. The fluorescence peak at each concentration was plotted against [SecYEG] to generate Fig 6C. In A and B, the schematic shows the binding reaction monitored and the corresponding FRET pair used in the experiment.

Table S1. Anisotropy measurements for 7-hydroxycoumaryl ethylglycine (Cm) and BODIPY-FL fluorophores.

Dye	Anisotropy
Cm	0.019
Cm-RNC (C-terminus)	0.139
Cm-RNC (N- terminus)	0.123
BODIPY-FL	0.011
SRP 415 BODIPY-FL	0.232
SRP 421 BODIPY-FL	0.171
SRP 425 BODIPY-FL	0.205
SRP 429 BODIPY-FL	0.204

Supplemental References

Holtkamp, W., S. Lee, T. Bornemann, T. Senyushkina, M.V. Rodnina, and W. Wintermeyer. 2012. Dynamic switch of the signal recognition particle from scanning to targeting. *Nat. Struct. Mol. Biol.* 19:1332-7.

Shan, S., S. Chandrasekar, and P. Walter. 2007. Conformational changes in the GTPase modules of the signal recognition particle and its initiation of protein translocation. *J. Cell Biol.* 178:611-620.

CHAPTER 4

Towards Understanding the Mode of SecYEG-Nascent Polypeptide Chain Interaction

Abstract

Translating ribosomes targeted to the sites of translocation at the endoplasmic reticulum or the bacterial inner membrane by the SR•SRP targeting complex are unloaded onto a conserved protein-conducting channel, Sec61 complex in eukaryotes and SecYEG in bacteria. In both cases, the ribosome-nascent chain complex (RNC) interacts in a bidentate manner with the channel: the cytosolic loops of SecYEG contact the ribosome at the ribosomal channel exit site, while the lateral gate accommodates the signal peptide. As the ribosome continues to synthesize the nascent chain, the trasmembrane domains (TMs) of a membrane protein exit SecYEG into the lipid bilayer, while the polypeptide chain of a secretory protein is translocated through the pore of the channel into the periplasmic space. Despite considerable progress in our understanding of protein translocation across the lipid bilayer and biogenesis of membrane proteins, little is known about the dynamics of the signal peptide-SecYEG interaction at early stages of these processes. Further, the role of the accessory components of the SecYEG complex, such as the abundant insertase YidC, in this interaction remains unclear. Here, we use a FRET assay to map the orientation of a signal peptide inside SecYEG as it interacts with RNC. We used a signal peptide mimic, an engineered 3A7L sequence, appended to the mature region of PhoA, and the only TM of FtsQ. We monitored their interaction with SecYEG while increasing the length of the mature region to mimic an elongating nascent chain. Although additional experiments are necessary to draw definite conclusions, the results of our study suggest that 3A7L and the TM of FtsQ bind SecYEG with different orientations. Interestingly, as the length of the nascent chain increases, the binding affinity of RNC for SecYEG first weakens and then tightens for both nascent chains. YidC affects both the conformation of the SecYEG-nascent chain complex and its stability. Collectively, the results of this study suggest that SecYEG in

DDM is capable of discriminating between the types of signal sequences and can sense the length of the nascent chain. Further, we propose that one of the roles of YidC may be to facilitate the exit of TMs from SecYEG. The biophysical assays described in this chapter set the stage for further characterization of SecYEG-RNC interaction in an in vitro system and promise to shed light on molecular details of the membrane protein biogenesis.

Introduction

Docking of a translating ribosome onto a protein-conducting channel, or translocon, at the target membrane is the final step in the cotranslational protein targeting pathway. Both in prokaryotes and eukaryotes, translocon is a heterotrimeric integral membrane protein that is an essential constituent of a multi-component complex involving accessory membrane proteins (Veenendaal, 2004; Kudva, 2013). The first crystal structure of the translocon from an archaeon *M. jannaschii*, SecYEβ, solved at 3.2 Å resolution was a significant breakthrough in the field of cellular protein export. The structure showed that the main subunit of the translocon, SecY, consists of ten transmembrane domains (TMs), forming a characteristic clamshell structure with TMs 1-5 composing one half and TMs 6-10 the second half of the "clam" (van den Berg, 2004). TMs 5 and 6 are connected by a short loop that acts as a hinge, linking the two halves of SecY. On the side opposite to the hinge, TMs 2b and 7 constitute the so-called lateral gate that is closed in the idle state of the translocon and is open in the translocation state (Fraunfeld, 2011; Egea, 2010; du Plessis, 2009). The gate functions as an exit site for TMs of the nascent membrane protein partitioning into the lipid bilayer.

The pore of SecY has an hourglass shape consisting of aqueous cytoplasmic and periplasmic funnels separated in the center by a constriction, the so-called pore ring, ~ 5-8 Å in diameter composed of six hydrophobic residues. The pore ring was proposed to form a gasket around the translocating nascent chain, preventing the leakage of small molecules and ions across the lipid bilayer (Park, 2011). In the idle state, a short helix 2a, called the plug domain, forms hydrophobic contacts with the lateral gate and seals the channel at the periplasmic side (Li, 2007). The plug domain was proposed to move away from the center of the channel, allowing the helices of the lateral gate to part and opening the passage through the pore. The extent of the

translocation of the plug domain in the open state of the translocon is still a matter of debate (Lycklama A Nijeholt, 2010; van den Berg, 2004).

Another interesting feature of the SecY subunit is the set of prominent cytosolic loops connecting TM6 to TM7 and TM8 to TM9 (Fraunfeld, 2011; Zimmer, 2008; van den Berg, 2004). These loops protrude approximately 20Å into the cytosol and contain conserved basic residues that interact with cytosolic factors such as the ribosome, FtsY, and SecA (Kuhn, 2011; Zimmer, 2008; Menetret 2007). The SecE subunit functions as a molecular hinge that clamps SecY on the side opposite to the lateral gate and is composed of two helices one of which lies on the cytosolic face of the lipid bilayer. The Secβ consists of one TM.

Sequence alignment of archaeal, bacterial, and eukaryotic translocons shows that the pore-forming subunits of translocons across the species share 50% sequence identity (van den Berg, 2004). The X-ray crystal structures and cryo-EM reconstructions of bacterial and eukaryotic translocons reveal great structural similarity to the archaeal SecYEβ. The *E. coli* translocon SecYEG differs from both archaeal and eukaryotic translocons by the number of TMs. While the SecY subunit is almost identical to that of SecYEβ, the E subunit consists of four α-helices instead of two, and the G subunit is composed of two TMs instead of one. Two of the four helices of SecE are non-essential and are not part of the helix bundle of SecYEG (Fraunfeld, 2011), with the two remaining helices forming a molecular clamp around SecY. While SecG is non-essential (Brundage, 1990), it was proposed to play a role in SecA-dependent translocation of precursor proteins across the lipid bilayer (Moser, 2013). The mammalian homolog of the translocon, Sec61p complex (Gorlich, 1993, 1992) resembles the archaeal SecYEβ and consists of three subunits Sec61α, Sec61γ, and Sec61β (Becker, 2009; Veenendaal, 2004; Beckmann, 2001).

A large body of evidence including both function and structural studies shows that SecYEG interacts with a translating ribosome in a bidentate manner. Prominent cytosolic loops of the SecY subunit contact the ribosomal proteins L23 and L29 at the ribosomal tunnel exit site (Menetret, 2007; Cheng, 2005), while the lateral gate of a translocon accommodates the signal peptide (van den Berg, 2004; Plath, 1998; Mothes, 1998; Jungnickel, 1995). Early crosslinking studies involving posttranslational substrates preproalpha factor, preprolactin, and proOmpA collectively defined the SecY subunit as the channel for translocating nascent chain and the lateral gate as the binding site for a signal peptide (Canon, 2005; Plath, 1998; Crowley, 1994; Joly, 1993). A number of cryo-EM structures of a translating ribosome bound to the translocon from prokaryotic and eukaryotic systems followed, defining the path of the nascent chain in the ribosome-translocon complex (Fraunfeld, 2011; Becker, 2009). Recently, the translocon-RNC complexes were formed *in vivo* as translocation intermediates, using either ER microsomes or intact *E. coli* cells, trapping the signal peptide or TM of the nascent membrane protein bound to the lateral gate. These intermediates were visualized using cryo-EM, showing conclusively the nascent chain bound to SecYEG (Gogala, 2014; Park, 2014).

The crosslinking studies and the structural data support and explain the earlier suggestion that SecYEG may be functioning as a checkpoint capable of distinguishing between the nascent proteins destined for export/incorporation into the lipid bilayer and cytosolic proteins devoid of signal sequences. The notion originated from genetic screens that isolated mutations (*prl* for protein localizations), allowing for correct localization of proteins with defective or even missing signal sequences (van der Wolk, 1998; Flower, 1994; Derman, 1993; Osborne, 1993; Emr, 1981). In particular, *prlA* mutations in the SecY gene produce a superactive translocon that no longer requires a signal peptide to mediate translocation of a precursor protein (Fekkes, 1998;

Derman, 1993). Significantly, most of the prlA mutations localize to the pore region, the lateral gate region, and the plug domain of SecY, likely destabilizing hydrophobic contacts between these structures (Li, 2007; van der Berg, 2004). Weakening of this hydrophobic cluster in prlA mutants would obviate the need for a hydrophobic signal sequence required to open the channel.

One of the most interesting questions of the SecYEG-nascent chain interaction is the mechanism whereby the correct topology of the signal peptide inside the SecY subunit is established during protein translocation and the orientation of transmembrane domains at early stages of the membrane protein biogenesis. While earlier functional and structural studies showed that the nascent chain interacts with SecY (Plath, 1998; Mothes, 1998; Jungnickel, 1995) and likely adopts a looped conformation with the N-terminus pointing towards the cytosol (Park, 2014, 2011; Shaw, 1988), they provide little information as to the dynamics of the SecYEG-nascent chain interaction. At best, these studies either observed the protein already integrated into the lipid bilayer (Kocik, 2012; Shaw, 1988) or were based on low resolution structural data (Park, 2014) or crosslinking assays, correlating the length of the nascent chain with the intensity of the crosslinked translocon-nascent chain product (Park, 2011).

A relatively recent study attempted to monitor Sec61p-nascent chain interaction in ER microsomes, using RNCs with progressively longer nascent chains containing TM1 of aquaporin 4 (Devaraneni, 2011). Using a variety of elegant biochemical and biophysical assays, the authors showed that the TM inserts head first, but flips the orientation to type II topology at the nascent chain length of approximately 125 aa, resulting in a translocated C-terminal mature region. Another study attempted to monitor the force exerted by SecYEG as it interacts with an elongating nascent chain *in vivo* (Ismail, 2012). The pulling force was observed at two distinct lengths of the nascent chain, indicating conformational changes undergone by the TM as it

interacts with SecYEG. While all of these studies contribute invaluable information as to the translocon-nascent polypeptide interaction, they do not attempt to map the orientation of the signal peptide of the elongating nascent chain inside the SecY subunit with high resolution. Further, whether detergent-solubilized SecYEG in the absence of accessory factors is capable of sensing an increasing length of the nascent chain and binds the signal peptide in different orientation depending on the length of the polypeptide chain remains an open question. Here, we use a FRET assay between BODIPY-FL-labeled SecYEG and the RNCs site-specifically labeled with coumarin at the signal sequence/TM to observe the conformational changes undergone by the signal peptide as SecYEG binds RNCs with progressively longer nascent chains. Our studies show that the nascent chain binds detergent-solubilized SecYEG in a loop conformation with the signal peptide adopting type II topology and suggest that SecYEG alone may be sufficient to correctly bind the signal peptide. Further, we observed the dependence of the binding affinity of SecYEG for RNC on the length of the nascent chain, suggesting that *in vivo* SecYEG may sense the length of the nascent chain and modulate the affinity of the translating ribosome for the target membrane. The physiological significance of the differential affinity of SecYEG for nascent chains of varying length is currently not clear and requires additional assays. It may constitute an important part of the mechanism regulating membrane protein biogenesis.

In vivo, SecYEG exists as a complex called holotranslocon, which consists of several membrane proteins, including SecDF, YajC, and YidC (Schulze, 2014; Dalbey, 2014; Nouwen, 2002; Scotti, 1999; Duong, 1997). The latter is a member of the YidC-Oxa1-Alb3 family and was shown to be essential for cell growth, with deletion causing global changes in cell physiology (Kiefer, 2007). It is present in a bacterial inner membrane in a 5-fold molar excess over SecYEG (Drew, 2003; Urbanus, 2001) and is thought to play an important role in

membrane protein biogenesis acting as an insertase/foldase (Dalbey, 2004; Houben, 2002; Urbanus, 2001; van der Laan, 2001; Houben, 2000). A number of substrates have been identified that require YidC for insertion, including F_0c subunit of ATP synthase (van Bloois, 2004; Yi, 2004; van der Laan, 2004), M13 bacteriophage procoat protein (Stiegler, 2011; Samuelson 2001), pf3 bacteriophage coat protein (Ernst, 2011), MscL (Facey, 2007), and the subunit a of cytochrome oxidase a (du Plessis, 2006). YidC also increases efficiency of integration of SecYEG-dependent substrates MalF and MalFGK (Wagner, 2008), subunits a and b of F_1F_0 ATP synthase (Yi, 2004) and was shown to interact with Lep (Houben, 2002; Houben, 2000) and FtsQ (Urbanus, 2001). An intriguing recent study showed that SRP substrates can be targeted to either SecYEG or YidC, with the analyzed substrates including TatC, MtlA, and YidC devoid of the periplasmic loop (Welte, 2012). A growing list of substrates whose biogenesis either requires or is facilitated by YidC raises a question at to the precise role of YidC as a part of the membrane protein biogenesis machinery. It appears that substrates that have unbalanced charge distribution in transmembrane domains and do not follow the "positive inside" rule, have TMs with reduced degree of hydrophobicity, or have a prevalence of negative charge in the regions flanking the TMs exhibit higher YidC-dependence (Zhu, 2013; Gray, 2011; Price, 2010). The precise features of a membrane protein that define it as a YidC substrate, however, are yet to be determined. Further, at present, it remains unclear whether or not YidC acts as an independent insertase capable of receiving the cargo protein from the targeting complex or functions in conjunction with SecYEG to facilitate biogenesis of membrane proteins.

Topological analysis of bacterial YidC revealed that this 548 aa long membrane protein is composed of six transmembrane domains with a large 330 aa long periplasmic loop connecting TM1 to TM2 (Saaf, 1998). Apart from the X-ray structure of the non-essential periplasmic

domain solved at 1.8Å resolution (Ravaud, 2008), no high resolution structural data exist. Structural information regarding the *E. coli* YidC is currently limited to a low resolution cryo-EM model of dimeric YidC alone (Lotz, 2008) or in complex with RNCs bearing F_0c nascent chains (Kohler, 2009). A monomeric YidC-ribosome complex at 8.6 Å resolution was also solved by cryo-EM, revealing the long C-terminal tail of YidC from *R. baltica* and *O. alexandrii* interacting with the ribosomal protein L29 (Seitl, 2014). Interestingly, the long C-terminal tail is absent in the *E. coli* YidC and is composed of 13 amino acids with prevalence of basic residues (Saaf, 1998). A recent fluorescence cross correlation study showed that the *E. coli* YidC interacts only with programmed ribosomes and does so in a monomeric state (Kedrov, 2013). Recently the crystal structure of YidC from *Bacillus halodurans* was solved at 2.4 Å resolution (Kumazaki, 2014). The structure revealed a novel fold that can be likened to a curved closed palm of the hand, in which the five membrane spanning helices form a hydrophilic groove in the lipid bilayer open towards the cytoplasm and the lipids and closed at the periplasmic side. A conserved arginine residue is situated in the center of the hydrophilic groove and was shown to be essential for efficient insertion of membrane proteins containing acidic residues in their N-termini. The structural data combined with functional assays allowed the authors to propose a model for how YidC facilitates membrane protein insertion. The hydrophilic surface of YidC with the charged arginine residue allows the extracellular domains containing negative charge to be translocated across the low-dielectric environment of the lipid bilayer. It is important to note, however, that the model is based on the functional assays examining insertion activity of the *Bacillus subtilis* YidC (SpoIIIJ) using single-spanning membrane proteins Pf3 and MifM. Similar assays were not performed with the *E. coli* YidC. Furthermore, mutations in the hydrophilic groove of the *E. coli* YidC did not impair the insertion of a double-spanning membrane protein M13 procoat,

suggesting that, in addition to the hydrophilic groove of YidC, other determinants of this insertase are important in insertion of membrane proteins.

The importance of YidC in biogenesis of membrane proteins emerged relatively recently and, despite the enormous progress in our understanding of its physiological role, many questions regarding its functions in the cell currently remain open. Biophysical assays to dissect the mechanism of the YidC activity are limited in part by the lack of structural information, and in part by the lack of a defined set of bona fide YidC substrates. The complex nature of the E. coli translocation machinery involving several components with two major pathways – co- and posttranslational – handling many substrates with overlapping requirements complicates the issue (Wu, 2012; Koch, 2000; Neumann-Haefelin, 2000; Qi, 1999; Saaf, 1995). Does YidC act independently or in conjunction with SecYEG? Does it act solely as a foldase assisting SecYEG? Does it function as a recipient of a translating ribosome? If yes, what determines targeting of the translating ribosomes to YidC rather than SecYEG? Is the targeting reaction promiscuous and substrate independent as suggested earlier (Welte, 2012)? If YidC assists SecYEG in biogenesis of membrane proteins, at what stage of the RNC-SecYEG interaction does it begin to exert its effect? A collective effort from multiple laboratories over the course of many years is required to address these questions. Here, we asked whether YidC affects SecYEG-RNC interaction in a system consisting of detergent-solubilized components. We show that YidC weakens affinity of RNC for SecYEG and changes the conformation of the signal anchor bound to SecYEG. Importantly, it does so at early stages of the interaction, suggesting its involvement in membrane protein biogenesis at early stages of the process. We propose that YidC modulates the SecYEG-RNC interaction and facilitates the exit of transmembrane domains into the lipid bilayer.

Results and Discussion

Determination of orientation of the 3A7L signal sequence in SecYEG

To examine the orientation of the signal peptide inside the tranlocation channel at early stages of translocation, we used FRET between BODIPY-FL-labeled SecYEG and RNCs containing coumarin-labeled signal peptides. We reasoned that judicial placement of the acceptor dye (BODIPY-FL) on various sites of the SecY subunit constituting the pore of the translocation channel and site-specific derivatization of the signal peptide with the donor dye (coumarin) either at its N- or C-terminus would allow us to map the intercalation mode of the signal peptide in the lateral gate of SecY. This approach would also allow us to examine the topological changes undergone by the signal peptide inside the translocon as it interacts with RNCs bearing progressively longer nascent chains. Taking the Forster radius of 45Å for the BODIPY-FL-coumarin FRET pair, modeling performed by the group of Tom Miller based on the cryo-EM reconstruction of the *E. coli* SecYEG has shown that two positions of the acceptor probe on the cytoplasmic site of SecY in combination with two positions on the periplasmic site would allow us to determine the topology of the signal peptide with 95% confidence, provided that the topology is either Type I or Type II. Various combinations of the acceptor and donor dye positions on the translocon and the signal peptide, respectively, would result either in low or high FRET values, which can be directly translated to distances (Figure 1A). We used stalled RNCs bearing PhoA nascent chains of increasing length with an engineered 3A7L signal peptide (Figure 1B) (see Materials and methods for detailed description of the RNCs). The fluorescent amino acid L-(7-hydroxycoumarin-4-yl)ethylglycine was site-specifically introduced either at the N- or C-terminus of the signal peptide, using amber technology (Saraogi, 2011). Single-cysteine mutants of SecYEG were labeled with BODIPY-FL-maleimide using thiol chemistry as described in Materials and methods. Two cytoplasmic and two periplasmic locations of the

acceptor probe were chosen on SecY and determined by modeling to be sufficient for mapping the signal sequence orientation (Figure 3A).

Multiple lines of evidence from structural and function studies showed that SecYEG interacts with RNCs in detergent with high affinity (Akopian, 2013; Becker, 2009; Beckmann, 2001; Mothes, 1998). This interaction is not an artifact observed in detergent, as it is abolished if critical residues in the cytosolic loops of SecY are mutated (Akopian, 2013; Menetret, 2007). Replacement of two leucine residues with arginines in 3A7L dramatically weakens SecYEG-RNC interaction, suggesting that the 3A7L signal peptide is likely intercalated into the lateral gate of SecY, and reducing the hydrophobic character of the sequence interferes with productive binding (Saraogi, 2014). Also, RNCs bearing different signal peptides interacted with SecYEG with markedly different affinities, suggesting that the signal peptide identity is an important factor in RNC-SecYEG interaction and is thus likely to be engaged by the translocon in a physiologically relevant manner (Figure 7D) (unpublished observations). Independently, engagement of the signal peptide by SecYEG was confirmed using a protease protection assay with radioactively labeled RNC_{1A9L} chains (Figure 13) (unpublished observations). A significant fraction of RNCs were protected from digestion by proteinase K in the presence of detergent-solubilized SecYEG. Further, wild-type SecYEG in DDM, and not the cytosolic loop mutant, was shown to specifically destabilize the early complex in the SRP pathway, stabilize the activated state of the complex, and remove the stalling effect of RNC on hydrolysis of GTP from the complex (Akopian, 2013; Shen, 2012). It was also shown to be sufficient for *in vitro* reconstitution of the RNC transfer reaction from the targeting complex (Saraogi, 2014). Taken together, multiple lines of evidence show that detergent-solubilized SecYEG interacts with RNCs in a physiologically relevant manner and is thus suitable for examining the intercalation

mode of the signal peptide. We therefore used this minimal system to ask if the topology of the signal peptide inside the channel changes as the length of the nascent chain increases and if SecYEG in detergent in the absence of other components is capable of establishing correct Type II topology of the model secretory protein signal peptide, 3A7L.

Upon interaction of SecYEG with RNCs site-specifically labeled with coumarin, a significant increase in fluorescence of coumarin is observed (Figure 2A) (see also Chapter 3, Figure 5). This increase in fluorescence due to environmental sensitivity of coumarin masks the decrease in the coumarin fluorescence due to FRET (Figure 2B). We therefore used fluorescence of coumarin in the presence of the dye-free SecYEG as the fluorescence of the donor only (D*+A) and fluorescence of coumarin in the presence of BODIPY-FL-labeled SecYEG as the fluorescence of the donor in the presence of the acceptor (D*+A*) (Figure 3A). FRET was calculated using the equation described in Figures 2 and 3.

FRET values obtained with N-terminally labeled RNCs were significantly higher when SecYEG with the acceptor dye on the cytosolic face was used (SecYEG180 and SecYEG344) compared to the FRET values obtained with SecYEG labeled at the periplasmic face (SecYEG211 and SecYEG295) (Figure 3B). This indicates that the donor fluorophore is closer to the cytoplasmic face of SecYEG when N-terminally labeled RNCs are used. Significantly, the trend was observed as the nascent chain was lengthened from 85 to 135 amino acids. Furthermore, slightly higher FRET values were observed with longer nascent chains (compare 85 aa to 135 aa in Figure 3B), suggesting that the signal peptide of the longest nascent acquires a slightly different orientation likely dictated by the length of the nascent chain. Interestingly, no distinct differences in FRET values were observed between the cytosolically and periplasmically labeled SecYEG when C-terminally labeled RNC was used (Figure 3C). Such seemingly

contradictory results can be readily explained if the length of the signal peptide is taken into account. 3A7L spans only half of the translocon height. Thus, upon intercalation of 3A7L into the lateral gate, its C-terminus is expected to be positioned somewhere in the center of the channel, with the donor probe equidistant from the acceptor probes on the cytosolic and periplasmic face (Figure 4).

Analysis of the FRET values and molecular modeling suggest that the nascent chain interacts with SecYEG in a loop conformation such that the signal peptide acquires Type II topology with its N-terminus pointing toward the cytosolic face of SecYEG (Figure 4). Such conformation was observed in other studies. In particular, orientation of 3A7L observed in our studies is similar to that seen in a recently obtained cryo-EM structure of the RNC-SecYEG trapped *in vivo* as translocation intermediates (Park, 2014). To the best of our knowledge, the results of our studies show for the first time that SecYEG alone without additional components can establish correct initial topology of the secretory protein signal peptide. Elongation of the nascent chain bound to SecYEG in Type II topology would result in translocation of the substrate into the periplasmic space and exposure of the leader peptidase cleavage site at the C-terminal end of the signal peptide, resulting in its removal with subsequent release of the mature region into the periplasm.

One of the surprising aspects of our results is the lack of dependence of the signal peptide conformation in SecYEG on the length of the nascent chains. Lengthening the nascent chain by 50 amino acids (85 to 135) did not significantly change the conformation. A previous crosslinking study examined formation of RNC-SecYEG complexes in intact *E. coli* cells using cysteine crosslinking (Park, 2011). RNCs bearing nascent chains of various lengths with the DsbA signal peptide at the N-terminus were crosslinked to SecYEG *in vivo* by forming a

disulfide bridge between Cys19 at the C-terminus of the DsbA signal peptide and Cys68 on the plug domain of SecY in the presence of copper phenanthroline. A sharp reduction in the amount of the crosslinked complex was observed when the nascent chain length was reduced from 100 to 90 aa, and no crosslinking occurred with RNCs bearing 80 aa long nascent chains, suggesting that at these lengths the nascent chain is too short to acquire a looped configuration and position Cys19 close to the plug domain. In light of these observations, our FRET results are intriguing. However, one caveat of the crosslinking studies is that the two cysteine residues must be within ~ 2Å to form the disulfide bond. Poor crosslinking efficiency or no crosslinking does not suggest that the nascent chain of a particular length can no longer acquire the loop configuration. The direct inference is only that the two cysteines are not within the disulfide bond distance from each other. Our results show that the Type II topology is acquired early in translocation when the nascent chain is only 85 aa long. In the future, it would be interesting to examine the topology of the signal peptide with even shorter nascent chains. It is likely that at the nascent chain length shorter than 85 aa, the signal peptide is inserted into the channel in Type I topology and subsequently flips the orientation as the nascent chain is elongated. This was observed with a model membrane protein in a relatively recent study (Devaraneni, 2011).

Determination of orientation of the FtsQ transmembrane domain in SecYEG

FtsQ is a bitopic membrane protein that acquires type II topology in the inner membrane with short N-terminal extension in the cytosol and a large periplasmic loop (Figure 5A) (Carson, 1991). We used the FRET assay between RNC_{FtsQ} and SecYEG to ask whether, and if so, at what stage the type II topology of the signal anchor (transmembrane domain) of FtsQ is acquired during SecYEG-RNC_{FtsQ} interaction. We prepared RNCs bearing FtsQ nascent chains of increasing length site-specifically labeled with coumarin either at the N- or C-terminus of the

signal anchor. The nascent chain length was varied from 90 aa to 155 aa to mimic the elongating nascent chain (Figure 5B-C) (see Materials and methods for a detailed description of RNC_{FtsQ}). Considering that the signal anchor of FtsQ is significantly longer than the 3A7L signal peptide, we expected to see a more pronounced difference in the FRET values with cytosolically vs. periplasmically labeled SecYEG. Surprisingly, no significant difference in FRET values was observed, making the determination of the intercalation mode impossible (Figure 6A and B). Several scenarios can explain the observed FRET values. First, it is conceivable that no one definitive intercalation mode of the FtsQ signal anchor exists; instead, a highly heterogeneous population of intercalation modes results in averaging of the FRET values in ensemble measurements. Perhaps, the translocon alone is insufficient to bind the signal anchor in one defined orientation and the correct topology is established with the aid of other factors, such as YidC (Urbanus, 2001). Second, the observed FRET values can be explained if the signal anchor breaks into two α-helical segments of approximately the same size, resulting in close proximity of the N- and C-termini. That would position the donor dye in the same region in SecYEG regardless of whether it is at the N- or C-terminus of the signal anchor (Figure 6C). The presence of glycine and serine in the approximate center of the TM suggests that the sequence may exist as two short α-helices. Third, the signal anchor may simply nonspecifically associate with SecYEG in a conformation that is not observed *in vivo*. Such possibility is not unlikely considering that highly purified SecYEG is used and may suggest the requirement for accessory factors. We are currently testing these possibilities. Our approach involves replacement of the helix-breaking GS with alanine residues with an attempt to confer rigidity to the FtsQ TM. In a different approach, we are reassigning the amber codon to move either the N- or C-terminal probe towards the center of the signal anchor. If the signal anchor is indeed broken leading to

spatial proximity of the N- and C-terminus, then moving one of the probes towards the center of the helix would result in greater spatial separation of the probes and change in FRET values.

Dependence of the avidity of RNC-SecYEG interaction on the length of the nascent chain

One of the interesting questions in the translocation field is how the synthesis of the nascent polypeptide chain affects the affinity of the translating ribosome for SecYEG. Attempts to address this question showed that SecYEG exerts a pulling force on the nascent chain, with the strength of the force directly dependent on the length of the polypeptide chain (Ismail, 2012). Such studies, although valuable, were performed in intact cells and thus examined the phenomenon in a complete system. To the best of our knowledge, no high resolution studies exist asking the question in a purified system. We asked if detergent-solubilized SecYEG in the absence of the lipid bilayer or accessory protein factors is capable of discriminating between the nascent chains of different lengths.

To determine the binding affinity of RNCs to SecYEG, we used a well-established binding assay based on the environmental sensitivity of the coumarin probe to SecYEG when derivatized at the signal peptide. The increase in the coumarin fluorescence in the presence of unlabeled SecYEG is robust and saturable, allowing us to perform equilibrium titration and derive dissociation constants from the fits to the data (see Materials and methods) (Figure 7A and B). We observed weakening and tightening of the affinity of RNC for SecYEG as the length of the nascent chain increased. Interestingly, the trend was observed with both 3A7L signal peptide and the FtsQ TM (Figures 7C and E), suggesting that the length of the nascent chain plays an important role in modulating the avidity of the SecYEG-RNC interaction. Taking into account the 24 aa long N-terminal extension preceding the signal anchor of FtsQ, the weakest binding with RNC_{FtsQ} was observed at the nascent chain length of 86 aa counted from the

peptidyl transferase center (PTC) to the N-terminus of the signal anchor, while the weakest binding with RNC_{3A7L} was observed with 105 aa long nascent chains. At present, the reason for this difference remains unclear. Most likely the nature of the signal peptide and its mode of interaction with SecYEG at least in part determine the length of the nascent chain at which the interaction is weak. Studies are underway to explore this phenomenon.

Weakening of the binding affinity of RNC_{FtsQ} for SecYEG upon increasing the length of the nascent chain from 90 to 110 aa is in agreement with a crosslinking study carried out by Joen Luirink and colleagues (Urbanus, 2001). The authors crosslinked RNC_{FtsQ} with various nascent chain lengths to IMVs and observed gradual decrease in efficiency of crosslinking to SecYEG as the nascent chain length was increased from 77 to 87, 97, and 108 aa. The crosslinking efficiency was very low with the 108aa nascent chain and significant with the 87 aa one, paralleling our results with binding affinity (Figure 7E). It would be interesting to see if, in accordance with our thermodynamics data, the efficiency of crosslinking increases as the nascent chain is lengthened.

In a recent study, von Heijne and coworkers investigated interaction of SecYEG with RNCs *in vivo* (Ismail, 2012). They examined the pulling force exerted by SecYEG on stalled nascent chains in intact *E. coli* cells. The authors engineered stalled RNCs containing the Lep nascent chain with one additional artificial transmembrane domain located at a certain distance from PTC. Full-length product would only be observed if the pulling force exerted by SecYEG on stalled RNCs is sufficient to remove the block on translation imposed by the arrest peptide. The pulling force was observed with 72 and 82 aa long nascent chains, with the first corresponding to the interaction of the TM with SecYEG and the second caused by the exist of the TM from the translocon into the lipid bilayer. The difference in the experimental set-up, nature of the substrate, and lengths of the nascent chains used in our and their studies prevent

direct comparison of the results. It is not far fetched to suggest, however, that the tight binding observed in our study may correspond to the pulling force exerted by SecYEG on the nascent chain. It is conceivable that as the nascent chain elongates the avidity of its interaction with SecYEG cycles between relatively weak and relatively tight due to changes in the signal peptide orientation and/or the accumulation of the polypeptide in the ribosome translocon junction. Performing these studies with the expanded repertoire of the nascent chain lengths may address this question in the future.

Our results here show that SecYEG in DDM without any accessory factors is capable of discriminating between the nascent chains of different lengths. This suggests an attractive hypothesis that *in vivo* SecYEG senses the length of the nascent chain and at some point loosens its grip on it, facilitating protein translocation across the lipid bilayer or biogenesis of membrane proteins.

To make sure that tight binding of RNCs to SecYEG is not an artifact of having SecYEG in detergent, we reconstituted SecYEG in lipid patches called nanodiscs (Figure 8). Nanodiscs are an attractive and widely-used system in which functional studies with membrane proteins are performed (Dalal, 2012; Gluck, 2011; Alami, 2007; Boldog, 2007; Nath, 2007). The nanodisc technology developed by the laboratory of Stephen Sligar involves incorporating a membrane protein of interest in a patch of phospholipids approximately 5 nm tall and 13 nm in diameter surrounded by a membrane scaffold protein, a derivative of apolipoprotein A (Denisov, 2004; Bayburt, 2002;). The technology allows one to obtain a monodisperse solution of a membrane protein in its native environment with tunable phospholipids composition. We expressed and purified membrane scaffold proteins, MSP1D1 and MSP1E3D1 (Figure 9A) and reconstituted SecYEG in nanodiscs using either *E. coli* lipids or phosphatidylglycerol (PG) according to the

previously-described method (Dalal, 2010). Successful assembly of the nanodiscs was confirmed by gel filtration chromatography (Figure 9B), native (Figure 9C) and denaturing gels (Figure 9D) (see Materials and methods for detailed description of the reconstitution of SecYEG in nanodiscs). Further, we checked binding of MSP1D1/PG/SecYEG nanodiscs to RNC using a well-established cosedimentation assay (Figure 9E) (see Materials and methods for detailed description of the assay). Empty nanodiscs did not cosediment with RNC_{1A9L}, while SecYEG nanodiscs were detected in the pellet, indicating that SecYEG specifically bound RNC.

We then examined binding of RNC_{3A7L} bearing nascent chains of increasing length to MSP1D1/PG/SecYEG nanodiscs. The extent of the signal change in the coumarin fluorescence due to environmental sensitivity was significantly lower compared to that observed with SecYEG in DDM (Figure 10A), probably reflecting the different environment of SecYEG and thus that of the signal peptide bound to the lateral gate region. Fitting of the titration data yielded dissociation constant similar to those obtained with SecYEG in detergent (Figure 10B). Significantly, like with SecYEG in DDM, weaker binding was observed with the nascent chain 105 aa long, suggesting that, at least with respect to thermodynamics, SecYEG in nanodiscs behaves similarly to SecYEG in DDM.

Effect of YidC on SecYEG-RNC interaction

In vivo, SecYEG does not function in isolation; it is a part of a holotranslocon complex that includes SecDF, YajC, and YidC (Schulze, 2014; Dalbey, 2014; Beck, 2001). The latter recently emerged as an important membrane foldase/insertase that handles a growing list of substrates independently or in cooperation with SecYEG. To begin to understand the role of YidC, we decided to examine its effect on SecYEG-RNC interaction *in vitro*. We purified YidC to homogeneity and solubilized it in DDM (Figure 11). Unlike SecYEG, YidC in DDM did not

produce a change in fluorescence of coumarin when incubated with either RNC_{3A7L} or RNC_{FtsQ} (data not shown). We then titrated RNC_{FtsQ} bearing a 90 aa long nascent chain with SecYEG in the presence of increasing concentrations of YidC (Figure 12A). Significantly, YidC changed both the K_d value and the fluorescence end point in a concentration-dependent saturable manner (Figure 12A and B), indicating that it forms a ternary YidC•SecYEG•RNC complex in which it lowers the affinity of RNC for SecYEG (higher K_d) and changes the conformation of the TM (lower titration end point). If YidC acted simply as a competitor of SecYEG for binding RNC, only the K_d value would be affected with the titration end point, finally reaching the same saturation value as in the absence of YidC. These results allow us to draw a thermodynamic cycle of the ternary YidC•SecYEG•RNC formation (Figure 12C). It is apparent from the cycle and the known K_d values (K_{d1} and K_{d4}) that YidC associates with SeYEG (K_{d3}) with ~ 8-fold higher affinity compared to its affinity for the SecYEG•RNC complex (K_{d4}). These results are in agreement with the recent SecYEG-YidC crosslinking study conducted by Hans Georg Koch and colleagues (Sachelaru, 2013). The authors showed that YidC contacts the lateral gate of SecYEG, and that in the presence of ribosomes and RNCs, the SecYEG-YidC crosslinking pattern changes, indicating conformational rearrangement of the SecYEG-YidC interface. Here, we show that in addition to affecting the SecYEG-YidC interaction interface, RNCs also weaken the affinity of YidC for SecYEG. This could be a direct consequence of the reduction of the number of contacts between SecYEG and YidC in the presence of RNC as YidC is in part displaced from the lateral gate. Combined with previous observations, our data suggest that YidC may facilitate the exit of transmembrane domains from SecYEG. It may also promote correct topology of membrane proteins. Weakening of the RNC-SecYEG interaction by YidC may lower the energy barrier of sampling various conformations by TMs on the pathway towards

establishing the correct final topology. At this point, this is only an attractive hypothesis, which requires rigorous testing. Significantly, the effects of YidC can be reproduced in a minimal system with detergent-solubilized components. The effect of YidC on the conformation of the nascent chain bound to SecYEG was observed not only with FtsQ, but also with 3A7L peptide (data not shown), suggesting that YidC may act as a general membrane chaperone. Future studies in detergent, as well as in native environment, are necessary to further explore this topic.

Developing an in vitro cotranslational protein targeting assay

Although *in vitro* assays with detergent-solubilized SecYEG offer invaluable mechanistic information as to the role of SecYEG in the SRP-mediated targeting pathway, they do not report on the ultimate function of SecYEG, its ability to mediate efficient insertion of a cotranslational substrate into the lipid bilayer. Ideally, any new finding with detergent-solubilized SecYEG should be validated with SecYEG in the native environment. A robust *in vitro* cotranslational targeting assay involving purified SecYEG reconstituted in lipid vesicles would allow one to link the observations in detergent to those in the lipid bilayer, examine the requirements for co- vs. posttranslational pathways, and test the effect of SecYEG mutants in substrate insertion/translocation. To the best of our knowledge, no robust cotranslational targeting assay involving the prokaryotic protein targeting/translocation machinery with a well-characterized set of substrates exists (Schulze, 2014; Houben, 2000;). In contrast, relatively robust assays examining SecA-dependent translocation have been established (van der Does, 2003; Hanada, 1994; Akimuru, 1991; Brundage, 1990). Moreover, efficient cotranslational targeting has been observed with the eukaryotic system, using both intact ER microsomes and the Sec61 complex reconstituted in proteoliposomes (Bernstein, 2001; Gorlich, 1992; Nicchitta, 1990).

We sought to develop a cotranslational protein targeting assay using the prokaryotic protein targeting/translocation machinery in a coupled transcription/translation/integration system supplemented with ^{35}S-methionine (Figure 14). The system combines the previously-developed system for coupled transcription/translation (Saraogi, 2011) with desired formulation of lipid vesicles. The reaction is initiated by adding a plasmid encoding the substrate of interest and incubated for 30 min at 37°C. As the DNA is transcribed, ribosomes assemble on the message and are targeted to the sites of translocation on the lipid vesicles. Upon completion of the reaction, protease protection can be used to check for insertion/translocation of the ^{35}S-labeled substrate (see detailed description of the assay in Materials and methods). This approach has been widely used in the field of protein targeting (Schulze, 2014; Welte, 2012; Houben, 2000).

Leader peptidase (Lep) is a polytopic membrane protein with a large C-terminal periplasmic segment and a short cytosolic loop connecting the two transmembrane domains (Wolfe, 1983) (Figure 15A). The substrate was previously used in co-translational targeting to *E. coli* inverted membrane vesicles (IMVs), and its integration into the lipid bilayer was checked by treating IMVs with proteinase K (Houben, 2000). If productive insertion of Lep is achieved, proteinase K digests only the P1 loop, producing two fragments. The H2-P2 protected fragment can be detected on a gel as a lower molecular weight band relative to Lep (Figure 15B). Absence of the fragment indicates complete digestion and thus no insertion. Luirink and colleagues reported 12% integration of Lep into IMVs (Houben, 2000). Using our cell free extract and IMVs with overexpressed levels of SecYEG, we obtained 11% efficiency of integration (Figure 15C). At present, it is unclear why the efficiency of cotranslational insertion of Lep is low. It is not unlikely that the cotranslational insertion machinery at least partly loses activity during inner

membrane breakage and IMV formation. Further, concentration of the targeting factors relative to the abundance of the translocation machinery is likely to change as the cells are lysed and the inner membrane is resealed. Also, the effect of the change in the lipid vesicle curvature on insertion cannot be excluded.

We then examined the efficiency of cotranslational insertion of Lep into proteoliposomes composed of the *E. coli* total lipid extract. SecYEG, YidC, or SecYEG/YidC proteoliposomes were prepared according to the established protocol (van der Does, 2003), and the presence of the proteins in the isolated lipid vesicles was checked by resolving an aliquot on a denaturing gel (Figure 16A). Stoichiometric amounts of SeYEG and YidC were incorporated. IMVs and urea-washed IMVs were included in the reaction as positive controls. The efficiency of insertion was highest with IMVs (~ 20%) and lower with urea-washed vesicles (~ 12%) (Figure 16B and C). This is not surprising since the peripherally associated proteins that may aid in insertion are removed by urea from the lipid bilayer. The efficiency of translocation was lower with synthetic vesicles: ~7%, 5%, and 1% with SecYEG/YidC, SecYEG, and YidC proteoliposomes, respectively. Importantly, almost no insertion was observed with empty lipid vesicles, indicating specificity of the reaction. Also noteworthy, is the observation that the efficiency of insertion was higher with SecYEG/YidC proteoliposomes compared to SecYEG proteoliposomes and very low with YidC proteoliposomes. YidC has emerged as the membrane protein foldase/insertase that is thought to assist SecYEG in membrane protein biogenesis (Dalbey, 2014). The results of our insertion assay suggest that cotranslational insertion of Lep requires SecYEG and may be assisted by YidC. This is in agreement with the observation that the nascent chain of Lep is in vicinity of YidC (Houben, 2000). Further studies are required to explore the role of YidC in cotranslational insertion of Lep. The effect of SecYEG and YidC in proteoliposomes can simply

be additive rather than cooperative. It would be informative to check if SecYEG and YidC form complexes in the lipid bilayer. Our studies of the effect of detergent-solubilized YidC on the SecYEG-RNC interaction suggest that they interact in detergent. SecYEG-RNC interaction was also observed in the lipid environment (Sachelaru, 2013), suggesting that the complexes are formed in our proteoliposomes. Labeling SecYEG and YidC with distinct fluorescent probes and performing colocalization experiments would be a direct way to observe and quantify SecYEG-YidC complexes in the lipid environment.

Why is the efficiency of insertion lower in synthetic proteoliposomes compared to the native vesicles? There are many equally plausible explanations. First, it is not unlikely that the amount of the translated substrate far exceeds the available translocation sites, resulting in jamming of SecYEG units and accumulation of Lep outside the vesicles. This possibility can be tested by lowering the amount of the plasmid and increasing the amount of proteoliposomes in the reaction. Second, SecYEG may lose activity in synthetic vesicles composed of total *E. coli* lipids. It is known that *in vivo* SecYEG is activated by anionic lipids (Gold, 2010), which are segregated into microdomains in the bacterial inner membrane (Barak, 2008; Vanounou, 2003; Fishov, 1999). The absence of such microdomains in proteoliposomes may adversely affect the activity of SecYEG. Increasing the concentration of PG and cardiolipin in the synthetic vesicles may lead to higher efficiency of insertion. Third, the lipid bilayer in synthetic vesicles may not have correct curvature in which the translocation machinery exhibits high activity. Activation of the proteoliposomes before the assay to break the multilamelar structure may also result in formation of small vesicles with high curvature in which the altered lateral pressure on the translocation machinery prevents efficient insertion. It would be informative to reconstitute SecYEG into giant unilamelar vesicles to exclude the effect of curvature (Kedrov, 2011). Four,

SecYEG reconstituted in proteoliposomes may lose activity due to altered conformation, collapse of the cytosolic loops, or jamming of the lateral gate with lipids. A recent study reports increased post-translational translocation capacity of synthetic proteoliposomes when SecYEG was reconstituted in the presence of SecA (Mao, 2013). Perhaps, SecA acts as a chaperone for proper integration of SecYEG into the lipid bilayer. It would be interesting to see if this approach also improves cotranslational insertion of Lep. Five, SecYEG may require other components of the holotranslocon complex, SecDF and YajC to mediate efficient cotranslational insertion of Lep. A recent study reports purification of holotranslocon and its reconstitution in proteoliposomes (Schulze, 2014). Cotranslational substrate CyoA was inserted into SecYEG proteoliposomes with only 1% efficiency and with 4% efficiency into holotranslocon proteoliposomes. This improvement of the efficiency of insertion, albeit very modest, suggests that the components of the holotranslocon assist SecYEG in the insertion process. It would be interesting to see if the insertion efficiency of Lep is also improved. Six, Lep may require proton motive force for efficient insertion. Arnold Driessen and colleagues showed that a transmembrane electrical potential ($\Delta\Psi$) is required for efficient insertion of FtsQ into IMVs (van der Laan, 2004). When IMVs prepared from *E. coli* strains defective in F_1F_0 ATPase were used or when the inophores valinomycin and nigerin were added to inhibit the ATPase, the insertion of FtsQ was blocked. Further, immunodepletion of SecA from the lysate abolished the insertion and the presence of $\Delta\Psi$ could only mediate insertion if SecA was present. It was earlier shown that SecA is required for insertion of membrane proteins containing large periplasmic domains (Deitermann, 2005; Saaf, 1995). Like FtsQ, Lep contains a long periplasmic segment (Figure 15A) and may thus require both SecA and $\Delta\Psi$ for efficient insertion. Generating $\Delta\Psi$ in proteoliposomes and adding exogenous SecA to the lysate is a straightforward way to test this possibility. Shortening the

periplasmic domain of Lep, and thus partly obviating the need for SecA and $\Delta\Psi$, may also improve the efficiency of insertion. A painstakingly systematic and rigorous approach towards understanding the role of various factors in cotranslational targeting of membrane proteins is required for developing an efficient cotranslational targeting assay *in vitro*.

Materials and methods

Expression and purification of SecYEG

The plasmid pEK20 plasmid (pSOS334) encoding cysteineless SecYEG was a kind gift from Arnold Driessen. Expression and purification of SecYEG were performed based on the previously-established protocol with modifications (Dalal, 2010).

1) Transform BL21(DE3) cells with pSOS334 plasmid encoding His_6-SecYEG (SecY N-terminally His_6-tagged). Add 2 μL of 30 ng/uL plasmid to 50 μL of the cell suspension. Mix by swirling on ice and allow to stand on ice for 30 min. Heat shock at 42°C for 45 seconds and allow to stand on ice for 2 min. Add 300 μL of LB, shake at 37°C for 1 hour. Plate the entire volume on amp plates.

2) Inoculate 40 mL of LB (containing 100 μg/mL of ampicillin) with a single colony and use it to make 3 100-fold serial dilutions. Grow cells ON.

3) Inoculate large culture (25g of LB powder per 1L of ddH_2O + 2 ml of 100 mg/ml Amp stock) (2L/6L-flask) with 8 mL of the ON culture at OD ~ 0.5. Grow at 37°C by shaking at 200 rpm. Induce at O.D. ~ 0.5 by adding 1 ml of 1 M IPTG (0.5 mM final). Continue to grow for 2 hours.

4) Place the flasks at 4°C when ready to pellet the cells. Harvest by centrifugation at 4°C, 6,000 rpm for 15 min, deceleration: slow. Use 4 1L-bottles in a JLA-9.1 rotor and harvest repeatedly in the same bottles.

Resuspend the total pellet mass in 35 mL of KS300G (50 mM KHEPES (pH 7.5), 300 mM NaCl, 10% Glycerol) at 4°C on ice. Add 2 pulverized protease inhibitor cocktail pills. Mix well. Distribute into 50-mL Falcon tubes (15 ml per tube) and freeze thoroughly in liquid nitrogen. Store the cells for up to a week at - 80°C.

5) Thaw the cell suspension in RT water bath. Once thawed, transfer the suspension to ice. Break the cells by sonication (around 45 ml each time), using 7 30s-cycles at duty cycle 50% and output 8 in a plastic beaker. NOTE: keep the suspension cool. Make sure the beaker is surrounded with ice. After each cycle, pour the contents into a 200-ml stainless steel beaker in ice-water bath, and swirl gently to cool. Cool for ~ 5 min after each cycle. Centrifuge the suspension of lysed cells at 12,000 g for 20 min in a JA-20 rotor. Decant the supernatant and the viscous material above the compact pellet into Ti 45 rotor centrifuge tubes.

6) Add KS50G buffer to the cell lysate to fill the ultracentrifuge tubes completely. The tubes will deform during centrifugation if half-filled. Centrifuge at 42,000 rpm in Ti 45 rotor for 55 min. Discard the supernatant. Resuspend the membrane pellet in 10 ml of KS50G (50 mM KHEPES (pH 7.5), 50 mM NaCl, 10% Glycerol). Homogenize the suspension in a 15-ml dounce homogenizer. Determine the concentration of protein using Bradford assay (OD 595) based on a BSA standard curve. To prepare a sample for Bradford assay, dilute the membrane suspension 10-fold in KS50G and add 5 μL of the dilution to 1 mL of 1X Bradford reagent. A reading of 0.40 corresponds to 13.4 mg/ml of total protein. Add 10% DDM to the membrane suspension so that the final solution contains 1% of the detergent and 10 mg of protein per ml of solution. Add enough KS50G to reach the final volume. Tumble the suspension gently at 4°C for 1 hour.

Centrifuge the homogenate for 45 min at 42,000 rpm in a Ti 45 rotor to pellet intact membranes. Fill the tube completely with KS50G/0.02% DDM. 7) Wash 12 mL of SP Sepharose resin with 400 mL of ddH_2O using a peristaltic pump (rate: 7). This step may be performed at RT. Wash the resin with KS50G/0.02% DDM at 4°C in a cold room. (Note: washing and equilibrating the resin takes a few hours; start it before thawing the cells.) Pass the supernatant

(60 mL) through the resin using the peristaltic pump (rate: 3). Reload the FT. Wash the resin with 125 mL (~ 10 CV's) of KS50G/0.02% DDM at the pump rate 6.00.

Elute with increasing concentration of NaCl using a gradient mixer. Light solution: KS50G/0.02% DDM. Heavy solution: KS1000G/0.02% DDM. Collect 30 fractions (round fraction collector set to 3.00). The pump rate 6.00. Run every 3rd fraction on a 15% (or 12.5%) SDS-PAGE to check for presence of SecYEG (10 μL of each fraction). Save the fractions that contain a significant amount of SecYEG with a minimal amount of contaminants. Flash freeze the solution containing SecYEG in 10 ml aliquots in 50-ml Falcon tubes.

8) Wash 2 mL of Ni-NTA agarose resin (NOTE: use regenerated resin for best results; fresh resin binds contaminants non-specifically and dramatically reduces purity) as follows. Transfer the resin into a 50 mL-Falcon tube, fill the tube with ddH_2O, mix well, spin at 3000 rpm for 2 min with the deceleration set at 1. Decant the liquid. Repeat the wash two more times. Equilibrate the washed resin with KS300G/0.02% DDM/20 mM Imidazole in the same manner that it was washed with water. (Note: prepare 5 mL of 4 M stock Imidazole solution in water and pH with concentrated HCl to pH 7.4. Store at 4°C.) Add enough 4M Imidazole to the combined SecYEG fractions to have 20 mM final Imidazole concentration. Mix the SecYEG fractions with the resin and stir gently for 1.5 hours at 4°C. Spin for 5 min at 3,000 rpm with the deceleration set at 1. Save the flow through (FT). Add 20 mL of KS300G/0.02% DDM/20 mM Imidazole to the resin and stir gently for 15 min. Spin as above and save the wash (W). Mix the resin with 7 ml of KS300G/0.02% DDM/20 mM Imidazole and transfer to a Poly-Prep chromatography column (0.8 x 4 cm) (Bio-Rad). Allow the resin to settle and combine the second wash with the first one. Elute SecYEG in 5 1-mL fractions using KS300G/0.02% DDM/300 mM Imidazole as follows. Add 1 ml of the elution buffer to the resin containing no buffer and collect the entire 1

ml by gravity (E1). Repeat four more times (E2-E5). Run FT, W, and E1-E5 on a 15% SDS-PAGE (10 µL of each fraction). Combine the fractions containing a significant amount of pure SecYEG (usually fractions #2 and #3).

Dialyze against 1L of 50 mM KHEPES (pH 7.5), 150 mM KOAC, 10 mM $Mg(OAc)_2$, 20% Glycerol, 0.02% DDM, 2 mM DTT ON using a 10,000 MW cut-off dialysis tubing for 2 hours. Repeat the dialysis against 1L of buffer for 4 hours. Dialysis is performed at 4°C with gentle stirring.

Determine the concentration of SecYEG using OD 280 (nanodrop 1 AU = 1 mg/ml). Concentrate to approximately 55 µM $SecY_2E_2G_2$ using a 50,000 MW cut-off Amicon filter at 2500 rcf. (Usually, 2 mL of the dyalysed solution to 0.5 ml). Mix well, determine concentration. Note: do not exceed 80 µM final concentration. Freeze 30 µL aliquots in liquid nitrogen. Store the aliquots at - 80°C.

Expression and purification of SecYEG single Cys mutant for labeling

Single cysteine residues were introduced into a cysteineless SecYEG sequence (pEK20 plasmid, pSOS334) at specific locations using site-directed mutagenesis (Stratagene), and the mutations were confirmed by sequencing. Expression and purification of single cysteine SecYEG mutants was performed based on the previous protocol with modifications (Dalal, 2010).

1) Transform BL21(DE3) cells with pSOS334 plasmid-derived plasmid encoding a single cysteine His_6-SecYEG mutant (SecY N-terminally His_6-tagged). Add 2 µL of 30 ng/µL plasmid to 50 µL of the cell suspension. Mix by swirling on ice and allow to stand on ice for 30 min. Heat shock at 42°C for 45 seconds and allow to stand on ice for 2 min. Add 300 µL of LB, shake at 37°C for 1 hour. Plate the entire volume on amp plates.

2) Inoculate 40 mL of LB (containing 100 μg/mL of ampicillin) with a single colony and use it to make 3 100-fold serial dilutions. Grow cells ON.

3) Inoculate large culture (25g of LB powder per 1L of ddH_2O + 2 ml of 100 mg/ml Amp stock) (2L/6L-flask) with 8 mL of the ON culture at OD ~ 0.5. Grow at 37°C by shaking at 200 rpm. Induce at O.D. ~ 0.5 by adding 1 ml of 1 M IPTG (0.5 mM final). Continue to grow for 2 hours.

4) Place the flasks at 4°C when ready to pellet the cells. Harvest by centrifugation at 4°C, 6,000 rpm for 15 min, deceleration: slow. Use 4 1L-bottles in a JLA-9.1 rotor and harvest repeatedly in the same bottles. Resuspend the total pellet mass in 35 mL of KS300G20 (50 mM KHEPES (pH 7.5), 300 mM NaCl, 20% Glycerol) at 4°C on ice. Add 2 pulverized protease inhibitor cocktail pills. Mix well. Distribute into 50-mL Falcon tubes (15 ml per tube) and freeze thoroughly in liquid nitrogen. Store the cells for up to a week at - 80°C.

5) Thaw the cell suspension in RT water bath. Once thawed, transfer the suspension to ice. Break the cells by sonication (around 45 ml each time), using 7 30s-cycles at duty cycle 50% and output 8 in a plastic beaker. NOTE: keep the suspension cool. Make sure the beaker is surrounded with ice. After each cycle, pour the contents into a 200-ml stainless steel beaker in ice-water bath and swirl gently to cool. Cool for ~ 5 min after each cycle. Centrifuge the suspension of lysed cells at 12,000 g for 20 min in a JA-20 rotor. Decant the supernatant and the viscous material above the compact pellet into Ti 45 rotor centrifuge tubes.

6) Add KS300G20 buffer to the cell lysate to fill the ultracentrifuge tubes completely. The tubes will deform during centrifugation if half-filled. Centrifuge at 42,000 rpm in Ti 45 rotor for 55 min. Discard the supernatant. Resuspend the membrane pellet in 10 ml of KS300G20 (50 mM KHEPES (pH 7.5), 50 mM NaCl, 20% Glycerol). Homogenize the suspension in a 15-ml

dounce homogenizer. Determine the concentration of protein using Bradford assay (OD 595) based on a BSA standard curve. To prepare a sample for Bradford assay, dilute the membrane suspension 10-fold in KS300G20 and add 5 μL of the dilution to 1 mL of 1X Bradford reagent. A reading of 0.40 corresponds to 13.4 mg/ml of total protein. Add 10% DDM to the membrane suspension so that the final solution contains 1% of the detergent and 10 mg of protein per ml of solution. Add enough KS300G20 to reach the final volume. Tumble the suspension gently at 4°C for 1 hour. Centrifuge the homogenate for 45 min at 42,000 rpm in a Ti 45 rotor to pellet intact membranes. Fill the tube completely with KS300G20/0.02% DDM. 7) Wash 2 mL of Ni-NTA agarose resin (NOTE: use regenerated resin for best results; fresh resin binds contaminants non-specifically and dramatically reduces purity) as follows. Transfer the resin into a 50 mL-Falcon tube, fill the tube with ddH_2O, mix well, spin at 3000 rpm for 2 min with the deceleration set at 1. Decant the liquid. Repeat the wash two more times.

Equilibrate the washed resin with KS300G20/0.02% DDM/20 mM Imidazole in the same manner it was washed with water. (Note: prepare 5 mL of 4 M stock Imidazole solution in water and pH with concentrated HCl to pH 7.4. Store at 4°C). Add enough 4M Imidazole to the combined SecYEG fractions to have 20 mM final Imidazole concentration. Mix the SecYEG fractions with the resin, and stir gently for 1.5 hours at 4°C. Spin for 5 min at 3,000 rpm with the deceleration set at 1. Save the flow through (FT). Add 20 mL of KS300G/0.02% DDM/20 mM Imidazole to the resin and stir gently for 15 min. Spin as above and save the wash (W). Mix the resin with 7 ml of KS300G/0.02% DDM/20 mM Imidazole and transfer to a Poly-Prep chromatography column (0.8 x 4 cm) (Bio-Rad). Allow the resin to settle and combine the second wash with the first one. Elute SecYEG in 5 1-mL fractions using KS300G20/0.02% DDM/300 mM Imidazole as follows. Add 1 ml of the elution buffer to the resin containing no

buffer and collect the entire 1 ml by gravity (E1). Repeat four more times (E2-E5). Run FT, W, and E1-E5 on a 15% SDS-PAGE (10 µL of each fraction). Combine the fractions containing significant amount of pure SecYEG (usually fractions #2 and #3). Determine the concentration of SecYEG using OD 280 (nanodrop 1 AU = 1 mg/mL). Freeze 0.7 mL aliquots at 2 to 3 mg/ml in liquid nitrogen. Store the aliquots at - 80°C.

Labeling SecYEG with BODIPY-FL

Labeling of single cysteine SecYEG mutants with BODIPY-FL was performed based on the established protocol with modifications (Kedrov, 2011).

1) Start with SecYEG single cysteine mutant purified via Ni-NTA and contained in 50 mM KHEPES pH 7.5, 300 mM NaCl, 0.02% DDM, 300 mM Imidazole (from elution).

2) Incubate approximately 800 µL of 2.3-3 mg/ml of protein solution with 2 mM DTT for 20 min with gentle tumbling on a rotary shaker at 4°C.

3) Remove both imidazole and DTT by dialyzing against approximately 700 mL of buffer A (50 mM KHEPES, pH 7.5, 150 mM NaCl, 10% Glycerol, 0.02% DDM) three times, 40 min each time.

4) Wash 800 µL of Ni-NTA resin with ddH_2O and equilibrate with buffer B (50 mM KHEPES pH 7.5, 150 mM NaCl, 10 % Glycerol, 0.02% DDM, and 10 mM Imidazole). Washing and equilibration are performed as follows. Fill the 15 mL Falcon tube containing the resin with water, swirl to mix, and spin down the resin at 3500 rpm, 5 min, deceleration 1, 4°C. Repeat the washing step twice. Equilibrate in the same manner three times. Decant the buffer and store the resin in ice.

4) Add the dialyzed protein solution to the equilibrated resin and adjust the volume to 12 ml in a 15 mL Falcon tube with buffer B. Tumble gently on a rotary shaker for 1.5 h at 4°C.

5) Spin down the SecYEG-bound resin at 3000 rpm, 4°C, 5 min, deceleration 1, and collect the flow through.

6) Wash the resin with 2 mL of buffer C (50 mM KHEPES, pH 7.0, 150 mM NaCl, 20 % Glycerol, 0.02 % DDM, 200 μM TCEP) as follows. Add the buffer to the spun-down resin and pipette gently. Spin as above and collect the wash. Repeat the washing step.

7) Transfer the washed resin to a 2 ml eppendorf tube by resuspending in buffer C. Adjust the volume of the suspension to 2 ml.

8) Add approximately 15-fold molar excess of BODIPY-FL-maleimide (4 μL of 100 mM stock), wrap the tube in foil, and tumble gently at 4°C for 3 h.

9) Transfer the suspension to a 15 mL Falcon tube. Rinse the eppendorf tube with buffer B and transfer the solution to the Falcon tube. Fill the tube with buffer B to the 12-ml mark, swirl gently to mix the resin with the buffer, and spin down the resin at 3000 rpm, 4°C, for 5 min. Collect the supernatant.

10) Add 12 ml of buffer B to the resin, tumble gently for 10 min at 4°C in the dark, spin down the resin and save the wash. Repeat the washing step twice. Remove as much of the supernatant as possible during the last washing step since it contains the dye. Occasionally, the dye forms an orange ring at the top of the solution, which can be removed using a pipette.

11) Transfer the resin to a Polyprep BioSpin column by resuspending in buffer B. Rinse the Falcon tube with a few mL of the buffer. Allow the resin to settle in the column and the buffer to drain by gravity. Wash the resin with a few mL of the buffer.

12) After the buffer is drained by gravity leaving a meniscus, close the column and add 1 ml of buffer D (50 mM KHEPES, pH 7.5, 150 mM NaCl, 10 % glycerol, 0.02 % DDM, 600 mM Imidazole) to elute the protein. Incubate for 10 min and collect the eluate by gravity. After most

of the eluate is collected, spin for a few seconds at several hundred rpm to collect the rest of the buffer. Only very low g force is required to collect the rest of the eluate.

13) Dialyze the labeled protein solution against 1L of buffer E (50 mM KHEPES, pH 7.5, 150 mM KOAc, 2 mM DTT, 10 % Glycerol, 0.02 % DDM) for 2 hours. Repeat the dialysis against fresh buffer for 2 hours.

14) Determine the concentration of the protein. Concentrate using a 50,000 MWCO concentrator to approximately 50 µM. Flash freeze 20 to 40 µL aliquots in liquid nitrogen. Store at - 80°C.

Expression and purification of membrane scaffold proteins

Below are the amino acid sequences of the membrane scaffold proteins used in reconstitution of SecYEG in nanodiscs. The sequences were obtained from the laboratory page of Stephen G. Sligar: http://sligarlab.life.uiuc.edu/nanodisc/sequences.html. The helices are color coded.

MSP1D1 211 aa

GHHHHHHHDYDIPTTENLYFQGSTFSKLREQLGPVTQEFWDNLEKETEGLRQEM
SKDLEEVKAKVQPYLDDFQKKWQEEMELYRQKVEPLRAELQEGARQKLHELQE
KLSPLGEEMRDRARAHVDALRTHLAPYSDELRQRLAARLEALKENGGARLAEY
HAKATEHLSTLSEKAKPALEDLRQGLLPVLESFKVSFLSALEEYTKKLNTQ

MSP1E3D1 278 aa

MGHHHHHHHHDYDIPTTENLYFQGSTFSKLREQLGPVTQEFWDNLEKETEGLRQE
MSKDLEEVKAKVQPYLDDFQKKWQEEMELYRQKVEPLRAELQEGARQKLHEL
QEKLSPLGEEMRDRARAHVDALRTHLAPYLDDFQKKWQEEMELYRQKVEPLRA
ELQEGARQKLHELQEKLSPLGEEMRDRARAHVDALRTHLAPYSDELRQRLAAR
LEALKENGGARLAEYHAKATEHLSTLSEKAKPALEDLRQGLLPVLESFKVSFLSA
LEEYTKKLNTQ

Expression and purification of MSP1D1 and MSP1E3D1 was performed according to the protocol kindly provided by the laboratory of Stephen G. Sligar at the University of Illinois at Urbana-Champaign with modifications (Bayburt, 2002). Plasmids encoding MSP1D1 and

MSP1E3D1 were purchased from Addgene (pMSP1D1: plasmid 20061, pET28a vector; kanamycin resistance; MSP1E3D1: plasmid 20066, pET28a vector, kanamycin resistance).

1) Transform BL21(DE3) cells with pMSP1D1 or pMSP1E3D1.

2) Inoculate 15 ml of LB (25g of LB powder per 1 L of ddH_2O) with a single colony and serially dilute 100-fold for a total of 5 15-ml cultures containing 100 μg/mL of kanamycin. Incubate the cultures with shaking overnight at 37°C.

3) Inoculate 2 liters of LB containing 100 μg/ml of kanamycin with 10 ml of the overnight culture at O.D of ~ 0.6. Incubate with shaking at 37°C. Induce at O.D. of 0.6 with 1 mM IPTG and in 30 minutes cool the culture to room temperature in 4°C water bath. Continue shaking at 28°C for 4 hours. Harvest the cells and freeze the wet cell mass in liquid nitrogen. Store the cell pellet at - 80°C.

4) Resuspend the cell mass from two liters of culture for either MSP1D1 or MSP1E3D1 in 25 mL of potassium phosphate buffer (23.1 g of KH2PO4 and 125.4 K2HPO4 per liter of solution) containing 20 mM Imidazole, 1% Triton X100, 1 mM PMSF, and two pulverized protease inhibitor cocktail pills (Complete, EDTA-free, Roche). Sonicate using 30 second cycles for a total of 3 minutes to lyse the cells (output: 8; % cycle duty 50).

5) Clear the lysate by centrifugation at 19,000 g for 25 min.

6) Load the lysate onto 3 mL of Ni-Sepharose High Performance resin equilibrated with 30 mL of the above potassium phosphate buffer containing 20 mM Imidazole.

7) Wash the loaded resin with 30 mL of 40 mM Tris•HCl (pH 8.0)/300 mM NaCl/1% Triton.

8) Wash the resin with 30 mL of 40 mM Tris•HCl (pH 8.0)/300 mM NaCl/50 mM Cholate/20 mM Imidazole.

9) Wash the resin with 30 mL of 40 mM Tris•HCl (pH 8.0)/300 mM NaCl/20 mM Cholate/50 mM Imidazole.

10) Elute the protein with 50 mM to 500 mM Imidazole gradient in 40 mM Tris•HCl (pH 8.0)/300 mM NaCl/10 mM Cholate.

11) Combine fraction containing the protein and dialyze against 20 mM Tris•HCL/100 mM NaCl/0.5 mM EDTA pH 7.4 overnight with several changes.

12) Concentrate the protein using 10,000 MWCO concentrators.

13) Determine the protein concentration using absorbance at 280 nm and the following extinction coefficients: MSP1D1 $\varepsilon = 21430\ M^{-}cm^{-}$, MSP1E3D1 $\varepsilon = 29910\ M^{-}cm^{-}$.

14) Flash freeze 50 µL aliquots and store at - 80°C.

Reconstitution of SecYEG in nanodiscs

Reconstitution of SecYEG in nanodiscs was performed according to the protocol provided by the laboratory of Franck Duong at the University of British Columbia without modifications (Dalal, 2010).

Preparation of lipids

Dissolve *E. coli* lipids or pure phosphatidylglycerol (PG) in chloroform. Transfer 1000 nanomoles of chloroform-solubilized lipids to 1.5 mL screwcap microtubes and evaporate chloroform under a gentle stream of nitrogen or argon. Dry the lipid under vacuum overnight and store the lipids at or below -20°C.

Reconstitution of SecYEG in nanodiscs using MSP1D1

Resuspend 1 micromole of dried lipid in 200 µL of TS50 buffer (50 mM Tris HCl pH 7.9/ 50 mM NaCl) and 10 µL of 10% DDM (to ensure initial solubilization of the lipids). Mix and sonicate briefly to dissolve the lipids.

In a 1.5 ml eppendorf tube, combine:

25 µL of 1% DDM in dd water

8 µL of the above lipid solution

12 µL of 15 mg/ml MSP1

172 µL of TS300G (50 mM Tris HCl pH 7.9/ 300 mM NaCl/ 10% glycerol)

83 µl of 1.8 mg/ml SecYEG

85 µL of BioBeads in TS50

Molar ratio of SecYEG:MSP1D1:Lipid = 1:4:40

Note: depending on the concentration of the starting reagents, adjust the volumes used to have the same molar ratio.

Incubate the mixture with gentle rocking at 4°C ON.

Transfer the mixture into a buffer-exchange column and spin at 1000 rpm to remove the BioBeads.

Ultracentrifuge in TLA 120.1 rotor at 70,000 rpm for 25 min to remove aggregates.

Transfer the supernatant to an eppendorf tube and mix gently. Store in ice.

Resolve 10 µL on a native gel.

<u>Reconstitution of SecYEG in nanodiscs using MSP1E3D1</u>

Resuspend 1 micromole of dried lipid in 200 µL of TS50 buffer (50 mM Tris HCl pH 7.9/ 50 mM NaCl) and 10 µL of 10% DDM (to ensure initial solubilization of the lipids). Mix and sonicate briefly to dissolve the lipids.

In a 1.5 ml eppendorf tube combine:

25 µL of 1% DDM in dd water

8 µL of the above lipid solution

20.4 µL of 9.19 mg/ml of MSP1E3D1 solution

163.6 µL of TS300G (50 mM Tris HCl pH 7.9/ 300 mM NaCl/ 10% glycerol)

67 µl of 2.25 mg/ml SecYEG

85 µL of BioBeads in TS50

Molar ratio of SecYEG:MSP1E3D1:Lipid = 1:2.75:20

Incubate the mixture in 1.5 ml eppendorf tubes overnight at 4° on an orbital shaker with gentle tumbling. Note: 5 hour incubation is sufficient.

Transfer the mixture to a buffer exchange column (used as a filter) without transferring Biobeads. Spin at 1000 rpm for 1 min to remove any transferred biobeads and contaminant particles.

Determine concentration using Bradford assay.

Concentrate nanodiscs to 1.2 mg/mL, using Amicon 50,000 MW cut-off filter rinsed with TS300G. Spin at 2500 rcf at 4°C.

Remove aggregates and liposomes by centrifugation in TLA 100.2 rotor at 70, 000 rpm, 4°C, 25 min. (Note: a tiny crescent-shaped pellet is observed. Protein concentration should not change since mainly empty liposomes are pelleted).

Determine the concentration using absorbance at 280. Convert to molarity using the MW of the species and the corresponding extinction coefficients.

Flash freeze aliquots of nanodiscs in liquid nitrogen and store at -80°C.

Expression and purification of YidC

E. coli YidC coding sequence was amplified using pET33 plasmid containing GFP-YidC fusion as a template (kindly provided by the laboratory of Bil Clemons at Caltech). The amplified sequence was used to replace the SecYEG sequence in the pEK20 plasmid (a gift from

Arnold Driessen). The promoter and other flanking sequences in pEK20 were left intact. Expression and purification of YidC was performed based on the protocol used for expression and purification of SecYEG with modification.

1) Transform BL21(DE3) cells with the pEK20/YidC plasmid.

2) Inoculate 40 ml of LB containing 100 mg/ml of ampicillin with a single colony and shake overnight at 37°C.

3) Inoculate 1 L of LB (25 g of powder per 1 L of ddH2O) with overnight culture at O.D. of ~ 0.3. Shake at 37°C until O.D. of 0.6. Induce with 1 mM IPTG and continue to shake for 2 hours. The final O.D. is ~ 0.95.

4) For expression analysis, collect cells from 1 mL of culture and resuspend the pellet in 30 µL of 1X BugBuster. Add 3 µL of Benzonase and incubate for 15 min at 37°C. Add 40 µL of 2X Laemmli Sample buffer. Load 20 µL onto 15% denaturing gel along with the pre-induction sample.

5) Collect the cells as described in purification of SecYEG and resuspend the total cell mass in 30 mL of KS300G buffer containing one pulverized protease inhibitor pill (Complete, EDTA-free, Roche).

6) Lyse the cells by sonicating at 50% duty of the cycle and output 8 on ice. Perform 5 1-min cycles. Cool the cell suspension between the cycles in ice water bath.

7) Clear the lysate as described in purification of SecYEG.

8) Centrifuge the supernatant to collect the membrane fraction as described in purification of SecYEG.

9) Resuspend the pellet in 20 mL of KS300G using dounce homogenizer, add 2 mL of 10% DDM, and tumble gently at 4°C for 1 hour.

10) Remove the intact membranes after extraction as described in purification of SecYEG.

11) Perform batch purification using Ni-NTA agarose as described in purification of SecYEG single Cys mutants. To maximize purity, use 250 μL of the resin. Significant loses of YidC, however, occur with this volume of the resin.

12) Dialyze YidC against 1L of 50 mM KHEPES pH 7.5/150 mM potassium acetate/10% glycerol/0.025% DDM/2 mM DTT.

13) Quantitate YidC using absorbance at 280 nm and $\varepsilon = 96,000\ M^{-}cm^{-}$.

Reconstitution of SecYEG and YidC in proteoliposomes

Reconstitution of SecYEG and YidC in proteoliposomes was performed according to the protocol provided by the laboratory of Arnold Driessen at the University of Groningen (van der Does, 2003). The procedure involves gradual removal of DDM from the mixture of lipids and SecYEG using adsorbent material. Seventy μL of 52 μM SecYEG were diluted to 1 mL with the buffer containing 10 mM Tris (pH 8.0), 10 % glycerol, 0.1% DDM, and 100 mM KCl. Two hundred μL of 20 mg/ml *E.coli* liposomes were activated in a bath sonicator until the solution was clear and diluted with 0.5% Triton X-100 to 4 mg/ml. SecYEG was mixed with the liposomes, and the mixture was incubated for 30 min at 4°C with gentle tumbling. Two hundred mg of Biobeads SM-2 adsorbent material (Bio-Rad Laboratories, Inc.) were washed twice with 5 ml of methanol, twice with 5 ml of double-deionized water, and three times with buffer A containing 50 mM Tris (pH 8.0), 50 mM KCl, and 1 mM DTT, mixed with the SecYEG/liposome mixture, and stirred gently for 2 hours at 4°C. The beads were sedimented by centrifugation at 500 g, the supernatant was mixed with 200 mg of washed Biobeads, and stirred gently at 4°C for 4 hours. The supernatant was incubated one more time with 400 mg of the

beads overnight, and the SecYEG proteoliposomes were pelleted by centrifugation in a TLA 100.3 rotor at 100,000 rpm for 30 min. The pellet was dissolved in 300 µL of the buffer A containing 10% glycerol using a dounce homogenizer. Concentration of SecYEG in proteoliposomes was determined by resolving an aliquot of the preparation on a denaturing gel along with the SecYEG standard of known concentration. Small aliquots of proteoliposomes were frozen in liquid nitrogen and stored at -80°C.

Reconstitution of YidC in proteoliposomes was performed exactly as reconstitution of SecYEG. Fifty µL of 56 µM YidC were diluted to 1 ml in the buffer containing 10 mM Tris (pH 8.0), 10 % glycerol, 0.1% DDM, and 100 mM KCl. Coreconstitution of SecYEG and YidC was performed according to the above protocol. Seventy µL of 52 µM SecYEG and 50 µL of 56 µM YidC were diluted to 1 mL in mM Tris (pH 8.0), 10 % glycerol, 0.1% DDM, and 100 mM KCl.

Concentration of the protein in the proteoliposome preparation was determined by diluting an aliquot in 2% SDS and measuring the concentration using absorbance at 280 nm. Quantitation was also performed by resolving an aliquot of proteoliposomes on a denaturing gel along with SecYEG standards of known concentration.

Native gels

The procedure for making and running native gels was kindly provided by the laboratory of Franck Duong at the University of British Columbia and performed without modifications.

Reagents and buffers

Anode buffer: Tris/Glycine pH 8.8 at 4°C (3g of Tris and 14g of Glycine per 1L of solution). Note. Do not pH this solution. The pH should be correct at 4°C.

Cathode buffer: Tris/Glycine pH 8.8 at 4°C (3g of Tris and 14g of Glycine per 1L of solution) / 0.015% Coomassie Brilliant Blue G 250 (in case of BN-PAGE). Exclude Coomassie Brilliant Blue G 250 from the cathode buffer in case of CN-PAGE.

1.5M Tris-HCl pH 8.8

Coomassie Brilliant Blue G 250 (C.I. 42655) from Serva.

2% solution of ultrapure bis-acrylamide in deionized water from BioShop

40% solution of ultrapure acrylamide in deionized water from BioShop

Making native gels

For 4-12% gradient native gel first prepare 12% and 4% acrylamide/bisacrylamide solutions as follows:

	12% (mL)	4% (mL)
Acrylamide 40%	14.6	4.9
Bis-acrylamide 2%	8	2.7
1.5M Tris-HCl pH 8.8	12.5	12.5
Glycerol	10	-----
ddH_2O	4.9	29.9
Total	50	50
APS 10%	58 µL	145 µL
TEMED	5.8 µL	14.5 µL

Mix the solutions thoroughly.

For six 8 cm x 10 cm gels, pour 27.5 ml of 12% and 4% solutions into the heavy and light chamber of a gradient former, respectively. Both chambers are equipped with magnetic stir bars.

Deliver the solutions using a peristaltic pump over the course of ten minutes. Note: a slow rate of delivery is crucial to forming a smooth gradient. The procedure is done at room temperature.

Insert the combs and allow the solution to solidify. (Note: there is no stacking gel). Wrap the gels in wet paper towel and store them at 4°C without removing the combs.

BN-PAGE

Fill the cathode chamber with the cathode buffer containing 0.015% Comassie Brilliant Blue G250.

Add the anode buffer to the anode chamber so that the electrodes are fully immersed in the buffer.

Make sure there are no air bubbles in the wells and that they are filled with the cathode buffer. Load 10 µL of the sample onto each well.

Perform electrophoresis at room temperature and constant current of 20 mAmp for 55 minutes. (Note: all electrophoresis buffers are at 4°C.)

Destain the gel in destain solution (1.6L of ethanol, 0.8L of acetic acid, and 5.6L of deionized water). Change the destain solution once after 2 hours of destaining and destain overnight or as desired for best contrast. Transfer the destained gel in water.

RNC_{3A7L} constructs

Below is the sequence of RNC_{3A7L} containing a 135 aa long nascent chain with the amber codon at the C-terminus. The color coding is described below the sequence. In N-terminally labeled RNCs, the glutamine residue at the N-terminus of the signal peptide was replaced with the amber codon.

M A S W S H P Q F E K G A M T G W S H P Q F E K R S A G S W S H P Q F E K L Q L V P R G S M K Q S T L A
L L L L L A L A T Stop V T K A R T P E M P V L E N R A A Q G D I T A P G G A R R L T G D Q T A A L R D S L

SDKPAKNIILLIGDGMGDSEITAARNYAEGAGGFFKGIDALDISEKGYRIDYAHFT
PQAKFSTPVWISQAQGIRAGP

- Triple Strep-tag (underlined)
- Thrombin cleavage site
- Signal anchor is in bold; with the gray color coded SecM, this construct constitutes RNC 65aa, boxed STOP is the location of the amber codon
- RNC_{FtsQ} 85 aa
- RNC_{FtsQ} 105 aa
- RNC_{FtsQ} 135 aa
- SecM stalling sequence, underlined region is inside the ribosomal tunnel

RNC3A7L 65 aa construct contains a 22 aa sequence upstream of the thrombin cleavage site inserted to increase the distance between the ribosomal surface and the Strep-tag for efficient binding to the resin (color coded cyan below)

MASWSHPQFEKGAMTGWSHPQFEKRSAGSWSHPQFEKTPVTKARTPEMPVLE
NRAAQGDLQLVPRGSMKQSTLALLLLLALATStopVTKARTPEMPVLENRAAQGD
ITAPGGARRLTGDQTAALRDSLSDKPAKNIILLIGDGMGDSEITAARNYAEGAGG
FFKGIDALDISEKGYRIDYAHFTPQAKFSTPVWISQAQGIRAGP

RNCs site-specifically labeled with coumarin were prepared according to the established protocol (Saraogi, 2011). RNCs were purified using the Strep-Tactin Sepharose resin as described and eluted in 10 ml of Solution I (50 mM KHEPES pH 7.5, 100 mM potassium acetate, and 25 mM magnesium acetate) containing 2 mg/ml of desthiobiotin. To remove the Strep-tag, 150 µL of 1unit/µL Thrombin in 1X PBS was added to the elution and incubated at room temperature for 4.5 hours. The solution was subsequently spun in at 38 000 rpm for 4 hours in Ti70 to pellet RNC. The pellet was dissolved in SRP buffer, RNC was quantitated as described, and 25 µL aliquots were frozen in liquid nitrogen. RNC was stored at -80°C.

RNC_{FtsQ} constructs

Below is the sequence of RNC_{FtsQ} containing a 155 aa long nascent chain with the amber codon at the N-terminus. The color coding is described below the sequence. In C-terminally labeled RNCs, the tryptophan residue at the C-terminus was replaced with the amber codon.

MASWSHPQFEKGAMTGWSHPQFEKRSAGSWSHPQFEKLQLVPRGSMGQAALN
TRNSEEEVSSRRNNGTRLStopGILFLLTVLTTVLVSGWVVLGWMEDAQRLPLSK
LVLTGERHYTRNDDIRQSILALGEPGTFMTQDVNIIQTQIEQRLPWIKQVSVRKQ
WPDELSEKGYRIDYAHFTPQAKFSTPVWISQAQGIRAGP

- Triple Strep-tag
- Thrombin cleavage site
- Signal anchor is in bold; with the gray color coded SecM, this construct constitutes FtsQ 90aa, boxed STOP is the location of the amber codon
- RNC_{FtsQ} 110 aa
- RNC_{FtsQ} 125 aa
- RNC_{FtsQ} 140 aa
- RNC_{FtsQ} 155 aa
- SecM stalling sequence, underlined region is inside the ribosomal tunnel

Preparation, purification, and thrombin treatment of RNCs bearing FtsQ nascent chains was performed exactly as with RNC_{3A7L}.

FRET assay with SecYEG and RNC

All FRET measurements were performed on a Horiba Jobin Yvon fluorolog in the modified SRP buffer (50 mM KHEPES pH 7.5/150 mM potassium acetate/10 mM magnesium acetate/10 % glycerol/0.3 mg/mL BSA/ 2 mM DTT/0.02% DDM). The concentration of RNC was kept at 20 nM. The final concentration of unlabeled and labeled SecYEG was from 200 to 600 nM and always saturating. FRET was calculated by taking the emission signal of coumarin in the presence of unlabeled SecYEG as the emission of the donor fluorophore in the absence of acceptor and the emission signal of coumarin in the presence of BODIPY-Fl-labeled SecYEG as the emission of the donor in the presence of the acceptor. FRET was calculated as described in Figures 2 and 3.

Equilibrium titration of RNC with SecYEG

Titrations were performed on a Horiba Jobin Yvon fluorolog in the modified SRP buffer. Twenty nM coumarin-labeled RNC was titrated with unlabeled SecYEG, and the increase in the emission of coumarin due to environmental sensitivity to SecYEG was monitored. Emission for each concentration of SecYEG was averaged around the peak emission value (typically from 440 nm to 460 nm), and the change in fluorescence was calculated using the emission of the coumarin-labeled RNC in the absence of SecYEG. The change in fluorescence was plotted against the concentration of SecYEG, and the data were fitted to the quadratic equation below:

$$F_{obsd} = F_1 \times \frac{[RNC]+[SecYEG]+K_d - \{([RNC]+[SecYEG]+K_d)^2 - 4[RNC][SecYEG]\}^{1/2}}{2\times[RNC]} \quad (1)$$

Cosedimentation assay with RNC and SecYEG nanodiscs

Assessment of binding of RNC to SecYEG nanodics was performed using a published cosedimentation assay with modifications (Fraunfeld, 2011; Menetret, 2007). Briefly, 200 nM RNC1A9L were incubated with 1 μM of SecYEG nanodiscs (MSP1D1/PG/SecYEG) or empty discs (MSP1D1/PG) in a 50 μL reaction volume for 35 minutes at room temperature in SRP buffer supplemented with 10% glycerol. Fifteen μL were removed and mixed with 15 μL of 2X Laemmli Sample buffer (L, see figure 9E), while 35 μL of the mixture were layered onto 200 μL of 30% sucrose solution in SRP buffer. The tubes were spun in TLA 100 rotor for 12 minutes at 100,000 rpm, 4°C. The supernatant was aspirated, the pellet was dissolved in 15 μL of 1% SDS, and 15 μL of 2X Laemmli Sample buffer were added to the solution (P, see figure 9E). The samples were resolved on a 15% denaturing gel.

Protease protection assay

Binding of the nascent chain to SecYEG was assessed using a protease protection assay. RNC1A9L containing 85 aa long nascent chain were prepared according to the published protocol in the translation mixture containing ^{35}S-methionine instead of cold methionine. Radioactively-labeled RNCs were sedimented through 30% sucrose cushion as follows. 186 µL of translation mixture were layered onto 2.2 mL of the sucrose cushion in SRP buffer and spun in TLA 100.3 rotor at 90,000 rpm for 3 hours. The pellet was dissolved in 100 µL of SRP buffer supplemented with 10% glycerol. The RNC was quantitated as described.

Twenty µL of 1 µM ^{35}S-RNC/ribosomes were diluted to 100 µL and distributed among 8 tubes (12 µL per tube). Five µL of 19 µM SecYEG/DDM, empty liposomes, 18 µM SecYEG proteoliposomes, or SRP buffer were mixed with RNC, the reactions were incubated either at 25°C or 37°C, and transferred to ice. Proteinase treatment was performed by adding 17 µL of 0.01 mg/mL proteinase K to each reaction and incubating on ice for 15 min. The reactions were quenched with 200 µL 5 mM PMSF in 20 mM KHEPES pH 7.5, and the protein was precipitated by adding 70 µL of 100% TCA. The samples were incubated on ice for 30 min. After centrifugation at 14,000 rpm for 40 min and washing with cold acetone, the pellets were dissolved in 60 µL of 2X Laemmli Sample buffer with vortexing and sonication. Seventeen µL were loaded onto a 15% denaturing gel. The gel was dried and visualized by autoradiography.

Cotranslational protein targeting assay

The chloramphenicol transferase coding sequence in CATAmb109Y plasmid was replaced with the *E. coli* Leader peptidase (Lep) sequence amplified from pDUET-cpSRP-Lep plasmid.

Cotranslational protein targeting of Lep was performed by combining coupled transcription/translation with translocation of the translated substrate into lipid vesicles. The

coupled transcription/translation system was used here as described in Saraogi et al., 2011 with the following modifications. The extract was cleared by centrifugation at 42,000 rpm, 4°C for 20 min in TLA 120-1 to remove the membrane. Cold methionine was replaced with ^{35}S-methionine, with the final concentration of radioactive methionine (316 nM) much lower than the concentration of the other amino acids (2 mM). Anti-ssrA oligo was excluded from the reaction.

For the targeting assay, the system was supplemented with lipid vesicles and the reaction was initiated with 65 μg/mL of Lep plasmid. The final concentration of SecYEG proteoliposomes and YidC proteoliposomes in the reaction were 3.2 μM and 2.9 μM, respectively. The reactions were incubated at 37°C for 30 minutes and cooled by transferring to ice. Triton X100 was added to select reactions for the final concentration of 1%, and 10 μL of the reaction were removed for treatment with proteinase K. Two μL of 2 mg/mL of proteinase K were added to the aliquot, the reaction was incubated on ice for 15 min, and quenched with 200 μL of 7 mM PMSF in 20 mM KHEPES pH 7.5. The protein was precipitated by adding 65 μL of 100% TCA. For – K samples, the protein was TCA precipitated from another 10 μL aliquot of the same targeting reaction by adding 200 μL of 20 mM KHEPES pH 7.5 and 65 μL of 100% TCA. The mixtures were incubated on ice for 40 min, centrifuged at 14,000 rpm, 4°C for 30 min, washed with cold acetone, air dried, and dissolved in 70 μL of 2X Laemmli Sample buffer with vortexing and sonication. Twenty μL were loaded onto 12.5% denaturing gel.

The gel was visualized by autoradiography, and the intensity of the bands was quantified using the ImageQuant software. The extent of insertion was calculated by comparing the intensity of the protected P2-H2 fragment (+K) to the intensity of the full-length Lep band (–K) using equation (2), where the factor of 1.33 accounts for the difference in the methionine content in H2-P2 vs. Lep and bckg is the background intensity of the gel.

$$\% \text{ Insertion} = \left\{ \frac{(H2\text{-}P2 \times 1.33) - bckg}{Lep - bckg} \right\} \times 100\% \qquad (2)$$

References

Akimuru, J., Matsuyama, S.I., Tokuda, H., and S. Mizushima. 1991. Reconstitution of a protein translocation system containing purified SecY, SecE, and SecA from *Escherichia coli*. Proc. Natl. Acad. Sci. USA *88*, 6545-6549.

Akopian, D., K. Dalal, K. Shen, F. Duong, and S.-o. Shan. 2013. SecYEG activates GTPases to drive the completion of cotranslational protein targeting. J. Cell Biol. *2* 397-405.

Alami, M., Dalal, K., Lelj-Garolla, B., Sligar, S.G., and F. Duong. 2007. Nanodiscs unravel the interaction between the SecYEG channel and its cytosolic partner SecA. EMBO J. *26*, 1995-2004.

Barak, I., Wilkinson, A.J., O'Toole, P.J., and N. Pavlendova. 2008. Lipid spirals in *Bacillus subtilis* and their role in cell division. Mol. Microbiol. *68*, 1315-1327.

Bayburt, T.H., Grinkova ,Y.V., and S.G. Sligar. 2002. Self-assembly of discoidal phospholipids bilayer nanoparticles with membrane scaffold proteins. Nano Letters *2*, 853-856.

Beck, K., Eisner, G., Trescher, D., Dalbey, R.E., Brunner, J., and M. Muller. 2001. YidC, an assembly site for polytopic *Escherichia coli* membrane proteins located in immediate proximity to the SecYE translocon and lipids. EMBO Rep. *2*, 709-714.

Becker, T., Bhushan, S., Jarasch, A., Armache, J., Funes, S., Jossinet, F., Gumbart, J., Mielke, T., Berninghausen, O., Schulten, K., Westhof, E., Gilmore, R., Mandon, E.C., and R. Beckmann. 2009. Structure of monomeric yeast and mammalian Sec61 complexes interacting with the translating ribosome. Science *326*, 1369-1373.

Beckmann, R., Spahn, C.M., Eswar, N., Helmers, J., Penczek P.A., Sali, A., Frank, J., and G. Blobel. 2001. Architecture of the protein-conducting channel associated with the translating 80S ribosome. Cell *107*, 361-372.

Bernstein, H.D. 2001. Cotranslational translocation of proteins into canine rough microsomes. Curr. Protoc. Cell Biol. doi: 10.1002/0471143030.cb1104s00.

Boldog, T., Mingshan, Li, and G.L. Hazelbauer. 2007. Using nanodiscs to create water-soluble transmembrane chemoreceptors inserted in lipid bilayers. Meth. Enzymol. *423*, 317-335.

Brundage, L., Hendrick, J.P., Schiebel, E., Driessen, A.J.M, and W. Wickner. 1990. The purified *E. coli* integral membrane protein SecY/E is sufficient for reconstitution of SecA-dependent precursor protein translocation. Cell *62*, 649-657.

Cannon, K.S., Or, E., Clemons, W. M., Jr., Shibata, Y., and Rapoport, T.A. (2005). Disulfide bridge formation between SecY and a translocating polypeptide localizes the translocation pore to the center of SecY. J. Cell Biol. *169*, 219-225.

Carson, M.J., Barondess, J., and J. Beckwith. 1991. The FtsQ protein of *Escherichia coli*: membrane topology, abundance, and cell division phenotypes due to overproduction and insertion mutations. J. Bacteriol. *173*, 2187-2195.

Cheng, Z., Jiang, Y., Mandon, E.C., and R. Gilmore. 2005. Identification of cytoplasmic residues of Sec61p involved in ribosome binding and cotranslational translocation. J. Cell Biol. *168*, 67-77.

Crowley, K.S., Liao, S., Worrell, V.E., Reinhart, G.D., and A.E. Johnson. 1994. Secretory proteins move through the endoplasmic reticulum membrane via an aqueous, gated pore. Cell *78*, 461-471.

Dalal, K., Chan, C.S., Sligar, S.G., and F. Duong. 2012. Two copies of the SecY channel and acidic lipids are necessary to activate the SecA translocation ATPase. Proc. Natl. Acad. Sci. USA *109*, 4104-4109.

Dalal, K. and F. Duong. 2010. Reconstitution of the SecY translocon in nanodiscs. Meth. Mol. Biol. *619*, 145-156.

Dalbey, R.E. and A. Kuhn. 2004. YidC family members are involved in the membrane insertion, lateral integration, folding, and assembly of membrane proteins. J. Cell Biol. *166*, 769-774.

Dalbey, R.E., Kuhn, A., Zhu, L., Kiefer, D. 2014. The membrane insertase YidC. *Biochim. Biophys. Acta* Advance online publication. doi: 10.1016/j.bbamcr.2013.12.022.

Deitermann, S., Sprie, G.S., and H.G. Koch. 2005. A dual function for SecA in the assembly of single spanning membrane proteins in *Escherichia coli*. J. Biol. Chem. *280*, 39077-39085.

Denisov, I.G., Grinkova, Y.V., Lazarides, A.A., and S.G. Sligar. 2004. Directed self-assembly of monodisperse phospholipids bilayer nanodiscs with controlled size. J. Am. Chem. Soc. *126*, 3477-3487.

Derman, A.I., Puziss, J.W., Bassford, Jr. P.J., and J. Beckwith. 1993. A signal sequence is not required for protein export in *prlA* mutants of *Escherichia coli*. EMBO J. 12, 879-888.

Devaraneni, P. K., Conti, B., Matsumura, Y., Yang, Z., Johnson, A. E., and W.R. Skach. 2011. Stepwise insertion and inversion of a type II signal anchor sequence in the ribosome-Sec61 translocon complex. Cell *146*, 134-47.

Duong, F. and W. Wickner. 1997. Distinct catalytic roles of the SecYE, SecG, and SecDFyajC subunits of preprotein translocase holoenzyme. EMBO J. *16*, 2756-2768.

du Plessis, D.J., Nouwen, N., and A.J. Driessen. 2006. Subunit a of cytochrome o oxidase requires both YidC and SecYEG for membrane insertion. J. Biol. Chem. *281*, 12248-12252.

du Plessis, D.J., Berrelkamp, G., Nouwen, N., and Driessen, A.J. (2009). The lateral gate of SecYEG opens during protein translocation. J. Biol. Chem. *284*, 15805-14.

Drew, D., Froderberg, L., Baars, L., de Gier, J.W. 2003. Assembly and overexpression of membrane proteins in *Escherichia coli*. Biochim. Biophys. Acta *1610*, 3-10.

Egea, P.F. and R.M. Stroud. 2010. Lateral opening of a translocon upon entry of protein suggests the mechanism of insertion into membranes. Proc. Natl. Acad. Sci. USA *107*, 17182-17187.

Emr, S.D., Helen-Way, S., and T.J. Silhavy. 1981. Suppressor mutations that restore export of a protein with a defective signal sequence. Cell *23*, 79-88.

Ernst, S., Schonbauer, A.K., Bar, G., Borsch, M., and A. Kuhn. 2011. YidC-driven membrane insertion of single fluorescent Pf3 coat protein. J. Mol. Biol. *412*, 165-175.

Facey, S.J., Neugebauer, S.A., Krauss, S., and A. Kuhn. 2007. The mechanosensitive channel protein MscL is targeted by the SRP to the novel YidC membrane insertion pathway of *Escherichia coli*. J. Mol. Biol. *365*, 995-1004.

Fekkes, P., de Wit, J.G., van der Wolk, J.P., Kimsey, H.H., Kumamoto, C.A., and A.J. Driessen. 1998. Preprotein transfer to the *Escherichia coli* translocase requires the co-operative binding of SecB and the signal sequence to SecA. Mol. Microbiol. 29, 1179-1190.

Fishov, I., and C.L. Woldringh. 1999. Visualization of membrane domains in *Escherichia coli.* Mol. Microbiol. *32*, 1166-1172.

Flower, A.M., Doebele, R.C., and T.J. Silhavy. 1994. PrlA and PrlG suppressors reduce the requirement for signal sequence recognition. J. Bacteriol. *176*, 5607-5614.

Fraunfeld, J., Gumbart, J., Sluis, E.O., Funes, S., Gartmann, M., Beatrix, B., Mielke, T., Berninghausen, O., Becker, T., Schulten, K., Beckmann, R. (2011). Cryo-EM structure of the ribosome-SecYE complex in the membrane environment. Nat. Struct. Mol. Biol. *18*, 614-621.

Gluck, J.M., Koenig, B.W., and D. Willbold. 2011. Nanodiscs allow the use of integral membrane proteins as analytes in surface plasmon resonance studies. Anal. Biochem. *408*, 46-52.

Gogala, M., Becker, T., Beatrix, B., Armache, J.P., Barrio-Garcia, C., Berninghausen, O., and R. Beckmann. 2014. Structure of the Sec61 complex engaged in nascent peptide translocation or membrane insertion. Nature *506*, 107-110.

Gold, V.A.M., Robson, A., Bao, H., Romantsov, T., Duong, F., and I. Collison. 2010. The action of cardiolipin on bacterial translocon. Proc. Nat. Acad. Sci. USA. *107,* 10044-10049.

Gorlich, D., Prehn, S., Hartmann, E., Kalies, K.U. and T.A. Rapoport. 1992. A mammalian homolog of Sec61p and SecYp is associated with ribosomes and nascent polypeptides during translocation. Cell *71*, 489-503.

Gorlich, D. and T.A. Rapoport. 1993. Protein translocation into proteoliposomes reconstituted from purified components of the endoplasmic reticulum membrane. Cell *75*, 615-630.

Gray, A.N., Henderson-Frost, J.M., Boyd, D., Sharafi, S., Niki, H., and M.B. Goldberg. 2011. Unbalanced charge distribution as a determinant for dependence of a subset of *Escherichia coli* membrane proteins on the membrane insertase YidC. mBio 2, doi: 10.1128/mBio.00238-11.

Hanada, M., Nishiyama, K., Mizushima, S., Tokuda, H. 1994. Reconstitution of an efficient protein translocation machinery comprising SecA and the three membrane proteins, SecY, SecE, and SecG (p12)*. *J. Biol. Chem.* **269**, 23625-23631.

Houben, E.N., Scotti, P.A., Valent, Q.A., Brunner, J., de Gier, J.L., Oudega, B., and J. Luirink. 2000. Nascent Lep inserts into the *Escherichia coli* inner membrane in the vicinity of YidC, SecY, and SecA. FEBS Lett. *476*, 229-233.

Houben, E.N., Urbanus, M.L., van der Laan, M., Ten Hagen-Jongman, C.M., Driessen, A.J., Brunner, J., Oudega, B., and J. Luirink. 2002. YidC and SecY mediate membrane insertion of a Type I transmembrane domain. J. Biol. Chem. *277*, 35880-35886.

Ismail, N., Hedman, R., Schiller, N., and G. von Heijne. 2012. A biphasic pulling force acts on transmembrane helices during translocon-mediated membrane integration. Nat. Struct. Mol. Biol. *19*, 1018-1022.

Jiang, F., Chen, M., Yi, L., de Gier, J.W., Kuhn, A., and R.E. Dalbey. 2003. Defining the regions of *Escherichia coli* YidC that contribute to activity. J. Biol. Chem. *278*, 48965-48972.

Joly, J.C. and W.T. Wickner. 1993. The SecA and SecY subunits of translocase are the nearest neighbors of a translocating preprotein, shielding it from phospholipids. EMBO J. *12*, 255-263.

Jungnickel, B., and Rapoport, T.A. (1995). A posttargeting signal sequence recognition event in the endoplasmic reticulum membrane. Cell *82*, 261-270.

Kedrov, A., Kusters, I., Krasnikov, V.V., Driessen, A.J. 2011. A single copy of SecYEG is sufficient for preprotein translocation. EMBO J. *30*, 4387-4397.

Kedrov, A., Sustarsic, M., de Keyzer, J., Caumanns, J.J., Wu, Z.C., and A.J.M. Driessen. 2013. Elucidating the native architecture of the YidC:ribosome complex. J. Mol. Biol. *425*, 4112-4124.

Kiefer, D. and A. Kuhn. 1999. Hydrophobic forces drive spontaneous insertion of the bacteriophage Pf3 coat protein without topological control. EMBO J. *18*, 6299-6306.

Kiefer, D., and A. Kuhn. 2007. YidC as an essential and multifunctional component in membrane protein assembly. Int. Rev. Cytol. *259*, 113-138.

Koch, H.G. and M. Muller. 2000. Dissecting the translocase and integrase functions of the *Escherichia coli* SecYEG translocon. J. Cell Biol. *150*, 689-694.

Kocik, L. Junne, T., and M. Spiess. 2012. Orientation of internal signal-anchor sequence at the Sec61 translocon. J. Mol. Biol. *424*, 368-378.

Kohler, R., Boehringer, D., Greber, B., Bingel-Erlenmeyer, I., Collinson, I., Schaffitzel, C., and N. Ban. 2009. YidC and Oxa1 form dimeric insertion pores on the translating ribosome. Mol. Cell *34*, 344-353.

Kudva, R., Denks, K., Kuhn, P., Vogt, A., Muller, M., and H.G. Koch. 2013. Protein translocation across the inner membrane of Gram-negative bacteria: the Sec and Tat dependent protein transport pathways. Res. Microbiol. *164*, 505-534.

Kuhn, P., Weiche, B., Sturm, L., Sommer, E., Drepper, F., Warscheid, B., Sourjik, V., and H.-G. Koch. (2011). The bacterial SRP receptor, SecA and the ribosome use overlapping binding sites on the SecY translocon. Traffic *12*, 563-578.

Kumazaki, K., Chiba, S., Takemoto, M., Furukawa, A., Nishiyama, K., Sugano, Y., Mori, T., Dohmae, N., Hirata, K., Nakada-Nakura, Y., Maturna, A.D., Tanaka, Y., Mori, H., Sugita, Y., Arisaka, F., Ito, K., Ishitani, R., Tsukazaki, T., and N. Osamu. 2014. Structural basis of Sec-independent membrane protein insertion by YidC. Nature. Advance online publication. doi: 10.1038/nature13167

Li, W., Schulman, S., Boyd, D., Erlandson, K., Beckwith, J., and T.A. Rapoport. 2007. The plug domain of the SecY protein stabilizes the closed state of the translocation channel and maintains a membrane seal. Mol. Cell *26*, 511-21.

Lotz, M., Haase, W., Kuhlbrandt, W., and I. Collinson. 2008. Projection structure of yidC: a conserved mediator of membrane protein assembly. J. Mol. Biol. *375*, 901-907.

Lycklama A Nijeholt, J.A., Bulacu, M., Marrink, S.J., and A.J. Driessen. 2010. Immobilization of the plug domain inside the SecY channel allows unrestricted protein translocation. J. Biol. Chem. *285*, 23747-23754.

Mao, C., Cheadle, C.E., Hardy, S.J., Lilly, A.A., Suo, Y., Sanganna Gari, R.R., King, G.M., and L.L. Randall. 2013. Stoichiometry of SecYEG in the active translocase of *Escherichia coli* varies with precursor species. Proc. Natl. Acad. Sci. USA *110*, 11815-11820.

Menetret, J., Schaletzky, J., Clemons, Jr.W.M., Osborne, A.R., Skanland, S.S., Denison, C., Gygi, S.P., Kirkpatrick, D.S., Park, E., Ludtke, S.J., Rapoport, T.A., and C.W. Akey. 2007. Ribosome binding of a single copy of the SecY complex: implications for protein translocation. Mol. Cell *28*, 1083-1092.

Moser, M., Nagamori, S., Huber, M., Tokuda H., and K. Nishiyama. 2013. Glycolipozyme MPIase is essential for topology inversion of SecG during preprotein translocation. Proc. Natl. Acad. Sci. USA *110*, 9734-9739.

Mothes, W., Jungnickel, B., Brunner, J., and Rapoport, T.A. (1998). Signal sequence recognition in cotranslational translocation by protein components of the endoplasmic reticulum membrane. J. Cell Biol. *142*, 355-364.

Nath, A., Atkins, W.M., and S.G. Sligar. 2007. Applications of phospholipid bilayer nanodiscs in the study of membranes and membrane proteins. Biochemistry *46*, 2059-2069.

Neumann-Haefelin, C., Schafer, U., Muller, M., and H.G. Koch. 2000. SRP-dependent co-translational targeting and SecA-dependent translocation analyzed as individual steps in the export of a bacterial protein. EMBO J. *19*, 6419-6426.

Nicchitta, C.V. and G. Blobel. 1990. Assembly of translocation-competent proteoliposomes from detergent-solubilized rough microsomes. Cell *60*, 259-269.

Nouwen, N. and A.J. Driessen. 2002. SecDFyajC forms a heterotetrameric complex with YidC. Mol. Microbiol. *44*, 1397-1405.

Osborne, R.S. and T.J. Silhavy. 1993. PrlA suppressor mutations cluster in regions corresponding to the three distinct topological domains. EMBO J. *12*, 3391-3398.

Park, E., Menetret, J.F., Gumbart, J.C., Ludtke, S.J., Li, W., Whynot, A., Rapoport, T.A., and C.W. Akey. 2014. Structure of the SecY channel during initiation of protein translocation. Nature *506*, 102-106.

Park, E., and Rapoport, T.A. (2011). Preserving the membrane barrier for small molecules during bacterial protein translocation. Nature *473*, 239-42.

Plath, K., Mothes, W., Wilkinson, B.M., Stirling, C.J., Rapoport, T.A. 1998. Signal sequence recognition in posttranslational protein transport across the yeast ER membrane. Cell *94*, 795-807.

Price, C.E., and A.J. Driessen. 2010. Conserved negative charges in the transmembrane segments of subunit K of the NADH:ubiquinone oxidoreductase determine its dependence on YidC for membrane insertion. J. Biol. Chem. *285*, 3575-3581.

Qi, H.Y. and H.D. Bernstein. 1999. SecA is required for the insertion of inner membrane proteins targeted by the *Escherichia coli* signal recognition particle. J. Biol. Chem. *274*, 8993-8997.

Ravaud, S., Stiepanovic, G., Wild, K., and I. Sinning. 2008. The crystal structure of the peripasmic domain of the *Escherichia coli* membrane protein insertase YidC contains a subsrate binding cleft. J. Biol. Chem. 283, 9350-9358.

Saaf, A., Anderson, H., Gafvelin, G. and G.von Heijne. 1995. SecA-dependence of the translocation of a large periplasmic loop in the *Escherichia coli* MalF inner membrane protein is a function of sequence context. Mol. Membr. Biol. *12*, 209-215.

Saaf, A., Monne, M., de Gier, J.W., and G. von Heijne. 1998. Membrane topology of the 60-kDa Oxa1 homologue from *Escherichia coli*. J. Biol. Chem. *273*, 30415-30418.

Sachelaru, I., Petriman, N.A., Kudva, R., Kuhn, P., Welte, T., Knapp, B., Drepper, F., Warscheid, B., and H.G. Koch. 2013. YidC occupies the lateral gate of the SecYEG translocon and is sequentially displaced by a nascent membrane protein. J. Biol. Chem. *288*, 16295-16307.

Samuelson, J.C., Jiang, F., Yi. L., Chen, M., de Gier, J.W., Kuhn, A., and R.E. Dalbey. 2001. Function of YidC for the insertion of M13 procoat protein in *Escherichia coli*: translocation of mutants that show differences in their membrane potential and Sec requirement. J. Biol. Chem. *276*, 34847-34852

Saraogi, I., Akopian, D., and S.-o. Shan. 2014. Regulation of cargo recognition, commitment, and unloading drives cotranslational protein targeting. J. Cell Biol. In press.

Saraogi, I., D. Zhang, S. Chandrasekaran, and S. Shan. 2011. Site-specific fluorescent labeling of nascent proteins on the translating ribosome. J. Amer. Chem. Soc. *133*, 14936-14939.

Schulze, R.J., Komar, J., Botte, M., Allen, W.J., Whitehouse, S., Gold, V.A., Lycklama A Nijeholt, J.A., Huard, K., Berger, I., Schaffitzel, C., Collinson, I. 2014. Membrane protein insertion and proton-force-dependent secretion through the bacterial holo-translocon SecYEG-SecDF-YajC-YidC. *Proc. Natl. Acad. Sci. USA* Advance online publication. doi/10.1073/pnas/1315901111.

Scotti, P.A., Urbanus, M.L., Brunner, J., de Gier, J.W., von Heijne, G., van der Does, C., Driessen, A.J., Oudega, B., and J. Luirink. 2000. YidC, the *Escherichia coli* homologue of mitochondrial Oxa1p, is a component of the Sec translocase. EMBO J. *19*, 542-549.

Scotti, P.A., Valent, Q.A., Manting, E.H., Urbanus, M.L., Driessen, A.J., and J. Luirink. 1999. SecA is not required for signal recognition particle-mediated targeting and initial membrane insertion of a nascent inner membrane protein. J. Biol. Chem. *274*, 29883-29888.

Seitl, I., Wickles, S., Beckmann, R., Kuhn, A., and D. Kiefer. 2014. The C-terminal regions of YidC from *Rhodopirellula baltica* and *Oceanicaulis alexandrii* bind to ribosomes and partially substitute SRP receptor function in *Escherichia coli*. Mol. Microbiol. *91*, 408-421.

Shaw, A.S., Rottier, P.J.M., and J.K. Rose. 1988. Evidence for the loop model of signal-sequence insertion into the endoplasmic reticulum. Proc. Natl. Acad. Sci. USA *85*, 7592-7596.

Shen, K., Arslan, S., Akopian, D., Ha. T., and S.-o. Shan. 2012. Activated GTPase movement on an RNA scaffold drives co-translational protein targeting. Nature *492*, 271-275.

Stiegler, N., Dalbey, R.E., and A. Kuhn. 2011. M13 procoat protein insertion into YidC and SecYEG proteoliposomes and liposomes. J. Mol. Biol. *406*, 32-370.

Urbanus, M.L., Froderberg, L., Drew, D., Bjork, P., de Gier, J.W., Brunner, J., Oudega, B., and J. Luirink. 2002. Targeting, insertion, and localization of *Escherichia coli* YidC. J. Biol. Chem. *277*, 12718-12723

Urbanus, M.L., Scotti, P.A., Froderberg, L., Saaf, A., de Gier, J.L., Brunner, J., Samuelson, J.C., Dalbey, R.E., Odega, B., and J. Luirink. 2001. Sec-dependent membrane protein insertion; sequential interaction of nascent FtsQ with SecY and YidC. EMBO rep. *2*, 524-529.

van Bloois, E., Jan Haan, G., de Gier, J.W., Oudega, B., and J. Luirink. 2004. F_1F_0 ATP synthase subunit c is targeted by the SRP to YidC in the *E. coli* inner membrane. FEBS Lett. 576, 97-100.

van den Berg, B., Clemons, Jr. W.M., Collinson, I., Hartmann, E., Harrison, S.C., Rapoport, T.A. 2004. X-ray structure of a protein-conducting channel. Nature *427*, 36-44.

van der Does, C., de Keyzer, J., van der Laan, M., and A.J. Driessen. 2003. Reconstitution of purified bacterial preprotein translocase in liposomes. Meth. Enzymol. *372*, 86-98.

van der Laan, M., Bechtluft, P., Kol, S., Nouwen, N. and A.J. Driessen. 2004 F_1F_0 ATP synthase subunit c is a substrate of the novel YidC pathway for membrane protein biogenesis. J. Cell Biol. *165*, 213-222.

van der Laan, M., Houben, E.N., Nouwen, N., Luirink, J., and A.J. Driessen. 2001. Reconstitution of Sec-dependent membrane protein insertion: nascent FtsQ interacts with YidC in a SecYEG-dependent manner. EMBO Rep. *2*, 519-523.

van der Laan, M., Nouwen, N., and A.J. Driessen. 2004. SecYEG proteoliposomes catalyze deltaphi-dependent membrane insertion of FtsQ. J. Biol. Chem. *279*, 1659-1664.

van der Wolk, J.P., Fekkes, P., Boorsma, A., Huie, J.L., Silhavy, T.J., and A.J.M. Driessen. 1998. PrlA4 prevents the rejection of signal sequence defective preproteins by stabilizing the SecA-SecY interaction during the initiation of translocation. EMBO J. *17*, 3631-3639.

Vanounou, S., Parola, A.H., and I. Fishov. 2003. Phosphatidylethanolamine and phosphatidylglycerol are segregated into different domains in bacterial membrane. A study with pyrene-labeled phospholipids. Mol. Microbiol. *49*, 1067-1079.

Veenendaal, A.K.J., van der Does, C., and A.J.M. Driessen. 2004. The protein-conducting channel SecYEG. Biochim. Biophys. Acta *1694*, 81-95.

Wagner, S., Pop, O.I., Haan, G.J., Baars, L., Koningstein, G., Klepsch, M.M., Genevaux, P., Luirink, J., and J.W. de Gier. 2008. Biogenesis of MalF and the MalFGK2 maltose transport complex in *Escherichia coli* requires YidC. J. Biol. Chem. *283*, 17881-17890.

Welte, T., Kudva, R., Kuhn, P., Sturm, L., Braig, D., Muller, M., Warscheid, B., Drepper, F., and H.G. Koch. 2012. Promiscuous targeting of polytopic membrane proteins to SecYEG or YidC by the *Escherichia coli* signal recognition particle. Mol. Biol. Cell *23*, 464-479.

Wolfe, P.B., Wickner, W., and J.M. Goodman. 1983. Sequence of the leader peptidase gene of *Escherichia coli* and the orientation of leader peptidase in the bacterial envelope. J. Biol. Chem. *258*, 12073-12080.

Wu, Z.C., de Keyzer, J., Kedrov, A., and A.J. Driessen. 2012. Competitive binding of the SecA ATPase and ribosomes to the SecYEG translocon. J. Biol. Chem. *287*, 7885-7895.

Yi. L., Celebi, N., Chen, M., and R.E. Dalbey. 2004. Sec/SRP requirement and energetics of membrane insertion of subunits a, b, and c of the *Escherichia coli* F_1F_0 ATP synthase. J. Biol. Chem. *279*, 39260-39267.

Zhu, L., Wasey, A., White, S.H., and R.E. Dalbey. 2013. Charge-composition features of model single-span membrane proteins that determine selection of YidC and SecYEG translocase pathways in *Escherichia coli*. J. Biol. Chem. *288*, 7704-7716.

Zimmer, J., Nam, Y., Rapoport, T.A. 2008. Structure of a complex of the ATPase SecA and the protein-translocation channel. Nature *455*, 936-943.

.

Figures

Figure 1

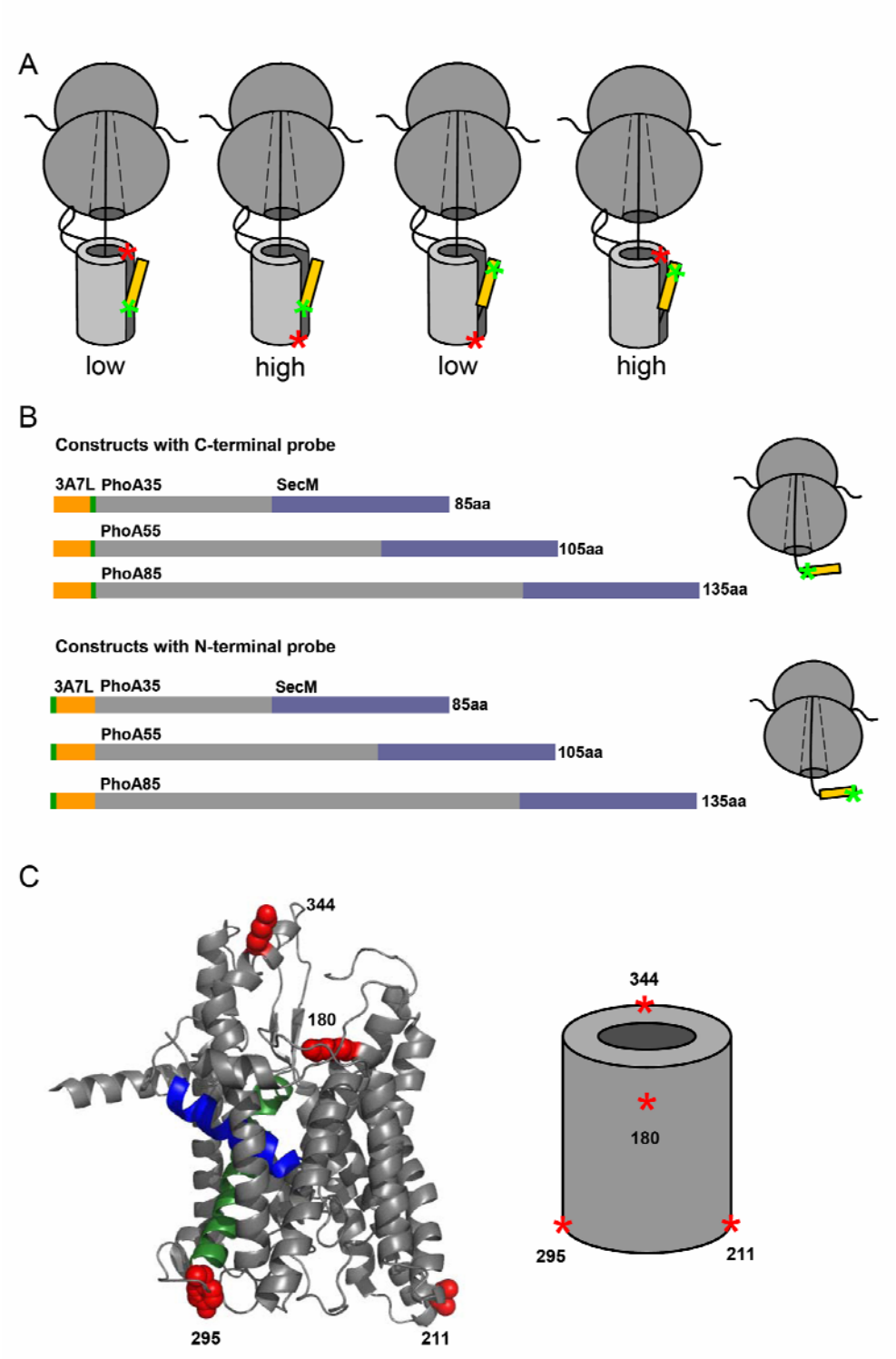

Figure 1. Experimental approach to map the signal peptide-SecYEG interaction. A. Schematic diagram of type II orientation of the signal peptide inside SecYEG. This is one of the possible intercalation modes and is shown to demonstrate the reasoning behind the FRET mapping assay. The donor (green) and acceptor (red) dyes positioned at different sites on the signal peptide and SecYEG, respectively, are expected to yield distinct FRET efficiency values and thus determine the orientation of the signal peptide. The orange rectangle depicts the signal peptide. "Low" and "high" refer to expected FRET efficiencies for each set of labeled species and configuration. **B**. The nascent chain constructs used in the FRET mapping experiment are schematically depicted. The numbers on the right indicate the length of the nascent chains. The green bar shows the location of the donor dye at the N- or C-terminus of the signal peptide. **C**. X-ray crystal structure of SecYEβ from *M. jannaschii* showing the location of the acceptor dye. The numbering corresponds to the amino acid residues of the *E. coli* SecYEG. On the right, SecYEG is represented as a cylinder to emphasize the spatial distribution of the labeled residues. See Materials and methods for detailed description of the constructs used in preparation of the RNCs and the procedure of SecYEG labeling.

Figure 2

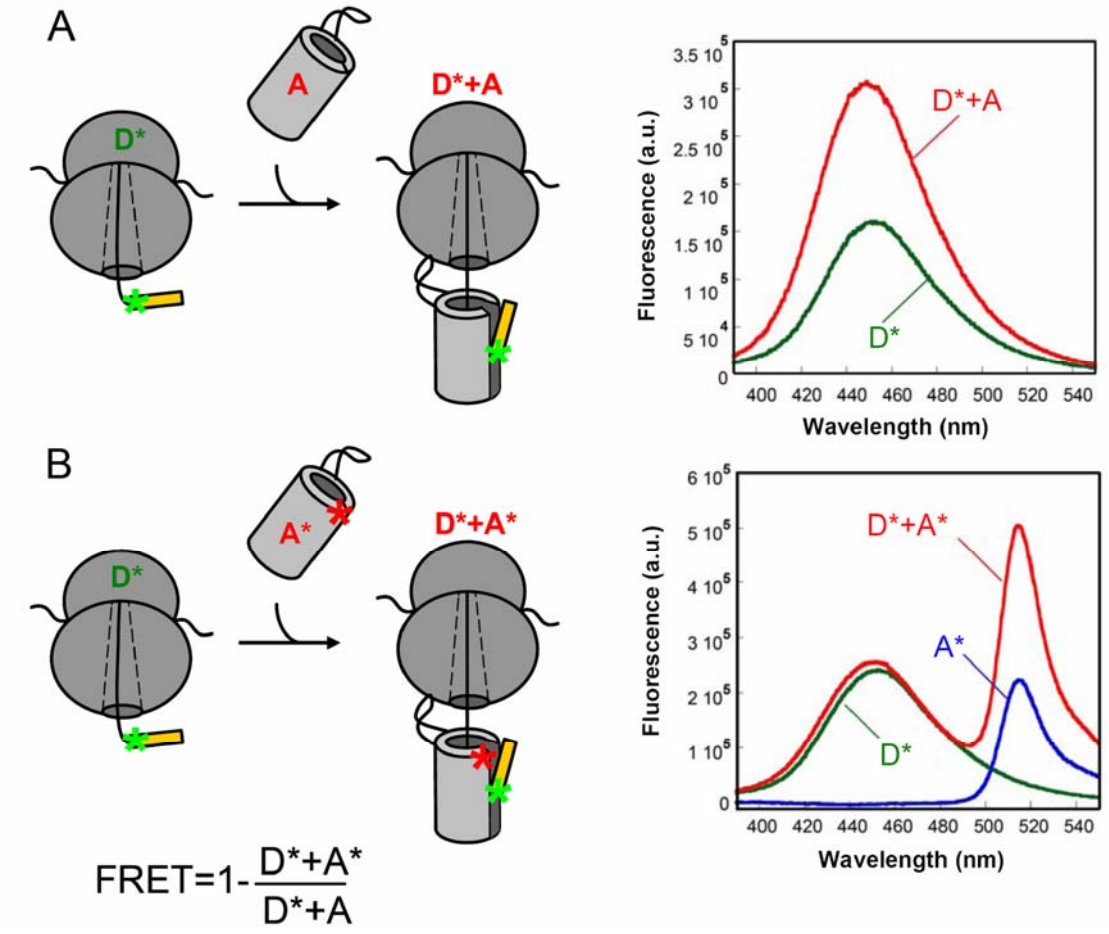

Figure 2. Fluorescence signal upon addition of unlabeled or acceptor-labeled SecYEG to the donor-labeled RNC. A. Upon addition of unlabeled SecYEG to the coumarin-labeled RNC (green, D*) a dramatic increase in coumarin fluorescence is observed (red, D*+A) due to the environmental sensitivity of the dye to SecYEG. **B**. No apparent change in the fluorescence of coumarin is observed when BodipyFL-labeled SecYEG is added to the solution of coumarin-labeled RNC since the increase in fluorescence due to the environmental sensitivity of coumarin is cancelled by the decrease of the signal due to FRET. RNCs containing 85 aa long nascent chains with 1A9L signal sequence were used in this experiment. Note the increase in the acceptor channel due to FRET (B). Forty nM RNC and 47 nM SecYEG were mixed in the SRP buffer supplemented with 10% glycerol and 0.02% DDM. SecYEG used in this experiment was tagged at the N-terminus of SecE with a His_6 tag. The formula at the bottom of the figure was used to calculate FRET efficiency.

Figure 3

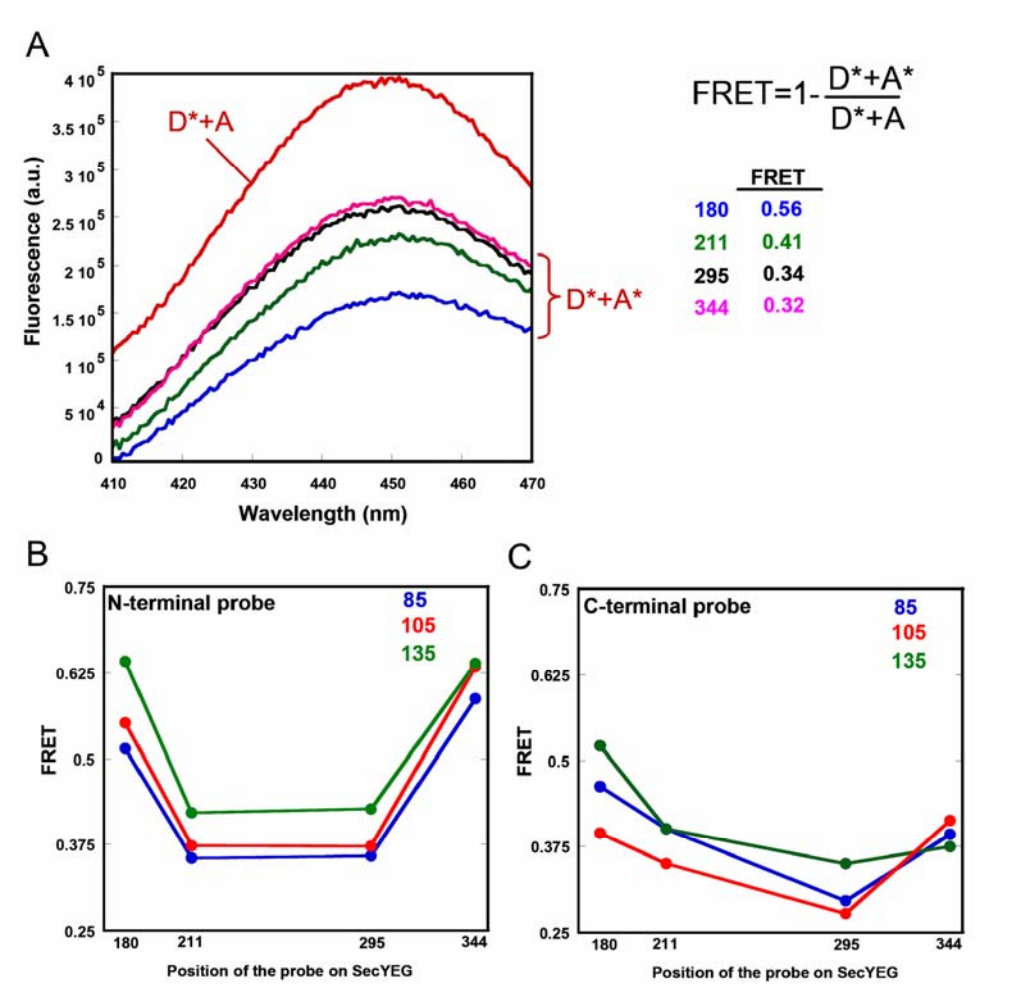

Figure 3. FRET between coumarin-labeled RNC_{3A7L} and BodipyFL-labeled SecYEG. A. Representative emission spectra of coumarin-labeled RNC_{3A7L} bearing a nascent chain 135 aa long upon addition of unlabeled (D*+A) and BODIPY-FL labeled (D*+A*) SecYEG. Twenty nM RNC and 315 nM SecYEG were used. The formula on the right of the panel was used to calculate FRET efficiency. The numbers on the right show FRET efficiency values observed with SecYEG labeled at corresponding residues. **B**. FRET efficiencies observed upon binding of N-terminally coumarin-labeled RNC of variable nascent chain length to BodipyFL-labeled SecYEG. Numbers inside the panel indicate the length of the nascent chains. FRET efficiencies were calculated as described in A. **C.** As in B, only C-terminally labeled RNCs were used. Twenty nanomolar RNC and at least two different concentrations of SecYEG were to saturate RNC. The final SecYEG concentration was from 250 to 600 nM in different experiments. Every FRET measurement was performed under saturating concentration of SecYEG.

Figure 4

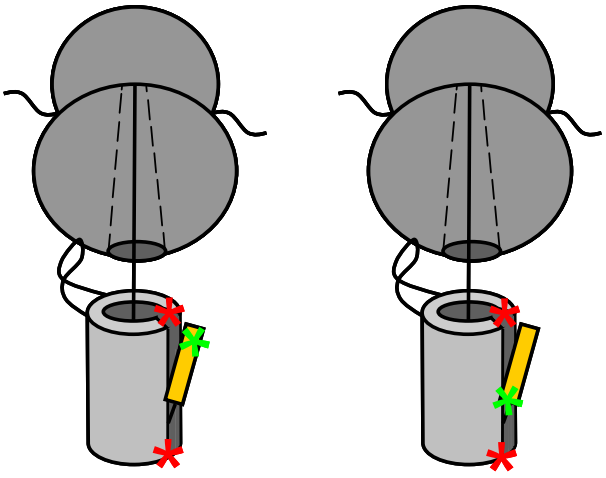

Figure 4. A model for Type II orientation of the 3A7L signal peptide inside SecYEG. The red star is the acceptor fluorophore on SecYEG. Both the cytoplasmic and periplasmic location of the probe are shown on the same SecYEG unit to explain the observed FRET values with N- and C-terminally labeled signal peptide (green star). See discussion for how the FRET data led to this model.

Figure 5

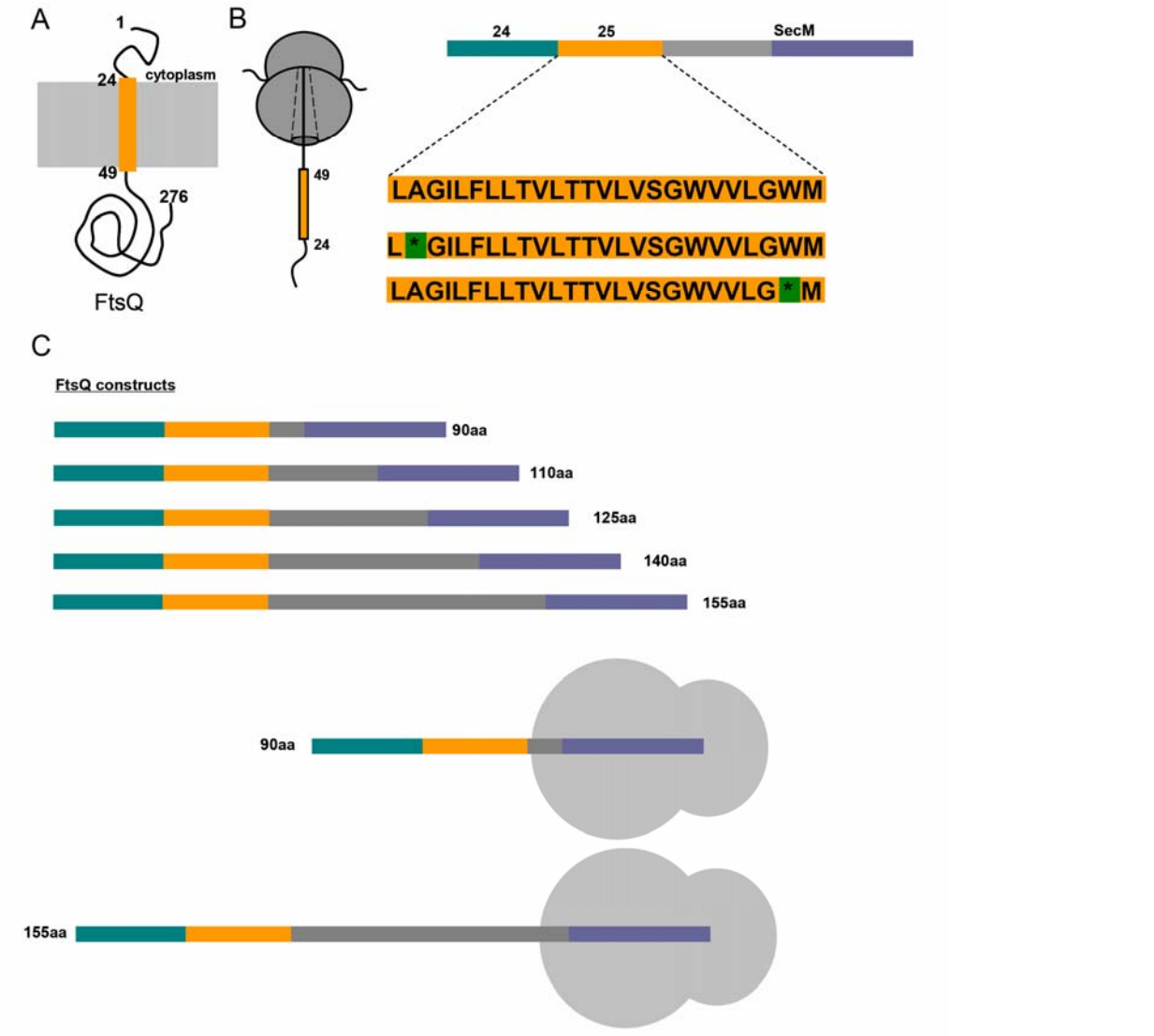

Figure 5. FtsQ constructs used in mapping orientation of the FtsQ TM upon binding SecYEG. A. Topology of the membrane protein FtsQ in the lipid bilayer. The orange rectangle represents the transmembrane domain (signal anchor) of FtsQ. The numbers show the size of each region of the protein. **B**. Pictoral representation of a stalled RNC bearing the FtsQ nascent chain (left) and location of coumarin on the N- or C-terminus of the signal anchor of FtsQ (right). **C**. FtsQ constructs of increasing length used in the FRET mapping assay. The number on the right of each construct indicates the length of the nascent chain. Below is the schematic representation of stalled RNCs containing the shortest (90 aa) and the longest (155 aa) nascent chains shown for comparison. See Materials and methods for detailed description of the constructs used in preparation of the RNCs.

Figure 6

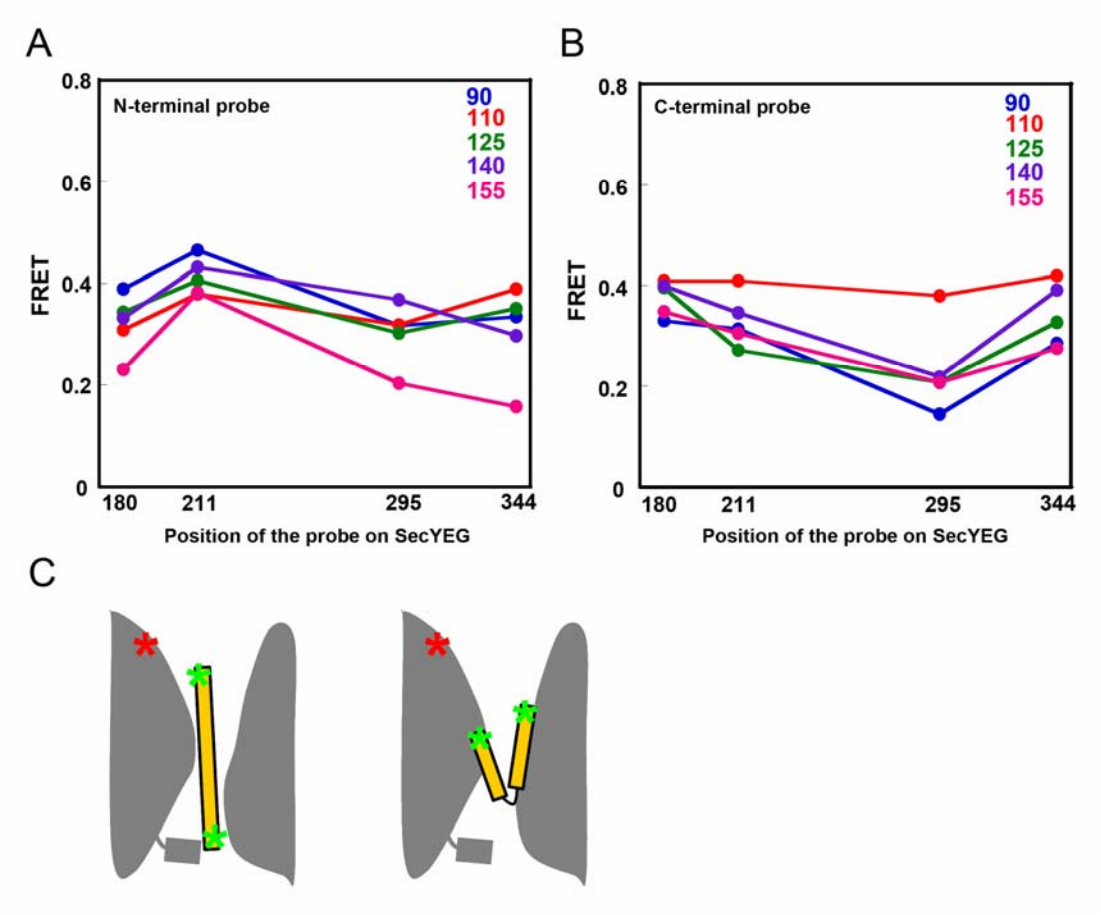

Figure 6. FRET efficiency values observed upon interaction of coumarin-labeled RNC_{FtsQ} with BodipyFL-labeled SecYEG. A. Twenty nM RNC_{FtsQ} with coumarin at the N-terminus of the signal anchor (see Figure 4B) were incubated with at least 10-fold molar excess of BodipyFL-labeled SecYEG in the SRP buffer supplemented with 10% glycerol and 0.02% DDM. FRET efficiencies were calculated as described in Figure 3. **B**. As in A, only N-terminally-labeled RNCs were used. C. Schematics of the expected intercalation mode of the FtsQ signal anchor into the lateral gate of SecYEG (left) and the likely orientation involving a break in the signal anchor helix (right) to explain the observed FRET data (see text for discussion).

Figure 7

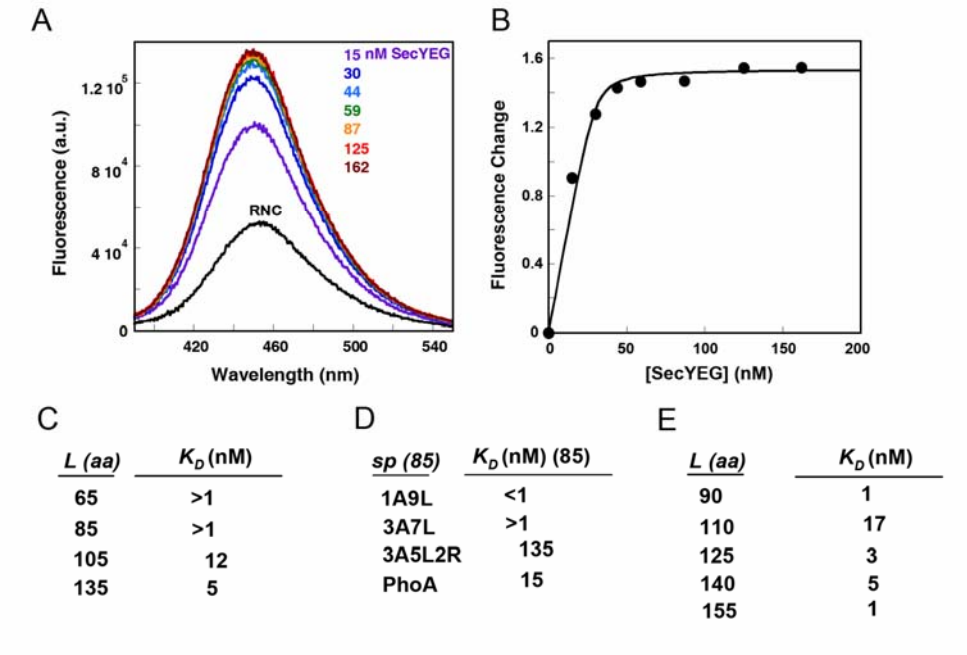

Figure 7. Equilibrium titration of RNC_{3A7L} bearing 85 aa long nascent chains with SecYEG. A. Emission spectra of 20 nM C-terminally coumarin-labeled RNC were collected in the absence or in the presence of increasing concentration of unlabeled SecYEG (see the indicated concentrations). **B**. Fluorescence change was plotted against the concentration of SecYEG and the data were fitted to a quadratic equation described in Materials and methods. **C**. Dissociation constants obtained upon titration of RNC_{3A7L} bearing the nascent chain of increasing length (*L aa*) (65 to 135 aa) with SecYEG. **D**. RNCs bearing the nascent chain 85 aa long and containing different signal peptides (*sp 85*) were titrated with SecYEG to obtain the tabulated dissociation constants. **E**. RNCFtsQ bearing the nascent chain of increasing length (90 to 155 aa) was titrated with SecYEG to obtain the tabulated dissociation constants. The data to obtain the K_d values in C, D, and E were treated as described in panels A and B.

Figure 8

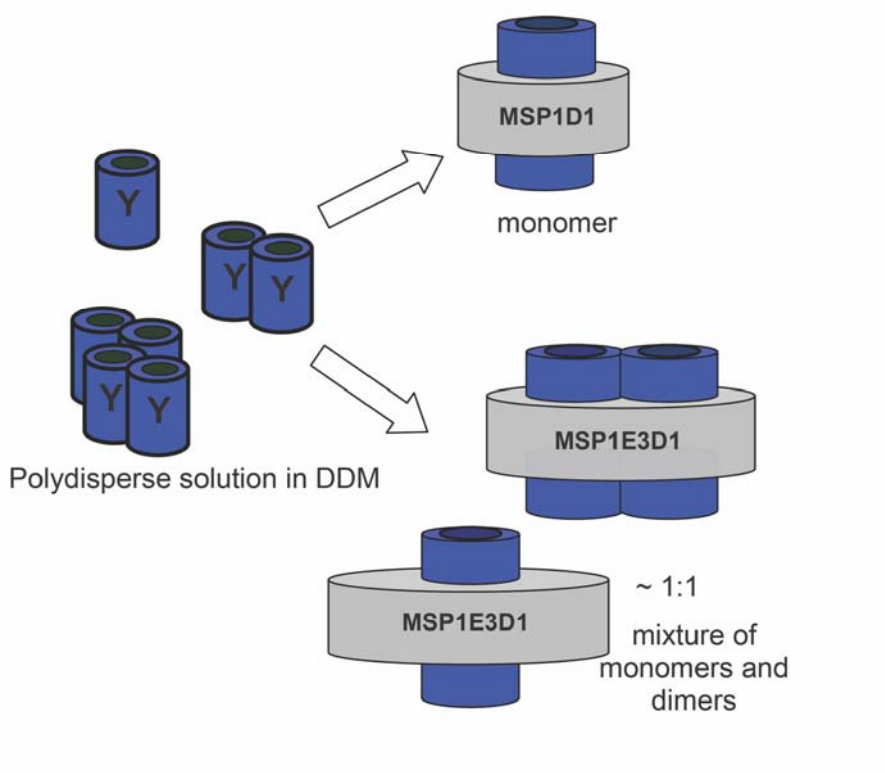

Figure 8. Schematics of reconstitution of detergent-solubilized SecYEG in nanodiscs. Using the membrane scaffold protein of a defined size allows control of the polydispersity of the SecYEG-Nd solution. A monodisperse solution of nanodiscs containing monomers of SecYEG can be formed with MSP1D1, while a larger scaffold protein MSP1E3D1 affords a stoichiometric mixture of monomers and dimers. See the Materials and methods section for a detailed description of the reconstitution procedure.

Figure 9

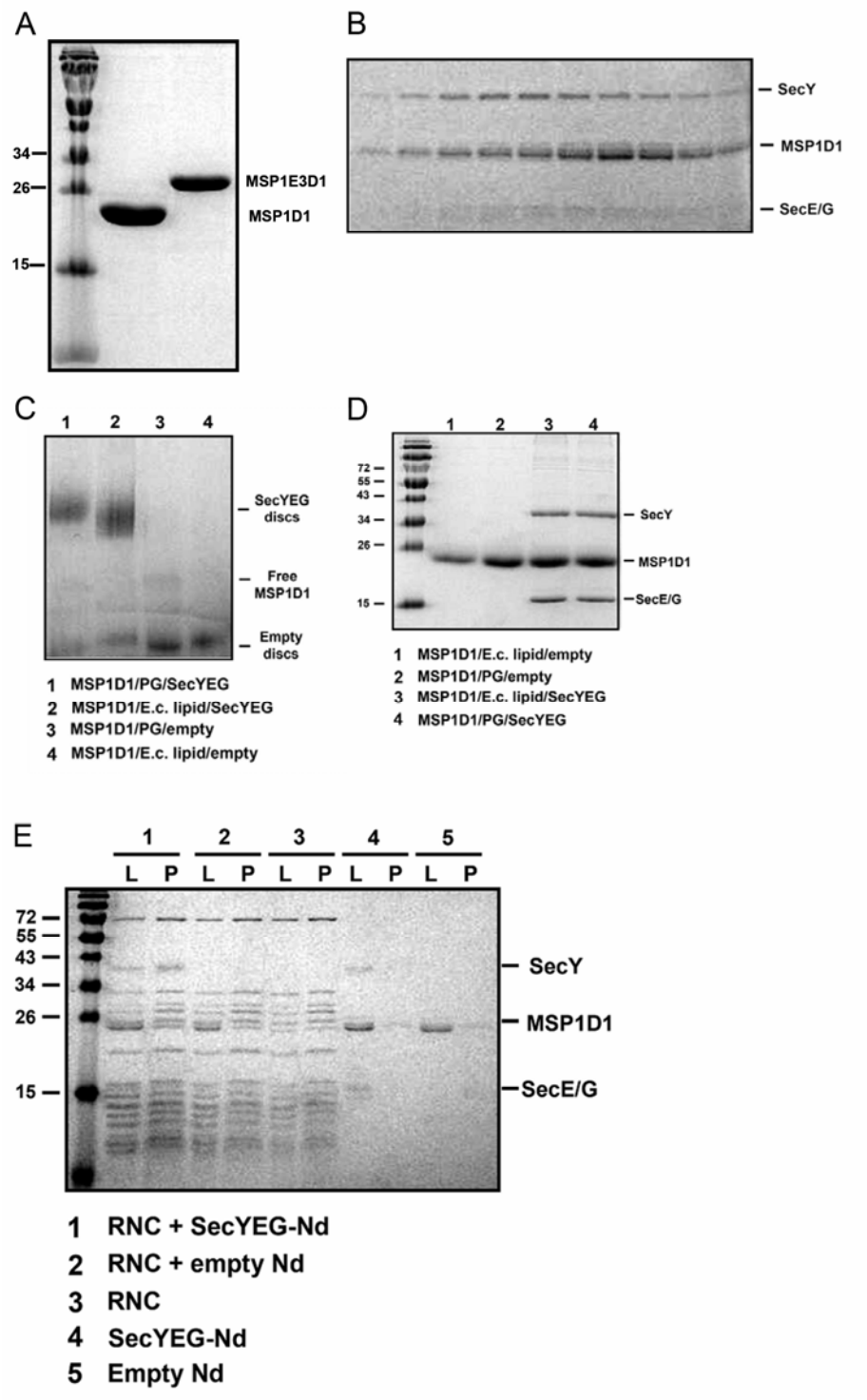
A
34
26
15
MSP1E3D1
MSP1D1
B
SecY
MSP1D1
SecE/G
C
1 2 3 4
SecYEG discs
Free MSP1D1
Empty discs
1 MSP1D1/PG/SecYEG
2 MSP1D1/E.c. lipid/SecYEG
3 MSP1D1/PG/empty
4 MSP1D1/E.c. lipid/empty
D
1 2 3 4
72
55
43
34
26
15
SecY
MSP1D1
SecE/G
1 MSP1D1/E.c. lipid/empty
2 MSP1D1/PG/empty
3 MSP1D1/E.c. lipid/SecYEG
4 MSP1D1/PG/SecYEG
E
1 2 3 4 5
L P L P L P L P L P
72
55
43
34
26
15
SecY
MSP1D1
SecE/G
1 RNC + SecYEG-Nd
2 RNC + empty Nd
3 RNC
4 SecYEG-Nd
5 Empty Nd

Figure 9. Reconstitution of SecYEG in nanodiscs. A. Coomassie-stained denaturing gel showing purified MSP1D1 and MSP1E3D1 (labeled). **B**. Elution profile of SecYEG nanodiscs resolved on a Superdex 200 10/300 gel filtration column. Fractions were collected and run on a denaturing gel. SecY, MSP1D1, and SecE/G bands are labeled. **C**. Blue-native gel to visualize intact SecYEG nanodiscs. SecYEG reconstituted nanodiscs was resolved on a non-denaturing gel in the presence of Brilliant Blue G250. The gel was destained and photographed using Bio-Rad gel documentation system. The reconstitution reactions loaded onto lanes 1 through 4 are described below the gel. **D**. Coomassie-stained denaturing gel showing the components of SecYEG-nanodiscs. The reactions loaded onto lanes 1 through 4 are described below the gel. **E**. Binding of RNC to SecYEG nanodiscs. RNC_{1A9L} was incubated either with SecYEG nanodiscs or empty discs. The RNCs were pelleted through sucrose cushion. The pellet was resuspended in 2X Laemmli sample buffer and resolved on a denaturing gel (P) along with the sample before centrifugation (L). The samples subjected to centrifugation are described below the gel. The gels were photographed using Bio-Rad gel documentation system. See Materials and methods for a detailed description of reconstitution of SecYEG in nanodiscs and the cosedimentation assay.

Figure 10

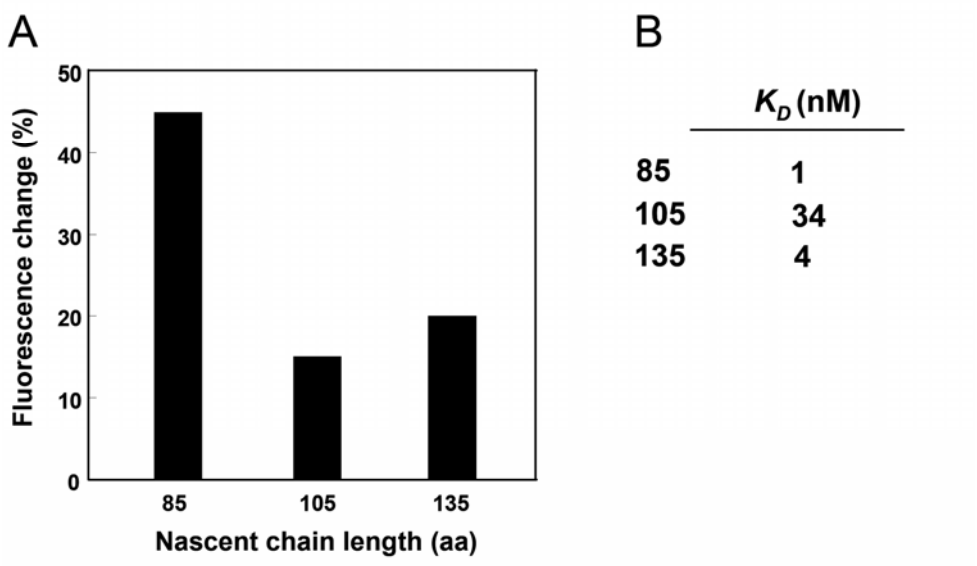

Figure 10. Binding of SecYEG nanodiscs to RNC_{3A7L}. A. Maximum fluorescence change due to environmental sensitivity of coumarin upon incubating RNC_{3A7L} labeled with coumarin at the C-terminus of the signal sequence with SecYEG reconstituted in nanodiscs. **B**. The K_d values were obtained as described in Figure 6.

Figure 11

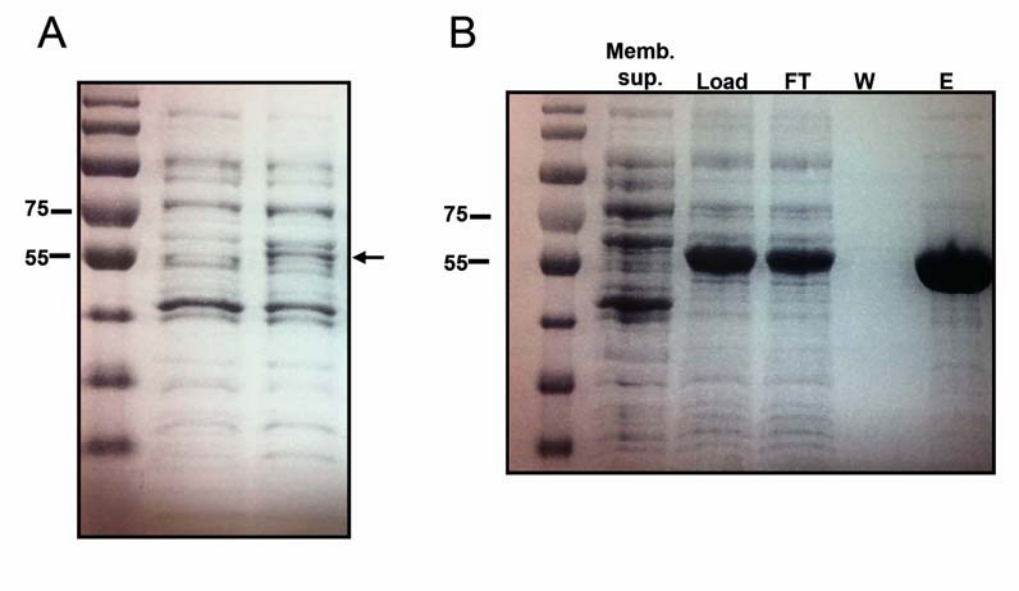

Figure 11. Expression and purification of YidC. A. Coomassie-stained denaturing gel showing expressioin of YidC. The arrow shows the location of the YidC band (3rd lane) from the induced sample missing in the 2nd lane (non-induced sample). See Materials and methods for detailed description of the expression vector as well as expression procedure and analysis of expression. **B**. Coomassie-stained denaturing gel showing affinity purification of YidC using Ni-NTA agarose resin. See Materials and methods for detailed description of the purification procedure. FT, flow through; W, wash; E, elution. The numbers on the left of each gel indicate molecular weight in kDa. The gels were photographed using iPhone 4 camera.

Figure 12

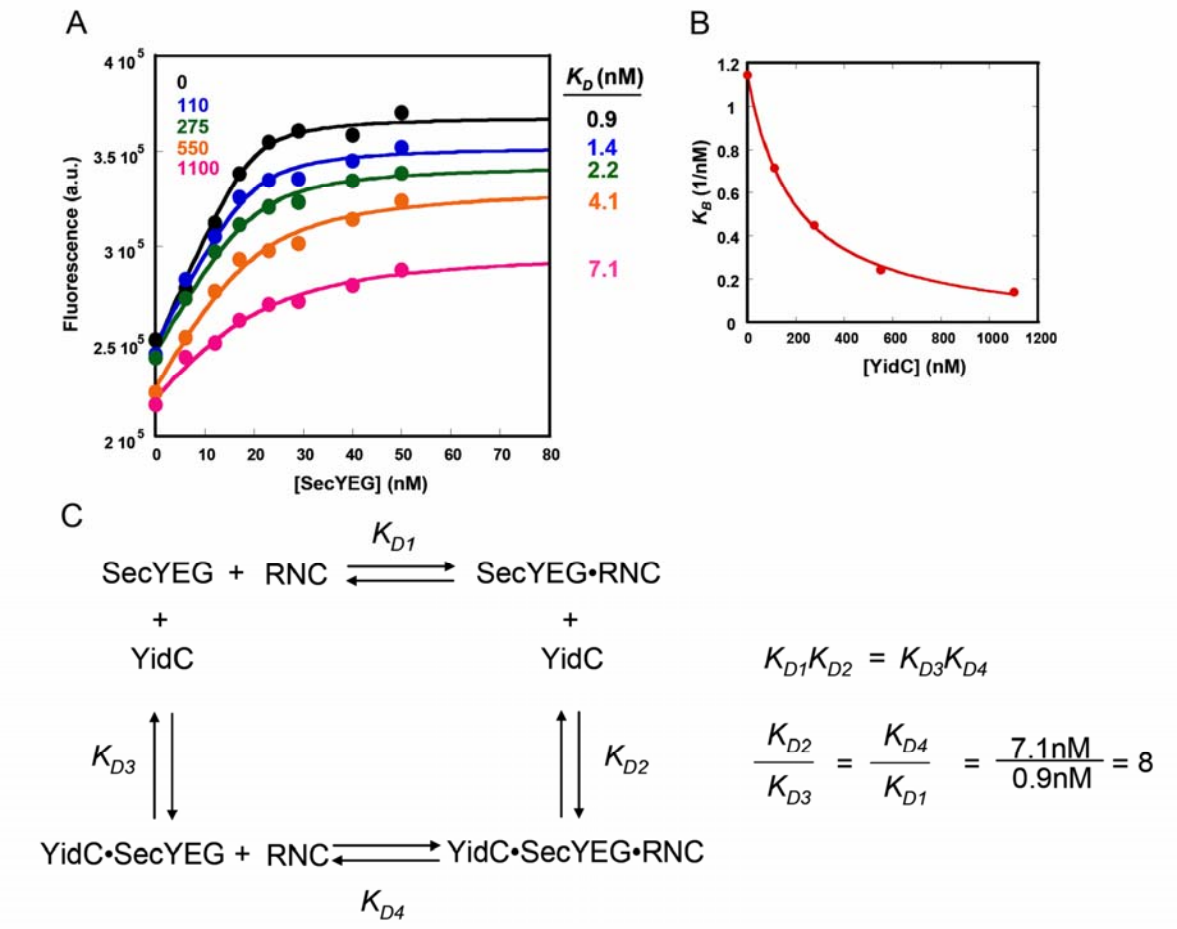

Figure 12. Effect of detergent-solubilized YidC on RNC-SecYEG interaction. A. Twenty nM N-terminally coumarin-labeled RNC_{FtsQ} containing a 90 aa long nascent chain was titrated with SecYEG in the presence of increasing concentration of YidC (indicated). Emission fluorescence of coumarin was plotted against the concentration of SecYEG, and the data were fit to a quadratic equation described in the Materials and methods. **B**. The dissociation constant values in A were converted to binding constants ($1/K_d$) and plotted against the concentration of YidC. **C**. A thermodynamic cycle of the ternary YidC•SecYEG•RNC complex formation. SecYEG binds RNC with 8-fold weaker affinity when in complex with YidC.

Figure 13

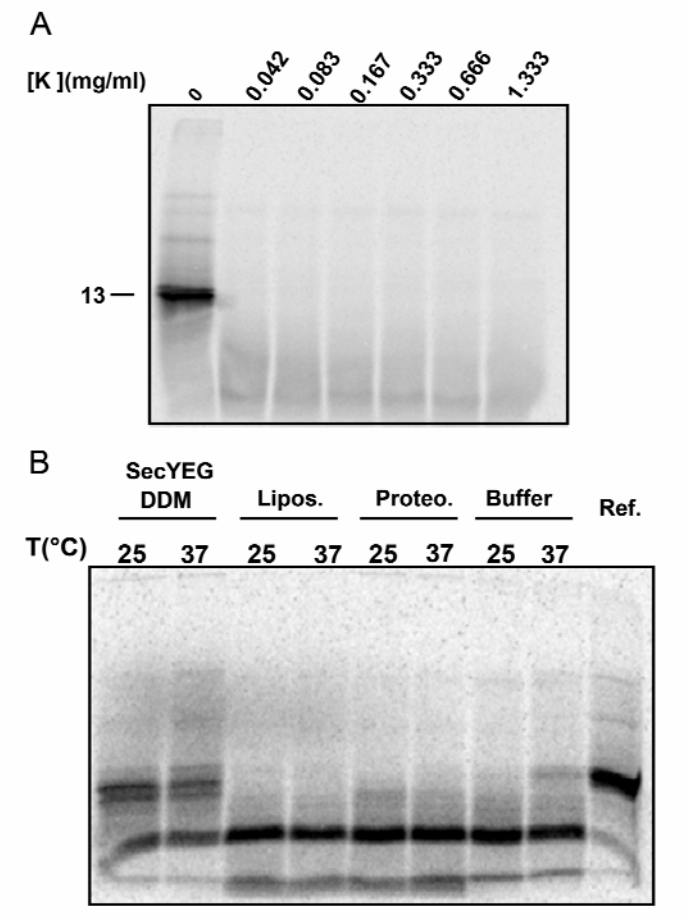

Figure 13. Assessment of the nascent chain insertion into SecYEG upon binding of ^{35}S-labeled RNC_{1A9L} to detergent-solubilized SecYEG or SecYEG in proteoliposomes. A. ^{35}S-labeled RNC_{1A9L} were treated with increasing concentration of proteinase K for 15 minutes on ice. The samples were quenched with PMSF, precipitated using trichloroacetic acid (TCA), dissolved in 2X Laemmli buffer, and resolved on 18% acrylamide denaturing gel. The gel was analyzed using autoradiography. **B**. S35-RNC1A9L was incubated was incubated either with detergent-solubilized SecYEG, empty liposomes, SecYEG proteoliposomes, or buffer at 25 or 37°C for 30 minutes. The mixtures were treated with 0.005 mg/ml proteinase K for 15 minutes on ice, and the reactions were analyzed as described in panel A. The samples were loaded onto 15% denaturing gel. 30% of TCA-precipitated RNC were loaded onto the reference lane (Ref.).

Figure 14

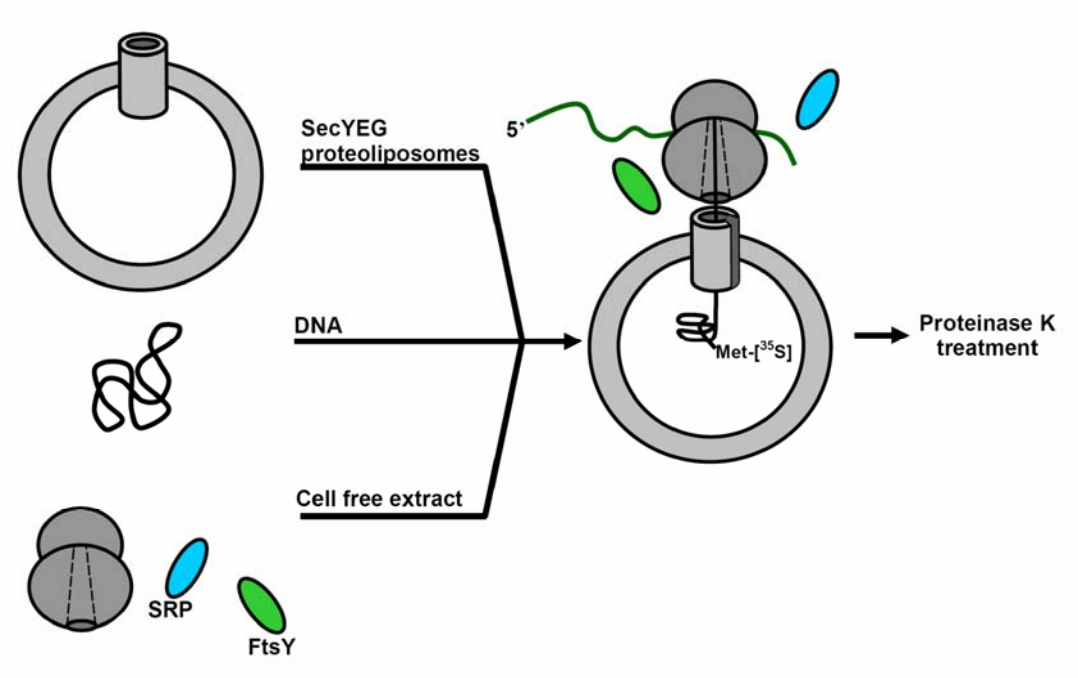

Figure 14. Shematics of an *in vitro* cotranslational protein targeting assay. SecYEG proteoliposomes were mixed with the plasmid encoding the substrate of interest and the cell free extract. The samples were supplemented with T7 RNA polymerase and incubated at 37°C for 30 min. As DNA is transcribed into mRNA, the components are assembled into complexes depicted on the right. The substrate is translated into the lipid vesicle. The extent of translocation or insertion is assessed by treating the reactions with proteinase K. See Materials and methods for detailed description of the assay.

Figure 15

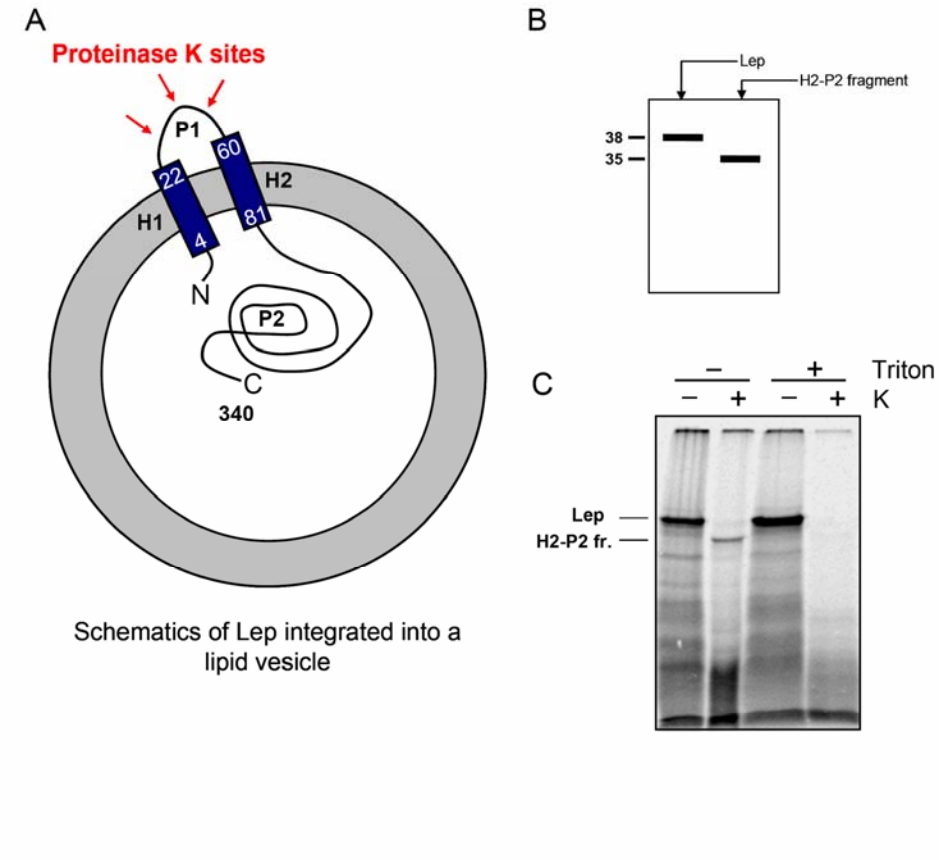

Figure 15. Cotranslational insertion of leader peptidase into *E. coli* inner membrane vesicles (IMVs) containing overexpressed levels of SecYEG. A. Schematics of Lep inserted into a lipid vesicle. The exposed loop P1 contains proteinase K sites. **B**. Treatment of Lep inserted into a lipid vesicle with proteinase K results in appearance of the protected H2-P2 fragment with MW of ~ 35 kDa indicative of productive insertion of Lep. **C**. IMVs with overexpressed SecYEG levels were incubated with cell free extract and the plasmid encoding Lep in the presence of T7 RNA polymerase for 30 min at 37°C. The samples were split into two aliquots, and one of the aliquots was treated with proteinase K in the absence or presence of Triton X100. The reaction was quenched with PMSF, and the protein was precipitated with TCA. The pellet was dissolved in 2X Laemmli sample buffer, and equal amounts of the samples were resolved on a 15% denaturing gel. The gel was visualized by autoradiography.

Figure 16

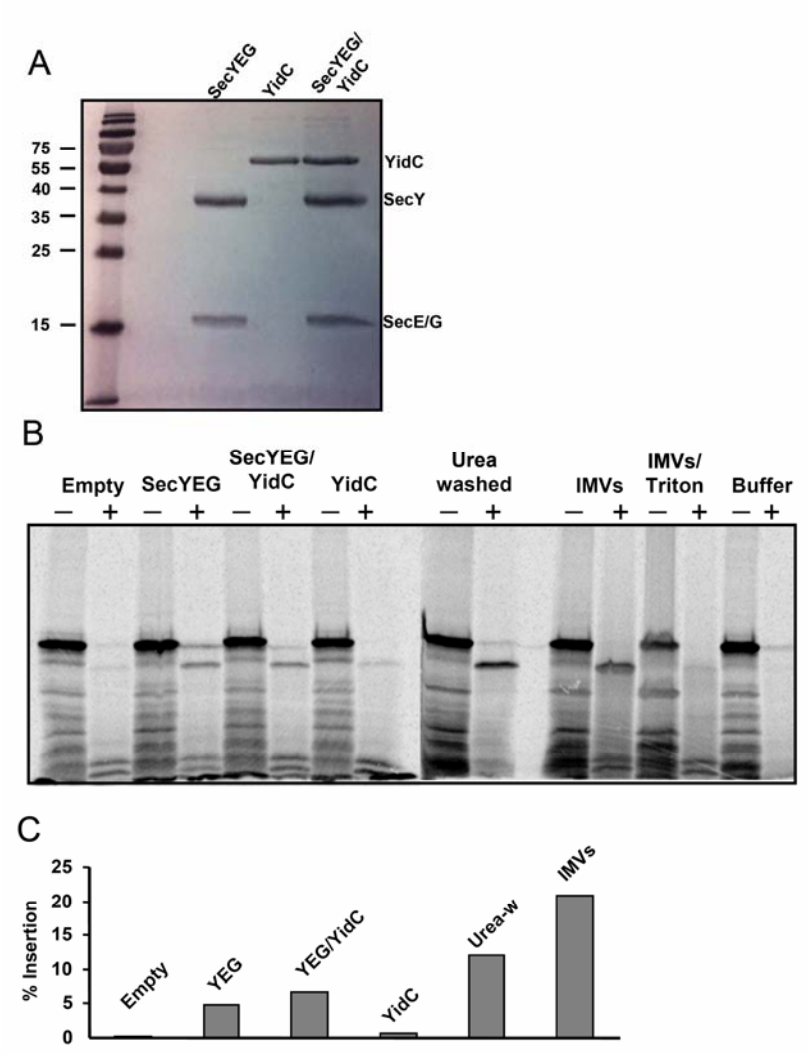

Figure 16. Cotranslational targeting assay with YidC and SecYEG proteoliposomes. A. Proteoliposomes containing either SecYEG, YidC, or both SecYEG and YidC were solubilized in 2% SDS and mixed with 2X Laemmli Sample buffer. Equal volumes were resolved on a 15% denaturing gel. The numbers on the left of the gel indicate MW in kDa. See Materials and methods for description of the detailed procedure of reconstitution of SecYEG and YidC in proteoliposomes. **B**. Cotranslational protein targeting assay performed with liposomes (empty), SecYEG proteoliposomes, SecYEG/YidC proteoliposomes, urea-washed IMVs, and IMVs. + and – indicate whether the solution was or was not treated with proteinase K, respectively. The assay was performed as described in Figure 14. **C**. Quantitation of the insertion efficiency. Percent insertion was calculated by comparing the intensity of the P2-H2 protected fragment to the intensity of the full-length Lep in the – proteinase K sample. See Materials and methods for a detailed description of the assay.